Consortium for Small-Scale Modelling

Newsletter

April 2005

No. 5

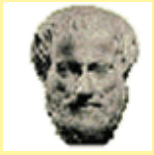

www.cosmo-model.org

Editors: Ulrich Schättler (DWD) and Andrea Montani (ARPA-SIM)
Printed at Deutscher Wetterdienst, PO. Box 100465, 63004 Offenbach am Main, Germany

Table of Contents

In Memoriam Günther Doms

1956-2004

The COSMO community was shocked in the week after the 20th of June when we heard of Günther Doms' sudden and unexpected decease one day after his 48th birthday. And even today, it seems to us quite unreal that he is no longer with us. We did not only loose an outstanding scientist in the field of meteorology, but an excellent colleague and dear friend.

Günther Doms started studying meteorology in 1975 at the University of Frankfurt. Here his outstanding talents in theoretical meteorology were discovered by Prof. Herbert. During the years 1980-84 he worked as a *wissenschaftliche Hilfskraft*, i.e. he assisted Prof. Herbert as an advanced student. In 1984 he finished his Diploma Thesis. From 1984-87 he was engaged in two projects as a junior scientist. He joined DWD in 1987. Since that time he worked in the Research Department in the field of numerical weather prediction.

Since the time of his Diploma Thesis his special subject was cloud modelling, in particular cloud microphysics and precipitation formation. But he also investigated problems in the planetary boundary layer. His first publication *Fluid- and microdynamics in numerical models for convective clouds* together with Prof. Herbert is mainly based on his Diploma Thesis. The chapters of this publication are covering a wide range of topics and many principles of nonhydrostatic modelling are addressed, such as basic equations, filtering of sound waves, shallow and deep convection, cloud microphysics, liquid water drag, turbulence in clouds including detrainment and entrainment. A lot of information can be found here

which has been used later for the development of LM by him.

Thanks to his excellent talents both in physics and numerics Günther Doms could use his know-how to contribute to the development of the *Europa-Modell* (EM) and *Deutschland-Modell* (DM). Based on his profound theoretical knowledge he clearly formulated later the equations of LM. In the course of time he became a nationally and internationally acknowledged expert in cloud microphysical parameterization. The cloud ice scheme developed by him was introduced into GME and LM in September 2003.

Günther Doms participated in all bilateral Swiss-German meetings in Bad Säckingen and in several EWGLAM/SRNWP workshops as a national or COSMO representative. *His presentations were a highlight both for their scientific content and for their didactical quality.* That was expressed by Jean Quiby in his e-mail to the representatives of the SRNWP community in Europe. Günther Doms was also an important contact person at LM User Seminars in Langen and SRNWP meetings in Bad Orb.

He was one of the fathers of LM and during the last years he became the *supportive pillar* of LM. Through his work, LM became nationally and internationally well-known and attractive. The Meteorological Services of Switzerland, Italy, Greece, Poland and Romania are now using the model operationally and are participating in the further development of LM in the framework of COSMO.

Günther Doms was the first Scientific Project manager of COSMO, a position he occupied from 2000 to 2003. Everybody who had questions concerning LM got answers from him because he had the best knowledge of LM both in physics and numerics. He also looked after the visiting scientists who wanted to work with LM or to learn from him. In addition, he was one of the editors of the COSMO Newsletter. He also took care of the technical aspects like the writing in LaTEX. Documentation was considered very important by him.

His last scientific position at DWD was the Scientific Project Manager of LMK (LM for very short-range forecasts) where he co-ordinated five project scientists together with their mentors. He did not hesitate to take over this task because he loved to work together with other colleagues. He proposed daily running test versions and invited the future internal users to have a look at the model results and to help in evaluating the LMK fields. The last mission he made was to Geneva in Switzerland at the beginning of May 2004 where he gave a presentation on LMK at the Work Package Coordinator meeting, proud of the results which had already been achieved.

The COSMO family is very thankful to him for his scientific work. We thank him for his knowledge and experience which he has shared with us, for his modesty and friendliness, and we thank him for the time which he has given to each of us. His advice, his judgement and his ideas for the further development of LM will be missed.

The COSMO community honoured Günther Doms at the 6th COSMO General Meeting in Milano 2004 which was held in his memory.

Günther Doms is survived by his wife Agneta and their two sons Fredrik and Henrik. Our sympathy is with them all.

Dieter Frühwald

1 Introduction

This is the fifth Newsletter of the Consortium for Small-Scale Modelling (COSMO). Up to now the Newsletter has been prepared once a year in February/March, but will be shifted to a date in autumn, after the COSMO General Meeting. Therefore, there will be two Newsletters this year.

The basic purpose of the Newsletter is threefold:

- to review the present state of the model system and its operational applications and to give information on recent changes;
- to present the principal events concerning COSMO during the last year and to summarize recent research and development work as well as results from the model verification and diagnostic evaluation;
- to provide the meteorological community and especially all external users of the model system with information on COSMO's activities and with new information on the model system and its current forecast quality.

The present Newsletter is organized as follows. Section 2 gives a general overview of the current organizational structure of the COSMO consortium. The present state of the model system, i.e. the LM-package, is summarized in Section 3, including a short description of the model and its data assimilation system, information on the preprocessor programs to provide initial and boundary conditions, and finally remarks on postprocessing utilities and hints on the available model documentation.

Operational and pre-operational applications of the LM-package at the COSMO meteorological centres are described in Section 4. Information about the recent changes to the model system as well as changes in the model set-up at the meteorological centres are outlined in Section 5. Section 6 gives you an overview of the six COSMO Working Groups and their recent research and development activities.

Section 7 provides short information on the main COSMO meetings and events during the last year. Other activities such as internal visits and guest scientist programs are also included. Finally, some forthcoming events planned for this year are announced.

Recent results from the verification of the operational models, both for surface parameters and for vertical profiles, are summarized in Section 8. This section also includes contributions related to the development of new methodologies for model verification as well as results from the verification of new model components.

Section 9 is devoted to reports on various research topics related to model development and application, including data assimilation, numerics, physics, interpretation, and technical aspects. Finally, all COSMO activities related to the LM-system within international and national projects of the member meteorological services are listed in Section 10. This list will be updated in the forthcoming issues.

The Appendices concern the use of the GRIB binary data format for the output and input analyses and forecast fields. These lists will also be updated, and we hope they will be helpful, especially for new users of the LM and its forecast products.

Information about COSMO and the LM can also be obtained from our web-site ***www.cosmo-model.org*** or the mirror site ***cosmo-model.cscs.ch***. Due to the activities of the greek weather service during the Olympic Games 2004, the official COSMO web-site has temporarily been

unvailable and additional work was necessary to maintain the site in Manno, Switzerland. Many thanks to Theodore Andreadis from HNMS and Marco Consoli from CSCS for running, updating and supervising the web-sites.

The present organization of the Newsletter may change in future. Please contact the editors for any comments and suggestions as well as proposals for items to be included or excluded in the next issue. The editors recognize that typographical and other errors or inconsistencies may be present. We apologize for this, and your assistance in correcting them will be welcome.

We would also like to encourage all the scientists in the COSMO Working Groups to document their work, e.g. in form of a short progress summary or a longer report, to be included in the next Newsletter. Special thanks to all who provided contributions and graphical material for the present issue:

Marco Arpagaus (MeteoSwiss)
Euripides Avgoustoglou (HNMS)
Michael Baldauf (DWD)
Davide Cesari (ARPA-SIM)
Ulrich Damrath (DWD)
Pierre Eckert (MeteoSwiss)
Jochen Förstner (DWD)
Alessandro Galliani (UGM)
Thomas Hanisch (DWD)
Emanuele Zala (MeteoSwiss)
Pirmin Kaufmann (MeteoSwiss)
Stefan Klink (DWD)
Detlev Majewski (DWD)
Chiara Marsigli (ARPA-SIM)
Lucio Torrisi (UGM)
Joanna Linkowska (IMGW)
Guy de Morsier (MeteoSwiss)
Heinz-Werner Bitzer (AGeoBW)
Jan Parfiniewicz (IMGW)
Tiziana Paccagnella (ARPA-SIM)
Patrizio Emiliani (UGM)
Ulrich Pflüger (DWD)
Christoph Schraff (DWD)
Francis Schubiger (MeteoSwiss)
Klaus Stephan (DWD)
Jürgen Steppeler (DWD))
Katarzyna Starosta (IMGW)
Jan-Peter Schulz (DWD)
Ermanno Veccia (UGM)

To run a complex NWP system at a COSMO meteorological centre requires the continuous effort of many people. Thanks to all of them, especially to those implementing new model versions, maintaining the operations, and organizing the data transfer between the centres:

– Michael Gertz and Thomas Hanisch at DWD,
– Jean-Marie Bettems, Guy deMorsier and Emanuele Zala at MeteoSwiss,
– Theodore Andreadis and Euripides Avgoustoglou at HNMS,
– Davide Cesari and Paolo Patruno at ARPA-SIM and
– Jan Parfiniewicz and Marek Lazanowicz at IMGW.

Finally, thanks to all who supported us concerning technical problems during the editorial work. For any comments, suggestions and questions please contact the editors:

Ulrich Schättler
ulrich.schaettler@dwd.de

Andrea Montani
montani@smr.arpa.emr.it

2 Organizational Structure of COSMO

2.1 General

The ***Consortium for Small-Scale Modelling*** (COSMO) was formed in October 1998 at the regular annual DWD/MeteoSwiss meeting. At present, the following national, regional and military meteorological services are participating:

DWD	Deutscher Wetterdienst, Offenbach, Germany
HNMS	Hellenic National Meteorological Service, Athens, Greece
IMGW	Institute for Meteorology and Water Management, Warsaw, Poland
MeteoSwiss	MeteoSchweiz, Zürich, Switzerland
UGM	Ufficio Generale per la Meteorologia, Roma, Italy
ARPA-SIM	Servizio Idro Meteorologico di ARPA, Bologna, Italy
ARPA-Piemonte	Agenzia Regionale per la Protezione Ambientale, Piemonte, Italy
AGeoBW	Amt für Geoinformationswesen der Bundeswehr, Euskirchen, Germany

The general goal of COSMO is to develop, improve and maintain a non-hydrostatic limited-area modelling system to be used both for operational and for research applications by the members of COSMO. The emphasis is on high-resolution numerical weather prediction by small-scale modelling. COSMO is initially based on the "Lokal-Modell" (LM) of DWD with its corresponding data assimilation system.

A Memorandum of Understanding (MoU) on the scientific collaboration in the field of non-hydrostatic modelling was signed by the Directors of DWD, HNMS, MeteoSwiss and UGM in March/April 1999. Meanwhile, the MoU has been replaced by an Agreement between the participating National Meteorological Services. The national weather service IMGW of Poland joined the consortium in 2002. Since 2004, the Romanian Meteorological Service, NMA, is an *associated member* of COSMO.

2.2 Agreement

The structure of the cooperation and both internal and external relationships of COSMO are defined and further detailed in an Agreement between the National Meteorological Services of the participating countries. On 3 October 2001, the final version of the COSMO Agreement has been signed by the representatives of the National Meteorological Services (DWD, HNMS, MeteoSwiss and UGM). The Director of the national weather service of Poland (IMGW) signed the Agreement on 4 July 2002.

There is no direct financial funding from or to either member. However, the partners have the responsibility to contribute actively to the model development by providing staff resources, by making use of research cooperations and by seeking for national funding whenever possible. A minimum of 2 scientists working in COSMO research and development areas is required from each member. In general, the group is open for collaboration with other NWP groups, research institutes and universities as well as for new members. For more details on the COSMO Agreement, please contact the present Chairman of the Steering Committee, Dieter Frühwald (dieter.fruehwald@dwd.de).

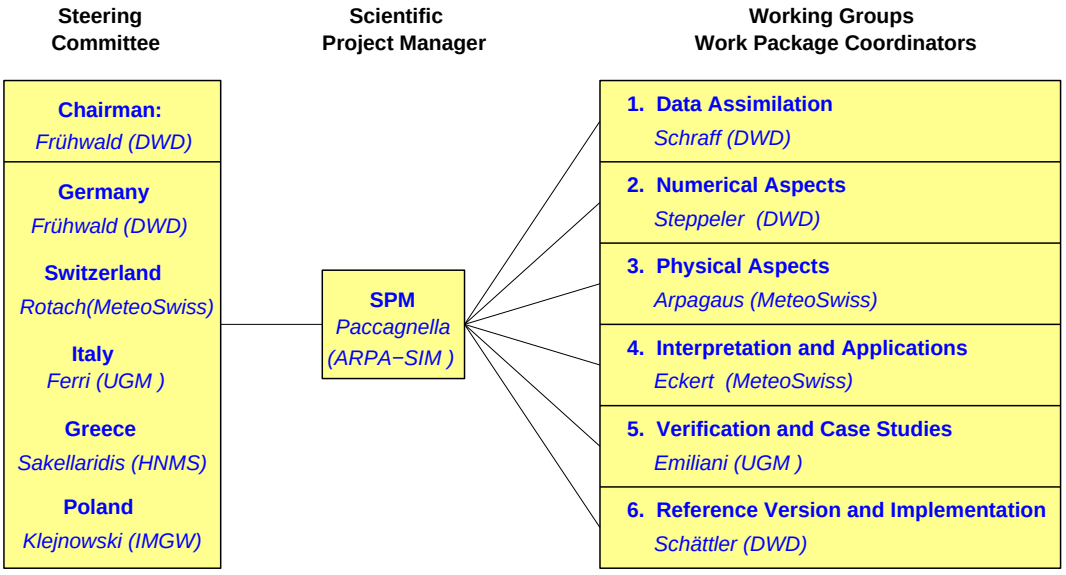

Figure 1: Organizational structure of COSMO as of January 2005

2.3 Organizational Structure

COSMO's organization consists of a Steering Committee (composed of one representative from each National Meteorological Service), a Scientific Project Manager, Work-package Coordinators and Scientists from the member institutes performing research and development activities in the COSMO working groups. At present, six working groups covering the following areas are active: Data assimilation, numerical aspects, physical aspects, interpretation and applications, verification and case studies, reference version and implementation. The current organizational structure is sketched in Fig. 1 (see Section 7 for changes in the Steering Committee and WP-Coordinators).

COSMO's activities are developed through extensive and continuous contacts among scientists, work-package coordinators, scientific project manager and steering committee members via electronic mail, special meetings and internal workshops. Once a year there is a General Meeting of the COSMO group in order to present results, deliverables and progress reports of the working groups and to elaborate a research plan with new projects for the next annual period. Following this meeting, a final work plan for each working group is set up. The recent 6th COSMO General Meeting was held on 22-24 September 2004 in Milano (Italy). For the first time, a representative from another European NWP consortium, Francois Bouttier (the project leader of the AROME-project), attended the COSMO General Meeting. The 7th General Meeting is scheduled for 20-23 September 2005 in Zürich (Switzerland).

3 Model System Overview

The limited-area model LM is designed as a flexible tool for numerical weather prediction on the meso-β and on the meso-γ scale as well as for various scientific applications using grid spacings from 50 km down to about 50 m. Besides the forecast model itself, a number of additional components such as data assimilation, interpolation of boundary conditions from a driving host model and postprocessing is required to run a NWP system at a meteorological service. In the following sections, the components of the LM package - as available to the COSMO group - are briefly described.

3.1 Short Description of the LM

This section gives only a brief overview of the Lokal-Modell. For a comprehensive description, the reader is referred to the documentation of the LM package (see section 3.6). An overview is given by Steppeler et al. (2003).

3.1.1 Dynamics and Numerics

The regional model LM is based on the primitive hydro-thermodynamical equations describing compressible nonhydrostatic flow in a moist atmosphere without any scale approximations. A basic state is subtracted from the equations to reduce numerical errors associated with the calculation of the pressure gradient force in case of sloping coordinate surfaces. The basic state represents a time-independent dry atmosphere at rest which is prescribed to be horizontally homogeneous, vertically stratified and in hydrostatic balance. The basic equations are written in advection form and the continuity equation is replaced by a prognostic equation for the perturbation pressure, i.e. the deviation of pressure from the reference state.

The model equations are formulated with respect to a rotated lat/lon-grid with coordinates (λ, φ). The rotated coordinate system results from the geographical (λ_g, φ_g) coordinates by tilting the north pole. In the vertical, we use a generalized terrain-following height coordinate ζ, where any unique function of geometrical height can be used for transformation. Since ζ does not depend on time, the $(\lambda, \varphi, \zeta)$-system represents a non-deformable coordinate system, where surfaces of constant ζ are fixed in space - in contrast to the pressure based coordinate system of most hydrostatic models, where the surfaces of constant vertical coordinate move in space with changing surface pressure. By default, a hybrid sigma-type (formulated with respect to the base-state pressure) vertical coordinate is used.

The model equations are solved numerically using the traditional Eulerian finite difference method. In this technique, spatial differential operators are simply replaced by suitable finite difference operators and the time integration is by discrete stepping using a fixed timestep Δt. The model variables are staggered on an Arakawa-C/Lorenz grid with scalars (temperature, pressure and humidity variables) defined at the centre of a grid box and the normal velocity components defined on the corresponding box faces. For a given grid spacing, this staggering allows for a more accurate representation of some differential operators than in the A-grid, where all variables are defined at the same point. In general, we use second order centered finite difference operators for horizontal and vertical differencing.

Because the governing nonhydrostatic equations describe a compressible model atmosphere, meteorologically unimportant sound waves are also part of the solution. As acoustic waves are very fast, their presence severely limits the time step of explicit time integration schemes. In order to improve the numerical efficiency, the prognostic equations are separated into terms

Table 1: LM Model Formulation: Dynamics and Numerics

Model Equations:	Basic hydro-thermodynamical equations for the atmosphere: – advection form, – non-hydrostatic, fully compressible, no scale approximations, – subtraction of horizontally homogeneous basic state at rest.
Prognostic Variables:	Horizontal and vertical Cartesian wind components, temperature, pressure perturbation, specific humidity, cloud water content. Options for additional prognostic variables: – turbulent kinetic energy, cloud-ice, rain, snow and graupel content.
Diagnostic Variables:	Total air density, precipitation fluxes of rain and snow.
Coordinate System:	Rotated geographical (lat/lon) coordinate system horizontally; generalized terrain-following height-coordinate vertically. Built-in options for the vertical coordinate are: – hybrid reference pressure based σ-type coordinate (default), – hybrid version of the Gal-Chen coordinate, – hybrid version of the SLEVE coordinate (Schär et al., 2002).
Grid Structure:	Arakawa C-grid, Lorenz vertical grid staggering.
Spatial Discretization:	Second order horizontal and vertical differencing.
Time Integration:	Leapfrog HE-VI (horizontally explicit, vertically implicit) time-split integration scheme by default; includes extensions proposed by Skamarock and Klemp (1992). Additional options for: – a two time-level split-explicit scheme (2nd order Runge-Kutta scheme (Gassmann, 2002), – a three time-level 3-d semi-implicit scheme (Thomas et al., 2000), – a two time level 3rd-order Runge-Kutta scheme (regular or TVD) with various options for high-order spatial discretization (Förstner and Doms, 2004).
Numerical Smoothing:	4th order linear horizontal diffusion with option for a monotonic version including an orographic limiter (Doms, 2001); Rayleigh-damping in upper layers; 3-d divergence damping and off-centering in split steps.
Lateral Boundaries:	1-way nesting using the lateral boundary formulation according to Davies (1976). Options for: – boundary data defined on lateral frames only, – periodic boundary conditions.

which are directly related to acoustic and gravity wave modes and into terms which refer to comparatively slowly varying modes of motion. This mode-splitting can formally be written in the symbolic form

$$\frac{\partial \psi}{\partial t} = s_\psi + f_\psi \,, \tag{1}$$

where ψ denotes a prognostic model variable, s_ψ the forcing terms due to the slow modes and f_ψ the source terms related to the fast acoustic and gravity wave modes. f_ψ is made up of the pressure gradient terms in the momentum equations, the temperature and pressure contributions to the buoyancy term in the equation for the vertical velocity, and the divergence term in the pressure and the temperature equation. The subset of equations containing the f_ψ-terms is then integrated with a special numerical scheme.

The default time integration method used in LM is a variant of the Klemp and Wilhelmson (1978) scheme including extensions proposed by Skamarock and Klemp (1992). It is based on a Leapfrog integration for the slow modes from time level $n-1$ to time level $n+1$ using an integration interval of $2\Delta t$. The slow mode tendencies are evaluated at time level n for horizontal advection and at time level $n-1$ for most physical forcings. Tendencies from vertical advection and diffusion are calculated by a quasi-implicit scheme. The integration step is then subdivided into a number N_s of small time steps $\Delta\tau_s$ according to $2\Delta t = N_s\Delta\tau$ and the prognostic equations (1) are stepped forward according to

$$\psi^{\nu+1} = \psi^{\nu} + f_{\psi}^{\nu}\Delta\tau + s_{\psi}^{n}\Delta\tau\,. \tag{2}$$

In the integration of (2), sound waves are treated explicitly for horizontal directions using the forward-backward method while implicitly for the vertical direction (HE-VI scheme). Thus, the small time step $\Delta\tau$ is limited by the CFL stability criterion for horizontal but not for vertical sound wave propagation. This makes the HE-VI scheme numerically very efficient for large grid aspect ratios, i.e. $\Delta x/\Delta z \gg 1$, which are typically used in meso-β and meso-γ applications. An additional 3-D divergence damping as well as a slight time off-centering in the vertical implicit formulation is applied to damp acoustic modes. On the big time step, the Asselin time filter and a 4th-order horizontal diffusion are used for numerical smoothing.

Three alternative time integration schemes have also been implemented for optional use: a two time-level time-split method based on a modified 2nd-order Runge-Kutta integration (Gassmann, 2002), a three-timelevel Leapfrog-based Eulerian 3-D semi-implicit scheme according to Thomas et al. (2000) and recently a new two time-level scheme based on 3rd-order Runge-Kutta integration with total variation diminishing (TVD) option (Förstner and Doms, 2004). The latter scheme is intended to be used for high-resolution applications of LM in near future. Table 1 summarizes the dynamical and numerical key features of the LM.

3.1.2 Initial and Boundary Conditions

For operational applications and real data simulations, LM is driven by the global model GME of DWD using the traditional boundary relaxation technique (see Section 3.3). Information on the GME as well as on recent changes to the global model are summarized in the *Quarterly Report of the Operational NWP-Models of the Deutscher Wetterdienst*. This report series is available online at the DWD web-site (*www.dwd.de*). Optionally, initial and boundary data may also be provided from the IFS global model at ECMWF. In this context, a new option for using boundary data which are defined on lateral frames only (by default, the boundary conditions are defined on the full 3-d model domain) has been introduced.

A four-dimensional data assimilation cycle based on a nudging analysis scheme (see Section 3.2) can be installed for operational NWP with the LM at COSMO meteorological services. In this case, the initial conditions come from the continuous LM assimilation stream and only boundary data have to be provided by GME forecasts. However, an operational NWP-system can also be set-up without a data assimilation cycle by relying on pure dynamical adaption of large-scale initial fields. In this case, the initial conditions come from interpolated (and initialized) GME analyses. To reduce noise generation and spin-up effects resulting from non-balanced interpolated data, a diabatic digital filtering initialization (DFI) scheme (Lynch et al., 1997) has been implemented. By default, the DFI initialization consists of a 1-h adiabatic backward integration followed by a 1-h diabatic forward integration of the model.

For various research applications as well as for model testing and evaluation, the LM provides a capability to handle idealized cases using user-defined artificial initial and boundary

data. For these types of application, periodic lateral boundary conditions can be specified optionally. Additionally, a 2-dimensional model configuration can be used.

3.1.3 Parameterization of Physical Processes

A variety of subgrid-scale physical processes is taken into account by parameterization schemes.

Table 2: LM Model Formulation: Physical Parameterizations

Grid-scale Clouds and Precipitation:	Cloud water condensation/evaporation by saturation adjustment. Precipitation formation by a bulk parameterization including water vapour, cloud water, rain and snow (scheme HYDOR), where rain and snow are treated diagnostically by assuming column equilibrium (default). Further options are: – the LM cloud ice scheme HYDCI (Doms, 2002), – a warm rain scheme following Kessler (1969), – prognostic treatment of rain and snow (Gassmann, 2002; Baldauf and Schulz, 2004), – a scheme including graupel content as prognostic variable.
Subgrid-scale Clouds:	Subgrid-scale cloudiness is interpreted by an empirical function depending on relative humidity and height. A corresponding cloud water content is also interpreted.
Moist Convection:	Mass-flux convection scheme (Tiedtke, 1989) with closure based on moisture convergence (default). Further Options: – a modified closure based on CAPE within the Tiedtke scheme. – the Kain-Fritsch convection scheme.
Radiation:	δ-two stream radiation scheme after Ritter and Geleyn (1992) for short and longwave fluxes; full cloud-radiation feedback.
Vertical Diffusion:	Diagnostic K-closure at hierarchy level 2 by default. Optional: – a new level 2.5 scheme with prognostic treatment of turbulent kinetic energy; effects of subgrid-scale condensation and evaporation are included and the impact from subgrid-scale thermal circulations is taken into account.
Surface Layer:	Constant flux layer parameterization based on the Louis (1979) scheme (default). Optional: – a new surface scheme including a laminar-turbulent roughness sublayer.
Soil Processes:	Soil model after Jacobsen and Heise (1982) with 2 soil moisture layers and Penman-Monteith transpiration; snow and interception storage are included. Climate values changing monthly (but fixed during forecast) in third layer. Optional: – a new multi-layer soil model including freezing of soil water (Schrodin and Heise, 2001).

Initially, the physics package of LM has been adapted from the former operational hydrostatic models EM/DM. Meanwhile, a number of additional schemes have been developed and implemented for optional use: a new scheme for vertical diffusion based on prognostic turbulent kinetic energy, a new diagnostic scheme for surface layer transports, a new grid-scale cloud and precipitation scheme including cloud ice, rain and snow water content and graupel content as (optional) prognostic variables, a new multi-layer soil model, and the

Kain-Fritsch scheme for deep moist convection. Work on a new lake model, a revised version of the surface layer scheme, a 3D turbulence scheme and a new scheme for shallow convection is in progress.

Table 2 gives a short overview on the parameterization schemes used by default and on additional options implemented so far.

3.1.4 External Parameters

The parameterization of physical processes and also the adiabatic model part require some parameters which are not derived by data assimilation or by interpolation from a driving model. These so-called external parameters are defined in additional data sets. The LM requires the following external parameters: mean topographical height, roughness length, soil type, vegetation cover, land fraction, root depth and leaf area index. The sources for these data are indicated below.

- Mean orography:
  Derived from the GTOPO30 data set (30"x30") from USGS. Also evaluated is the GLOBE dataset from the National Geophysical Data Center (NGDC) with a resolution of 30"x30".
- Prevailing soil type:
  Derived from the DSM data set (5'x5') of FAO.
- Land fraction, vegetation cover, root depth and leaf area index:
  Derived from the CORINE data set of ETC/LC and the GLCC (Global Land Cover Characterization) from USGS.
- Roughness length:
  Derived from the GTOPO30 and CORINE datasets.

External parameters for LM can be derived by a preprocessor program for any domain on the globe at any required spatial resolution. However, this is very time consuming because of the size of the high-resolution global data sets. Within the COSMO group, we thus have prepared some predefined data sets with external parameters on three different domains. These domains are shown in Fig. 2.

Domain 1 covers Europe and surrounding countries; data sets for this domain are available at 28 km, 21 km, 14 km and 7 km grid spacing. The smaller Domain 2 covers Germany and surrounding countries; the corresponding data set gives the external parameters at 7 km resolution. Domain 2 is only used at DWD. Finally, Domain 3 covers central and southern parts of Europe. For this domain, the external parameters are given at 2.8 km resolution. The LM can very easily be positioned anywhere within these domains.

Details on the location of the three domains are shown in Table 3, where longitude (λ) and latitude (ϕ) of the rotated coordinates and those of the geographical lat-lon grid (λ_g, ϕ_g) are given in degree. The resolution and the corresponding file names (these are required by the interpolation programs to generate initial and boundary data from a host model) are indicated in Table 4. The specifications refer to a rotated lat-lon grid of LM with the north-pole at geographical latitude 32.5° N and longitude 170.0° W.

Two new data sets were provided recently for nearly the same area as Domain 1 but with a different rotated pole. In order to keep the size of the grid boxes as equal as possible,

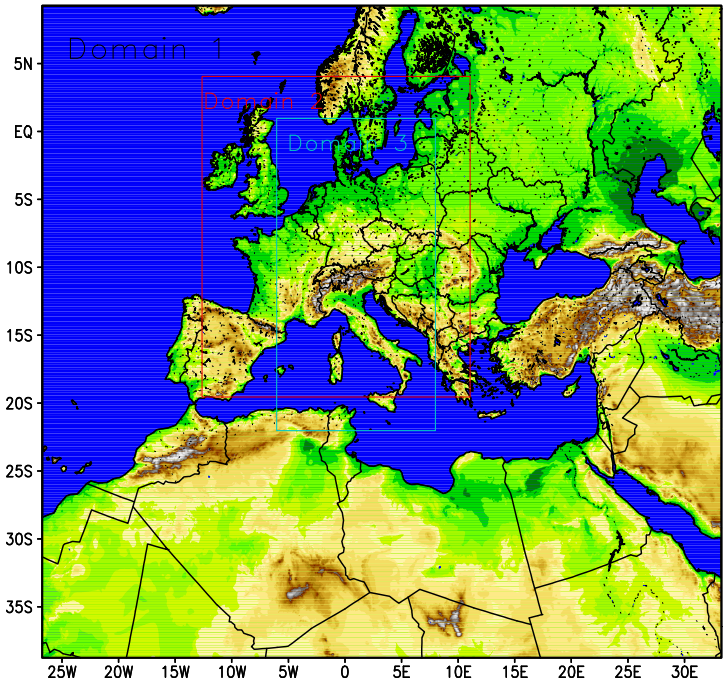

Figure 2: Domains of external parameter datasets used by COSMO partners

Table 3: Location of domains in rotated and in geographical coordinates

Name	Domain corners	λ	φ	λ_g	φ_g
Domain 1	upper left	- 26.75	+ 9.25	- 42.74	+ 56.07
	upper right	+ 33.25	+ 9.25	+ 70.36	+ 51.49
	lower left	- 26.75	- 38.75	- 11.26	+ 14.54
	lower right:	+ 33.25	- 38.75	+ 35.96	+ 12.34
Domain 2	upper left	- 12.625	+ 4.125	- 15.25	+ 59.26
	upper right	+ 11.125	+ 4.125	+ 32.48	+ 59.77
	lower left	- 12.625	- 19.50	- 4.87	+ 36.62
	lower right:	+ 11.125	- 19.50	+ 23.15	+ 36.92
Domain 3	upper left	- 6.00	+ 1.00	- 1.37	+ 58.00
	upper right	+ 8.00	+ 1.00	+ 25.06	+ 57.61
	lower left	- 6.00	- 22.00	+ 3.19	+ 35.20
	lower right:	+ 8.00	- 22.00	+ 19.06	+ 34.97

the equator was put to the center of the domain. The north-pole of this rotated grid is at geographical latitude 40.0° N and longitude 170.0° W. The two resolutions are 7 km (Domain 5) and 2.8 km (Domain 0), resp. These data sets are used by DWD for testing the LME (LM over whole Europe) and the LMK (LM Kürzestfrist: very high resolution LM for nowcasting purposes). The domains are shown in Fig. 3

The specifications of the new datasets are given in Table 5 and Table 6.

Table 4: Grid spacing $\Delta\lambda$ (= $\Delta\varphi$) in degrees, approximate resolution Δs in m, number of grid points and file name of the datasets for the domains

Name	$\Delta\lambda, \Delta\varphi$ (°)	Δs (m)	no. of grid points	File name
Domain 1	0.2500	28000	241 × 193	lm_d1_28000_241x193.g1
	0.1875	21000	321 × 257	lm_d1_21000_321x257.g1
	0.1250	14000	481 × 385	lm_d1_14000_481x385.g1
	0.0625	07000	961 × 769	lm_d1_07000_961x769.g1
Domain 2	0.0625	07000	381 × 379	lm_d2_07000_381x379.g1
Domain 3	0.0250	02800	561 × 921	lm_d3_02800_561x921.g1

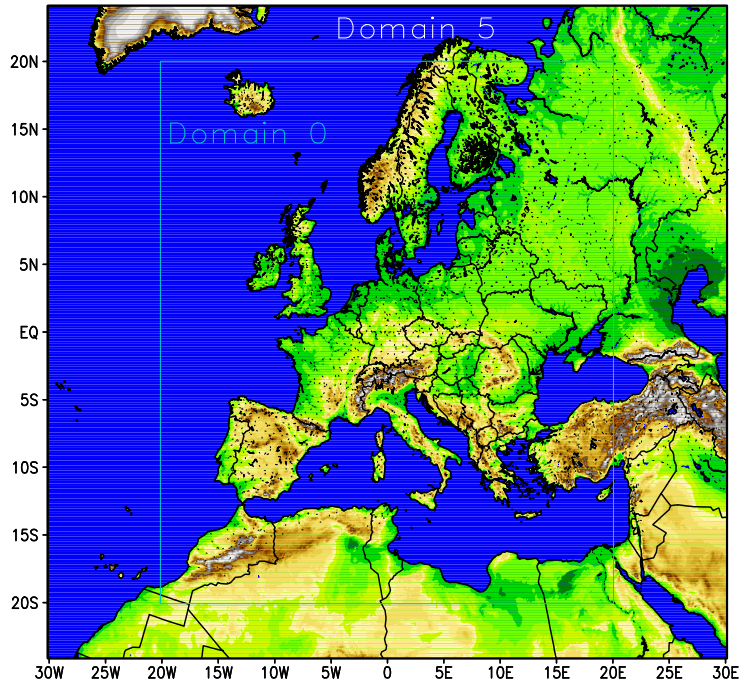

Figure 3: Domains of external parameter datasets with different rotated pole

Table 5: Location of new domains in rotated and in geographical coordinates

Name	Domain corners	λ	φ	λ_g	φ_g
Domain 5	upper left	- 30.125	+ 24.125	- 57.01	+ 60.16
	upper right	+ 30.125	+ 24.125	+ 77.01	+ 60.16
	lower left	- 30.125	- 24.125	- 19.17	+ 20.00
	lower right:	+ 30.125	- 24.125	+ 39.17	+ 20.00
Domain 0	upper left	- 20.05	+ 20.05	- 36.60	+ 63.69
	upper right	+ 20.05	+ 20.05	+ 56.60	+ 63.69
	lower left	- 20.05	- 20.05	- 11.21	+ 27.11
	lower right:	+ 20.05	- 20.05	+ 31.21	+ 27.11

Table 6: Grid spacing $\Delta\lambda$ (= $\Delta\varphi$) in degrees, approximate resolution Δs in m, number of grid points and file name of the datasets for the domains

Name	$\Delta\lambda, \Delta\varphi$ (°)	Δs (m)	no. of grid points	File name
Domain 5	0.0625	07000	965 × 773	lm_d5_07000_965x773.g1
Domain 0	0.025	02800	1605 × 1605	lm_d2_07000_1605x1605.g1

3.1.5 Coding and Parallelization

In order to meet the computational requirements of the model, the program has been coded in Standard Fortran 90 and parallelized using the MPI library for message passing on distributed memory machines. Thus it is portable and can run on any parallel machine providing MPI. Besides this, the model can still be executed on conventional single-processor computers without MPI.

The parallelization strategy is the two dimensional domain decomposition which is well suited for grid point models using finite differences (see Fig. 4). Each processor gets an appropriate part of the data to solve the model equations on its own subdomain. This subdomain is surrounded by halo grid-lines which belong to the neighboring processors. The number of halo grid-lines is soft-coded to be able to choose different values, when necessary. At present, we use two grid-lines for the three time-level leapfrog scheme and three grid-lines for the two time-level Runge-Kutta scheme that uses higher order advection schemes. During the integration step each processor updates the values of its local subdomain; grid points belonging to the halo are exchanged using explicit message passing. The number of processors in longitudinal and latitudinal direction can be specified by the user to fit optimal to the hardware architecture (vector, scalar, cache-size, etc.).

Table 7 shows the timings of the LM for a one-hour full-physics simulation on a 325×325×35 grid points domain using 7 km grid spacing and a 40 sec time step for various numbers of processors on an IBM SP3. Starting with 15 processors - which are required to fit the model into core memory - the number of processors has been doubled up to 240. The speedup behaviour of the LM shows an almost ideal scaling (half the CPU-time for twice the number

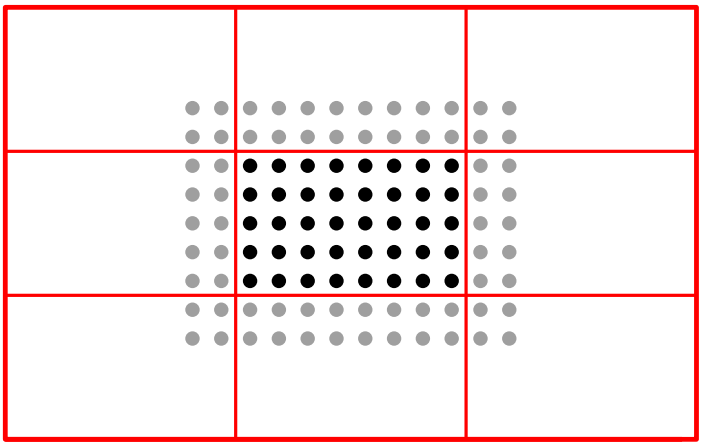

Figure 4: 2-D domain decomposition with a 2 gridline halo

of processors) up to 120 processors. With 240 processors, the execution time becomes larger than expected from ideal scaling. Here, the subdomain treated by a processor is so small that the ratio between physics-dynamics calculations – which scale superlinear – and the time for communication (data exchange and wait times due to load imbalances) and I/O – which both scale sub-linear – becomes disadvantageous.

Table 7: Timings for a 1-h LM forecast for various numbers of processors on an IMB-SP3

Number of Processors	15	30	60	120	240
Total CP-Time	571.53	284.04	136.34	67.61	38.10
Dynamics, Physics, Diagnostics	541.13	261.39	118.25	51.59	22.96
Communication	22.05	16.69	12.81	11.25	9.23
Input and Output	8.35	5.96	5.28	4.77	5.91

3.2 Data Assimilation

The requirements for the data assimilation system for the operational LM are mainly determined by the very high resolution of the model and by the task to employ it also for nowcasting purposes in the future. Hence, detailed high-resolution analyses have to be able to be produced frequently, and this requires a thorough use of asynoptic and high-frequency observations such as aircraft data and remote sensing data. Note that the synoptic scales are largely determined by the lateral boundary conditions provided by the driving model, and the main purpose of the assimilation scheme is to analyze the meso scales.

By design, 3-dimensional analysis methods tend to be less appropriate for this purpose. They do not allow to account for the exact observation time of asynoptic data, and they make it necessary to neglect most of the high-frequent data unless the analysis scheme is applied very frequently at significant computational costs. Moreover, the geostrophic approximation, a key ingredient of some of these schemes as used e.g. for the GME, is of limited validity on the meso scale. Therefore, 4-dimensional methods offer potential advantages since they include the model dynamics in the assimilation process directly. However, the 4-dimensional variational (4DVAR) method is too expensive for operational application of the LM considering the small amount of time available to produce the analyses and forecasts.

As a result, a scheme based on the observation nudging technique has been developed to

define the atmospheric fields. It is based on an experimental nudging analysis scheme which had been developed for DM and the Swiss model version SM (Schraff, 1996; 1997) and which compared favorably with the operational OI-analysis of the DM in various case studies. The new LM-scheme, however, has been adapted to the nonhydrostatic modelling framework and runs on distributed memory machines using domain decomposition. To compute the analysis increments locally for the grid points of each sub-domain, the observational information of the total domain is previously distributed to the sub-domains.

In addition to this, for some of the surface and soil fields, a set of 2-dimensional intermittent analysis schemes is applied. This comprises the snow analysis, the sea surface temperature (SST) analysis, and the variational soil moisture analysis scheme.

3.2.1 Nudging-Based Assimilation Scheme

Nudging or Newtonian relaxation consists of relaxing the model's prognostic variables towards prescribed values within a predetermined time window (see e.g. Davies and Turner (1977), Stauffer and Seaman (1990)). In the present scheme, nudging is performed towards direct observations which is more appropriate for high-resolution applications than nudging towards 3-dimensional analyses (Stauffer and Seaman, 1994). A relaxation term is introduced into the model equations, and the tendency for a prognostic variable $\psi(\mathbf{x}, t)$ is given by

$$\frac{\partial}{\partial t}\psi(\mathbf{x},t) \quad = \quad F(\boldsymbol{\psi},\mathbf{x},t) \quad + \quad G_\psi \cdot \sum_{k_{(obs)}} W_k \cdot [\psi_k - \psi(\mathbf{x}_k,t)] \tag{3}$$

F denotes the model dynamics and physical parameterizations, ψ_k the value of the k^{th} observation influencing the grid point $\mathbf{x}$ at time t, $\mathbf{x}_k$ the observation location, G_ψ the constant so-called nudging coefficient and W_k an observation-dependent weight which usually varies between 0 and 1. Neglecting the dynamics and physics and assuming a single observation with a constant weight W_k equal 1, the model value at the observation location relaxes exponentially towards the observed value with an e-folding decay rate of $1/G_\psi$ corresponding to about half an hour.

In practical applications, the nudging term usually remains smaller than the largest term of the dynamics so that the dynamic balance of the model is not strongly disturbed. The coupling between the mass and wind field innovations is primarily induced implicitly by the model dynamics. If the assimilation process is successful the model fields will be close to dynamic balance at the beginning of the forecast, and an initialization step is not required.

The factors W_k determine the relative weights given to the different observations at a specific grid point. For a single observation, this weight (w_k) comprises of the quality (and representativeness) of the observation (ϵ_k) and of weights which depend on the horizontal (w_{xy}) or vertical (w_z) distance, respectively, or the temporal (w_t) difference between the observation and the target grid point. If an increasing number of observations influence the grid point the total nudging weight should be limited to avoid the nudging term to become dominant over the dynamics. This is achieved by complementing the individual weight w_k by a relative weight (Benjamin and Seaman, 1985):

$$W_k \quad = \quad \frac{w_k}{\sum_j w_j} \cdot w_k \tag{4}$$

$$w_k \quad = \quad w_t \cdot w_{xy} \cdot w_z \cdot \epsilon_k \tag{5}$$

Currently, only conventional observations are used operationaly, namely from TEMP and PILOT (temperature and wind, including the significant levels; humidity up to 300 hPa;

geopotential only to derive one pressure increment at the lowest model level), AIRCRAFT (all data), WIND PROFILER and SYNOP, SHIP and DRIBU reports (station pressure; wind for stations below 100 m above msl; humidity; 2-m temperature is used only for the soil moisture analysis). Note that given a cut-off time of 2.5 hours, observations from up to about 2 hours after the actual analysis time can still be assimilated in the first hours of the operational forecast runs. As a quality control, the observed values are compared with the model fields of the assimilating run itself. For multi-level temperature data, a hydrostatic height and thickness check is included, and a spatial consistency check is performed for the station pressure data.

Equation (3) indicates that in principle the scheme consists of two main steps, i.e. the determination of the observation increments and the computation of the weights. With respect to the vertical interpolation required for the first step, the vertical scale of multi-level temperature and wind observations is adjusted to the vertical model resolution by averaging the observed profile over the thickness of model layers. As a result, the simulated thickness between two pressure levels is automatically relaxed towards the observed thickness when nudging temperature data. In contrast, humidity data are interpolated without averaging in order to capture thin layers of clouds as well as possible. Note that the increments are determined as differences in relative humidity which implies that relative rather than specific humidity is relaxed towards the observed humidity. In this sense, the analyzed quantities are horizontal wind, potential temperature, relative humidity, and pressure at the lowest model level.

Related to the second step, incomplete profiles and single-level increments are vertically extended and provided with vertical weights w_z according to a Gaussian (approx.) in log pressure (correlation scale is $1/\sqrt{3}$ for upper-air wind and 0.2 for upper-air temperature and humidity, and the cut-off is 850 m for surface-level wind resp. the lowest model layer for surface-level humidity). Thereafter, upper-air increments are spread laterally along horizontal surfaces since spreading along the terrain-following model levels as usually applied in nudging-type schemes has disadvantages near steep orography particularly in cases with low stratus (Schraff, 1997). In contrast, surface-level increments are spread along the model levels to limit the influence to the area close to the ground. The spreading includes the computation of the horizontal weights w_{xy} using the function $(1 + \Delta r/s) \cdot e^{-\Delta r/s}$ for the scalar quantities (Δr being the horizontal distance between observation and target grid point). The wind correlations are split into a longitudinal and transverse part, and this allows to specify the degree of divergence (γ) of the resulting wind analysis increment field (Lorenc et al., 1991). Both the correlation scales s and the non-divergence factor γ increase with height and with distance to the observation time and vary between about 60 km and 160 km resp. 0.4 and 0.7 . The function used for the temporal weights w_t is 1 at the observation time and decreases linearly to zero at 3 hours (for radiosonde data) resp. 1.5 hours (for other data) before and 1 resp. 0.5 hours after the observation time. Hourly or more frequent data are linearly interpolated in time.

In the current scheme, the resulting analysis increment fields are partly balanced explicitly in a third major step before being added to the model fields. Three types of balancing are applied. First, a hydrostatic upper-air temperature correction balances the pressure analysis increments at the lowest model layer. It is nearly constant within the lowest 1500 m (therefore hardly modifies the stability within the boundary layer) and decreases rapidly further above such that the geopotential above 400 hPa is not directly modified by the surface pressure nudging (for hydrostatic conditions). This significantly reduces the vertical extent of the mass field disturbance imposed by the pressure nudging and results in a better adjustment of the wind field and a greatly improved assimilation of the pressure data. Secondly, a geostrophic wind correction partly balances the wind field with respect to the mass field

increments imposed by the surface pressure nudging including the temperature correction. Finally, an upper-air pressure correction balances the total analysis increments of the mass field hydrostatically. This is the only feature directly related to the fact that the model is non-hydrostatic. Note that it does not change the non-hydrostatic properties of the full model fields. The correction prevents the introduction of direct sources of vertical wind for which there is no direct control without vertical wind observations being available to be assimilated. This is important since the vertical velocity is still small on the scales to be analyzed with the current scheme and observations (in contrast e.g. to a latent heat nudging scheme). Table 8 summarizes the main features of the LM nudging scheme.

Table 8: Data assimilation for LM

Method	Nudging towards observations
Implementation	continuous cycle of 3-hour assimilation runs
Realization	identical analysis increments used during 6 advection time steps
Balance	1. hydrostatic temperature increments (up to 400 hPa) balancing 'near-surface' pressure analysis increments 2. geostrophic wind increments balancing 'near-surface' pressure analysis increments 3. upper-air pressure increments balancing total analysis increments hydrostatically
Nudging coefficient	$6 \cdot 10^{-4} s^{-1}$ for all analyzed variables except pressure $1.2 \cdot 10^{-3} s^{-1}$ for 'near-surface' pressure
Analyzed variables	horizontal wind vector, potential temperature, relative humidity 'near-surface' pressure (i.e. at the lowest model level)
Spatial analysis	Data are analyzed vertically first, and then spread laterally along horizontal surfaces. vertical weighting: approximately Gaussian in log(p) horizontal weighting: isotropic as function of distance
Temporal weighting	1.0 at observation time, decreasing linearly to 0.0 at 3 hours (upper air) resp. 1.5 hours (surface-level data) before and 1.0 resp. 0.5 hours after observation time; linear temporal interpolation of frequent data.
Observations	SYNOP, SHIP, DRIBU: - station pressure, wind (stations below 100 m above msl) - humidity TEMP, PILOT: - wind, temperature: all standard levels, significant levels up to 150 hPa - humidity: all levels up to 300 hPa - geopotential used for one 'near-surface' pressure increment AIRCRAFT: - all wind and temperature data WIND PROFILER: - all wind data (except from blacklisted stations)
Quality control	Comparison with the model fields from assimilation run itself

3.2.2 Sea Surface Temperature Analysis

Since the latent and sensible heat fluxes over water depend crucially on the surface temperature, a sea surface temperature (SST) analysis is performed once per day (00 UTC). The global SST analysis for GME is deployed as first guess, which incorporates satellite data indirectly by making use of a global SST analysis from NCEP. All the ship and buoy observations from the previous 4 days are then used in a correction scheme based on Cressman-type weighting. For the sea-ice cover in the Baltic Sea, an external analysis (from the Bundesamt für Seeschifffahrt und Hydrographie) is used.

3.2.3 Snow Depth Analysis

The occurrence of a snow cover strongly influences the radiative absorption and reflection properties of the land surface and therefore the screen-level temperature. The snow water content is a prognostic quantity of the model, and is analyzed once every 6 hours. The method is based on a simple weighted averaging of SYNOP snow depth observations. The weighting depends both on the horizontal and vertical distances to the target grid points. In areas, where the density of these data is not sufficient, an average of snow depth increments derived from SYNOP precipitation, temperature, and weather reports as well as the model prediction are also included.

3.2.4 Soil Moisture Analysis

In land areas without snow, the soil water content influences significantly the screen-level temperature (and humidity) on clear-sky days. An inadequate specification of soil moisture can lead to forecast temperature errors of several degrees. The variational analysis scheme (Hess, 2001) derives improved moisture contents once per day by minimizing a cost functional J which depends on the deviations of the forecast temperature $T(\eta)$ from the observed (resp. analyzed) temperature T^o and of the soil moisture η from a given background state η^b:

$$J(\eta) \;=\; \frac{1}{2}\Big(T^o - T(\eta)\Big)^T \mathbf{R}^{-1}\Big(T^o - T(\eta)\Big) + \frac{1}{2}\Big(\eta - \eta^b\Big)^T \mathbf{B}^{-1}\Big(\eta - \eta^b\Big) \qquad (6)$$

The observation error covariance $\mathbf{R}$ and background error covariance $\mathbf{B}$ reflect the trust in the observations resp. the background. To solve the minimization problem, two assumptions are made. Firstly, since the 2-m temperature mainly depends on the soil moisture at the same location, the problem can be decoupled horizontally, and a low-dimensional (equal to the number of analyzed soil layers) minimization can be performed for each grid point individually. Secondly, (moderate) changes of soil moisture are assumed to lead to linear changes in temperature. This allows to derive the linear relationships Γ by means of one additional forecast run per analyzed soil layer where each of these forecasts has slightly different initial soil moisture values for the respective layer. The minimum of J can then be found by solving $\nabla J(\eta) = 0$ directly without using the adjoint method.

In the current implementation, two additional 15-hour forecasts are required to analyze two (sets of) soil layers for 00 UTC of the previous day by comparing forecast and observed temperature at 12 and 15 UTC. The analysis increments are then added to the soil moisture of the 24 h free forecast valid for 00 UTC of the current day. The resulting soil moisture is used both as initial state for the operational LM forecast of the current day and as background state for the next soil moisture analysis. This background state η^b is important in order to reduce the daily variation of the soil moisture contents and to stabilize the minimization in

cases of weak soil-atmosphere coupling (i.e. cloudy situations). Together with η^b (see above), the background error covariance $\mathbf{B}$ for the following day is provided in a Kalman-filter cycled analysis:

$$(\mathbf{B})^{next} \quad = \quad \mathbf{A} \; + \; \mathbf{Q} \quad , \quad where \;\; \mathbf{A} = (\nabla^2 J)^{-1} = \left(\Gamma^T \mathbf{R}^{-1} \Gamma + \mathbf{B}^{-1} \right)^{-1} \tag{7}$$

This takes into account both an increase of confidence in the retrieved soil moisture values due to the utilized screen-level observations (as part of the analysis error covariance $\mathbf{A}$) and a decrease of confidence due to the model error $\mathbf{Q}$ of the soil model. While $\mathbf{A}$ can be computed explicitly, $\mathbf{Q}$ is the main tuning parameter of the scheme. It influences the relative weight given to the past and the present observations and has an impact on the temporal variability of the soil moisture. The scheme has been successfully tested in various case studies and it is operated at DWD since March 2000.

3.3 Boundary Conditions from Driving Models

The LM can be nested in the global model GME of DWD (Majewski, 1998; Majewski et al., 2002), the ECMWF global spectral model IFS and also in itself. The lateral boundaries are treated by the Davies (1976) relaxation technique, where the internal model solution is nudged against an externally specified solution within a narrow boundary zone by adding a relaxation forcing term to the equations.

The external solution is obtained by interpolation from the driving host model at discrete time intervals. The interpolated fields are hydrostatically balanced, i.e. a hydrostatic pressure is prescribed for the nonhydrostatic pressure variable in LM at the lateral boundaries. Within these specified time intervals, the boundary data are interpolated linearly in time (which is done inside the model). Normally the boundary update interval is chosen to be one hour for meso-β scale applications of the LM. The boundary values (and initial values, if no data assimilation suite is operated) are obtained by a preprocessing program from the host model.

The different interpolation tools (GME2LM, IFS2LM, LM2LM) have now been combined to a single program INT2LM, which takes the data from GME, IFS or LM as input and interpolates to a specified LM grid.

A User Guide of the INT2LM preprocessor program is available at the COSMO Web-site.

3.4 Postprocessing

Postprocessing includes all applications that use the direct model output of LM runs. In general, there is a wide range of such applications at each meteorological service, ranging from simple graphical display of weather charts or meteograms for single grid points, or statistical correction of near surface weather elements by Kalman filtering, to more complex derived products supplying information on environment and health, transportation, agriculture and media presentation. Most of these postprocessing tools are very specific to the computer platform, data base system and visualization software of each service and thus cannot be shared within the COSMO group. There is, however, a number of postprocessing programs available within COSMO.

(a) Graphics

Work on two common plotting packages has been completed. The first has been developed at MeteoSwiss and uses Metview with an interface to the GRIB1 LM output data; the other one has been developed at ARPA-SIM and is based on the public domain VIS5D packages; a special routine converts the GRIB1 binary format to the VIS5D data format.

(b) Models

A *Lagrangian Particle Dispersion Model* (LPDM) may be used operationally in case of radioactive accidental releases to predict long-range transport, dispersion, and wet and dry deposition of radioactive material. The calculation of about $10^5 - 10^6$ trajectories of tracer particles is based on wind fields from LM (at hourly intervals) and superimposed turbulent fluctuations (TKE, Monte Carlo method). Radioactive decay and convective mixing are included. The concentration is calculated by counting the particle masses in arbitrary grids.

A *Trajectory Model* may provide guidance on transport routes. The meteorological input is derived from LM at hourly intervals.

An integral part of the NWP system at DWD is a *Wave Prediction Suite* comprising two models, namely the global model GSM (global sea state model), and a local one (LSM) which covers the Baltic Sea, the North Sea and the Adriatic Sea with a high-resolution mesh. GSM and LSM have been developed by the research institute GKSS in Geesthacht (Germany).

(c) Interpretation

An objective weather interpretation scheme (developed at DWD) derives the forecasted 'weather', i.e. the WMO weather code, based on LM output fields. Pressure, temperature, dew point temperature, liquid water content, cloud cover, precipitation and wind speed values are used as input parameters to define the present weather.

3.5 Data Flow of the LM Package

The various components of the LM package and the corresponding data flow are illustrated in Figure 5. In case of a set-up without data assimilation (right part of Figure 5), the interpolation program INT2LM provides initial and boundary conditions for the LM forecast runs (LM-FCT) from the corresponding driving models. This step involves the data set of the external parameters (see Section 3.1.4).

With a system set-up using the LM nudging analysis (left part of Figure 5), the INT2LM provides boundary conditions (LM-BC) from the GME assimilation cycle for the LM runs in nudging analysis mode (LM-NUD) within the assimilation stream. The LM-NUD runs start from a given LM analysis (LM-ANA) to generate an analysis for the next analysis time. The forecasts then start from these LM-ANA initial data using boundary conditions from the GME forecast.

To run the LM in nudging mode, a preprocessor program is required which provides the observational data in a special data file format (AOF). The LM analysis file may be modified by incremental analyses of sea surface temperature, snow depth and soil moisture (see Section 3.2). All these programs use GTS and non-GTS observational data, which are archived in a local data base system. The interface to these data is usually not portable as it depends on the data base system of each meteorological centre.

The LM runs in forecast mode generate direct model output, which includes also fields from the LM internal postprocessing (see Appendix B). These data are then subject to various visualization tools, external postprocessing and other applications such as follow-up models at COSMO Met Services.

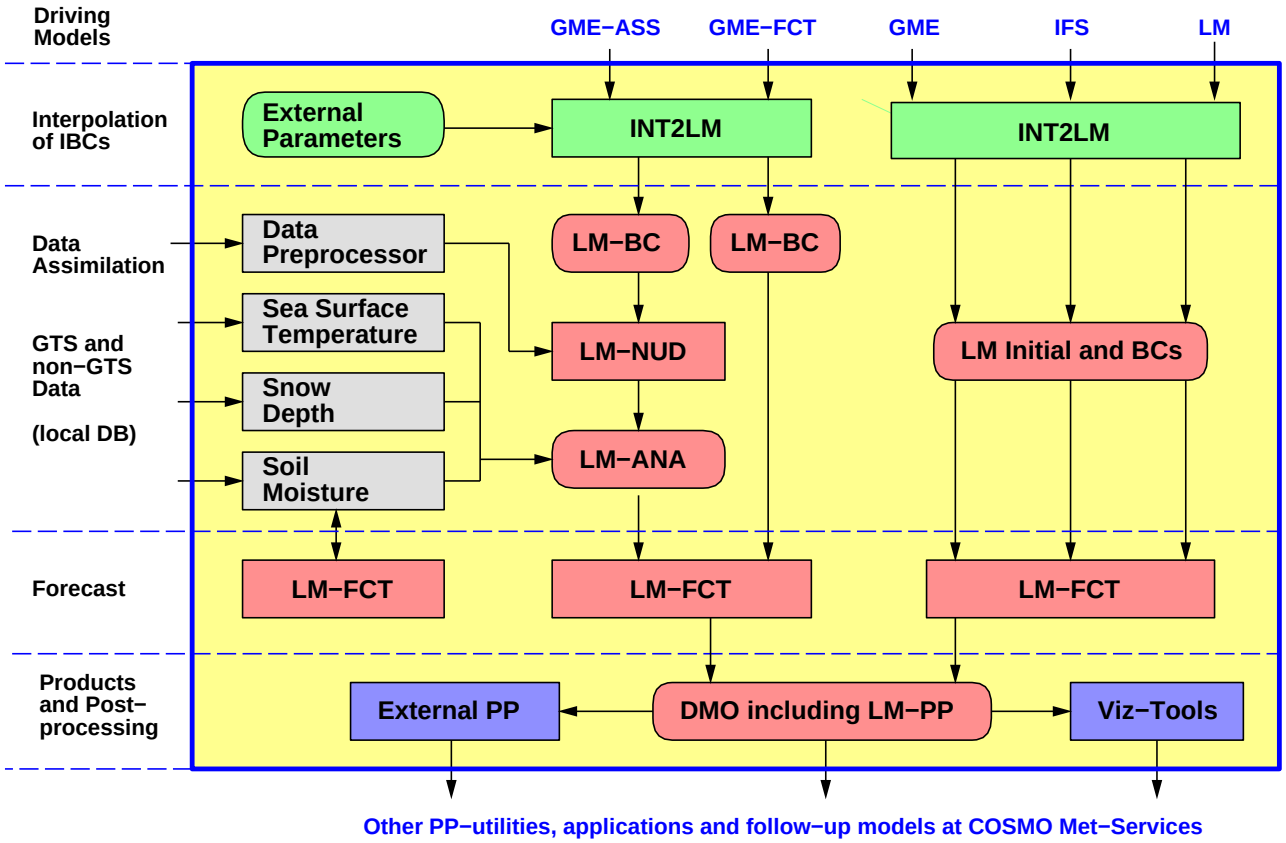

Figure 5: Process and data flowchart of the LM package for a set-up using data assimilation (left part) and a set-up without data assimilation (right part). Rectangular boxes indicate components of the package (programs), rounded boxes indicate data files generated by the components.

3.6 Documentation

The new release of the LM documentation covers the following parts:

A Description of the Nonhydrostatic Regional Model LM

Part I: *Dynamics and Numerics*
Part II: *Physical Parameterization*
Part III: *Data Assimilation*
Part IV: *Implementation Documentation*
Part V: *Preprocessing*
Part VI: *Postprocessing*
Part VII: *User's Guide*

Parts I - III form the scientific documentation, which provides information about the theoretical and numerical formulation of the model, the parameterization of physical processes and the four-dimensional data assimilation including soil moisture analysis. The scientific documentation is independent of (i.e. does not refer to) the code itself.

Part IV describes the particular implementation of the methods and algorithms as presented in Parts I - III, including information on the basic code design and on the strategy for parallelization using the MPI library for message passing on distributed memory machines.

The generation of initial and boundary conditions from coarse grid driving models is described in Part V. Available internal and external postprocessing utilities are described in Part VI.

Finally, the User's Guide (Part VII) provides information on code access and how to install, compile, configure and run the model. The User's Guide contains also a detailed description of various control parameters in the model input file (in NAMELIST format) which allow for a flexible model set-up for various applications.

Available at the COSMO web-site *www.cosmo-model.org* during 2004 are Parts I, II, III, V and VII. Part IV and VI will follow as soon as possible.

4 Operational Applications

The LM is operated in five centres of the COSMO members (ARPA-SIM, DWD, HNMS, IMGW, MeteoSwiss) and since early 2005 also at the associated member in Romania (NMA). Figure 6 shows the integration domains of the different implementations. This chapter informs about the basic set-up of the LM configurations and about some specific details for every partner.

ARPA-SIM, HNMS, IMGW and NMA use interpolated boundary conditions from forecasts of the global model GME of DWD. Only a subset of GME data covering the respective LM-domain of a centre are transmitted from DWD via the Internet. HNMS, IMGW and NMA start the LM from interpolated GME analyses. In this case it is possible to smooth the initial fields using the digital filtering scheme of Lynch et al. (1997). At DWD, a comprehensive data assimilation system for LM has been installed, comprising the LM nudging analysis for atmospheric fields, a sea surface temperature (SST) analysis, a snow analysis and the soil moisture analysis according to Hess (2001). A data assimilation system based on the LM nudging scheme is also used at MeteoSwiss (since November 2001) and at ARPA-SIM (since October 2003). Since September 2003, MeteoSwiss uses lateral boundaries from interpolated IFS-forecasts.

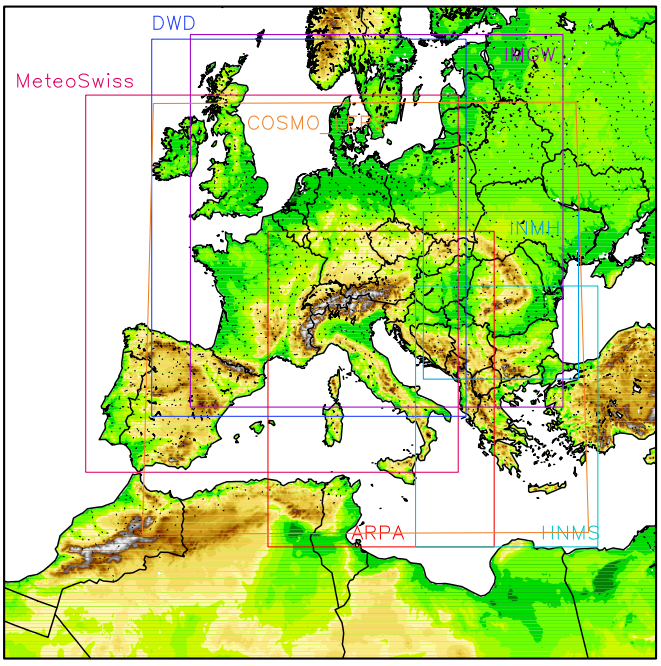

Figure 6: LM integration domains used at the partners and for the COSMO-LEPS

ARPA-SIM installed the COSMO-LEPS (Limited Area Ensemble Prediction System) based on LM and ECMWF ensemble forecasts at the ECMWF computing centre. Several operational LM runs are performed (10 km grid spacing, 32 levels) starting at 12 UTC on initial and boundary conditions for selected representative members of an ECMWF-EPS superensemble.

In addition, the national weather service of Italy, UGM in Rome, runs the LM at the ECMWF computing centre for a domain comparable to the COSMO-LEPS domain. The lateral boundaries for these runs are taken from the IFS.

The following sections give a brief overview on the configurations of the operational LM systems in the COSMO meteorological centres. MeteoSwiss, ARPA-SIM and UGM have

renamed the model within their services: the LM application in Switzerland is called ***aLMo*** (Alpine Model), the LM application in Italy is called ***LAMI*** (Limited Area Model Italy) and the LM run by UGM at ECMWF is called ***Euro-LM***.

4.1 ARPA-SIM (Bologna)

Basic Set-Up of LM
The regional meteorological service ARPA-SIM in Bologna operates the LM (as LAMI) at 7 km grid spacing. The rotated lat-lon coordinates of the lower left and the upper right corner of the integration domain are $(\lambda = -5°, \varphi = -24.0°)$ and $(\lambda = 9.5625°, \varphi = -7.0625°)$, respectively. See Figure 6 for this model domain. The main features of the model set-up are summarized in Table 9.

Table 9: **Configuration of the LAMI at ARPA-SIM**

Domain Size	234 x 272 gridpoints
Horizontal Grid Spacing	0.0625° (∼ 7 km)
Number of Layers	35, base-state pressure based hybrid
Time Step and Integration Scheme	40 sec, 3 time-level split-explicit
Forecast Range	72 h
Initial Time of Model Runs	00 and 12 UTC
Lateral Boundary Conditions	Interpolated from GME at 1-h intervals
Initial State	Nudging data assimilation cycle, no initialization
External Analyses	None
Special Features	Use of filtered topography, new TKE scheme, new surface-layer scheme, cloud-ice scheme
Model Version Running	lm_f90 3.9
Hardware	IBM SP pwr4 (using 64 of 512 processors)

Changes in the last year
In June 2004 all the LAMI operational suites have been upgraded to use LM version 3.9 and GME2LM version 1.19. Some output fields, since that date, are produced every hour rather than every 3 hours. Starting from July 2004, the LM backup suite running on ARPA-SIM Linux cluster makes use of the prognostic precipitation scheme; since October the run with prognostic precipitation has been activated also at CINECA on IBM-SP as an experimental suite, while the main operational run remains without prognostic precipitation. LAMI usually runs on 64 processors at CINECA (IBM) and on 42 at ARPA-SIM (Linux cluster).

Data assimilation
Since October 2003 an operational assimilation suite based on the LM nudging is running to produce the initial state for the atmospheric variables. The assimilation suite includes two 12-h cycles with AOF-file provided by UGM Rome with SYNOPs, AIREPs, TEMPs and PILOTs. Two forecasts up to 72 hours, at 00 and 12 UTC, are performed daily starting from the analyses provided by the assimilation cycles. Figure 7 illustrates the scheme of the assimilation suite.

Computer system
For the operational runs at CINECA, an IBM SP with pwr4 processors is used. The backup

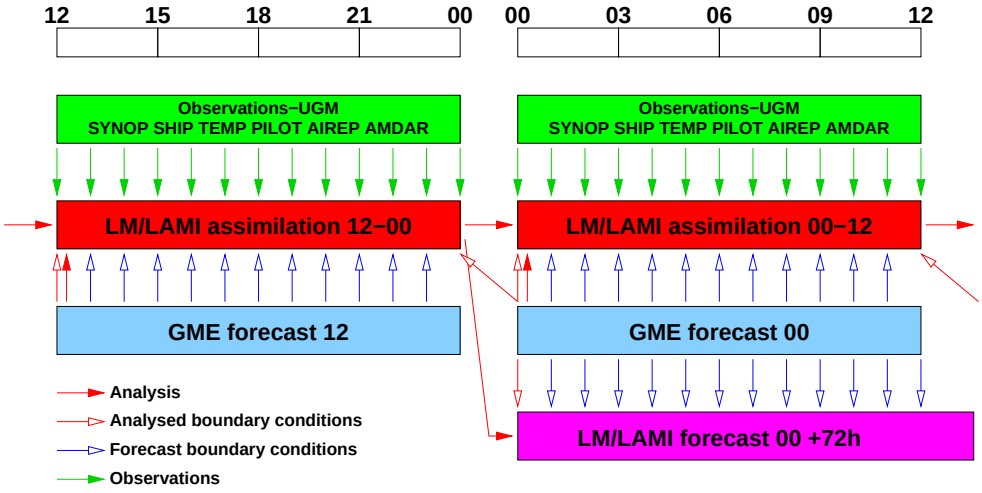

Figure 7: The assimilation suite at ARPA-SIM

suite is being set up at ARPA on a cluster of i386 computers using 42 processors INTEL Xeon 2.4Ghz (out of 44), connected by Gigabit ethernet network and running the Linux/GNU operating system. The setup is similar as the one at Cineca (with additional prognostic precipitation) and the suite is controlled by ECMWF SMS software.

4.2 DWD (Offenbach)

Basic Set-Up of LM

The LM runs operationally at DWD using a 7 km grid spacing and 35 vertical levels. The rotated lat-lon coordinates of the lower left and the upper right corner of the integration domain are $(\lambda = -12.5°, \varphi = -17.0°)$ and $(\lambda = 7.75°, \varphi = 3.25°)$, respectively. See Figure 6 for this model domain. The main features of the model set-up are summarized in Table 10.

Table 10: **Configuration of the LM at DWD**

Domain Size	325 x 325 gridpoints
Horizontal Grid Spacing	0.0625° (∼ 7 km)
Number of Layers	35, base-state pressure based hybrid
Time Step and Integration Scheme	40 sec, 3 time-level split-explicit
Forecast Range	48 h
Initial Time of Model Runs	00, 12 and 18 UTC
Lateral Boundary Conditions	Interpolated from GME at 1-h intervals
Initial State	Nudging data assimilation cycle, no initialization
External Analyses	Sea surface temperature (00 UTC) Snow depth (00, 06, 12, 18 UTC) Variational soil moisture analysis (00 UTC)
Special Features	Use of filtered topography, new TKE-scheme new surface-layer scheme, cloud-ice scheme prognostic precipitation
Model Version Running	lm_f90 3.15
Hardware	IBM SP (NighthawkII; using 185 of 1920 pwr3-processors)

Changes in the last year

These are the main changes in the operational setup in the last year:

- Introduction of *prognostic precipitation*: The prognostic treatment of grid-scale rain and snow is handled by semi-Lagrange advection.
- Reduction of turbulent fluxes over sea by changing the ratio of the laminar scaling factor for heat.
- Computation of synthetic satellite images using the RTTOV-library.
- Use of data from European windprofiler in the assimilation suite.
- Introduction of rain and snow as initial fields for LM (necessary because of their prognostic treatment.

Data Assimilation

At DWD, a comprehensive data assimilation system for LM has been installed. Besides the analysis by observational nudging, three external analyses are run: a sea surface temperature (SST) analysis (00 UTC), a snow depth analysis (00, 06, 12 and 18 UTC) and a variational soil moisture analysis (00 UTC).

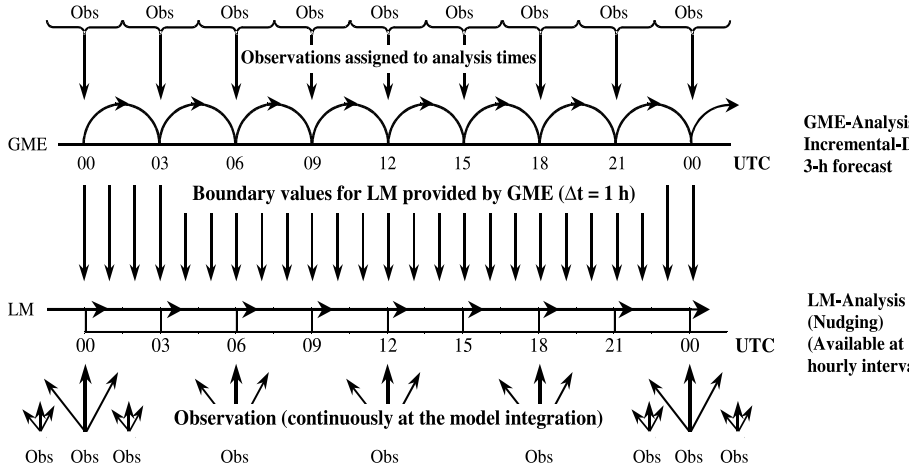

Figure 8: 4-D data assimilation for GME and LM

The data assimilations for the models GME and LM proceed as parallel streams which are coupled only via the boundary data. (see Fig. 8). The GME analysis is based on a 3-D multivariate optimum interpolation (OI) of deviations of observations from 3-h forecasts (first guess), generating an intermittent assimilation cycle with 3-h analysis frequency. All observations within a time window of $\pm$ 1.5 hours are considered as instantaneous, i.e. to be valid at analysis time.

The 3-h GME forecasts to produce the first guess are used to generate boundary data at 1-h intervals for the LM assimilation cycle. The nudging scheme produces a continuous analysis stream, where data are assimilated at the time they are observed - but using a time-weighting function to spread the information in time. For practical reasons, 3-hour LM assimilation runs are done. LM analysis files are written every hour.

Operational Schedule

The operational schedule is structured by data assimilation for GME and LM every three

hours, i.e. for 00, 03, 06, 09, 12, 15, 18 and 21 UTC. The data cut-off time for the 00 UTC and 12 UTC model runs of both GME and LM is 2 h 14 min. Based on this analyses, GME performs a 174-h forecast, and LM performs a 48-h forecast. Another 48-h prediction of both models is performed starting at 18 UTC with a data cut-off time of 4 hours. Besides the forecast models, a wave prediction suite comprising a global and a local sea state model (GSM and LSM) is run operationally.

4.3 HNMS (Athens)

Basic Set-Up of LM

The national meteorological service of Greece, HNMS in Athens, operates the LM in a pre-operational mode at 7 km grid spacing. The rotated lat-lon coordinates of the lower left and of the upper right corner of the integration domain are ($\lambda = 4.5°, \varphi = -24.0°$) and ($\lambda = 16.25°, \varphi = -10.0°$), respectively. See Figure 6 for this model domain.

In Athens, the LM (Version 3.1) is run 4 times a day (00, 06, 12, 18 UTC) on a HP-cluster and 2 times also at ECMWF (Version 3.9; 00, 12 UTC) The forecasts starting at 06 and 18 UTC are based on an experimental nudging suite.

Table 11 shows the main features of both model set-ups for the greek runs.

Table 11: **Configuration of the LM at HNMS and at ECMWF**

Domain Size	189 x 225 gridpoints	
Horizontal Grid Spacing	0.0625° (~ 7 km)	
Number of Layers	35, base-state pressure based hybrid	
Time Step	30 sec	
Integration Scheme	3 time-level split-explicit	
Forecast Range	48 h	
Initial Time of Model Runs	00, 06, 12, 18 UTC	00, 12 UTC
Lateral Boundary Conditions	GME, 1-h intervals	IFS, 3-h intervals
Initial State	from GME	from IFS
External Analyses	None	
Special Features	Use of filtered topography; new TKE-scheme new surface layer scheme; cloud-ice scheme	
Model Version Running	lm_f90 3.1	lm_f90 3.9
Hardware	HP	IBM SP

Implementation of LM during the 2004 Athens Olympics

Due to the need of improved accuracy regarding forecasting using the Non-Hydrostatic Local Model (LM), HNMS considered that hourly boundary conditions from both the ECMWF and DWD Global Models would help towards this goal.

Within this framework, ECMWF and DWD consistently provided hourly boundary conditions (full fields for 00 and 12 UTC analysis) covering the period starting from the end of July until the end of September 2004 where Athens Olympics and Paralympics took place.

HNMS was able to successfully implement these boundary conditions in order to initialize LM model by using software developed within the COSMO consortium. LM model run at

the IBM supercomputer of ECMWF through the available computational units of HNMS. The Centre generously gave the adequate priority to the submitted jobs for the prompt delivery of the output towards its operational use.

In particular, LM run at ECMWF in the following modes regarding grid size and hourly boundary conditions with analysis from 00 and 12 UTC (i.e. two runs a day per mode):

a) 7.0 km grid initialized from the Global Model of ECMWF.

b) 7.0 km grid initialized from the Global Model of DWD.

c) 5.0 km grid initialized from the Global Model of ECMWF.

d) 2.3 km grid over the wider area of the Olympics initialized from the LM output of (a) and through the Nesting Version of LM (1-way option).

From a first investigation, we may conclude that by using hourly boundary conditions, the incoming and outcoming flow, being to some extent more free from artificial boundary problems, gave the possibility to the model equations to resolve better the whole range of weather disturbances.

The Meteorological support of the 2004 Olympics has been officially considered a most successful one. HNMS would like to deeply acknowledge the invaluable help from all COSMO Members and ECMWF towards this achievement.

4.4 IMGW (Warsaw)

Basic Set-Up of LM

The national meteorological service of Poland, IMGW in Warsaw, operates the LM in an operational mode at 14 km grid spacing twice a day (00 and 12 UTC). The rotated lat-lon coordinates of the lower left and of the upper right corner of the integration domain are $(\lambda = -10.0^\circ, \varphi = -16.5^\circ)$ and $(\lambda = 14.0^\circ, \varphi = 3.5^\circ)$, respectively. See Figure 6 for this model domain. The main features of the model set-up are summarized in Table 12.

Table 12: **Configuration of the LM at IMGW**

Domain Size	193 x 161 gridpoints
Horizontal Grid Spacing	0.125° (∼ 14 km)
Number of Layers	35, base-state pressure based hybrid
Time Step and Integration Scheme	80 sec, 3 time-level split-explicit
Forecast Range	72 h
Initial Time of Model Runs	00 and 12 UTC
Lateral Boundary Conditions	Interpolated from GME at 1-h intervals
Initial State	Interpolated from GME
External Analyses	None
Special Features	Use of filtered topography, new TKE-scheme new surface-layer scheme, cloud-ice scheme
Model Version Running	lm_f90 3.5
Hardware	SGI 3800 (using 88 of 100 processors)

The results of the LM forecasts are provided to the Weather Offices and to the RADAR and HYDRO units of IMGW (also for verification). Figure 9 shows some of these forecast products.

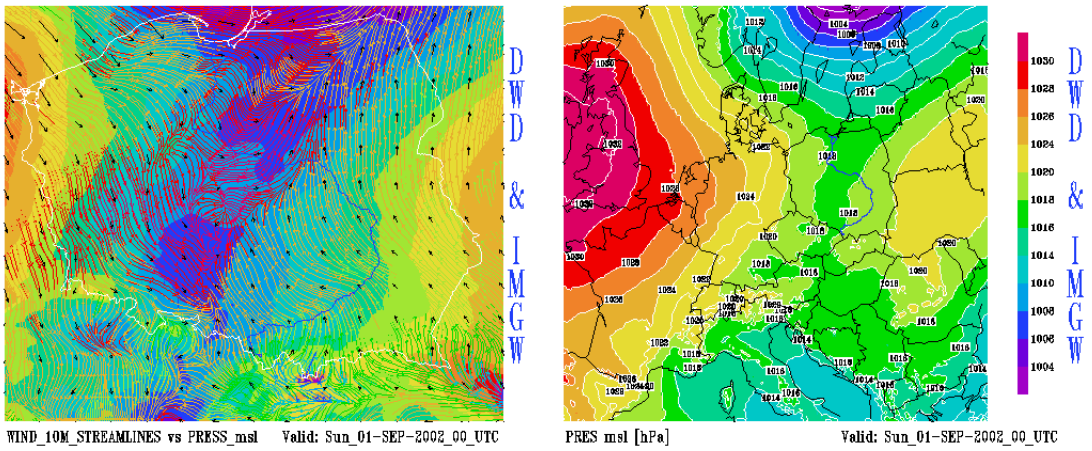

Figure 9: Forecast products used at IMGW, Warsaw

In addition to the operational runs with dx=14 km the LM also runs with a resolution of 7 km, but only for a forecast range of 30 hours.

4.5 MeteoSwiss (Zürich)

Introduction

The Alpine Model (aLMo) is the operational 7km version of the LM at MeteoSwiss. The model is computed on a NEC SX5 operated by the Swiss Centre for Scientific Computing (CSCS) in Manno. During the operational forecasting slots the SX5 enters near-dedicated mode: 14 CPUs are then reserved for the model integration, 1 for the interpolation of the initial and lateral boundary fields provided by the driving global model. From the global model (Integrated Forecast System, IFS, from ECMWF) only frames are used. The operational suite is controlled by the LM Package. This is a set of scripts running on SUN/SGI machines.

Basic Set-Up of aLMo

The aLMo domain extends from 35.11 N, 9.33 W (lower left) to 57.03 N, 23.41 E (upper right). This domain is covered by a grid of 385×325 points with a horizontal resolution of 7 km (see Figure 6). The borders are placed prevalently over sea in order to reduce negative interferences generated in the transition zone of the orographies of the driving model (IFS) and aLMo. The main features of the model set-up are summarized in Table 13.

Vertical Coordinates

In operational mode the model runs with 45 levels vertically distributed as shown in Fig. 10.

Hardware and Communications

The computational work of the aLMo suite is managed by 3 systems:

- SUN Enterprise 3000	at MeteoSwiss	(dissemination)
- SGI Origin 3000	at CSCS	(control, pre- and postprocessing, trajectories)
- NEC SX5	at CSCS	(IFS2LM, aLMo, LPDM)

Table 13: **Configuration of the aLMo at MeteoSwiss**

Domain Size	385 x 325 gridpoints
Horizontal Grid Spacing	0.0625° (∼ 7 km)
Number of Layers	45, base-state pressure based hybrid
Time Step and Integration Scheme	40 sec, 3 time-level split-explicit
Forecast Range	72 h
Initial Time of Model Runs	00 UTC and 12 UTC
Lateral Boundary Conditions	Interpolated from IFS at 3-h intervals
Initial State	Nudging data assimilation cycle, no initialization
External Analyses	Merging of LM-DWD snow analysis
Special Features	Use of filtered topography
Model Version Running	lm_f90 3.12
Hardware	NEC SX5 (using 14 of 16 processors)

Figure 11 shows the present configuration of hardware and communication used for the operational application of aLMo.

Data Flow
All operational processes are illustrated in the flow diagram of Figure 12. The format of the different products is shown by the different colours of the connections.

LM Package
The operational suite is driven by "LM Package", a software developed at Meteo Swiss. It has a modular structure and is composed by 50 shell scripts. It can be executed in three different modes: operational, test and personal mode. In operational mode preprocessing, aLMo and postprocessing are running concurrently; warnings and exits are transmitted to the permanently on-duty operators, who have the possibility to do manual interventions.

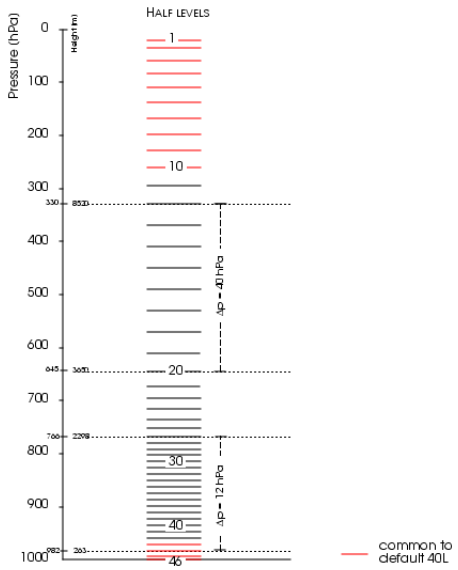

Figure 10: Vertical distribution of levels used at MeteoSwiss

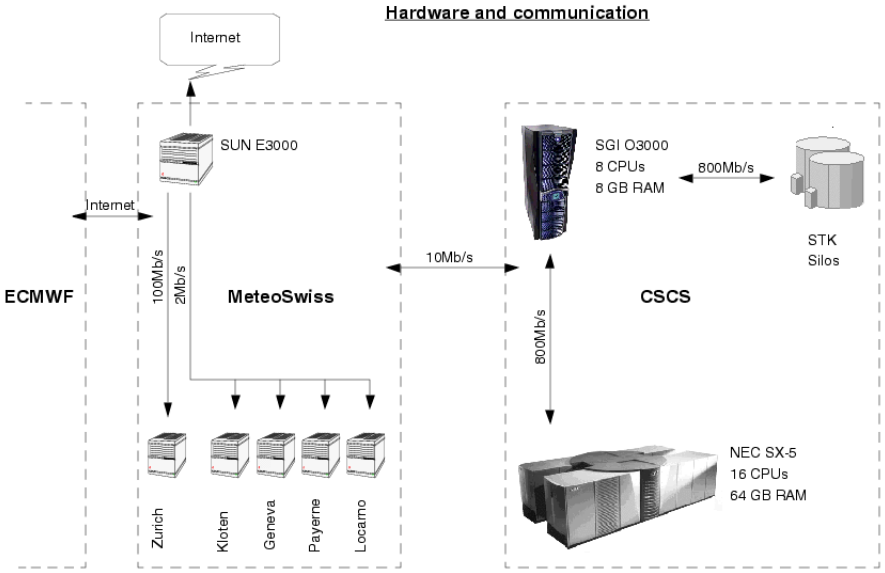

Figure 11: Present configuration of hardware and communications at MeteoSwiss

Products

- 2-D plots: produced by MetView every 3 or 6 hours
- Animations: Hourly loops produced with IDL and AVS
- Tables and extracts of the model output in different formats
- Trajectories
- Concentrations calculated by the LPDM module

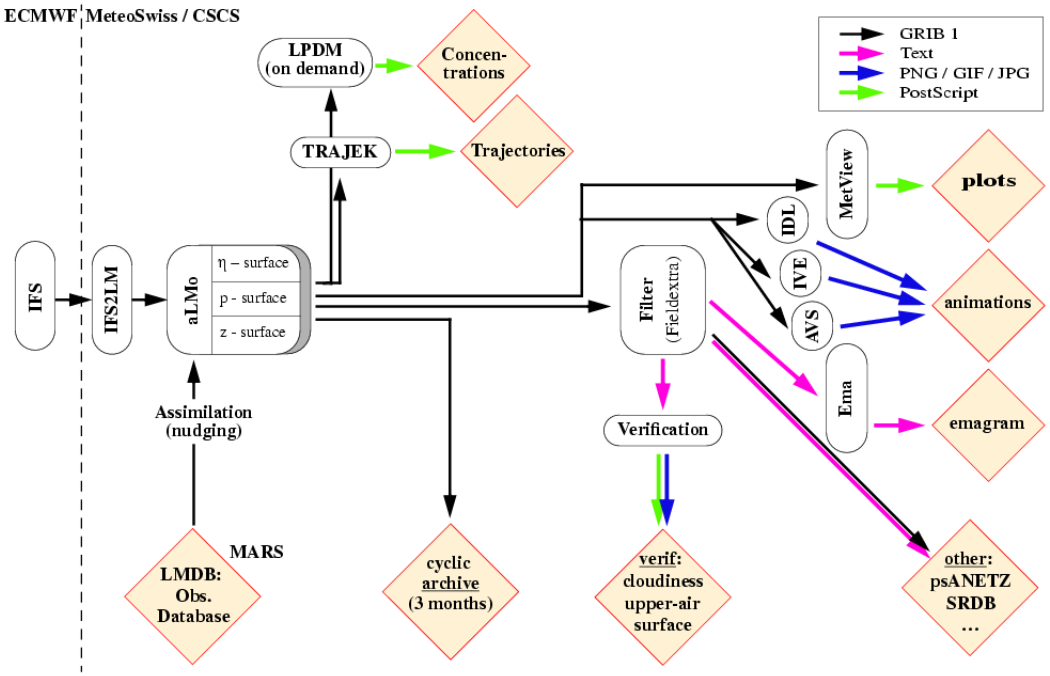

Figure 12: Dataflow of the current operational system at MeteoSwiss

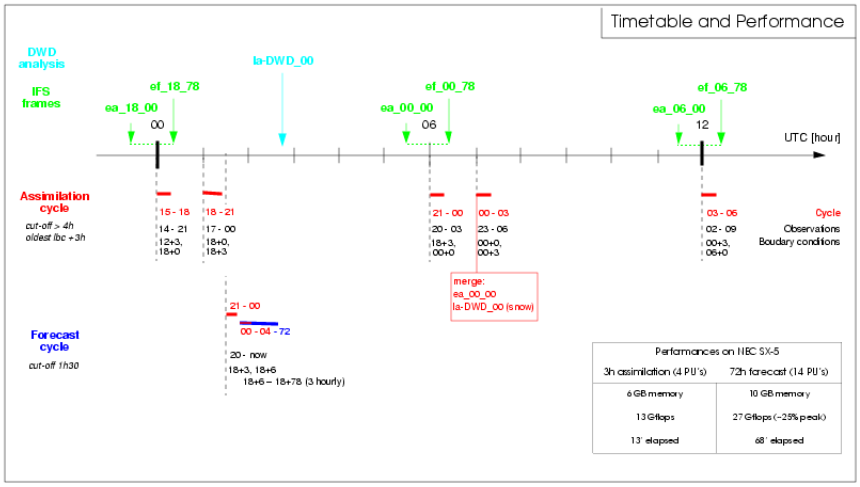

Figure 13: Time table of the aLMo assimilation cycle at MeteoSwiss

Assimilation Cycle
The data assimilation at MeteoSwiss is implemented with 3-hour assimilation runs. aLMo files are written every hour. The cut off time is at least 4 hours. The observations are taken from the aLMo data base, basically a copy of the ECMWF message/report data base. At the beginning of the 00-03 UTC and 12-15 UTC assimilation runs the ozone, vegetation and soil parameters are updated from the IFS analysis. In a similar way the LM snow analysis from DWD is merged into aLMo initial conditions. The schedule for half a day is displayed in Fig. 13.

Time Table
The analysis used by the main 72h forecasts is produced just ahead of the main runs (aLMo forecast) with a 3h run of aLMo in assimilation mode with the IFS frames from 6h earlier (18 or 06 UTC). The boundary conditions in the frames are updated every 3 hours. During the main forecast runs assimilation continues during the first 4 hours. The postprocessing is divided into a time critical and a non time critical part. During the first part the crucial products for Meteo Swiss internal clients (mainly forecasters) are generated and disseminated. During the second part the remaining products for internal and external clients are created. Archiving and statistics take place at the very end of the task. The concurrent processes of the operational production are illustrated in Fig. 14.

Verification
The output of the Model undergoes four different types of verification:

- Surface verification: The surface parameters are compared to measurements taken by synoptical and automatic stations.
- Upper air verification: verification of the model against measured radiosonde ascents;
- Cloud verification: verification of the model cloudiness based on METEOSAT visible images.
- Radar verification: verification of the precipitation against swiss radar network measurements.

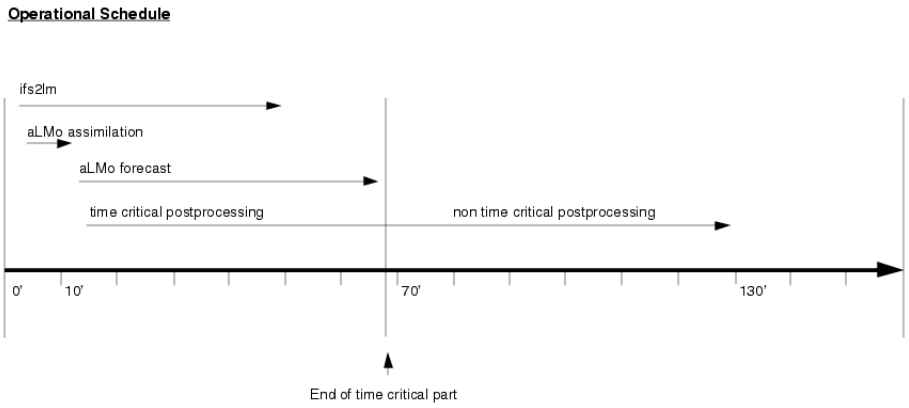

Figure 14: Time table of the operational suite at MeteoSwiss

4.6 UGM/CNMCA (Rome)

Basic Set-Up of LM

The EuroLM is the operational LM version of UGM using a 7 km grid spacing and 35 vertical levels. The rotated lat-lon coordinates of the lower left and of the upper right corner of the integration domain are $(\lambda = -14.0°, \varphi = -27.0°)$ and $(\lambda = 15.0°, \varphi = -3.0°)$, respectively. See Figure 6 for the model domain. EuroLM is driven by IFS boundary conditions (frames) and initialized by interpolated analysis from the EuroHRM variational data assimilation system (UGM hydrostatic NWP system). The new option of the Rayleigh damping, using filtered LM forecast fields instead of external boundary condition fields, is switched on to reduce the spurious reflection from the top boundary of the model domain. The main features of the model set-up are summarized in Table 14. UGM has started to run EuroLM at ECMWF from February 2004.

Table 14: **Configuration of EuroLM**

Domain Size	465 x 385 gridpoints
Horizontal Grid Spacing	0.0625° (∼ 7 km)
Number of Layers	35, base-state pressure based hybrid
Time Step and Integration Scheme	40 sec, 3 time-level split-explicit
Forecast Range	60 h
Initial Time of Model Runs	00 UTC
Lateral Boundary Conditions	Interpolated from IFS frames at 3-h intervals
Initial State	Interpolated from EuroHRM 3D-Var analysis
External Analyses	None
Special Features	Use of filtered topography, new TKE scheme, new surface-layer scheme, cloud-ice scheme new option for Rayleigh damping
Model Version Running	lm_f90 3.15
Hardware	IBM P690 (at ECMWF; using 120 processors)

Data assimilation

EuroLM initial fields are interpolated from the EuroHRM analysis. The EuroHRM intermittent, 3-hourly, data assimilation system is based on the UGM 3D-Var PSAS analysis scheme

and the hydrostatic model HRM. Temperature, wind and pseudo relative humidity on 30 pressure levels plus surface pressure are currently analysed. The observations assimilated in a 3 hours time window are: SYNOPs, SHIPs, BUOYs, WIND PROFILERs, TEMPs, PILOTs, QSCAT winds, ERS2 winds, AIREPs, AMDARs, AMVs and AMSU-A radiances. The EuroHRM model domain has a 0.25 grid spacing and 40 vertical levels.

Operational Schedule
The operational schedule is dependent on the data assimilation of EuroHRM. The data cut-off time is 3 hours. As the 00 UTC EuroHRM analysis is produced, the EuroLM model integration is performed up to 72 hours. 3-hourly IFS frames from 18 UTC run are used, as boundary conditions.

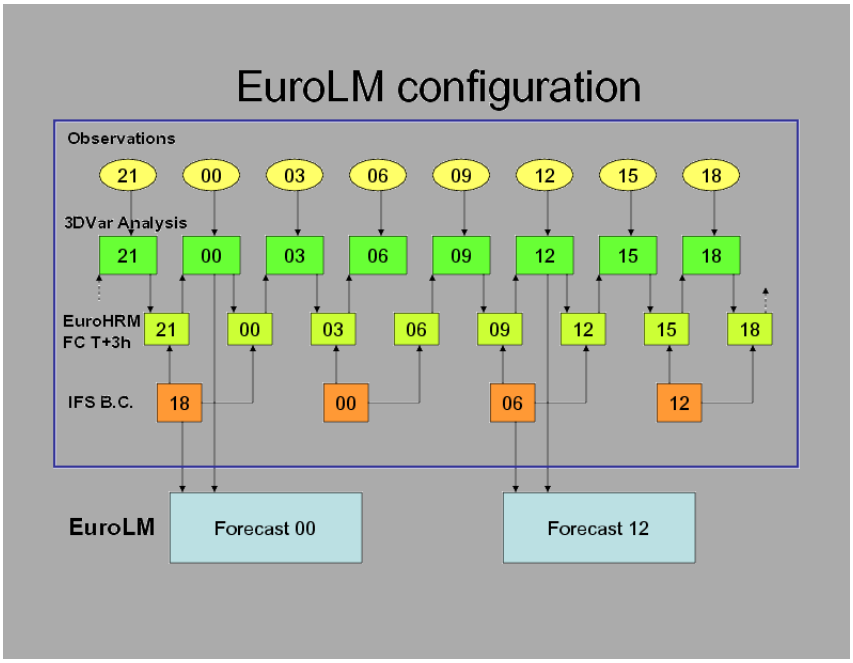

Figure 15: The assimilation suite of UGM/CNMCA

4.7 NMA (Bucharest)

Basic Set-Up of LM
The national meteorological administration of Romania, NMA in Bucharest, operates the LM in an operational mode at 14 km grid spacing twice a day (00 and 12 UTC). The rotated lat-lon coordinates of the lower left and of the upper right corner of the integration domain are $(\lambda = 5.0°, \varphi = -15.0°)$ and $(\lambda = 15.0°, \varphi = -6.0°)$, respectively. See Figure 6 for this model domain. The main features of the model set-up are summarized in Table 15.

In addition to the operational runs with dx=14 km the LM also runs with a resolution of 7 km on the same domain.

Table 15: **Configuration of the LM at NMA**

Domain Size	81 x 73 gridpoints
Horizontal Grid Spacing	0.125° (∼ 14 km)
Number of Layers	35, base-state pressure based hybrid
Time Step and Integration Scheme	80 sec, 3 time-level split-explicit
Forecast Range	48 h
Initial Time of Model Runs	00 and 12 UTC
Lateral Boundary Conditions	Interpolated from GME at 3-h intervals
Initial State	Interpolated from GME
External Analyses	None
Special Features	Use of filtered topography, new TKE-scheme new surface-layer scheme, cloud-ice scheme prognostic precipitation
Model Version Running	lm_f90 3.9
Hardware	Linux cluster (26 processors)

4.8 COSMO Limited-Area Ensemble Prediction System

The COSMO limited area ensemble prediction system (COSMO-LEPS) based on LM and ECMWF ensemble forecasts has been installed at ECMWF by our colleagues at ARPA-SIM in Bologna (Montani et al., 2003) The system is ready for a quasi-operational trial since November 2002, using 120-h forecasts of 10 LM runs starting at 12 UTC on initial and boundary conditions for 10 representative members of an ECMWF-EPS superensemble. Supervision and scheduling of the suite is done by ARPA-SIM. COSMO-LEPS probability products (derived and processed by the group in Bologna) are ready at about 23.00 GMT. The dissemination to COSMO centres is by GRIB-files.

Basic Set–Up of COSMO–LEPS
Within COSMO–LEPS framework, LM runs operationally at ECMWF using a 10 km grid spacing and 32 vertical layers. In contrast to all other applications, COSMO–LEPS uses a rotated pole with `pollat=40.0` and `pollon=-170.0`. The rotated lat-lon coordinates of the lower left and upper right corner of the integration domain (with this rotated pole) are ($\lambda = -12.5^o$, $\varphi = -16.0^o$) and ($\lambda = 14.95^o$, $\varphi = 7.13^o$), respectively. The main features of the model set–up are summarized in Table 16.

Changes in the last year
Since June 2004, the 10–member suite is operational using the two most recent EPSs to select the representative members. In March 2005, another LM run based on the high-resolution deterministic ECMWF forecast was added to the COSMO-LEPS suite. Products are archived at ECMWF from fc+0h to fc+120h every 3 hours.

COSMO-LEPS Products
At present, the following products are available.

- Probability of 24-h precipitation amount exceeding 1, 20, 50, 100 and 150 mm thresholds.
- Probability of 72-h precipitation amount exceeding 50, 100, 150 and 250 mm thresholds.
- Probability of maximum 2m-temperature above 20, 30, 35 and 40 Celsius thresholds.

Table 16: **Configuration of COSMO–LEPS, run at ECMWF by ARPA-SIM**

Domain size	306 × 258 gridpoints
Horizontal grid spacing	0.09^o ($\sim$ 10 km)
Number of layers	32, basic-state presure based hybrid
Time Step and Integration Scheme	60 sec, 3 time–level split–explicit
Forecast Range	120 h
Initial Time of Model Runs	12 UTC
Lateral Boundary Conditions	Interpolated from EPS members at 6-h intervals
Initial State	Interpolated from EPS members' analyses
Special Features	Use of filtered topography
Model version running	lm_f90 3.9
Hardware	IBM p690 clusters (using 84 processors)

- Probability of minimum 2m-temperature below 5, 0, -5 and -10 Celsius thresholds.
- Probability of maximum 10m wind speed above 10, 15, 20 and 25 m/s thresholds.
- Probability of maximum CAPE (in 24 hours) exceeding 750., 1000., 1500., 2000., 2500., 3000. and 3500. J/kg thresholds.
- Probability of minimum SHOWALTER INDEX (in 24 hours) below 0, -2, -4 and -6 thresholds.
- Probability of minimum 'height of 0 °C isotherm' (HZEROCL) over 24 hours below 1500, 1000, 700 and 300 m thresholds.
- Mean sea level pressure and accumulated precipitation from 10 deterministic LM runs (every 6 hours).
- Geopotential at 700 hPa and temperature at 850 hPa from 10 deterministic LM runs (every 6 hours).

5 Changes to the Model System

In this section, important changes to the LM-system which have been introduced during the last year are briefly described, and the possible impact on the forecast products are summarized. Of course, changes in the host model GME can also have a significant impact on the LM forecasts. Important changes to GME and its data assimilation are summarized below.

- GME now uses a prognostic treatment of sea-ice. The climatological ice temperatures, which were used before, have been replaced by a forecast for the thickness and the surface temperature of the ice. The part of a grid box, that is covered by ice, is determined in the 00 UTC analysis and only those grid elements, that are fully covered, are considered. During a GME forecast, the ice can melt, but new ice points can only be treated by the analysis scheme. The new scheme gives a more realistic horizontal distribution of the ice surface temperature in polar regions (March 2004).

- A new version of GME has been introduced which uses a horizontal resolution of about 40 km (60 km before) and 40 vertical layers (31 before). The lowest model level is now 10 meters above ground. The mean area covered by a grid box is 1384 km^2 (3100 km^2 before). This version of GME uses the new multi-layer soil model, that is also tested in the LM. Objective verification shows that the forecast of near-surface weather parameters (temperature and dew-point temperature) is improved significantly (September 2004).

- In the assimilation system the use of humidity from the Pseudo-Temps of ECMWF levels below 700hPa level has been excluded. The ECMWF model has a different humidity structure over sea, compared to GME, which led to a too moist atmosphere in the GME (December 2004).

- Atmospheric Motion Vector Winds (AMVs) are now used in BUFR format in the global assimilation system. Compared to the use of the SATOB format, the information is now obtained at a higher temporal and spatial resolution. It can be distinguished, whether the wind is derived from cloudy or clear-sky parts of the water vapor picture. In the BUFR format an information is included about the quality of the derived wind. Besides, the MSG satellites will not deliver the SATOB code any more. Monitoring of the AMV's in SATOB and in BUFR format shows a good, in large parts even higher quality of the BUFR format (February 2005).

For more detailed information on changes to GME and its data assimilation, please refer to the *Quarterly Report of the Operational NWP-Models of the Deutscher Wetterdienst* (available at `www.dwd.de`).

5.1 Major Changes to LM

During 2004/05 a number of updates of LM, cycle 3, have been introduced. The changes from version 3.8 up to version 3.15 are described below. The main features are – besides code optimization and bug corrections – the preparation of 1DVar satellite retrievals for data assimilation, the introduction of the graupel scheme and a second option for the Rayleigh damping.

Notes on lm_f90 Version 3.8

This version was created on 23 March 2004. Inconsistencies in the treatment of the linked lists for the namelist group `/GRIBOUT/` between the output of the model levels and the output of the synthetic satellite images have been removed. Besides a bug correction in the prognostic precipitation scheme, some optimizations and technical changes for the Runge-Kutta scheme have been implemented.

Notes on lm_f90 Version 3.9

This version was created on 22 April 2004. Bugs in the computation of the backward trajectories for the semi-Lagrange advection of precipitation have been corrected.

Notes on lm_f90 Version 3.10

This version was created on 23 June 2004. The treatment of the error-values from the RTTOV-library has been changed. If only soft-limits are violated, the synthetic satellite images are computed anyhow. If a violation of the hard-limits occurs, only the computation of the images for this special step are skipped. Only if a general error occurs, the computation of the synthetic satellite pictures is switched off, but LM integration is going on.

Notes on lm_f90 Version 3.11

This version was created on 28 July 2004. As only change it contains the introduction of Floating Point Exception trapping for IBM machines. At the beginning of the main program `lmorg.F90`, a special routine is called that initializes a special IBM trap handler.

With this change, the first `ifdef` has been implemented in the LM. The reason is the call of this specific IBM routine that allows an efficient trapping of floating point exceptions without using compiler options that would slow down program execution. To activate this trap handler, the main program has to be compiled with the option `-DFPEABORT`. The main program now has the extension `.F90`.

Notes on lm_f90 Version 3.12

This version was created on 15 September 2004. It prepares the assimilation of 1DVar satellite retrievals, introduces an option for a revised quality control for humidity and a new multi-level check, and re-organizes the observation processing.

- Preparation of 1DVar satellite retrievals from MSG or ATOVS radiances:
  A new module `src_obs_1dvar_org.f90` has been introduced, which contains the framework of organizing the observation processing (i.e. production) of satellite retrievals. The retrieved profiles are included in the process of computing the observation increments (without further quality control), spreading and nudging. This means, once the retrievals are available, they can be nudged immediately. New variables have beed defined in the module `data_nudge_all.f90`, which may become namelist variables in a later version, when the production of the retrievals by means of a 1DVar minimization is included.

- Revised quality control of vertical profiles (option):
  If this option is turned on (if `qcvf(4) > 0`), new (smaller) stability-dependent thresholds for the quality control of (radiosonde) humidity profiles and a new formulation of the multi-level check are used. This option is based on the formulation in the global analysis scheme.

- Re-organization of the observation processing:
  Several subroutines from the module `src_obs_processing.f90` have been outsourced to new modules. All `include`-files are now really included in the source code of the modules.

- Initialization of prognostic precipitation:
  When running with prognostic precipitation, there is the need to initialize the three-dimensional rain- and snow-field in the beginning of the forecast. Up to now these fields have been set to zero, with the results that there is a lack of total precipitation of about 30 % at the surface in the first hours. Two options have been implemented:

  - Diagnostic initialization: The microphysics scheme is used with minor modifications to diagnose the grid scale rain and snow. This option can be chosen by the new namelist parameter `ldiniprec=.TRUE.`.
  - Prognostic initialization: Initial values have to be provided for grid scale rain and snow from the nudging run. This option can be chosen by the new namelist parameter `lana_qr_qs=.TRUE.`

  If there is no assimilation suite to provide rain and snow (if e.g. starting from interpolated GME-analyses), only the option `ldiniprec=.TRUE.` can be used.

Notes on lm_f90 Version 3.13

This version was created on 3 December 2004. Three new features have been introduced and a modified version of the multi-layer soil model has been implemented. At the moment, all schemes are for testing only.

- Graupel scheme: This scheme can be chosen by setting `itype_gscp=4`. Then the hydrometeor graupel is added for the microphysics calculation.

- 3D turbulence scheme: This scheme is possible only in combination with the new Runge-Kutta dynamical core. It can be switched on with the namelist-variable (from /PHYCTL/) `itype_turb=5/7`. Together with this scheme a prognostic treatment of TKE can be chosen (namelist variable `lprog_tke=.TRUE.`.

- Latent Heat Nudging: The basic version of the latent heat nudging has been implemented. This scheme is still under testing and development.

- The multi-layer soil model, already implemented in LM, has been adapted to the GME version.

Notes on lm_f90 Version 3.14

This version was created on 25 January 2005. A new option for the Rayleigh-damping in the upper layers has been introduced and updates of the Runge-Kutta-scheme and the latent

heat nudging have been implemented. Bugs in the computation of the land-sea-mask and in the lower boundary for the latent and sensible heat flux have been corrected.

- There was an inconsistency in the treatment of grid boxes having a fraction of land of exactly 50 %. They are considered as land points, but because of a bug in the computation of the land-sea-mask, used in the LM, no soil model has been computed for these points. This has been corrected.

- The diagnostic computation of the latent and sensible heat flux in the dynamics now uses the same lower boundary formulation than the other prognostic calculations.

- Rayleigh damping: The new option allows a Rayleigh-damping in the upper layers, even when only frames for the boundary fields (e.g. from the IFS model) are provided. This procedure does not use the boundary fields, but LM forecast fields, which have been filtered to remove small-scale phenomenons. This kind of damping can be chosen with the new namelist variable `itype_spubc=2` (=1: already implemented kind of damping using boundary fields).

- Runge-Kutta scheme: The possibility for using an upwind 1st order and centered differences 2nd order advection operator has been implemented.

- Latent Heat Nudging: A scaling factor for diagnostic reference precipitation has been implemented as new namelist variable `rlhn_scale_dp`.

Notes on lm_f90 Version 3.15

This version was created on 3 March 2005. It contains two bug fixes and some technical adaptations for running with a big model domain (LME development at DWD):

- There was a bug in the computation of vertical aerosol profiles. This lead to a wrong vertical distribution of the different aerosol components and therefore to wrong optical thicknesses of the aerosols in the atmospheric layers. The optical thickness of some aerosol types was over- and the one of other types underestimated. This resulted in a partial compensation of the error for the radiation computation and masked the error in the overall results. Influences of this correction are expected for solar radiation fluxes for clear-sky conditions, but are rather small.

- After reading the first boundary file, the surface pressure has to be calculated again, if the initial data come from an analysis and the boundary data from a forecast of a different model. This is necessary, because the initial data set and the first boundary data set are mixed in this case, which changes the atmospheric pressure.

- For the calculation of the maximal wind gusts, the two lowest model levels are interpolated to a height of approximately 30 meters, then the gusts are derived from these values. This is an intermediate solution until a more sophisticated algorithm (e.g. regarding to Brasseur) has been implemented.

- A new namelist variable `nunit_of_time` has been implemented, to specify this Grib value. The following values are possible:

Value	Meaning
0	1 minute
1	1 hour
2	1 day
10	3 hours
11	6 hours
12	12 hours
13	15 minutes
14	30 minutes

Note that the values 13 and 14 are not Grib standard, but are necessary if Grib outputs in a frequency less than 1 hour are done.

5.2 Major Changes to GME2LM

There were two changes of the GME2LM in the last year. Only the first one was a real update, the second update only introduced the IBM trap handler for floating point exceptions similar to LM 3.11.

Notes on GME2LM Version 1.19

This version of GME2LM was created on 18 March 2004. The changes are:

- Adaptations for working with bitmaps and the 40 km / 40 level version of GME
- Interpolation of the new soil variable `FRESHSNW` from GME- to LM-fields for the multi-layer soil model.
- Additional treatment of the orography for the Z-coordinate version of the LM. A new namelist-variable `l_topo_z` has been introduced. The default of this variable is `.FALSE.`.
- Some Grib-names and tables have been changed to be consistent with the LM.

All changes only concerned non-operational parts of GME2LM, the operational results therefore are not changed.

Notes on GME2LM Version 1.20

This version of GME2LM was created on 21 July 2004. The IBM trap handler for detecting floating point exceptions has been introduced (see also LM Version 3.11).

5.3 The new Interpolation Program INT2LM

The new interpolation program is an extension of the GME2LM. It can interpolate data from the global model of ECMWF, the IFS, and from the LM itself. INT2LM is a joint COSMO development, where the tasks have been distributed to the centers as follows:

- DWD: parallel framework of the program; GME2LM

- ARPA-SIM: IFS2LM
- MeteoSwiss, DWD: LM2LM

After the implementation of several development- and testing-versions, the first official version of the new library `int2lm` is available since 12 April 2005 (Version 1.1). INT2LM will replace GME2LM and the former test versions IFS2LM and LM2LM in the near future.

6 Working Groups

COSMO's scientific and technical activities are organized in *Working Groups* (WG) which cover the main research areas related to a NWP-system. Each Working Group is headed by a *Work Package Coordinator* (WPC), who is responsible for the consistency of the execution of the work packages and for the coordination, planning, and supervision of the scientific and technical activities related to the work packages in his group. The WGC normally meet twice a year to discuss the status of the work packages and to prepare the work plans for the next period. The plans are then elaborated in detail during the COSMO General Meeting

This section gives an overview on the current personnel composition of the WGs. All scientists contributing actively to the work packages are included in the lists, also those from outside COSMO member institutions. For each WG, the main research activities from the recent COSMO period (Oct 2003 - Sep 2004) are briefly summarized and a short note on the planned activities for the present period (Oct 2004 - Sep 2005) is given. The work plan lists as well as a detailed description of each work package within a WG, are available at the member area of our web-site.

6.1 Working Group 1: Data Assimilation

This working group considers various aspects of 4-dimensional assimilation of observation data, especially using the nudging analysis technique. For soil moisture and some surface fields, a set of 2-dimensional intermittent analysis schemes is applied in addition. The group is headed by Christoph Schraff (DWD) as WPC. The following scientists are members of this group.

Name	Institution	e-mail
Jerzy Achimowicz	IMGW	jerzy.achimowicz@imgw.pl
Jean-Marie Bettems	MeteoSwiss	jean-marie.bettems@meteoswiss.ch
Massimo Bonavita	CNMCA	bonavita@meteoam.it
Michael Buchhold	DWD	michael.buchhold@dwd.de
Davide Cesari	ARPA-SIM	dcesari@smr.arpa.emr.it
Francesca di Giuseppe	ARPA-SIM	fdigiuseppe@smr.arpa.emr.it
Reinhold Hess	DWD	reinhold.hess@dwd.de
Stefan Klink	DWD	stefan.klink@dwd.de
Blazej Krzeminski	IMGW	blazej.krzeminski@imgw.pl
Martin Lange	DWD	martin.lange@dwd.de
Daniel Leuenberger	MeteoSwiss	daniel.leunenberger@meteoswiss.ch
Fabrizio Nerozzi	ARPA-SIM	fnerozzi@smr.arpa.emr.it
Christoph Schraff	DWD	christoph.schraff@dwd.de
Klaus Stephan	DWD	klaus.stephan@dwd.de
Antonio Vocino	CNMCA	vocino@meteoam.it
Antonella Sanna	ARPA Piemonte	antonella.sanna@arpa.piemonte.it

During the last COSMO period, the following topics were of major importance:

- The assimilation of European wind profiler data has been introduced operationally (at DWD) after that some profilers have been blacklisted and an impact study showed slight positive impact.
- A main focus continued to be on the assimilation of radar-derived precipitation by means of latent heat nudging (LHN). Sensitivity experiments in an OSSE framework for an idealised supercell storm indicate that errors in the ambient low-level humidity affect mainly the rain amounts, while wind errors may distort the dynamincal structures and precipitation distributions. Effects of prognostic treatment of precipitation (including drifting) limit the validity of the basic assumption of LHN, and this is found to adversely affect LHN in real-case studies on 2.8 km resolution compared to runs with diagnostic precipitation (see *Latent Heat Nudging and Prognostic Precipitation* by S. Klink and K. Stephan in Section 9). Efforts are devoted to diagnose, better understand and reduce these problems.
- Deriving 3D wind retrievals with a simple variational adjoint method provides another approach to use both radar reflectivity and radial velocity. Preliminary results indicate that the method is very sensitive to the pre-processing of the radar data, and spurious wind patterns may be obtained.
- Some further case studies on the assimilation of ground-based GPS-derived total precipitable water (PW) have basically confirmed earlier results, that although these data do have a potential to improve precipitation forecasts, the incorrect vertical distribution of the PW information has a significant negative impact in some cases. A feasibility study has been performed on GPS tomography which in principle could solve this problem by providing vertical humidity profiles. While this has worked reasonably well in some cases, problems in other cases indicate the need for much more work to be done on this method.
- The work has been continued on retrieving temperature and humidity profiles from NOAA polar orbiting satellite data by 1DVAR and assimilating them in a 3D-PSAS scheme for lower-resolution HRM applications. However, the effort has been extended to use these data also in the framework of the nudging-type scheme for LM and to apply the 1DVAR approach to MSG data.
- Using 2-m humidity observations in the 2D variational soil moisture analysis (SMA) in addition to 2-m temperature data has not shown any positive impact.

In 2005, the work on the above topics will continue along the lines described, except that it will probably not be possible to allocate any resources to the use of ground-based GPS data. The variational soil moisture analysis will be extended from the current 2-layer soil model to the new multi-level soil model. Further plans relate to tuning issues in the nudging scheme, the use of cloud information, and the incorporation of satellite information in the snow analysis.

(Christoph Schraff, DWD)

6.2 Working Group 2: Numerical Aspects

The WG on numerical methods and basic model dynamics is headed by Jürgen Steppeler (DWD) as WPC. Currently, the following scientists are members of this group.

Name	Institution	e-mail
Michael Baldauf	DWD	michael.baldauf@dwd.de
Heinz-Werner Bitzer	AWGeophys	heinz-werner.bitzer@dwd.de
Davide Cesari	ARPA-SIM	dcesari@srm.arpa.emr.it
Jochen Förstner	DWD	jochen.foerstner@dwd.de
Almut Gassmann	DWD	almut.gassmann@dwd.de
Guy de Morsier	MeteoSwiss	guy.demorsier@meteoswiss.ch
Tiziana Paccagnella	ARPA-SIM	tpaccagnella@smr.arpa.emr.it
Jan Parfiniewicz	IMWG	jan.parfiniewicz@imgw.pl
Peter Prohl	DWD	peter.prohl@dwd.de
Georgios Sakellaridis	HNMS	sak@hnms.gr
Ulrich Schättler	DWD	ulrich.schättler@dwd.de
Jürgen Steppeler	DWD	juergen.steppeler@dwd.de
Lucio Torrisi	UGM	torrisi@ecmwf.int

The main research activities of WG 2 for the period Oct 2003 - Sep 2004 and the planned activities for the current year are summarized below.

Apart from smaller work, which is described on the private part of the COSMO web-site, there are two important lines of work, which are the development of the Runge-Kutta time integration and the Z-coordinate. Both developments are contiued from the 2003/2004 period. A preliminary version of the RK-scheme was developed by September 2004 and the z-coordinate version had a preliminary physics interface and realistic runs were possible with the Euler version of the LM_Z. Also, the Semi-Lagrangian version of LM_Z was integrated in the same program library.

For 2004/2005 it is planned to develop the RK-scheme further by developing further versions and finding a suitable version using a series of tests, which in addition to realistic integrations involve convergence tests in idealised situations. For the z-coordinate, it is planned to develop the Semi-Lagrangian into three dimensions and to do realistic tests using the Eulerian version. This should include a refinement of the physics interface. The condensation should be computed on the z-levels.

(Jürgen Steppeler, DWD)

6.3 Working Group 3: Physical Aspects

The main effort of this working group is to develop new physics packages for future operational applications and to improve existing parameterizations. The WG on physical processes, which is coordinated by Marco Arpagaus (MeteoSwiss), consists of the following scientists:

Name	Institution	e-mail
Euripides Avgoustoglou	HNMS	euri@hnms.gr
Marco Arpagaus	MeteoSwiss	marco.arpagaus@meteoswiss.ch
Giovanni Bonafè	ARPA Emilia-Romagna	gbonafe@smr.arpa.emr.it
Matteo Buzzi	MeteoSwiss	matteo.buzzi@meteoswiss.ch
Claudio Cassardo	Università di Torino	cassardo@ph.unito.it
Alain Clappier	EPF Lausanne	alain.clappier@epfl.ch
Francesca di Giuseppe	ARPA Emilia-Romagna	fdigiuseppe@smr.arpa.emr.it
Grzegorz Duniec	IMGW	grzegorz_duniec@imgw.pl
Marco Elementi	ARPA Emilia-Romagna	melementi@smr.arpa.emr.it
Almut Gassmann	Universität Bonn	almut.gassmann@uni-bonn.de
Erdmann Heise	DWD	erdmann.heise@dwd.de
Hans-Joachim Herzog	DWD	hans-joachim.herzog@dwd.de
Witek Interewicz	IMGW	witold_interewicz@imgw.pl
Nicola Loglisci	ARPA Piemonte	n.loglisci@arpa.piemonte.it
Tiziano Maestri	Università di Bologna	t.maestri@adgb.df.unibo.it
Chiara Marsigli	ARPA Emilia-Romagna	cmarsigli@smr.arpa.emr.it
Massimo Milelli	ARPA Piemonte	m.milelli@arpa.piemonte.it
Dmitrii Mironov	DWD	dmitrii.mironov@dwd.de
David Oesch	Universität Bern	oesch@giub.unibe.ch
Tiziana Paccagnella	ARPA Emilia-Romagna	tpaccagnella@smr.arpa.emr.it
Paola Papetti	ARPA Emilia-Romagna	ppapetti@smr.arpa.emr.it
Antonio Parodi	Università di Genova	antonio@cima.unige.it
Renata Pelosini	ARPA Piemonte	r.pelosini@arpa.piemonte.it
Matthias Raschendorfer	DWD	matthias.raschendorfer@dwd.de
Thorsten Reinhardt	DWD	thorsten.reinhardt@dwd.de
Bodo Ritter	DWD	bodo.ritter@dwd.de
Rolando Rizzi	Università di Bologna	r.rizzi@adgb.df.unibo.it
Mathias Rotach	MeteoSwiss	mathias.rotach@meteoswiss.ch
Reinhold Schrodin	DWD	reinhold.schrodin@dwd.de
Jan-Peter Schulz	DWD	jan-peter.schulz@dwd.de
Zbigniew Sorbjan	Marquette University	zbigniew.sorbjan@marquette.edu
Linda Smoydzin	Universität Bonn	linda.smoydzin@uni-bonn.de
Ennio Tosi	Università di Bologna	e.tosi@adgb.df.unibo.it
Gerd Vogel	DWD	gerd.vogel@dwd.de

Most of the tasks of this working group are fairly big, and hence topics typically stay on the agenda for a few years. This is also true for most of the main work packages of the last COSMO period:

- Work continued on the new turbulence scheme based on a prognostic treatment of turbulent kinetic energy (TKE) as well as on the new surface transfer scheme. Both schemes are operational at DWD, ARPA-SIM, IMGW and HNMS, and are expected to become operational at MeteoSwiss soon. A technical report on parts of this work package ("Evaluation of Empirical Parameters of the New LM Surface-Layer Parameterisation Scheme") can be obtained on the COSMO web-site in *Publications* > *Technical Reports*.
- The new multi-layer version of the soil model TERRA, which includes freezing and melting of soil layers and a revised formulation of the snow model, has been thoroughly tested and is currently undergoing final pre-operational testing. A technical report describing the changes to TERRA ("The Multi-Layer Version of the DWD Soil Model TERRA_LM") is also available on the COSMO web-site in *Publications* > *Technical Reports*. Additionally, work on the development of the new lake model FLake continued.

- Implementation work on the Kain-Fritsch convection scheme continued, although very slowly. Tests show promising results, but rigorous validation is still pending and the code eventually needs substantial re-writing to improve the performance on vector machines. Therefore, alternative implementations of the Kain-Fritsch scheme are also being looked at.

- A three-category ice scheme has been developed and implemented into the LM. Tests, including comparison with a two-moment microphysics scheme, are ongoing.

- Implementation and adaptation of a 3D turbulence formulation is under way, and will be followed by extensive testing, especially at higher resolutions.

The plan for 2005 includes further work on most of the schemes mentioned above. For the new turbulence scheme, this consists of parameter tuning, further extension of the scheme as well as writing up an extended documentation. The soil model mainly awaits operational implementation, and the implementation of the Kain-Fritsch convection scheme is "work in progress".

New packages for the work plan of 2005 include the intercomparison of soil models with respect to soil moisture, the development of a shallow convection scheme to be used for LM runs at 2-3 km grid-spacing, sensitivity studies concerning boundary layer clouds and testing of different sub-grid scale cloudiness approaches as well as testing of different aspects of LM runs at 2-3 km, or even smaller grid-spacing.

(Marco Arpagaus, MeteoSwiss)

6.4 Working Group 4: Interpretation and Applications

The main effort of this working group is to develop methodologies and tools for the interpretation of high-resolution direct model output, including model applications to limited area ensemble prediction and various postprocessing methods. The WG on interpretation and applications is coordinated by Pierre Eckert (MeteoSwiss). The following scientists are members of the group:

Name	Institution	e-mail
M. Anadranistakis	HNMS	anad@hnms.gr
Marco Arpagaus	MeteoSwiss	marco.arpagaus@meteoswiss.ch
Carlo Cacciamani	ARPA-SIM	ccaciamani@arpa.emr.it
Daniel Cattani	MeteoSwiss	cat@meteoswiss.ch
Pierre Eckert	MeteoSwiss	pierre.eckert.@meteoswiss.ch
R. Kretzschmar	MeteoSwiss	krr@meteoswiss.ch
Andre-Charles Letestu	MeteoSwiss	acl@meteoswiss.ch
Chiara Marsigli	ARPA-SIM	cmarsigli@smr.arpa.emr.it
Andrea Montani	ARPA-SIM	amontani@smr.arpa.emr.it
Andrzej Mazur	IMGW	andrzej.mazur@imgw.pl
Tiziana Paccagnella	ARPA-SIM	tpaccagnella@smr.arpa.emr.it
Volker Renner	DWD	volker.renner@dwd.de
Susanne Theis	Universität Bonn	susanne.theis@uni-bonn.de
Andrea Walser	MeteoSwiss	andrea.walser@meteoswiss.ch

(Pierre Eckert, MeteoSwiss)

6.5 Working Group 5: Verification and Case Studies

The activities of this group focus on an administrative point of view, in order to have some objective measures of how well LM forecasts are performing, and on an scientific viewpoint, in order to have detailed assessment of the strengths and weaknesses of the model. Thus, at the moment, the main activities of the working group deal with the following issues:

- The verification of operational model forecasts,
- The verification with feedback on the physical parameterizations (which means verification of new LM versions on a set of test cases)
- The development of new verification methods and diagnostic tools
- The collection of LM case studies.

The WG was coordinated ad interim from September 2003 to September 2004 by Francis Schubiger (MeteoSwiss), and now by Patrizio Emiliani (CNMCA, Italy).

The following scientists are members of this group:

Name	Institution	e-mail
Theodore Andreadis	HNMS	andreadis@hnms.gr
Marco Arpagaus	MeteoSwiss	marco.arpagaus@meteoswiss.ch
Jean-Marie Bettems	MeteoSwiss	jean-marie.bettems@meteoswiss.ch
Carlo Cacciamani	ARPA-SIM	ccacciamani@smr.arpa.emr.it
Theagenis Charantonis	HNMS	tchara@hnms.gr
Flora Gofa	HNMS	fgofa@hnms.gr
Ulrich Damrath	DWD	ulrich.damrath@dwd.de
Patrizio Emiliani	UGM-CNMCA	p.emiliani@meteoam.it
Alessandro Galliani	UGM	galliani@meteoam.it
Pirmin Kaufmann	MeteoSwiss	pirmin.kaufmann@meteoswiss.ch
Chiara Marsigli	ARPA-SIM	cmarsigli@smr.arpa.emr.it
Andrezj Mazur	IMGW	andrzej.mazur@imgw.pl
Malgorzata Mierkiewicz	IMGW	malgorzata.mierkiewicz@imgw.pl
Massimo Milelli	ARPA Piemonte	massimo.milelli@arpa.piemonte.it
Marco Turco	ARPA Piemonte	marco.turco@arpa.piemonte.it
Guy de Morsier	MeteoSwiss	guy.de.morsier@meteoswiss.ch
Elena Oberto	ARPA Piemonte	elena.oberto@arpa.piemonte.it
Jan Parfiniewicz	IMGW	jan.parfiniewicz@imgw.pl
Renata Pelosini	ARPA Piemonte	renata.pelosini@arpa.piemonte.it
Ulrich Pflüger	DWD	ulrich.pflueger@dwd.de
Dominique Ruffieux	MeteoSwiss	dominique.ruffieux@meteoswiss.ch
Francis Schubiger	MeteoSwiss	francis.schubiger@meteoswiss.ch
Katarzyna Starosta	IMGW	katarzyna.starosta@imgw.pl
Joanna Linkowska	IMGW	joanna.linkowska@imgw.pl
Ermanno Veccia	UGM-CNMCA	e.veccia@meteoam.it
Emanuele Zala	MeteoSwiss	emanuele.zala@meteoswiss.ch
Claus-Jürgen Lenz	DWD	claus-juergen.lenz@dwd.de
Gerd Vogel	DWD	gerd.vogel@dwd.de
Maria-Stefania Tesini	ARPA-SIM	mstesini@smr.arpa.emr.it
Francesco Boccanera	Regione Marche	francesco.boccanera@regione.marche.it

The main activities of WG 5 for the period Oct 2003 - Sep 2004 covered the following points.

- Operational verification of surface parameters, using SYNOP stations and also regional high resolution networks. Results are summarised in verification reports which are distributed on a quarterly basis on the COSMO website.

- Operational verification of upper-air parameters, using TEMP stations. Like in the case of surface verification, results are summarized in reports distributed on a quarterly basis on the COSMO website.

- Exchange of LM maps (24hrs cumulated precipitation and MSLP) of each operational LM running on the COSMO web-site.

- High resolution verification of precipitation, using available high resolution dense non-GTS surface data. Consolidation of a common data set of non-GTS daily precipitation data.

- Daily cloudiness verification at 12 UTC with the Meteosat VIS channel.

- Verification of integrated water vapour content using GPS data.

- Validation of near-surface boundary layer processes and radiation budget from operational weather prediction runs (LM, GME, aLMo) at selected observatory measurement sites with different land surface properties.

- Weather regime type verification of vertical profiles and precipitation using radar composite network.

- Verification of precipitation forecast using radar composite network.

- Realization of a common Verification Package;

- Verification of runoff over river basins.

A WG4/WG5 workshop was held on 5-6 May 2004 in Geneva. Besides presentations of recent developments in the different services and preliminary results of the common verification package at ECMWF, the main topic of this joint workshop was a sessin named *how to present verification results to forecasters and feedbacks from forecasters to WG4 and WG5.* Presentations were given both from forecasters and scientists of the COSMO community. The discussion will lead into a document *LM Guidelines for forecasters.*

The work plan for 2005 includes new ideas and packages like verification on high resolution and with new techniques (like CRA (Contiguous Rain Area) verification, or by using fuzzy logic), verification of near surface boundary layer processes, conditional verification of new LM versions on a predefined set of test cases, implementation and installation of the Common Verification Suite at ECMWF and WGs 3-5 joint workshop in March 2005.

(Patrizio Emiliani, CNMCA-Italy)

6.6 Working Group 6: Reference Version and Implementation

The WG on code maintenance, reference version, documentation and implementation is headed by Ulrich Schättler (DWD) as WPC. The following scientists contribute to the work of this group:

Name	Institution	e-mail
Theodore Andreadis	HNMS	andreadis@hnms.gr
Euripides Avgoustoglou	HNMS	euri@hnms.gr
Jean-Marie Bettems	MeteoSwiss	jean-marie.bettems@meteoswiss.ch
Davide Cesari	ARPA-SIM	dcesari@srm.arpa.emr.it
Marco Consoli	CSCS / MeteoSwiss	mconsoli@cscs.ch
Guy de Morsier	MeteoSwiss	guy.demorsier@meteoswiss.ch
Marek Lazanowicz	IMGW	marek.lazanowicz@imgw.pl
Jan Parfiniewicz	IMGW	jan.parfiniewicz@imgw.pl
Paolo Patruno	ARPA-SIM	p.patruno@smr.arpa.emr.it
Ulrich Schättler	DWD	ulrich.schaettler@dwd.de
Jan-Peter Schulz	DWD	jan-peter.schulz@dwd.de
Lucio Torrisi	UGM	torrisi@meteoam.it
Emanuele Zala	MeteoSwiss	emanuele.zala@meteoswiss.ch

In the period Oct. 2003 - Oct. 2004 the following work was done by WG 6:

- Updates of the GME2LM (Versions 1.18/1.19) and LM (Versions 3.6-3.12) have been programmed, tested and implemented at all sites. See Section 5 for the program updates and Section 4 for the changes in the operational applications in the COSMO centres. No new Reference Version has been defined, so the update procedure for the reference version has not been activated.
- Due to the support of the Olympic Games in Athens, there were problems with the availability of the official COSMO web-site. Updating of the site could only be done in Manno. Therefore, many pages are rather old now and have to be updated.
- There was progress in updating the LM Documentation. Besides *Numerics and Dynamics* (Part I) and the *Data Assimilation* (Part III) there are drafts available now of the *Physical Parameterizations* (Part II) and the *User Guide* (Part VII).
- The common interpolation program INT2LM has been implemented as a test version. It includes GME2LM, IFS2LM and LM2LM and will, after a testing phase, replace these programs.
- There was little work on the Nesting Version of LM. Some more bugs were found and could be solved, but there still is no operational implementation in sight.

Activities on the maintenance and the update of the COSMO software will go on as usual in the next period. More emphasis will be put on updating the web-site, because this is a very important tool for information inside and also outside of COSMO. Also work on updating the whole LM documentation is going on. Some Grib related issues are investigated at MeteoSwiss and a comparison between the Nesting Version and the new INT2LM (LM2LM-part) is done at HNMS.

(Ulrich Schättler, DWD)

7 COSMO Meetings and Events

This section summarizes the main meetings, workshops and seminars as well as management decisions from the previous year. Other COSMO activities such as guest scientists and internal visits are also considered. Finally, an overview of the forthcoming activities in the present COSMO working period is given.

7.1 Meetings in 2004-2005

(1) LM User Seminar

This seminar on scientific applications of the LM is organized by Jürgen Steppeler and is always held at DWD in Langen. Two seminars have been held since the last COSMO Newsletter, from 8-10 March 2004 and from 7-9 March 2005. The User Seminar is dedicated to research activities with the LM at universities and research institutes and covers various scientific topics. Central issues usually are data assimilation, dynamics and numerics, physical processes, high-resolution experiments and LM applications. In the 2005 Seminar, several presentations of climate applications with the LM were shown. The 2004 User Seminar included also tutorials on the LM Package and on numerical methods. Proceedings of the seminars have not been published.

(2) WG6 Meeting (Zürich, 22 April 2004)

Some members of Working Group 6 together with staff from the Swiss Centre for Scientific Computing (CSCS) in Manno met to discuss various issues of *Reference Version and Implementation*. The status of the WPs was presented by the WG coordinator. Most WPs are on a good way, but there are problems with the official COSMO web-site in Athens. The current state of LM regarding *Code optimization and portability* was reviewed. LM now has a satisfying performance on the vector processors. Some further investigations are necessary for scalar architectures. A new benchmark version `LM_RAPS_3.0` is planned for summer 2004. Another point of discussion was the program for producing the external parameters. There is interest from the COSMO partners to access this program, developed at DWD. After implementing some modifications, DWD will provide this program as *Software Tool for Exchange*.

(3) WG4-WG5 Joint Meeting (Geneve, 4-5 May 2004)

The members of Working Group 4 for Interpretation and Applications and of Working Group 5 for Verification and Case Studies met at MeteoSwiss in Geneva (Switzerland) for a joint internal COSMO workshop.

(4) Meeting of the Working Group Coordinators (Geneve, 6-7 May 2004)

The Working Group Coordinators (WGCs, i.e. C. Schraff, J. Steppeler, M. Arpagaus, P. Eckert, F. Schubiger and U. Schättler), the Scientific Project Manager (SPM, T. Paccagnella) and the Chairman of the Steering Committee (D. Frühwald) met at MeteoSwiss in Geneve. Günther Doms (DWD) and Mathias Rotach (MeteoSwiss) joined this meeting.

The status of the different activities have been presented by the WP coordinators. As usual ongoing activities and critical aspects were discussed in details. Some initiatives and internal meetings have been planned. A report about the LMK project has been presented by Günther

Doms. LMK is at the moment the strongest driving force toward the further development of LM for applications at very high horizontal resolution. The LMK operational configuration will be, in the present planning, based on a horizontal resolution less than 3 km, 50 model layers, a rapid updating assimilation cycle to run LM every 3 hours for a range of 18 hours. A test suite for the 2.8 km version of the LM (LMK) has been installed at DWD. The model domain has 421×462 grid points with 50 vertical levels covering Germany and the Alps. The integrations start from interpolated initial conditions from LM/DWD using the LM2LM. Two integrations per day (00 and 12 UTC) are performed.

Dieter Frühwald reported about the recent actions and activities from the Steering Committee. An important initiative was the proposal to extend to other European countries, out of COSMO, the possibility to collect non GTS data for verification. The proposal, brought to the attention of Jean Quiby, chairman of SRNWP, will be presented and discussed during the SRNWP workshop on Verification in De Bilt in June 2004.

The major outcomes of the meeting have been reported in the minute which is available on the web-site member area.

(5) Meeting of the Working Group Coordinators (Bologna, 9-10 September 2004)

The work package coordinators and the Scientific Project Manager met a second time shortly before the General Meeting in Bologna.

Advancements of the activities were examined during the presentations of the WP coordinators. Part of the workshop was devoted to a general discussion about the COSMO internal technical organization. The strategy to make a planning of the activities better focussed on the basis of the **Goals** and **Perspectives** and has been also deeply discussed. A strong cooperation between the WP Coordinators group, the SPM and the STC is necessary to foster the accomplishment of the commitments related to top priorities in the COSMO scientific plan.

The last part of the meeting was devoted to the final tuning of the general meeting organization. As usual, the minutes of this meeting are available in the member area of the web site.

(6) COSMO WG2 Meeting on Numerical Methods (Milano, 21 September 2004)

Members of the COSMO numerics group (WG2) met one day before the General Meeting on 21 September 2004 in Milano. The participants discussed the current state of dynamics and numerics in European NWP models. The discussion then concentrated on the two major numerical developments for LM, the LM_Z and the LMK.

(7) 6th COSMO General Meeting

The 6th COSMO General Meeting was held in Milano hosted by UGM on 22 -24 September 2004. Over 60 participants attended the meeting (see Fig. 16).

The welcome address was given by the chief of UGM, Gen. Roberto Sorani, followed by the opening of the meeting by Dieter Frühwald who dedicated most of his talk to remember our colleague Günther Doms suddenly deceased in June 2004. The scientific value of Günther has been reminded going through his work of the last 25 years together with his rare human qualities experienced by all the colleagues working with him. Günther was the leader of LM and also of the COSMO scientific cooperation. All the DWD and COSMO colleagues will miss his scientific leadership and his rare human charisma.

After the organizational aspects presented by Massimo Ferri, D. Frühwald made the reporting of the Steering Committee activity and Tiziana Paccagnella made the SPM report about the scientific activities of the past COSMO year referring also about the WP Coordinators meetings.

An important new contribution to the meeting was the presentation by Francois Bouttier from MeteoFrance about Progress and Plans of the AROME project. This very interesting and stimulating presentation represents a first formal step toward the start of future cooperation between COSMO and the other European consortia on Limited Area modelling.

The presentation of F. Bouttier was followed by the presentation of M. Baldauf about the status of LMK project. Even if LMK is a DWD project, the high impact of this project on the future development of LM is obvious as regards its foreseen future implementations at higher resolution (cloud resolving scales).

With regard to COSMO activities, the meeting was divided into the two usual sessions: the session dedicated to the reporting and discussion about past activities and session devoted to the discussion and planning of the future work packages.

The status of the different work packages and related developments have been presented for each of the six working groups. The WP Coordinators made the introductory presentations followed by some specific talks over selected scientific contributions. Each working group included a poster session (a total of about 20 posters) to allow each scientist to present relevant activities carried on during the year.

The second part of the meeting was dedicated to the planning of future COSMO activities. After the introductory presentations about the general guidelines and goals by D. Frühwald and T. Paccagnella, the basis for the discussions have been illustrated by the coordinators before starting the separate meetings of the six working groups where detailed work plans have been set-up.

The general COSMO Goals 2005 to be considered during the activity planning are:

- Improvement of LM system at the current resolution.
- Doing high resolution forecast at the meso-γ scale.
- Enhance use of remote-sensing data in data assimilation.
- Development of ensemble systems based on LM.
- Improve internal exchange and communications.
- Improve exchange with other consortia.

In parallel with the working group session, the STC members met for the 12th STC meeting.

The last part of the meeting, the plenary session, started with the presentation of the workshop outcomes and planned activities have been described and discussed. The activity lists are available on the COSMO web site member area.

International and national projects related to COSMO have been also illustrated during the last part of the meeting.

The new structure of the future general meeting has also been discussed. The SPM has been charged to set up a proposal to be discussed and approved at the next December STC meeting.

Figure 16: Participants at the 6th COSMO General Meeting 22-46 September 2004, held in Milano, Italy.

The meeting was closed by Dieter Frühwald who showed appreciation to UGM for the successful organization of the meeting.

(8) 12th Meeting of the COSMO Steering Committee

Dieter Frühwald opened the meeting on welcoming all the participants to the meeting. Prof Sorbjan represented the General Director Prof Zielinski (IMGW).

Mathias Rotach on behalf of the directorate of MeteoSwiss and the other members of the STC congratulated HNMS for the successful meteorological support to the Olympic Games in Athens. Patrizio Emiliani from UGM was nominated as the new WG5 coordinator (Verification and Case Studies). The STC approved the proposal that a representative from those Partners, who do not hold a WGC position, should take part to the WGC meetings.

A new structure of the COSMO General Meeting will be designed. The STC discussed introducing of a *mentors program* for young scientists in countries participating in COSMO. DWD, MCH, and perhaps HNMS will consider hosting short visits, offering working places, mentors at their institutes, and financial support (if required) for such a *visiting scientist program*.The program will be coordinated by the Working Group Coordinators.

Mathias Rotach invited the COSMO scientists for the next COSMO General Meeting at the end of September 2005 to Switzerland.

(9) 13th Meeting of the COSMO Steering Committee

As usual for the December meeting, the activity plan proposed for the COSMO year 2004-2005 was discussed in detail. Activities have been approved and priorities confirmed. Several suggestions and comments have been formulated by the STC to be transmitted to the WG coordinators by the SPM.

The proposal for a new organization of the COSMO general meeting has been presented by the SPM; the proposal has been discussed and the new structure finalized. Further comments and remarks from the WP coordinators and from scientists will be collected before the final approval.

Mathias Rotach invited for the next General Meeting from 20-23 September 2005 to Switzerland, probably in Zürich.

Other items discussed, and all the outcomes, are available in the minute on the member area of the web site.

Since Dieter Frühwald and Georgios Sakellaridis will leave the STC in summer 2005, because of their retirement, an additional meeting of STC will be organized before July 2005 to introduce the new STC members.

(10) WG3-WG5 Joint Meeting

The members of Working Group 3 for Physical Aspects and of Working Group 5 for Verification and Case Studies met in combination with the LM User Seminar on 9 March 2005 in Langen, Germany.

(11) WG1-WG6 Joint Meeting

Also in connection with the LM User Seminar, WG1 and WG6 organized a joint workshop, where the different *Operational Applications* of some partners have been presented. Of special interest was the setup of a data assimilation suite without using a database system (as DWD uses it). Other points of discussion were the processing of satellite data and the external parameters necessary for LM. There are various products coming from satellites and also several software packages to process the satellite data. It would be a good thing if COSMO could nominate a *Satellite Specialist* who should get an overview over these topics. At DWD, the program for producing the external parameters has been modified and enhanced to process more global data sets. It was discussed whether a web interface could be used to access this program and the necessary data sets, so that the COSMO partners could produce their own external parameter sets, if wanted. At MeteoSwiss there is an interest to also test other global data sets, e.g. the ECOCLIMAP set. In the afternoon also the status of the work packages of WG 6 has been discussed.

7.2 Guest Scientists

During May 2004 Jürgen Steppeler from DWD again visited the research group of J. Klemp and B. Skamarock at NCAR in Boulder (USA). Various numerical aspects, especially higher-order spatial disretizations and implicit methods, have been investigated.

7.3 Internal Visits

Francesca di Giuseppe, Tiziana Paccagnella from ARPA-SIM and Blazej Krzeminski from IMGW visited the assimilation group at DWD (Christoph Schraff) to coordinate the activities on 1DVar assimilation of satellite data.

Heinz Bitzer from AGeoBW visited ARPA-SIM for one week to work with Davide Cesari on the implementation of a common LM_Z library.

Giovanni Bonafè from ARPA-SIM visited Matthias Raschendorfer (DWD) to start a cooperation about the boundary layer and the surface layer scheme.

Mathias Rotach and Andrè Walser from MeteoSwiss visited ARPA-SIM for two days to start the planning of the MAP D-Phase project.

Andrè Walser from MeteoSwiss visited ARPA-SIM for a week to discuss various issues of the COSMO-LEPS.

Theodore Andreadis and Euripides Avgoustoglou from HNMS visited MeteoSwiss for a week to have support for the management of the LM data assimilation system.

7.4 Upcoming COSMO Meetings

The following COSMO workshops and meetings are planned for 2005.

3-4 May 2005: 10th Meeting of the Working Group Coordinators
at DWD, Offenbach (D)
In this meeting, the progress of the WPs will be discussed with emphasis on problems and delays with respect to the original schedule of the activities. The agenda of the next COSMO General Meeting will be finalized. Minutes of this meeting will be posted on the member area.

June 2005: 14th Meeting of the Steering Committee
at DWD, Offenbach (D)
This will be an extra business meeting. Dieter Frühwald and Georgios Sakellaridis will introduce the new STC members who are going to represent Germany and Greece after their retirement.

September 2005: Meeting of the Working Group Coordinators
at ARPA-SIM, Bologna (I)
The exact date will be defined during the previous WGC meeting. During this meeting the different activities will be analyzed and discussed to have a clear picture of achievements and problems. The goals for the next COSMO year will be drafted as guidelines to be further discussed during the different WG workshops to be held the day before the general COSMO meeting. The last modifications to the agenda will be also defined.

20-23 September 2005: 7th COSMO General Meeting
at MeteoSwiss, Zürich (CH)
Progress Reports from the Working Groups; presentations of results from the work packages; discussions and set-up of a scientific work plan for the next period.

September 2005: 15th Meeting of the Steering Committee
at MeteoSwiss, Zürich (CH)
Regular business meeting in connection with the General Meeting.

6-8 March 2006: LM User Seminar
at DWD, Langen (CH)

7.5 Announcements

This section lists a number of meetings which are of specific interest for active participation. Of course, this list is by no means complete.

First SRNWP-PEPS Workshop
6 April 2005, Bologna (Italy).

Second SRNWP Workshop on Short-Range EPS
7-8 April 2005, Bologna (Italy).

4th WMO Symposium on Data Assimilation
18-22 April 2005, Prague (Czech Republic).

Conference on Regional Weather Predictability and Modelling
20-22 April 2005, Trieste (Italy).

General Assembly 2005 of the European Geosciences Union
24-29 April 2005, Vienna (Austria).

NEC Special Interest Group on Meteorological Applications
24 May 2005, Exeter (UK).

MAP Meeting 2005 and 28th International Conference on Alpine Meteorology
23-27 May 2005, Zadar (Croatia).

3rd SRNWP Workshop on Statistical and Dynamical Adaptation
1-3 June 2005, Vienna (Austria).

15th ALADIN workshop
6-10 June 2005, Bratislava, Slovakia.

ECMWF Workshop on Representation of sub-grid processes using stochastic-dynamic models
6-10 June 2005, Reading, UK.

15th AMS Conference on Atmospheric and Oceanic Fluid Dynamics
13-17 June 2005, Cambridge, MA (USA).

International Supercomputer Conference
21-24 June 2005, Heidelberg (Germany).

21st AMS Conference on Weather Analysis and Forecasting
17th AMS Conference on Numerical Weather Prediction
1-5 August 2005, Washington, D.C. (USA).

ECMWF Seminar - Global Earth-System Monitoring
5-9 September 2005, Reading, (UK).

WWRP Symposium on Nowcasting and Very Short Range Forecasting
5-9 September 2005, Toulouse (France).

Computing in Atmospheric Sciences Workshop
11-15 September 2005, Annecy (France).

7th ECAM Conference & 5th EMS Annual
12-16 September 2005, Utrecht (Netherlands).

2005 EUMETSAT Meteorological Satellite Conference
19-23 September 2005, Dubrovnik (Croatia).

27th EWGLAM and 12th SRNWP Meeting
3-6 October 2005, Slovenia.

12th AMS Conference on Mesoscale Processes
24-28 October 2005, Albuquerque, NM (USA).

32nd AMS Conference Radar Meteorology
24-29 October 2005, Albuquerque, NM (USA).

6th SRNWP Workshop on Nonhydrostatic Modelling
31 Oct - 2 Nov 2005, Bad Orb (Germany). Special topic: Convection resolving models

ECMWF/NWP-SAF Workshop on Bias estimation and correction in data assimilation
8-11 November 2005, Reading, (UK).

ECMWF 10th Workshop on Meteorological Operational Systems
14-18 November 2005, Reading, (UK).

8 Results and Methods of Model Verification

The operational verification results for the LM forecasts at various COSMO meteorological centres, both for near-surface and upper-air parameters, are summarized in this section. More detailed verification results are presented on a quarterly basis at the COSMO web-site. In this section are also included research oriented contributions related to the development and test of new methods of model verification, including the use of high-resolution non-GTS data, remote sensing data from GPS-satellites and radar composite data.
Most of the papers included in this section are write-ups from the COSMO annual meeting 2004 in Milano (I).
Many thanks to all of you who provided contributions for the present issue of the Newsletter.
The numbering of equations and figures in this section refers to each paper.

Before continuing with the contributions, we summarize shortly some conclusions on model deficiencies from the recent verification results as well as from diagnostic evaluations and from case studies.

Model Deficiencies

From the verification results for the last year, 2004, we can summarize some basic problems:

- The mean diurnal cycle of 2m-temperature still shows too rapid increase during early morning and too rapid decrease in the afternoon (for both the old and new turbulence schemes) During evening and night-time, the 2m-temperature has a quite large cold bias, especially during winter; this effect is less pronounced with the new model version (using the TKE turbulence scheme, surface layer scheme and the soil moisture analysis), but is still a problem.

- The diurnal cycle phase of the 2m-dewpoint-temperature is relatively well by the model even if the diurnal wave amplitude is not so good. The improvement in the diurnal cycle is due to the new TKE and surface layer scheme.

- 10-m winds generally appear to be underestimated on mountain stations and especially during the night, for low altitude stations as well as there is a constant overestimation of wind gusts.

- Cloud cover cycle is not well reproduced, generally overestimated (comparison SYNOP and METEOSAT VIS Channel), particularly there is an overestimation of high cloud cover. In the diurnal cycle of total cloudiness (especially in Spring and Summer) there is a mostly negative bias independent on the season.

- The mean daily cycle of both total cloudiness and precipitation is not well represented. Especially, during the summer the model shows too early onset of convective precipitation and too rapid increase of convective precipitation during afternoon. In Summer there is a too strong diurnal cycle on the mountain gridpoints (due to a too pronounced convection at daytime) and the daily maxima are forecasted too early.

- Low precipitation amounts appear to be overestimated by the model. Over regions with complex and steep topography (especially over the Alps and Appenini), the simulated precipitation patterns are still not very satisfactory and still show great precipitation amount upwind and an underestimation of rainfall downwind mountain chains.

- The integrated water vapor content is underestimated (as verified with GPS data) and shows a seasonal cycle with a greater negative bias in summer and in complex terrain (probably due to height differences).

- The temperature vertical profiles (as verified with TEMP soundings) show a cold bias from the surface up to 750 hPa (mainly during summer season) and a small positive one above 500 hPa. The mean error in wind speed is small, with a generally positive bias in the boundary layer and negative bias above 800 hPa. The relative humidity profiles give generally a positive error up to 700 hPa, above this level they seem to systematically be biased towards positive values. The two model set-ups, LM and LAMI (driven by the same boundary conditions), show a similar drop-off of the near-surface geopotential at the 48 h forecast range.

- Statistical verification results have shown that the enlargement of the domain have a measurable negative impact on LM forecast skill. In particular the wind vector and the MSLP have the worst scores after T+24h. It seems that LM dynamics does not give a good representation of the meteorological evolution in the larger domain.

At the recent COSMO meeting, new work packages have been defined to investigate these problems and to find short-term solutions as well as to improve effectively the model (medium and long term solutions) with the verification of new LM versions, originating from latest development within WGs 1-3, made on predefined set of test cases collected for this purpose.

Progresses on LAMI, LM-DWD, aLMo verification over Northern Italy

M. Turco, E. Oberto, P. Bertolotto

ARPA Piemonte, Italy

1 Comparative high resolution verification over Piedmont

1.1 The method

In this section we compare the performances over Piedmont of the three versions of LM (LAMI, LM-DWD, aLMo), using cumulated precipitation maps for each season from June 2003 to November 2004 and objective methods of verification using statistical indices. In this kind of verification we consider only Piedmont region because of the high density, spatial homogeneity, and high operativeness percentage of the observational network.

This non-GTS network is very dense and it is composed by more than 350 rain gauges. In order to obtain the cumulated QPF maps, we use ordinary Kriging techniques to interpolate the observed values over Piedmont, taking into account only the rain gauges with a 100% percentage of valid data in a season ($\sim$ 250 stations). In Fig. 1 we show the percentage of valid data over the whole considered period.

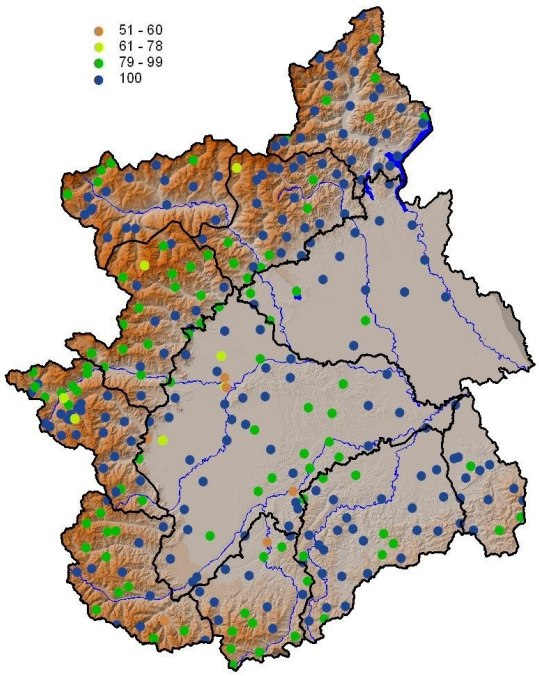

Figure 1: Percentage of rain gauges valid data used for the verification over the whole period and Piedmont warning areas.

The observed precipitation in each season from June 2003 to November 2004 is compared with the forecasted cumulated precipitation in order to obtain a visual comparison of the three versions of LM (LAMI, LM-DWD, aLMo) in terms of overestimation and underestimation. We consider the 24h cumulated precipitation every day for the first 24h of forecast time.

At the same time we perform an objective verification with statistical indices (BIAS, ETS) among the three model versions and the observations. We consider eleven basins, with mean size of 3000 km^2 that represent groups of neighboring hydrological catchments used as warning areas (see Fig. 1).

We average 24h forecasted and observed rain amounts over these basins in order to obtain contingency tables and statistical indices from June 2003 to November 2004. We compare the results fixing the 24h threshold and calculating the contingency tables season by season (using the first and the second 24 hours of forecast time).

In order to compare two model versions, a confidence interval is necessary to assess the real differences between skill scores. This is computed using a bootstrap technique, first developed by Hamill; for an exhaustive description of the method see Hamill, 1999. This test requires that the time series considered have negligible autocorrelations. Spatial correlation of data is taken into account by calculating the scores without considering any geographical partition of the data; time correlation is considered by choosing an accumulation period (24h) larger than the time correlation scale (as shown in Accadia et.al., 2003).

1.2 Main results

In Fig. 2 the seasonal cumulated precipitation (observed and forecasted) are exhibited.

From the maps of Fig. 2 we can derive different results:

- globally the best performances are in fall 2003, fall 2004 and over the plains;
- better performances of LM-DWD in summer (jja 2003 especially) with respect to the others, presumably because of the soil moisture external analysis (it has to be pointed out that in summer 2003 all the versions used the I.C. and B.C. from GME-DWD);
- there is a constant overestimation of LAMI and aLMo over the North-Western Alpine region of Piedmont;
- LM-DWD overestimated over the North-Western Alpine region too, but not in summer 2003 and not after the introduction of the prognostic rain scheme (summer 2004 and fall 2004);
- in summer 2004 aLMo dramatically overestimated.

In addition we can look at the seasonal model performances using statistical indices. In Fig. and the three versions are compared season by season in terms of BIAS score and Equitable Threat Score for a fixed threshold of $10mm/24h$. We consider the average precipitation values over the hydrogeological basins shown in Fig. 1. The error bars in Fig. and indicate 2.5th and 97.5th percentiles of resampled distribution, applied to the "reference" model. Note that the bootstrap technique is symmetric: the "reference" model could be the "competitor" model and viceversa. The score difference is statistically significant if it lies outside a given confidence interval (95% in this case) on the PDF produced by means of a bootstrap resampling technique.

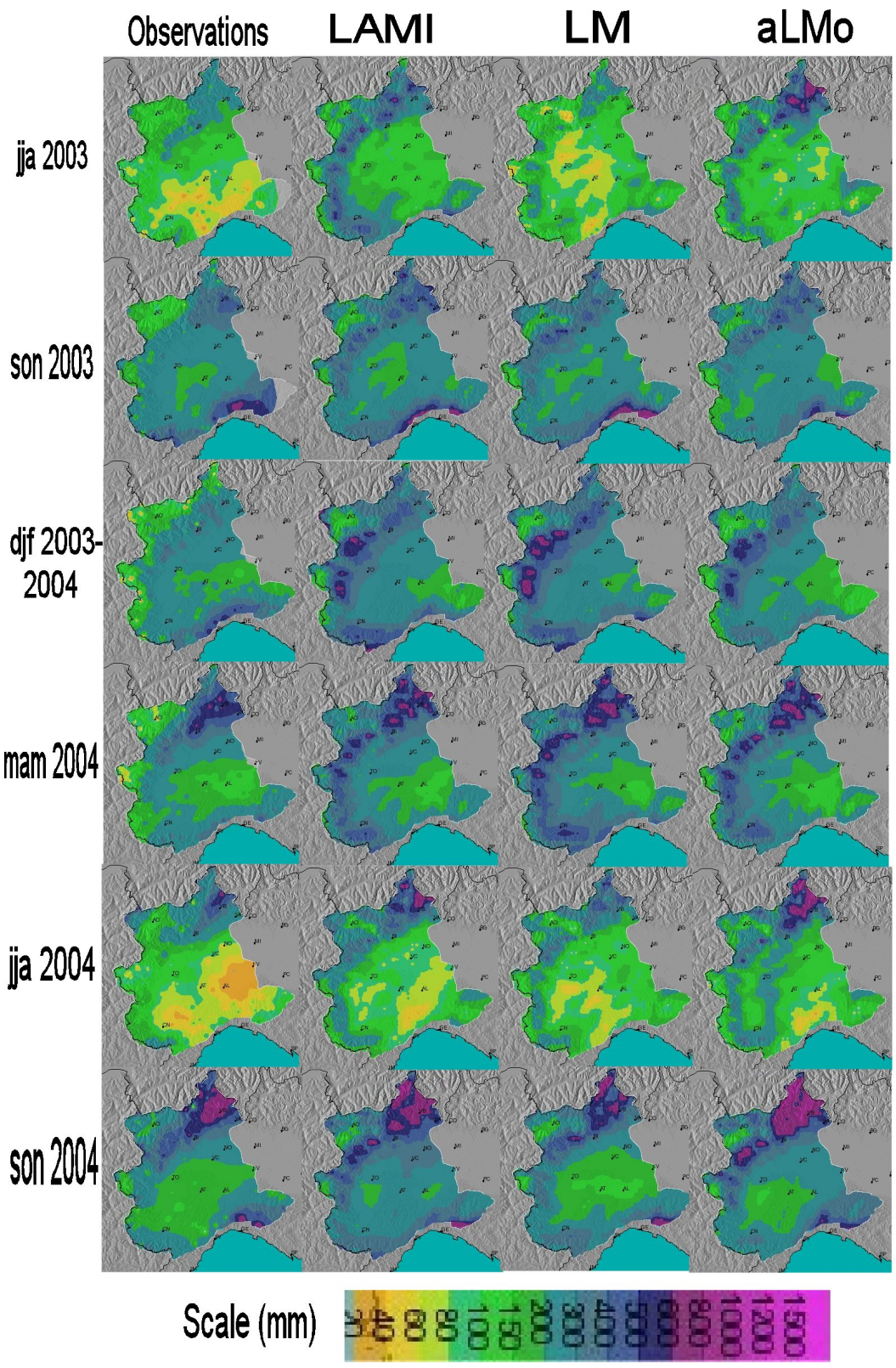

Figure 2: Comparison between observed and forecasted precipitation for each season in the period 200306-200411

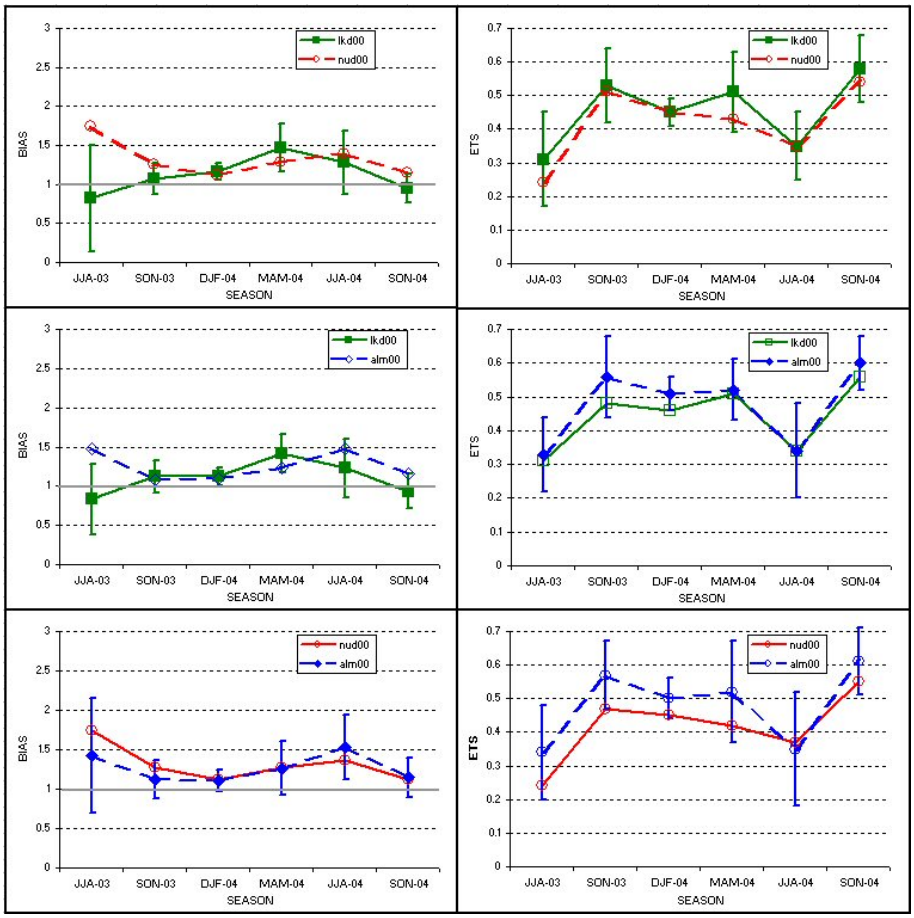

Figure 3: Seasonal trend of BIAS and ETS in the period 200306-200411 – Threshold=$10mm/24h$ – Forecast time: $00/+24$. The error bars indicate the 2.5th and the 97.5th percentiles of resampled distribution, applied to the "reference" model.

In the first 24 hours (day 1) of forecast time we note that:

- generally the model tends to overestimate the precipitation;
- globally the worst performances are in summer;
- also in this case we confirm the behavior of LM-DWD in summer 2003, presumably because of the soil moisture external analysis;
- LM-DWD recorded the best BIAS score also in fall 2004, this can be due to the presence of the prognostic rain scheme (aLMo introduced it only at the end of November 2004);
- there are no significant differences in ETS plots, with the exception of aLMo superior ETS values in some seasons (son-2003, djf-2004).

Regarding the second 24 hours (day 2) of forecast time, the results are:

- globally, as seen for the first 24 hours of forecast time, the worst performances are in summer;

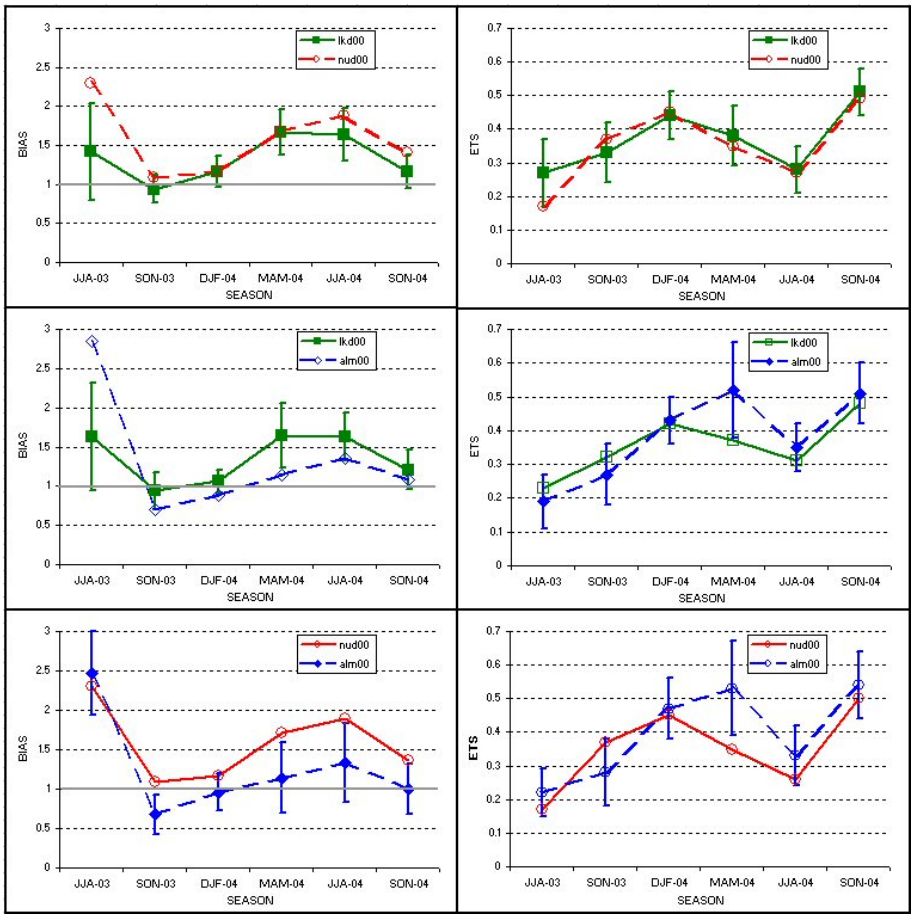

Figure 4: Seasonal trend of BIAS and ETS in the period 200306-200411 – Threshold=$10mm/24h$ – Forecast time: $+24/+48$. The error bars indicate the 2.5th and the 97.5th percentiles of resampled distribution, applied to the "reference" model.

- aLMo gives results better than the others in terms of BIAS score in all the seasons with the exception of summer 2003, this may be due to the IFS initial and boundary conditions;
- in summer 2003 LM-DWD showed the best scores;
- no significant differences in the ETS comparison, except for the superiority of aLMo in spring 2004.

2 Comparative high resolution verification over Northern Italy

2.1 The method

The aim of this section is to compare the performance of the three model versions (aLMo, LAMI, LM-DWD) over a common domain composed by 47 meteo-hydrological basins (see Fig. 5) of Northern Italy, in which fall 1023 station points (see Fig. 6). Further, we summarize the main results obtained during the last two years, presenting only the most representative and significant outcomes. We take into account a common period in which

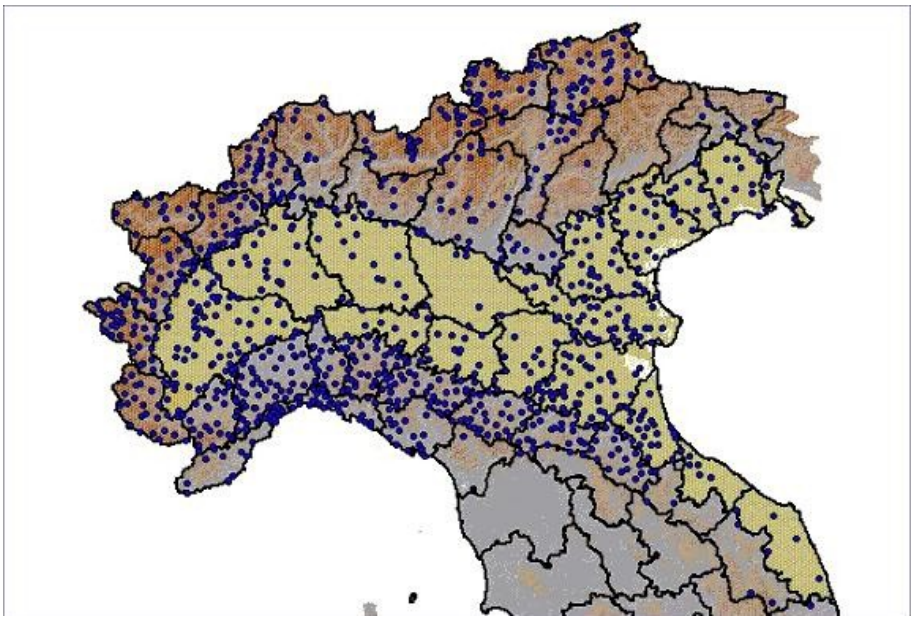

Figure 5: Map of Northern Italy: 47 meteo-hydrological basins, 30 brown areas representing mountainous basins, 17 yellow areas representing plain basins.

REGION	AVAILABILITY PERIOD	N. OF STAZIONS	AREA (km2)	RESOLUTION (km)	ORIGIN	USE
Piemonte + Valle D'Aosta	Jan '01- Dec '04	352	28700	9	Cosmo Project	used
Liguria	Jan '01- Dec '04	76	5400	8	Cosmo Project	used
Prov. Auton.	Jan '01- Dec '04	88	7400	9	Cosmo Project	used
Prov. Auton.	Jan '01- Dec '04	20	6200	18	Cosmo Project	used
Marche	Jan '01- Dec '04	12	9700	2	Cosmo Project	used
Veneto	Jan '02- Dec '04	89	18000	14	Cosmo Project	used
Friuli	Jan '02- Dec '04	27	7800	17	Cosmo Project	used
Emilia Romagna	Dec '00- May '03	42	22000	23	Cosmo Project	used
	Jun '03- Dec '04	271		9	Cosmo Project	used
Lombardia	Jan'02- Nov '04	88	23900	16	Civil Protection	used
Sardegna	Jan '02- Dec '04	49	24000	22	Cosmo Project	not used/out of common domain

Figure 6: Available Italian dataset table.

all the model versions are available, from June 2003 to December 2004, where we have got a complete dataset for 00UTC runs. Regarding to 12UTC runs, we hold a comparable period of data only for LM-DWD, so we will focus our efforts on 00UTC runs. We calculate skills and scores considering 24h cumulated precipitation averaged over basins for several precipitation thresholds, for +24h and +48h forecast time. In addition, in order to test the model sensitivity over complex terrain and the capability to distinguish a complex orography, we subdivide the 47 meteo-hydrological basins into two big subset, mountain (30 meteo-hydrological basins, Fig. 5 brown areas) and plain (17 meteo-hydrological basins, Fig. 5 yellow areas) areas. Therefore we estimate skill and scores considering 24h cumulated precipitation averaged over these different kind of basins for several precipitation thresholds, for +24h and +48h forecast time. Moreover, in order to evaluate the model changes and improvements, we show seasonal scores with a fixed chosen threshold (5 mm) considering 6h cumulated precipitation averaged over basins.

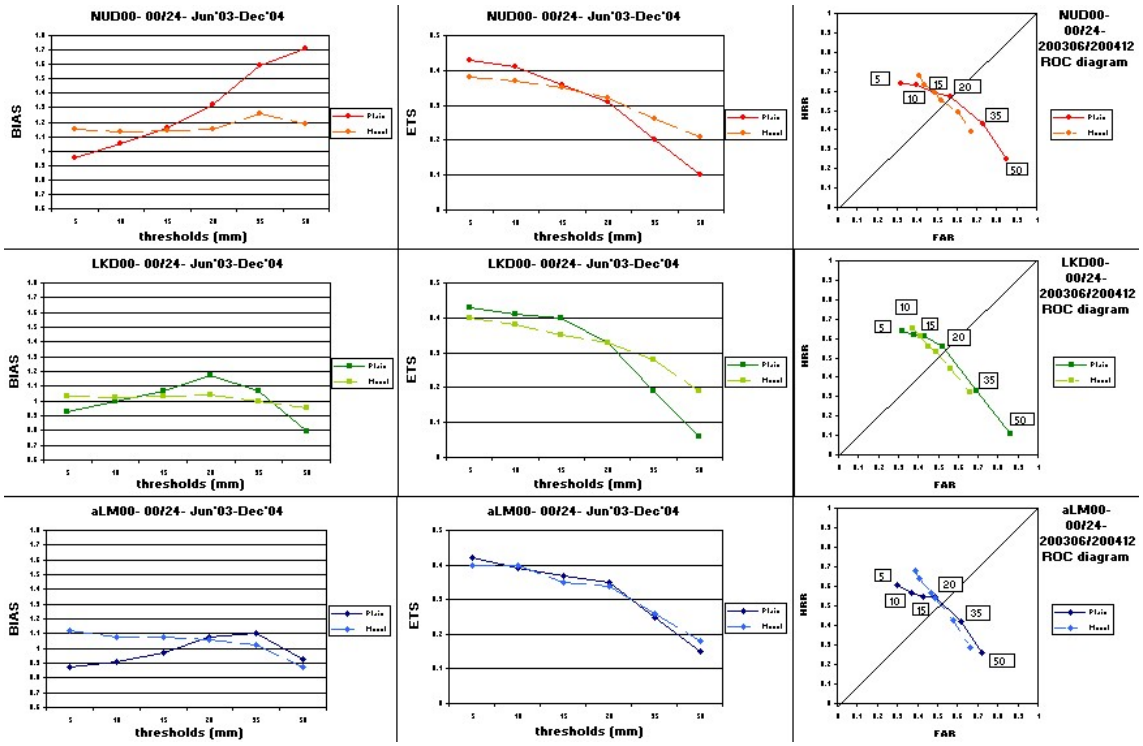

Figure 7: Skill and Scores for $24h$ average cumulated precipitation over mountain and plain basins. Runs 00UTC $+24h$ forecast time. Jun'03-Dec'04.

2.2 Main results

First of all we want to analyze the three model version performance over mountainous and flat basins, with respect to 24h cumulated average precipitation, for +24h (see Fig. 7) and +48h (see Fig. 8) forecast time. We can deduce some main features concerning to the three versions behavior, using statistical indices as BIAS, ETS and ROC diagram:

- the BIAS for small precipitation amount on plain areas is greater than on mountainous areas;
- this trend seem to be inverted as thresholds increase: in fact we generally obtain a greater BIAS on plain than on mountain for high thresholds;
- in particular, with regard to the first 24h, we find a BIAS on mountain more or less constant with respect to threshold and around 1;
- on the other hand, we derive better scores (see ETS and ROC diagram) on plain areas than mountain areas up to $10/15mm$, above these thresholds the trend is inverted.

To summarize, we note a different behavior in the model performance over mountain and plain zones: in the first case there is probably a balance of the up-wind/down-wind orographic effect that seems to compensate the underestimation/overestimation systematic error; in the second case the results are worse in term of BIAS especially for medium/high thresholds, but better in term of ETS for low/medium thresholds. In addition, according to the comparative study among the three model versions, we observe a fairly similar scores in term of ETS and ROC diagram, whereas we obtain a different results for BIAS skills, in fact LAMI model tends to overestimate more than the others particularly for high thresholds.

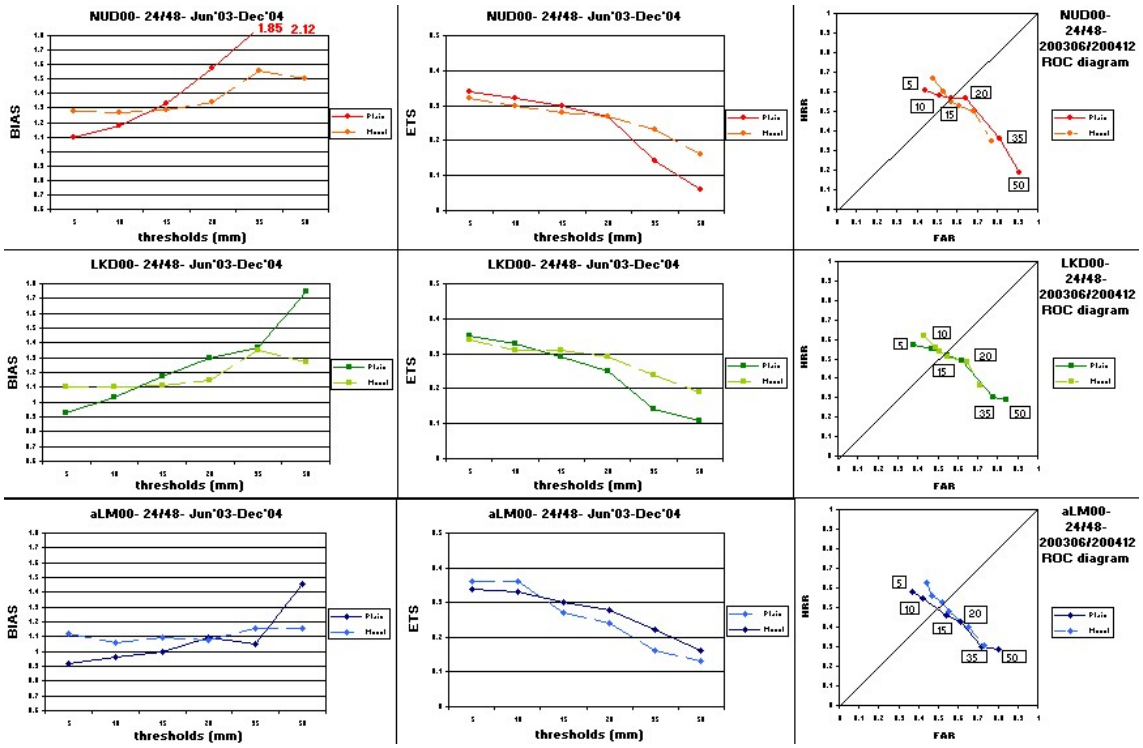

Figure 8: Skill and Scores for 24h average cumulated precipitation over mountain and plain basins. Runs 00UTC +48h forecast time. Jun'03-Dec'04.

Concerning the daily cycle and seasonal trend, we present BIAS and ETS graphs considering 6h cumulated precipitation averaged over basins for a fixed precipitation thresholds (5mm) to investigate the three versions behavior. Some differences exist (see Fig. 9). In particular, regarding to summer 2003, that was an exceptional dry season, we note some remarkable features:

- a similar trend for all the models, with a pronounced diurnal cycle, with a big overestimation in the morning and underestimation around nocturnal hours (this characteristics can be found also in JJA2004);

- during the strong convection peaks, LM-DWD seems to perform better than the others, probably because of the soil moisture analysis, that plays a basic role during summer seasons;

- a very bad ETS, maybe due to a low models capability to localize and predict accurately the precipitation pattern when it is larger the convective contribution.

Further, we note some differences among the model versions initialized by GME and aLMo, which has boundary condition from ECMWF (IFS-frames) since September 2003. In fact aLMo gives the lowest BIAS index for fall 2003, winter and spring 2004, and the highest ETS (at least from winter 2004). It has to be pointed out that LM-DWD BIAS behavior tends to be similar to aLMo behavior during the last two considered season (that is after the introduction of the prognostic rain scheme).

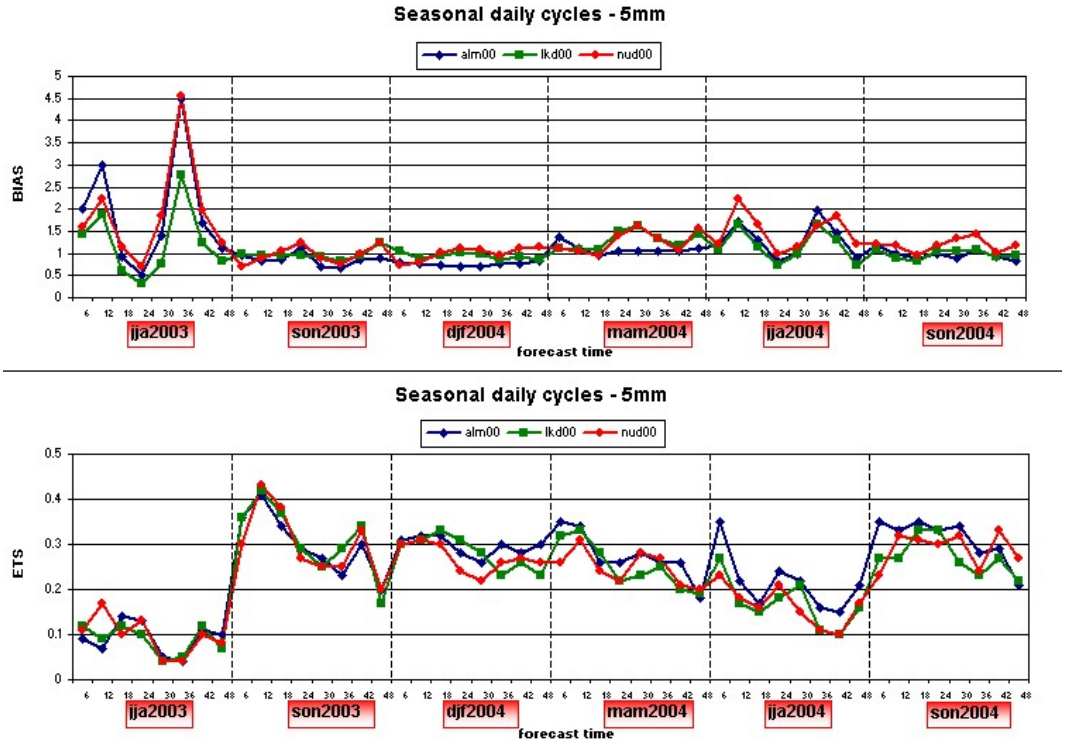

Figure 9: Seasonal daily cycles for 6h average cumulated precipitation. Runs 00UTC. Jun'03-Nov'04. Threshold=5mm

3 General conclusions

The main goal of this report is to compare the performance of the three model versions (aLMo, LAMI, LM-DWD). We consider two common domain (Northern Italy and Piedmont) and a period in which all the model versions are available (from June 2003 to December 2004). The main outcomes are:

- a strong skill dependence on the model changes. In particular aLMo has a trend different from the others, may be due to the IFS initial and boundary conditions. Considering the second day forecast for Piedmont, aLMo gives the best score for all the seasons except for summer 2003;
- LM-DWD gives the best scores in summer 2003 presumably because of the soil moisture external analysis. Good results for the last two seasons considered probably due to the prognostic rain scheme;
- regarding Northern Italy there is a systematic QPF difference among plain and mountain areas; about the eye-ball verification, we note an overestimation of LAMI and aLMo over the North-Western Alpine region of Piedmont, while over the whole mountainous area the results seem to be better, but this may be due to a balance between upwind and downwind effect.

References

Accadia C., Casaioli M., Mariani S., Lavagnini A., Speranza A., De Venere A., Inghilesi R., Ferretti R., Paolucci T., Cesari D., Patruno P., Boni G., Bovo S., Cremonini R., 2003.

Application of a statistical methodology for limited area model intercomparison using a bootstrap technique. *Il Nuovo Cimento*, Vol. 26, Issue 01, p.61, 2003.

Hamill, T.M., 1999. Hypothesis tests for evaluating numerical precipitation forecasts. *Wea. Forecasting*, 14, 155-167, 1999.

Verification Results for LM at DWD

Ulrich Damrath

Deutscher Wetterdienst, P.O.Box 100465, 63004 Offenbach a.M.,Germany

1 Surface weather elements, verification based on SYNOP reports

Verifcation results are presented for stations in Germany with an elevation below 800 m. The following graphics (Figs. 1-4) with time series of forecast quality during the last year show the following remarkable model errors:

Diurnal cycle of temperature 2m:

- A phase shift of maximum temperature is visible. Maximum occurs too early, especially during spring.
- Temperature decreases too rapid during afternoon.
- During winter temperature is generally too low. During night time bias values of more than 1K occur.

Diurnal cycle of dew point 2m:

- The phase of daily wave is well modelled.
- The amplitude shows too wet forecasted values during spring and summer, too dry forecasted values during winter (except noon) and good agreement with observations during autumn.

Diurnal cycle of wind speed 10m:

- Maximum and minimum values are modelled for the time when they occur.
- Too high values are in general modelled for night time.
- Maximum values are correct during Spring.
- Maximum are too high during other seasons.

Diurnal cycle of maximum wind speed 10m:

- The phase of daily wave is well modelled.
- Too high average values are modelled for all seasons and all times of the day.
- Frequency biases are much higher than 1, especially for thresholds of 12 and 15 m/s.

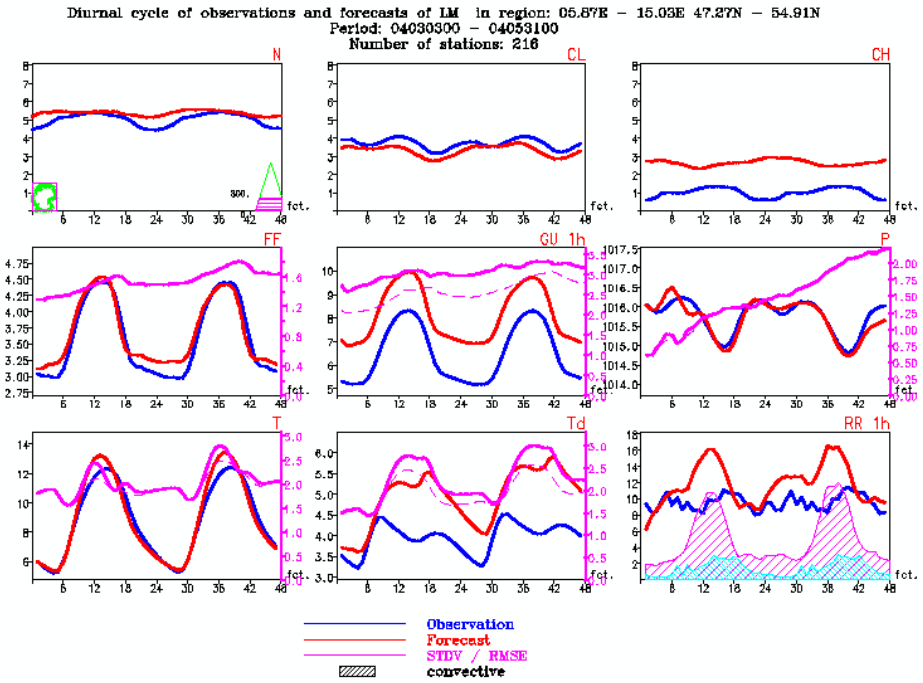

Figure 1: Time series of averaged observations and forecasts Spring 2004.

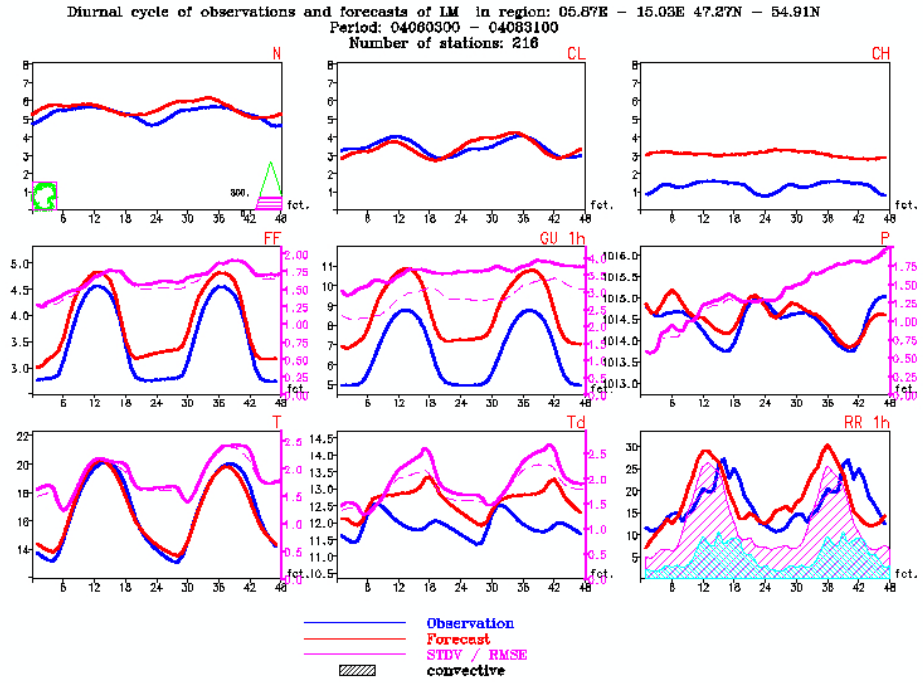

Figure 2: Time series of averaged observations and forecasts Summer 2004.

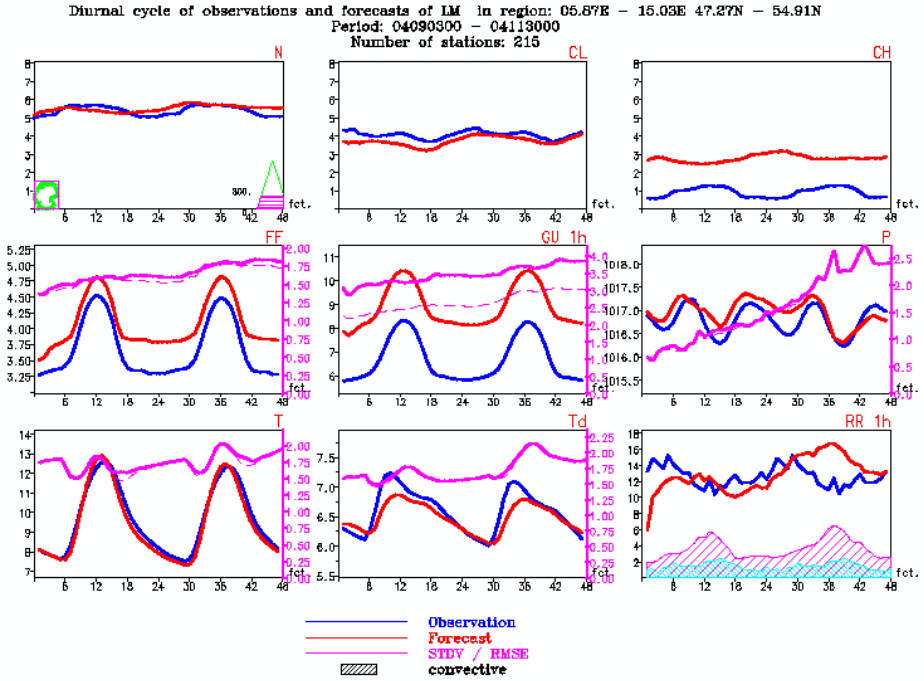

Figure 3: Time series of averaged observations and forecasts Autumn 2004.

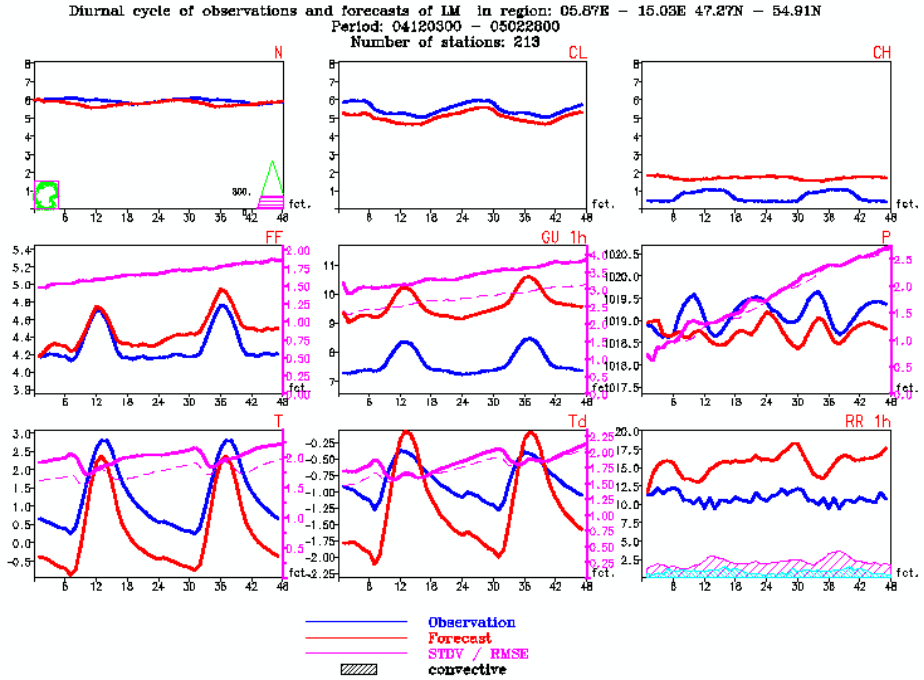

Figure 4: Time series of averaged observations and forecasts Winter 2004/2005.

Diurnal cycle of precipitation:

- The onset of convection (if happens) occurs too early.
- Convective precipitation amount are too high during morning and noon.
- During summer precipitation amount is too low during afternoon and first part of the night.
- An overestimation of precipitation amount around 50% occurs during winter. But his can be related to problems of snow height measurements.

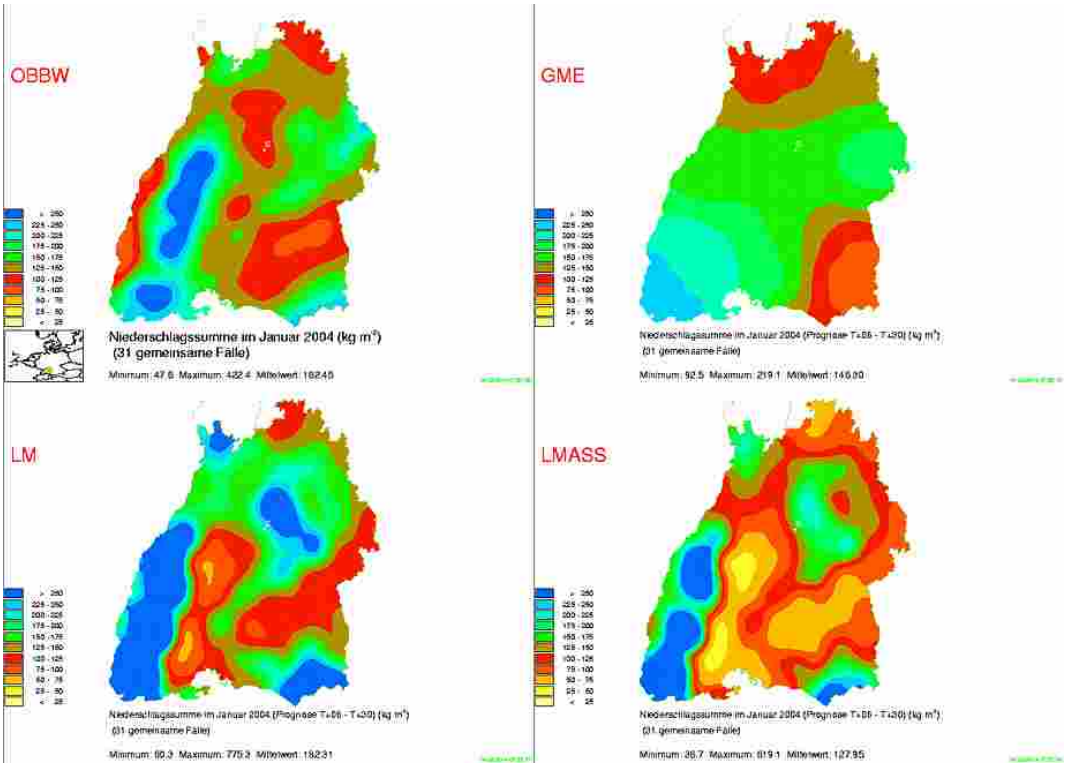

Figure 5: Horizontal distribution of precipitation over the Black Forest January 2004 (OBBW: observation, LM: LM-forecasts, GME: GME-forecasts, LMASS: Assimilation runs (8 forecasts over 3 hours)

2 Verification of precipitation based on measurements with high density network

This type of verification has been continued. The most interesting result is the demonstration of the effect of advected precipitation. This model version was introduced at the end of April 2004 into operational use. Fig. 5 shows the distribution of forecasted and observed precipitation over the Black Forest (Southwest Germany) during January 2004. This typical pattern occured during all months with intense precipitation over this area durng the whole time of operational use of LM. Maximum values were dramatically overestimated by the model. A phase shift of the zone with maximum precipitation towards the windward side of the mountains was modelled and in the areas of the leeward side a more or less strong underestimation of precipitation occured in the model output. With introduction of the advected precipitation this pattern has been changed in the following manner: The maximum of forecasted precipitation is shifted towards the peak of the mountains compared with the

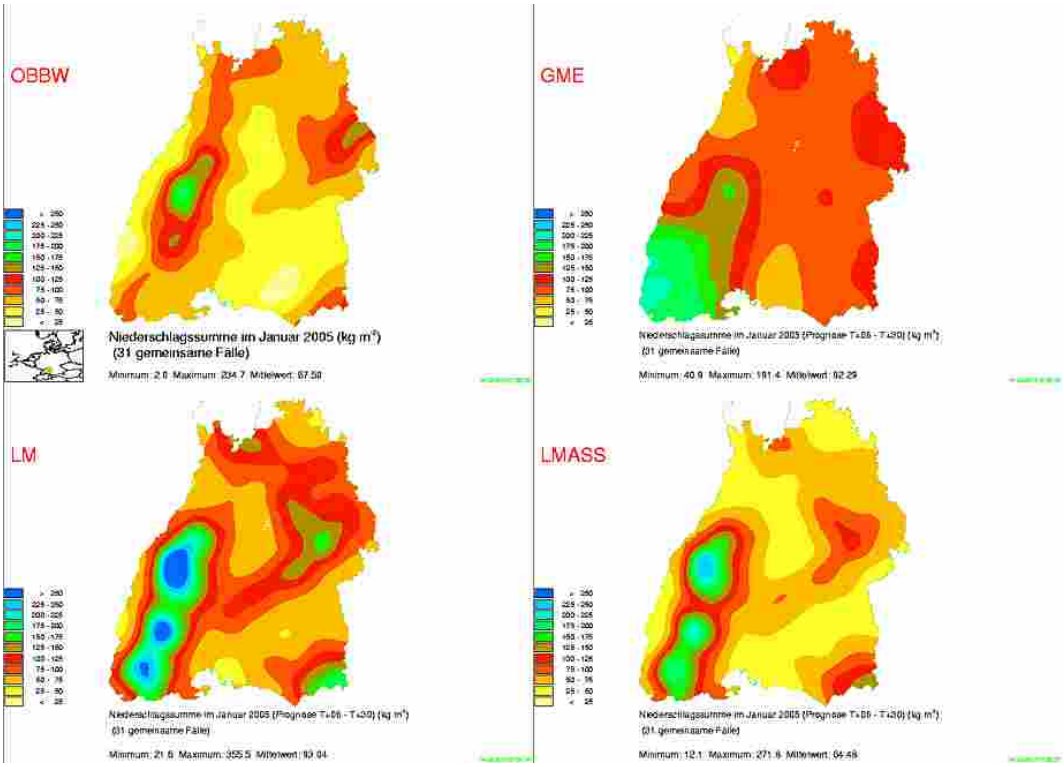

Figure 6: Horizontal distribution of precipitation over the Black Forest January 2005.

results of the years before. The strong underestimation of leeward minimum is damped. The remaining problems are the overestimation of precipitation in general (this could be a typical result for winter due to problems in measurements of fresh snow) and the fact that maximal precipitation amounts still occur in the windward side of the mountains instead near the top.

Verification of LAMI at Synop Stations

Patrizio Emiliani, Alessandro Galliani

(CNMCA), Roma, Italy

1 Introduction

A synthesis of LAMI (the Italian version of LM) verification results for the year 2004 is presented. The surface parameters analysed are 2m Temperature (2m T), 2m Dew Point Temperature (2m TD), 10m Wind Speed (10m WS), Mean sea Level Pressure (MSLP), and rainfall for which verification has been considered only for the period Nov. 2003 - May 2004. The LAMI version here verified is lm_f90 3.5 with initial state given by Nudging data assimilation scheme (see Table 1). These five parameters are not explicit model variables but they are computed through some internal post-processing which may introduce extra errors. Nevertheless, since the internal post-processing is generally based on some diagnostic balance among the model variables, which is derived from physical constraints, it is still possible to have some important information about problems in the formulation and in the configuration of the model itself.

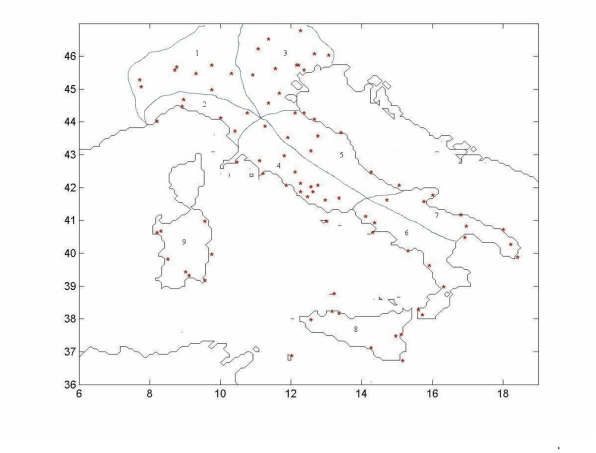

Figure 1: Synoptic Italian network and a classification of Italy in 9 climatological areas.

The observations forming the control data set were collected on 3-hourly basis from synoptic Italian network, including 89 manned stations and distributed over the Italian area. Figure 1 shows the distribution of the stations used to compute verification. Stations were divided in three classes according to geographical location; mountain stations ($>$ 700m), valley stations or inner lowland stations and coastal stations. Station classification has designed in order to check systematic errors related with different geographical and surface conditions. This approach can give two type of results: information about the model ability in reproducing correct surface processes through a correct climatology in different geographical areas and indication of possible source of error through a comparison in different areas. In the following some results will be shown obtained from the verification of daily cycle for 2m Temperature, 2m Dew Point Temperature, 10m Wind Speed, MSLP and for the categorical rainfall verification.

Table 1: *UGM, ARPA–SIM, ARPA Piemonte LM configuration running at CINECA in Bologna.*

Domain size	234×272 gridpoints
Horizontal grid spacing	0.0625^o ($\cong 7$) km
Number of layers	35, base–state presure based hybrid
Time step and integration scheme	40 s, 3 time–level split–explicit
Forecast range	72 h
Initial time of model runs	00 UTC
Lateral boundary conditions	Interpolated from GME at 1h interval
Initial state	Nudging data assimilation scheme, no initialisation
External analysis	None
Special features	Use of filetered topography, new TKE scheme, new surface–layer scheme
Model version	lm_f90 3.5
Hardware	IBM SP pwr4 (using 32 of 512 processors)

2 Daily Cycle

In order to verify the diurnal behaviour of the model, the couples forecast-observation, for which the mean error (ME, forecast minus observation) and the mean absolute error (MAE) have been computed, were stratified according to the hour of the day (3-hourly frequency), the month of the year and the forecast range (day 1 and day 2). Synchronous and co-located couples forecast-observation, independently from the station position, form each sample. In such way systematic errors due to inconsistency in the surface representation of the model (inconsistency in the terrain elevation and in the percentage of the surface covered by water are the main error sources over Italy) are somewhat dumped and the signal of daily and seasonal oscillation is retained.

3 2m-Temperature

Figures 2a, 3a, 4a and 5a show the behaviour of 2m-Temperature forecast error respectively for all Italian stations, for coastal stations, for valley and mountain stations.

A clear diurnal cycle is present in all the figures and for all months in the mean error pattern. All figures, except coastal stations (see Fig. 3a), show a common feature characterized by a cold bias during the cold months (January, February, November and December), more accentuated for mountain sites with values of about -1.5^{o}C.

Coastal ME patterns (Fig. 3a), present, both for day 1 and day 2, positive peaks around sunrise (06 UTC in the cold months and 03 UTC in the warm months) and negative peaks during the afternoon, near sunset, with a cycle amplitude of about 2.5^{o}C in the warm season and about 1^{o}C in the other period of the year. A different behaviour is shown by valley and mountain stations figures where positive peaks occur around midday, with a delay of 3-6 hours respect to coastal station, while negative peaks still occur near sunset.

Concerning the Mean Absolute Error a diurnal cycle is still present in the curve, even if it is not so clear like in ME curves. Minimum in MAE, corresponding to better absolute accuracy, occur in the early morning both for valley and mountain area and in the evening for coastal stations; lower absolute accuracy, that is MAE maximum, occurs for all the sites around midday, 12UTC. Another difference is evident in MAE curves for mountain stations where low values occur in the warm season while the opposite happen for valley and coastal

stations, where maximum MAE values occurs during summer.

4 10m wind speed

In Figures 2b, 3b, 4b and 5b the curves relative to mean error and mean absolute error of 10m wind speed are shown, for a technical reason were not available wind data for May and June. Even if the amplitude is small (less then 1 m/s) a diurnal cycle is present in ME curves. An overestimation of wind speed, positive bias, occurs for valley and coastal stations, more pronounced when dynamical circulation is dominant, that is during the cold months. It is interesting to point out the attention to low MEA values during summer for coastal stations, meaning a good model interpretation of local breeze circulation, but with a general low underestimation of the wind in the warm hours, with negative ME values during late morning and afternoon.

5 2m Dew Point Temperature

In Figures 2c, 3c, 4c and 5c 2m Dew Point Temperature ME is shown. First of all a clear general positive bias is present (Fig. 2c. More in detail, a positive bias occurs for coastal stations (about 0.4^oC in the warm season and more than 0.7^oC in the other periods of the year, see Fig. 3c), and mountain stations (with a bias of 1°C but with a cycle amplitude between 2°C and 3°C, see Fig. 5c). During October an anomaly appear for mountain stations with too low MAE and ME values. Valley stations, on the contrary, didn t present positive bias, during the cold season a negative bias, -0.5°C, is observed. Both, valley and mountain stations (Fig. 4-5c) present a well evident ME diurnal cycle with positive peaks occurring around midday, in phase with maximum MAE values, and minimum values occurring close to sunrise hours.

6 Mean Sea Level Pressure

Figures 2d, 3d and 4d show MSLP mean error and mean absolute error for the year 2004. Mean error curves don t show any diurnal cycle; a positive bias affect the d+1 ME line with exception in December. ME d+2 curve (pink line) shows a different situation, in fact starting with a positive bias at 03 UTC (corresponding at forecast range +27hrs) ME decrease systematically to negative values, meaning a systematic loss of mass in function of time. MAE curves show how the mean sea level pressure is less affected by local circulations or by model physics and is dominated by the atmosphere dynamics; in fact, MAE increases quasilinearly in function of forecast range (for each month, d+1 curve starts with +03 hrs and stops with +24 hrs while d+2 curve starts with +27 hrs to +48hrs forecast range) with a high degradation in MAE values during the months characterized by strong atmospheric motions.

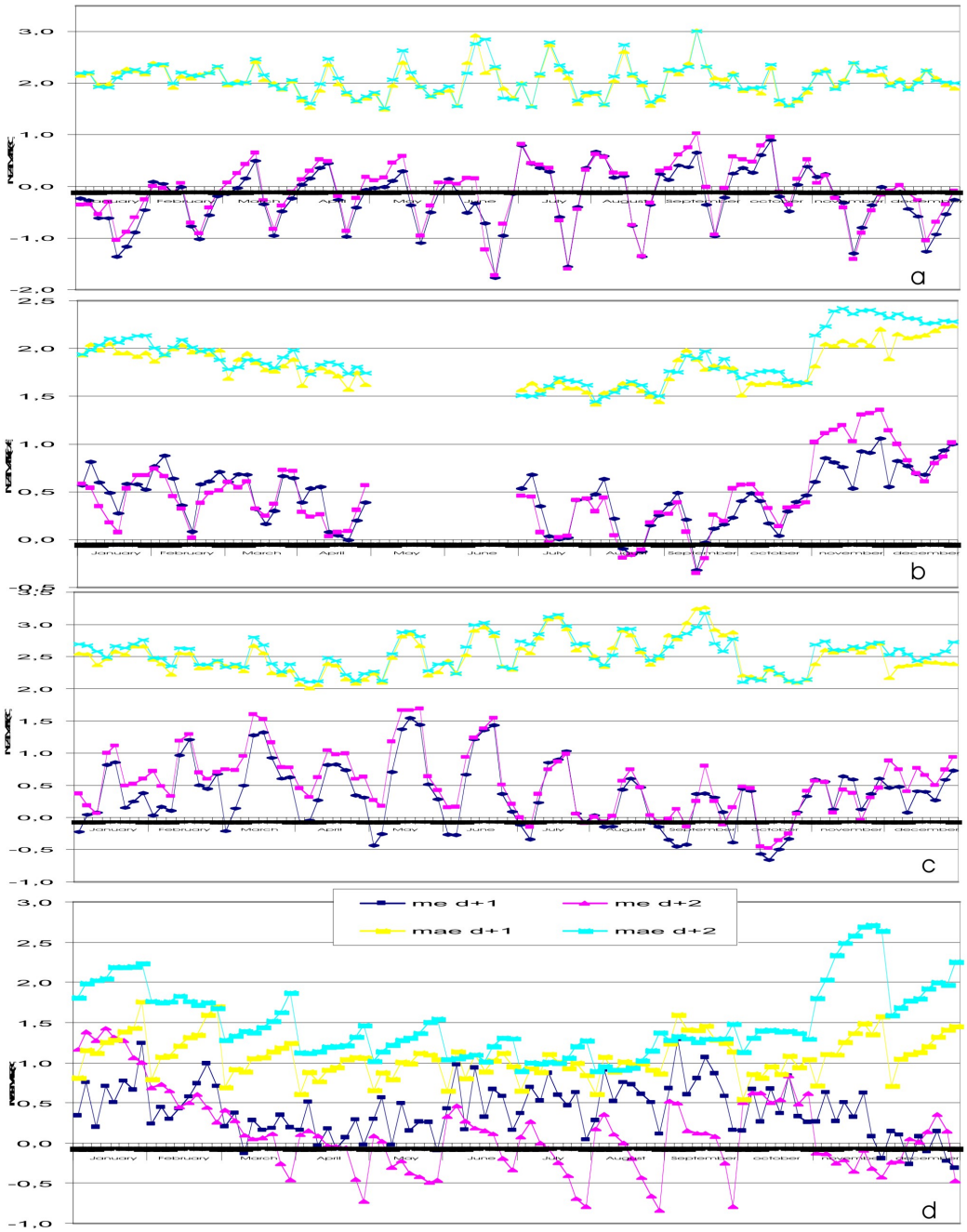

Figure 2: LAMI monthly mean error and mean absolute error of 2m Temperature (a), 10m wind speed (b), 2m dew point temperature (c) and mean sea level pressure (d) for Italian stations, 2004.

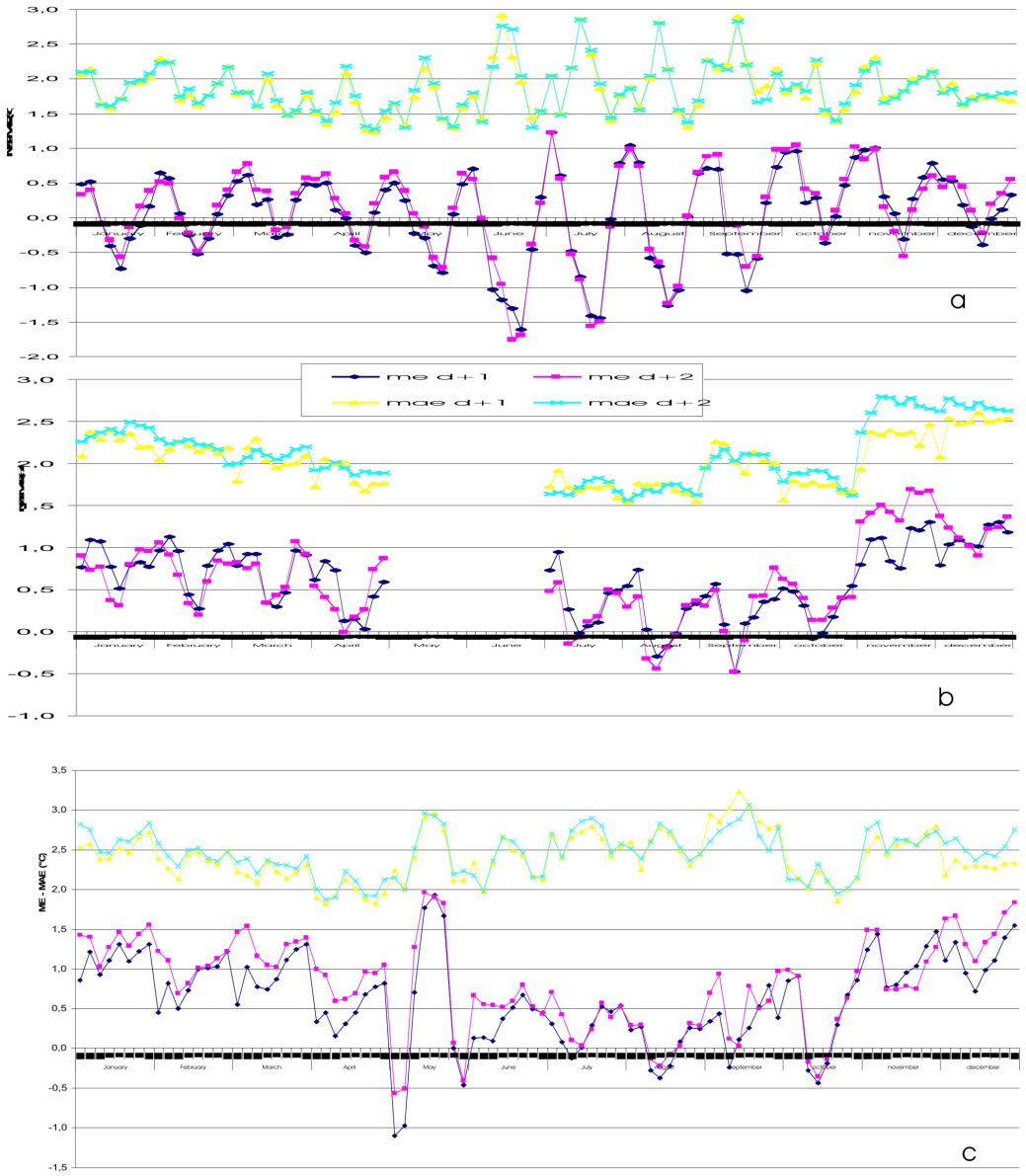

Figure 3: LAMI monthly mean error and mean absolute error of 2m Temperature (a), 10m wind speed (b), 2m dew point temperature (c) for coastal stations, 2004.

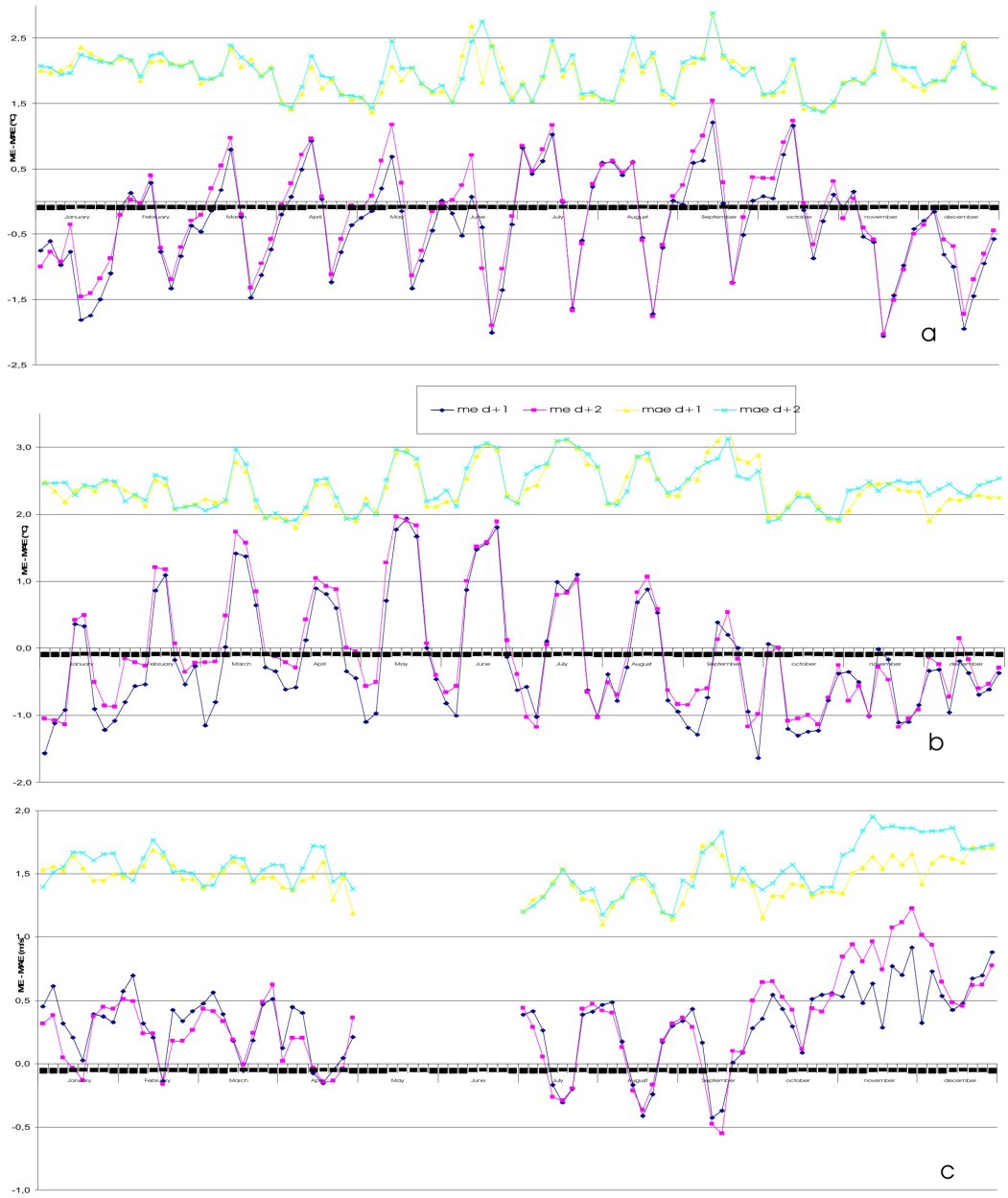

Figure 4: LAMI monthly mean error and mean absolute error of 2m Temperature (a), 10m wind speed (b), 2m dew point temperature (c) for valley stations, 2004.

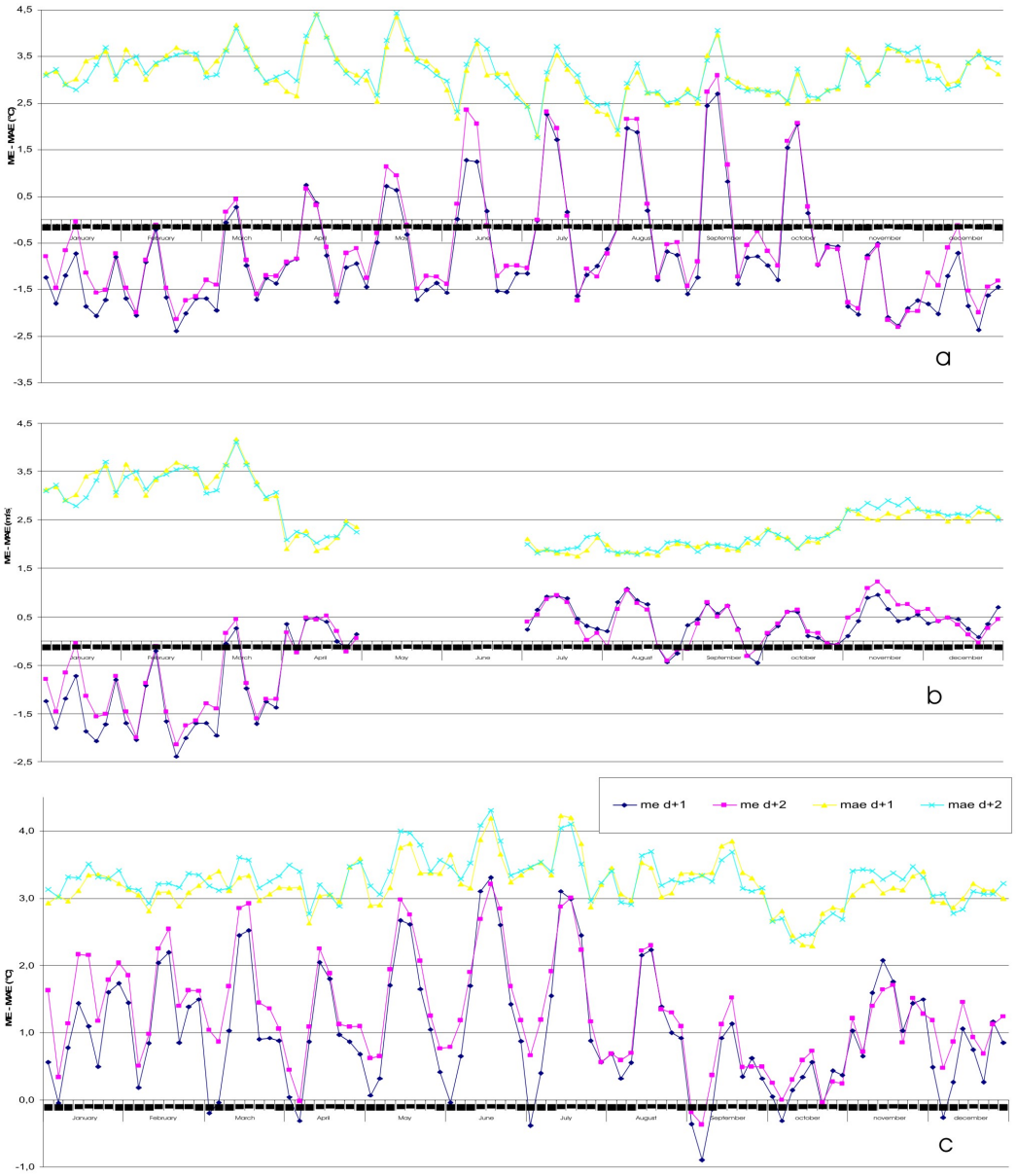

Figure 5: LAMI monthly mean error and mean absolute error of 2m Temperature (a), 10m wind speed (b), 2m dew point temperature (c) for mountain stations, 2004.

7 Precipitation

The verification results for the period from Oct/2003 to May/2004 are summarized in Fig. 6, where FBIAS, TS, POD and FAR scores are presented for all Italian stations, without any stratifications (for stratified precipitation scores see the COSMO web site). Fig. 6a shows a FBIAS comparison between LAMI, 00-UTC run, and ECM global model, 12-UTC run. For low threshold values, until 4mm/day, LAMI shows an overestimation of 20-30% (60% for ECM model). LAMI FBIAS increases with threshold valuesday curve has a small FBIAS increment, showing for high threshold values an overestimation of about 50%, while the second day line increase up to FBIAS value of 2.5, even if for intense precipitation the results coming out from this verification method should be carefully taken in account. Threat Score for 24 hours cumulated rainfall are reported in Fig. 6b. Both models show comparable TS values for d+1 forecast, decreasing in function of thresholds; while d+2 LAMI line shows a more pronounced forecast degradation respect to ECM model.

POD and FAR analysis plots (Fig. 6c) show, for low threshold, higher ECM values respect to LAMI. The obtained results are in agreement with the ECM rainfall overforecast (see Fig. 6a). A different situation appears starting from threshold values of about 10mm/day, where LAMI is characterized by high POD and FAR values. These differences in single POD and FAR analysis disappear considering d+1 POD/FAR ratio (Fig. 6d), that gives comparable values for both models, instead of d+2 forecast for which ECM works better than LAMI.

In the next session, rainfall verifications for the analysed period are presented, considering events due to south-west wind field regime and associated to frontal systems. At the beginning, stations were stratified in five regions: North, Centre, South, Adriatic and Tyrrhenian. Verification results obtained using this kind of stratification are summarized in Fig. 7. As expected, the model shows better performances in respect to the analysis effected without any kind of weather regime filter (precipitation associated to south west flux are well extended and well defined and so are easier to detected by the Model), and the scores for the different areas (North, Cent., South, Adriat. And Tyrrh.) are closer to one each other, even if Central region has better scores.

Considering the same weather pattern (South-West flux), rainfall verification was computed adopting another stations stratification. Italy was divided in 9 areas (see Fig. ugm-fig:1) more or less characterized by the same weather events.

This time a marked difference in the model performances (Fig. 8) associated to the considered areas occurs. Verification scores for day+1 forecast indicate good model performances associated to NW areas (1 and 2 curves) and bad results for the two islands (Sardinia and Sicily, 8 and 9 curves). It is interesting to note how LAMI over Liguria region shows high scores values also for high precipitation thresholds, meaning good spatial and time phase forecast in the development of Genoa Gulf cyclogenesis and the associated weather phenomena.

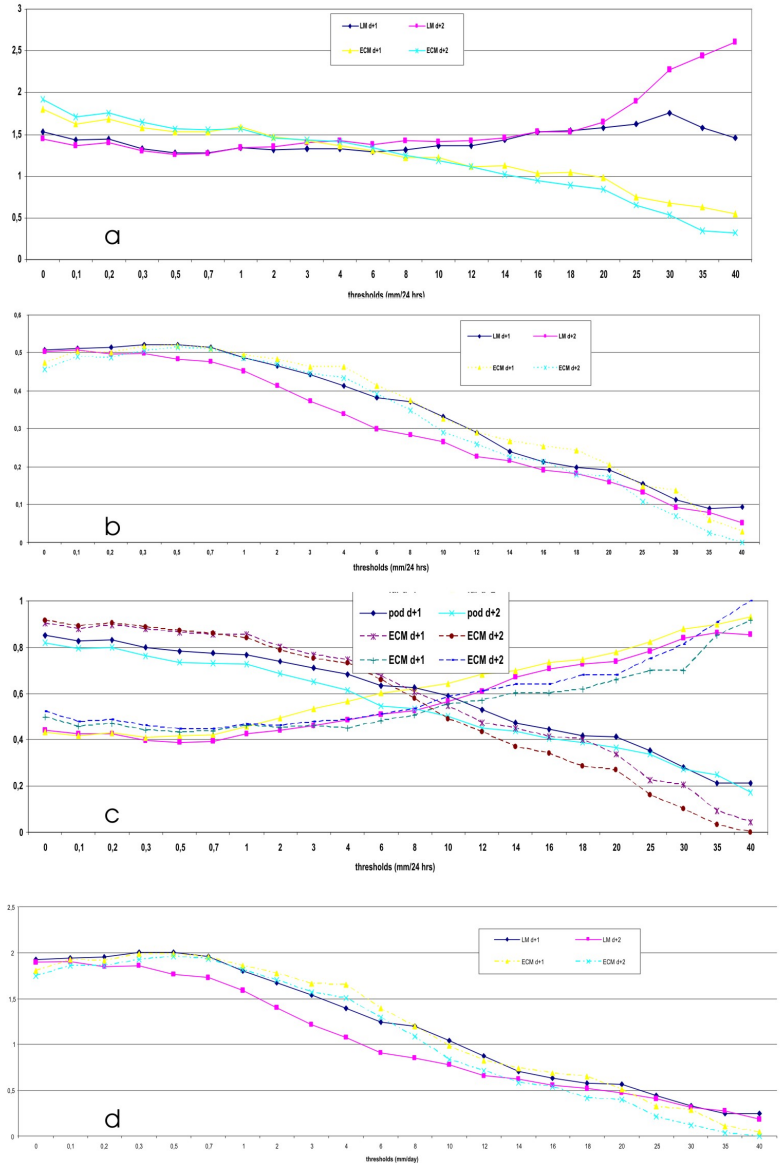

Figure 6: LAMI (00 UTC run) and ECM (12 UTC run) for all Italian stations without any stratification: FBIAS (a), TS (b), FAR-POD (c), POD/FAR (d).

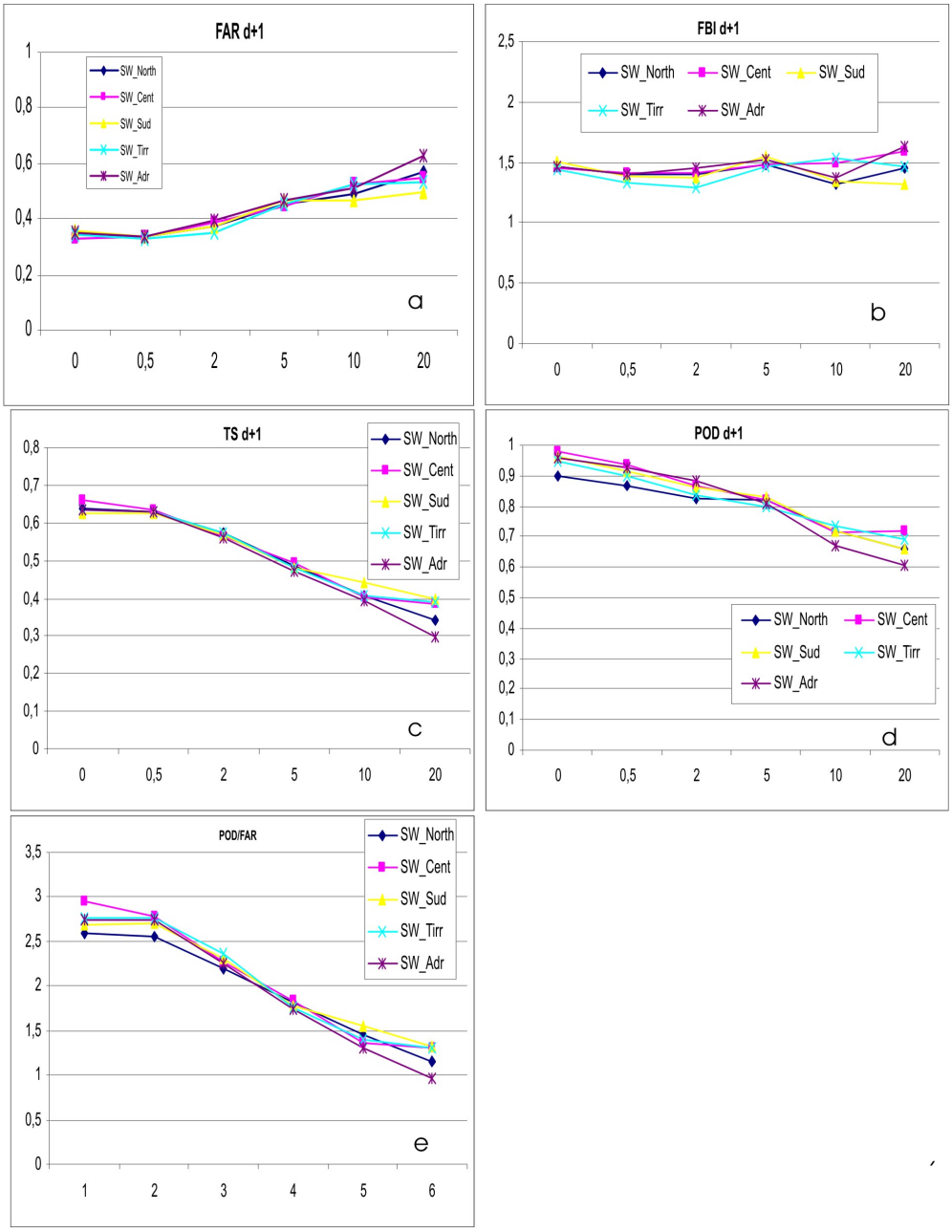

Figure 7: LAMI scores, d+1 cumulated rainfall, for precipitation due to South West fluxes stratifying Italy in five areas: North, Centre, South, Adriatic and Tyrrhenian. FAR (a), FBI (b), TS (c), POD (d), POD/FAR (e).

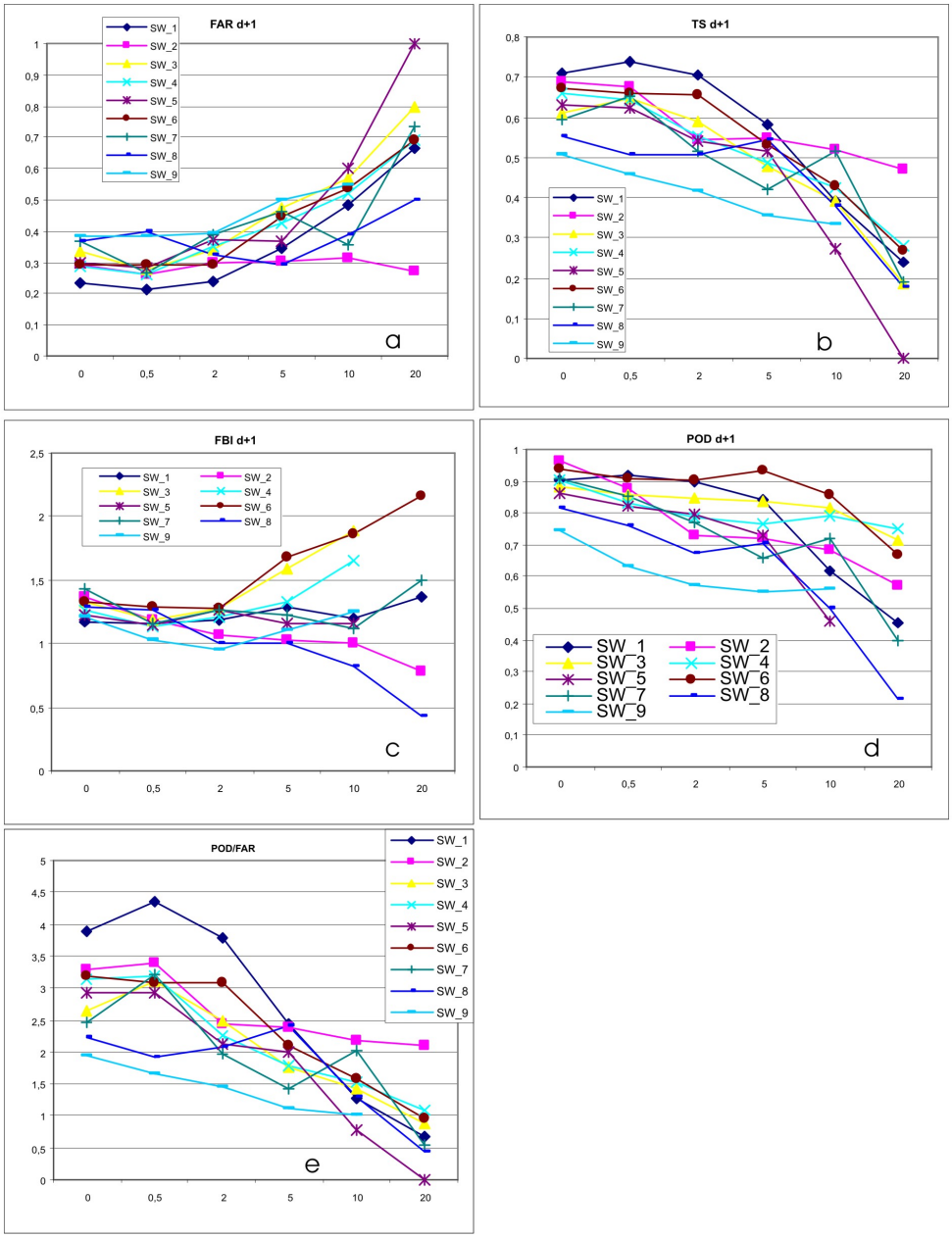

Figure 8: LAMI scores, d+1 cumulated rainfall, for precipitation due to South West fluxes stratifying Italy in nine areas: see 1. FAR (a), FBI (b), TS (c), POD (d), POD/FAR (e).

High Resolution Verification of Daily Cycle over Switzerland

FRANCIS SCHUBIGER

MeteoSwiss, Zürich, Switzerland

The following nomenclature for LM is used in the text below: aLMo means "Alpine Model", the LM version operational at MeteoSwiss and LMD means the operational LM version at DWD. Verification is done with hourly observations from the automated network of MeteoSwiss (ANETZ: 72 stations) and is stratified for 3 different height ranges (gridpoints < 800m, 800–1500m and > 1500m).

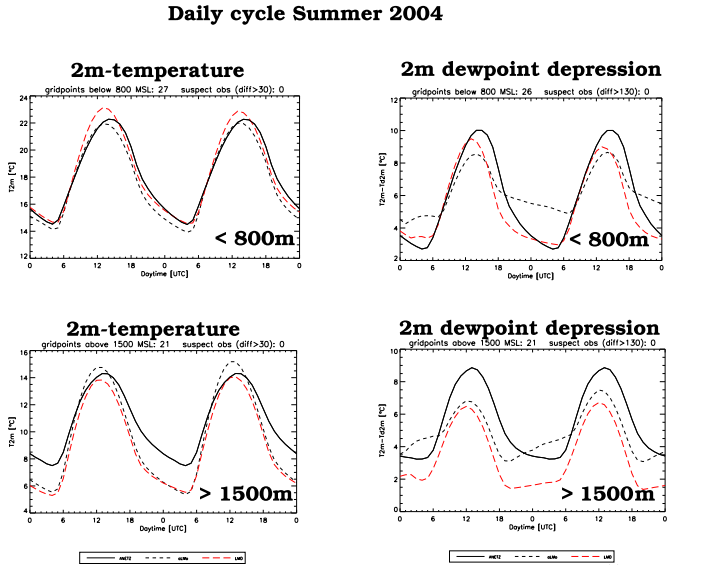

Figure 1: Verification of the daily cycle in Summer 2004 over Switzerland of 2m-temperature (left) and 2m-dewpoint depression (right) for gridpoints < 800m (upper part) and gridpoints > 1500m (lower part). Observations (ANETZ): full line black; aLMo: black dashed; LMD: red long dashes.

Results of aLMo and LMD have been computed monthly and seasonally for 2m-temperature, 2m-dewpoint and 2m-dewpoint depression, 10m-wind, precipitation (hourly sums for daily cycle and 6h sums for scores) and for cloud cover (3-hourly intervals). Three of the main differences between aLMo and LMD during the year 2004 are (1) the prognostic TKE-scheme, (2) the soil-moisture analysis (both operational at DWD, but not at MeteoSwiss) and (3) the different boundary conditions. Since 16 September 2003 aLMo runs with boundary conditions from ECMWF (IFS-frames) and this renders the interpretation of the differences with LMD (boundary conditions from GME) more difficult.

The following points are of main interest:

(1) The 2m-temperature cooling in the evening is too pronounced and there is a negative bias in Winter and Spring during night-time (in the late evening up to 1.5-2.0 K in aLMo and 1 K in LMD). The diurnal amplitude is too large. It is less pronounced in Summer for gridpoints < 800m and is a little bit larger in LMD than in aLMo. The daily maxima is reached ∼ 1.5 hour too early. In LMD with the prognostic TKE

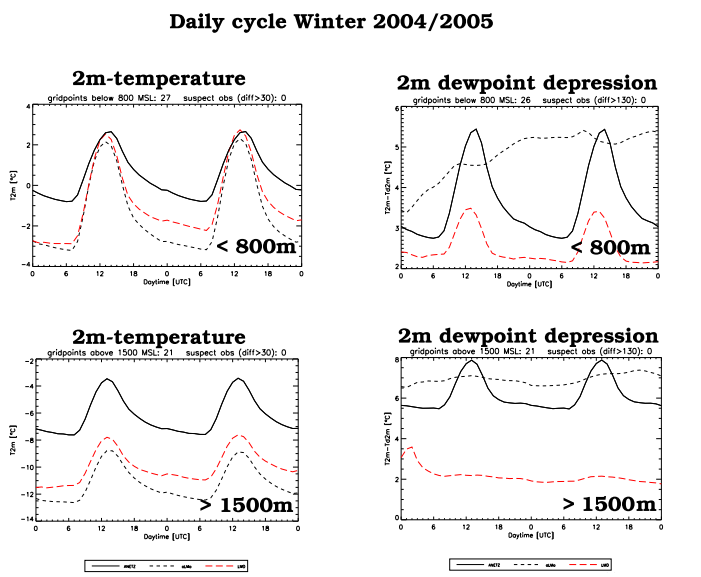

Figure 2: Verification of the daily cycle in Winter 2004/2005 over Switzerland of 2m-temperature (left) and 2m-dewpoint depression (right) for gridpoints < 800m (upper part) and gridpoints > 1500m (lower part). Observations (ANETZ): full line black; aLMo: black dashed; LMD: red long dashes.

scheme and soil moisture analysis the daily maxima for gridpoints < 800 m is 1K higher than in aLMo. This gives a greater positive bias in LMD with exception of the Winter. See Fig. 1 and 2 (left side) for results of Summer 2004 and Winter 2004/2005 for gridpoints < 800 m (upper part) and 1500 m (lower part).

(2) The daily cycle of 2m-dewpoint depression is not well reproduced (aLMo too moist during daytime and too dry during night-time). The TKE scheme, operational in LMD, corrects partly (in Summer and Autumn mostly) this cycle but the values are too low in Winter and Spring (constant negative bias, i.e. too moist). aLMo shows in Winter for gridpoints < 800m an increasing drying (positive bias) with increasing forecast time. See Fig. 1 and 2 (right side) for results of Summer 2004 and Winter 2004/2005 for gridpoints < 800 m (upper part) and 1500 m (lower part).

(3) The results for precipitation are summarized in Table 1 with the scores for the frequency bias of the five seasons (from Winter 03/04 to Winter 04/05) for the thresholds 0.1, 2, 10 and 30 mm/6h for aLMo and LMD. It shows an overestimation for low amounts (0.1 mm/6h) of 35-65% (except in Summer only 20%): this overestimation is most pronounced in the Prealps (altitude range 800-1500m). The high amounts (10 mm/6h) are in aLMo slightly underestimated by $\sim$ 10% and in LMD overestimated in Winter and Spring (40-50%) and underestimated in Summer and Autumn (by 10-25%). In Summer there is a too strong diurnal cycle on the mountain gridpoints (due to a too pronounced convection at daytime) and the daily maxima are forecasted about 4h too early (see Fig. 3 upper part). Differences between aLMo and LMD are more pronouced in Winter (surprisingly when the soil-moisture analysis operational in LMD but not in aLMo should not be important): LMD shows a stronger overall overerstimation (see Fig. 3 lower part). Since Autumn 2003 the differences between aLMo and LMD are partly due to the different lateral boundary conditions (aLMo runs with IFS-frames, LMD with GME) and the comparison between aLMo and LMD is not obvious (See

threshold	winter 03/04	spring 04	summer 04	autumn 04	winter 04/05
0.1 mm/6h					
aLMo	151	162	120	135	162
LMD	151	164	121	145	183
2.0 mm/6h					
aLMo	122	124	101	109	162
LMD	139	147	97	112	219
10 mm/6h	1.69	1.37	2.61	1.92	0.88
aLMo	89	91	84	106	91
LMD	137	130	76	94	231
30 mm/6h	0.033	0.090	0.222	0.091	0.0501
aLMo	139	75	114	268	0
LMD	475	93	82	166	7

Table 1: Frequency bias (%) of predicted precipitation over Switzerland. For all 6h-sums from +6h until +48h of all 00 UTC and 12 UTC-forecasts, compared to 69 ANETZ stations. The LM precipitation is the mean over 5 gridpoints. For the high amounts (10 and 30 mm/6h) the percentage of occurrences (%)is given. The columns give the values for the four seasons and (on the right part) for the period where aLMo run both with GME- and IFS-boundary conditions.

COSMO Newsletter 4, 63–66: the overestimation of precipitation in aLMo is partly removed with the IFS-frames).

(4) Verification of 10m-wind (for representative stations corresponding to a gridpoint $<$ 800m) gave an overestimation of the wind speed of $\sim$ 0.5-0.8 m/s both in aLMo and LMD (except in Spring and Summer daytime with an overestimation of $<$ 0.5 m/s). The diurnal cycle is qualitatively better in LMD (due to TKE-scheme) but the daytime values are even higher, i.e. positive bias greater (see also COSMO Newsletter 2, page 201). For the gridpoints $>$ 1500m the wind speed is strongly underestimated, due to the same PBL-parametrization over mountains than over flat terrain. See Fig. 4 for results of Summer 2003 and Winter 2004/2005 for gridpoints $<$ 800 m.
The mean error in 10m-wind direction (verified for observed wind speed $>$ 3 m/s) is very little, but it changed in sign during this year for LMD from a range of +5 to +10 degrees (i.e. a little bit biased in clockwise direction) to 0 to -5 degrees. LMD gives a bias that is in overall about 5 degrees more in anti-clockwise direction.

(5) The diurnal cycle of total cloudiness is not well reproduced (especially in Spring and Summer): there is a mostly a negative bias (up to $\sim$ 0.5 octa), except during the night (postive bias up to 0.5-1.0 octa in Spring). Except the first 6-9 h of forecast, LMD has higher values than aLMo by $\sim$ 0.2 octa. See Fig. 5 for results of Summer 2004 and Winter 2004/2005 for gridpoints $<$ 800 m and $>$ 1500m. In Winter 2004/2005 with frequent high pressure situations in December and January (stratus with top below 1000 m asl) the low cloud amount (stratus) was not well reproduced even at analysis time (with the nudging assimilation scheme): aLMo and LMD gave about the same cloud amount for gridpoints $<$ 800m and $>$ 1500m, but the observations gave a cloud amount of 1.5-2 octa higher for gridpoints $<$ 800m as compared to those $>$ 1500m.
As in Summer 2003, it is interesting to compare the following two behaviours on the

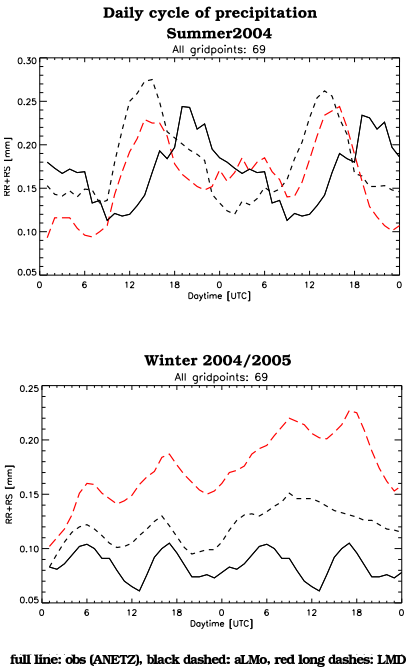

Figure 3: Verification of the daily cycle of precipitation for all 69 gridpoints corresponding to an ANETZ-station in Summer 2004 and Winter 2004/2005.

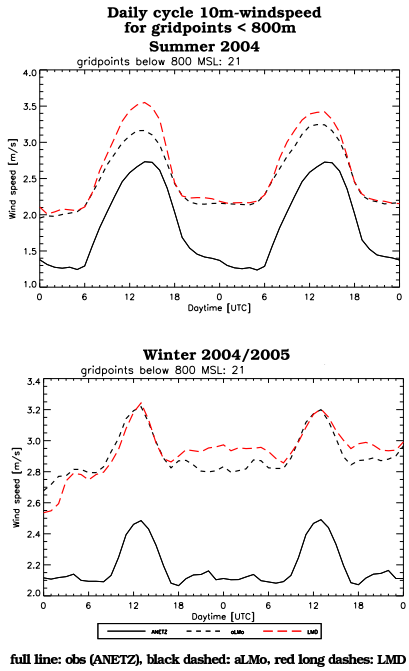

Figure 4: Verification of the daily cycle of 10m-wind speed for gridpoints $<$ 800m over Switzerland in Summer 2004 (upper part) and Winter 2004/2005 (lower part). Observations (ANETZ): full line black; aLMo: black dashed; LMD: red long dashes. Observations (ANETZ): full line black; aLMo: black dashed; LMD: red long dashes.

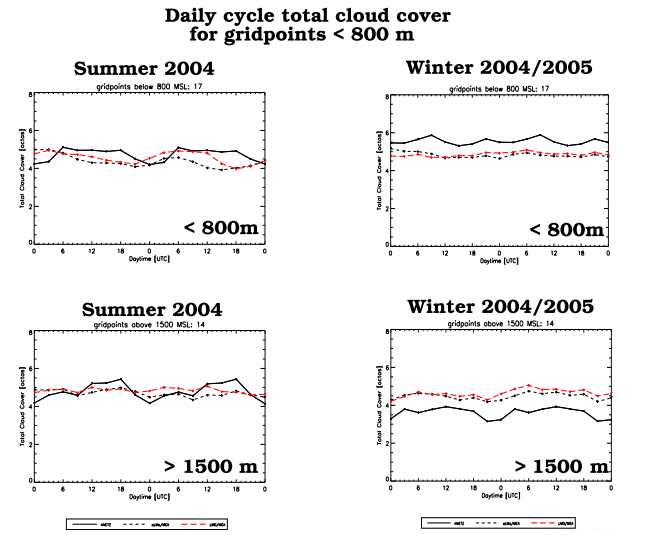

Figure 5: Verification of the daily cycle of total cloud cover over Switzerland in Winter 2002/2003 (left) and Summer 2003 (right) for gridpoints $<$ 800m (upper part, 17 locations) and for gridpoints $>$ 1500m (lower part, 16 locations). Observations (ANETZ): full line black; aLMo: black dashed; LMD: red long dashes. The LM total cloud cover is the mean of 41 gridpoints around the observation station and for three hours, to take in account that an observer sees in the mean a sky radius of $\sim$ 30 km.

diurnal cycle for mountain gridpoints in Summer: missing of the cycle for cloud cover and too exaggerated cycle for precipitation (see Fig. 6). It suggests that cloud amount in convective situations is too low.

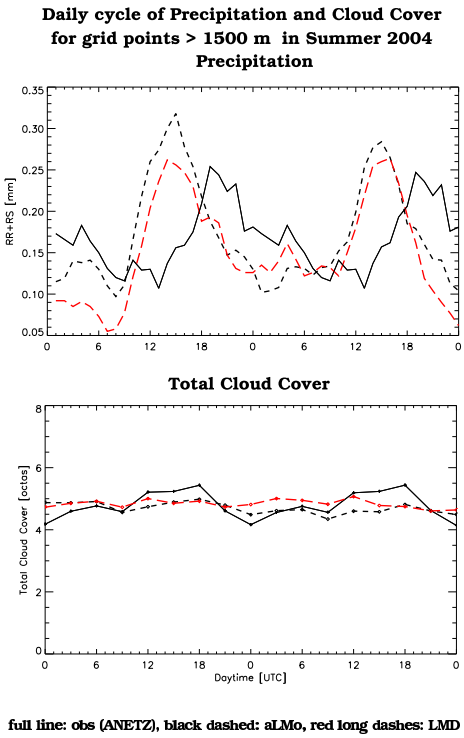

Figure 6: Verification of the daily cycle of precipitation (upper part) and total cloud cover (lower part) for gridpoints > 1500m over Switzerland in Summer 2004. Observations (ANETZ): full line black; aLMo: black dashed; LMD: red long dashes.

Verification of LM-COSMO Model in Poland with SYNOP and Rain Gauge Data

Katarzyna Starosta and Joanna Linkowska

Institute of Meteorology and Water Management, Centre for Development of Numerical Weather Forecasts. 61 Podleona str, 01-673 Warsaw, Poland

1 Introduction

In our article we presented the results of the verification of LM-COSMO model for Poland during 2004. For the calculations we interpolated the gridded forecast values on the station points where observations are available. The interpolation of forecast values on the station points was performed by averaging the values on the four nearest grid points. For this purpose we used the bilinear interpolation. We compared data from the model starting at 00 UTC with data 56 Polish SYNOP stations (Fig. 1).

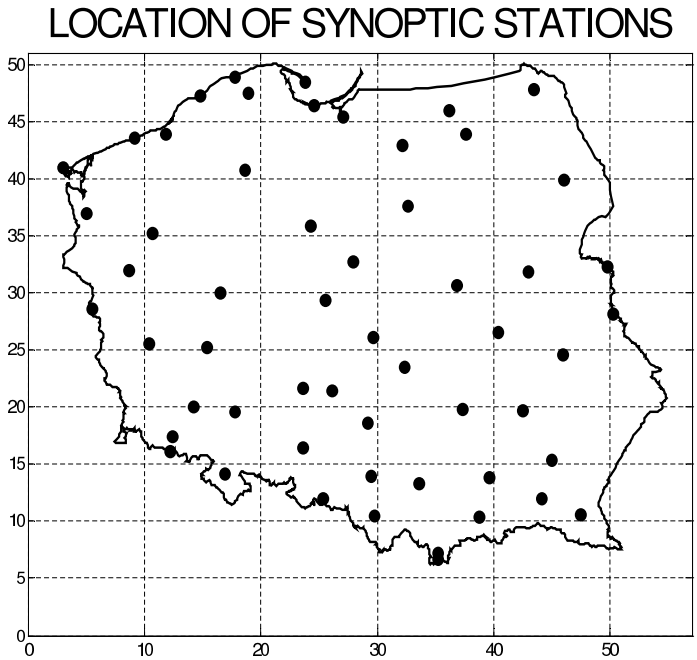

Figure 1: Location of synoptic stations

We used the following meteorological parameters for verification:

- Temperature at 2 m above ground level
- Dew point temperature at 2 m a.g.l
- Air pressure at sea level
- Wind speed at 10 m a.g.l

For comparison we used mean error (ME), root mean square error (RMSE) and correlation coefficient at six hour intervals from the range 6h - 72h. We calculated the errors for all the separate stations and they proved different in each station. We have also mountainous

stations (in the south of Poland) and coastal ones (in the north). We finally calculated the monthly mean errors in Poland (mean of all stations). We also made verification for the 24h precipitation amount (from 6h - 6h next day). We compared the precipitation data from the model started at 00 UTC with data from 308 rain gauges (Fig. 2). We calculated some verification indices from the contingency table for the different precipitation thresholds.

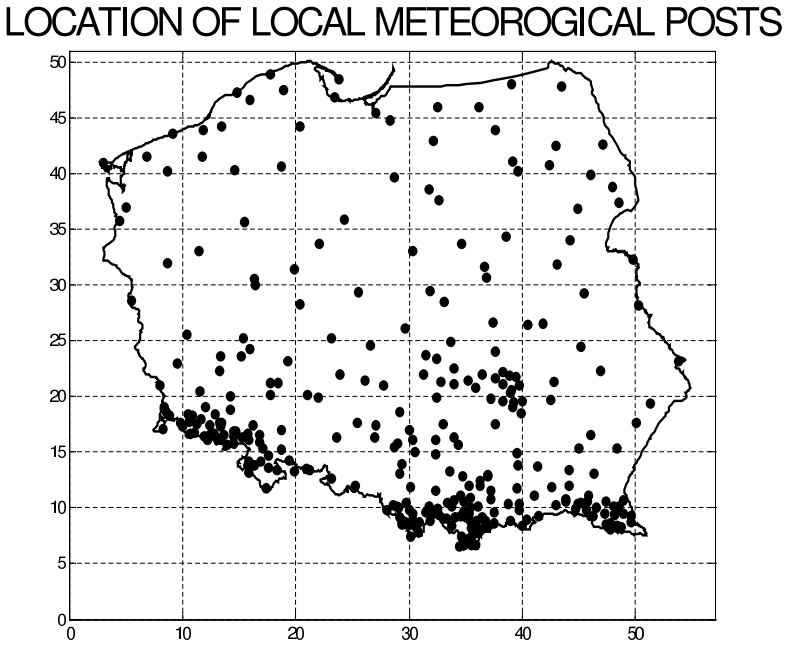

Figure 2: Location of local meteorological posts

2 Results

2.1 Comparison with SYNOP station.

Figures 3-10 show monthly the verification results during 2004.

The 2m temperature

The bias is bigger and positive (0-2) during spring and summer, while lower and negative (0-1) during winter (Fig. 3). We observed large diurnal amplitude in spring (April, May) and a little smaller in summer (June, July, August) with maximum of ME at 12 UTC (and 24 UTC) and minimum at 18 UTC (and 6 UTC). In the remaining months (autumn and winter) daily cycle is not well reproduced.

For RMSE error (Fig. 4) we observed explicit diurnal run for months from April to August with maximum of error at 12 UTC and minimum at 6 UTC.

The 2m dew point temperature

The dew point temperature is overpredicted for all months and the daily cycle is observed (especially in summer) with maximum at day time and minimum at night time (Fig. 5).

The RMSE reaches a maximum at 12 UTC and minimum at 6 UTC (Fig. 6). The errors are larger in summer than in winter. From October to December the daily cycle is not well observed.

Pressure sea level

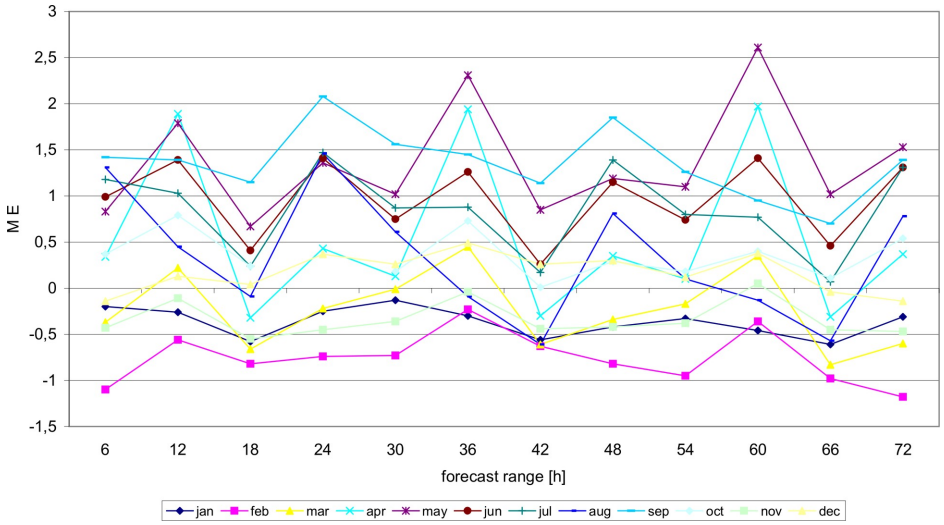

Figure 3: Mean error, Temperature 2m [C], Poland, 2004

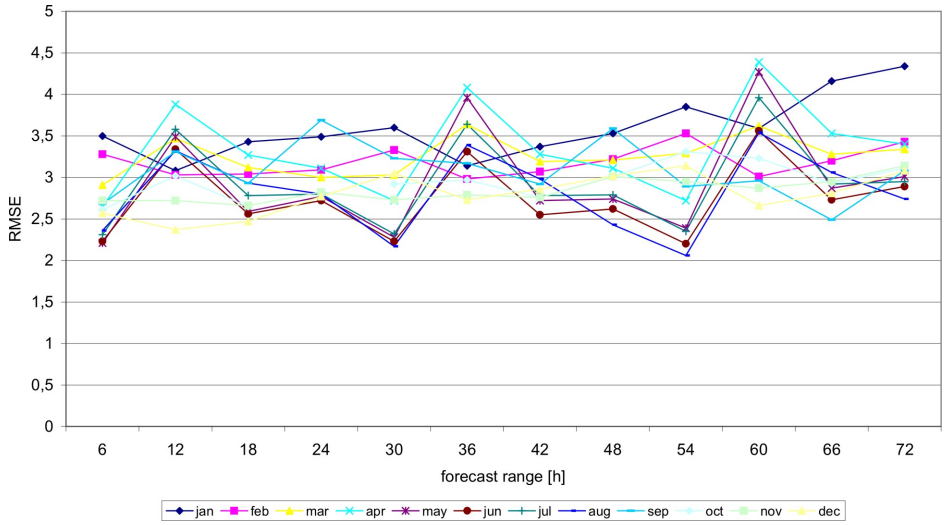

Figure 4: RMSE, Temperature 2m [C], Poland, 2004

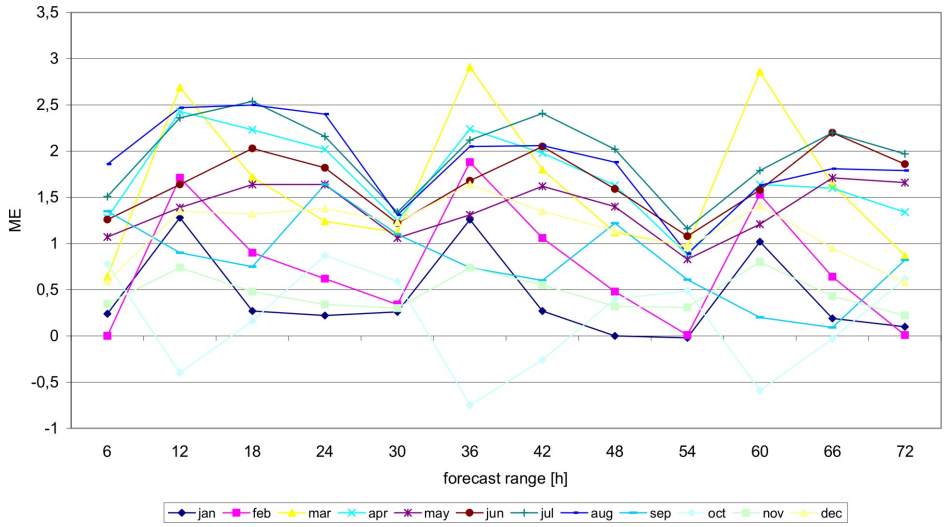

Figure 5: Mean error, Dew point 2m [C], Poland, 2004

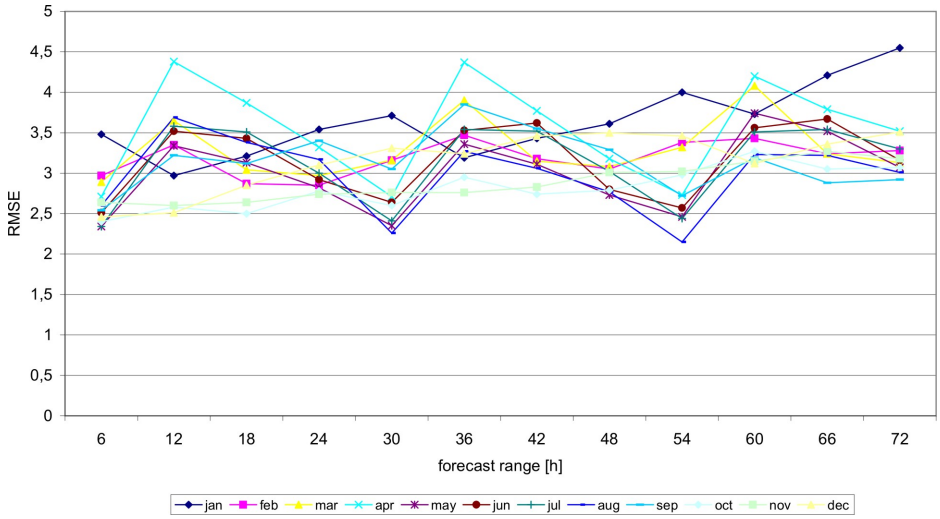

Figure 6: RMSE, Dew point 2m [C], Poland, 2004

The sea level pressure is underestimated for winter and summer (Fig. 7).

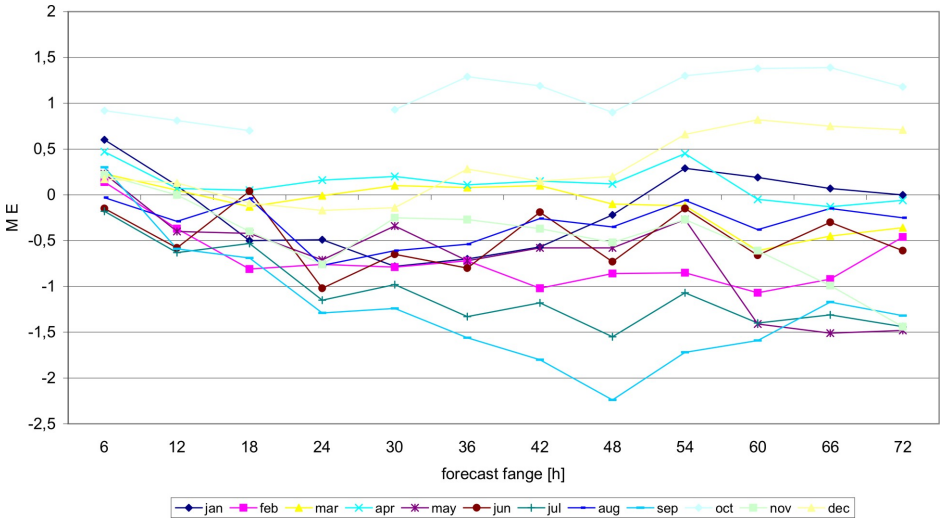

Figure 7: Mean error, Pressure [hPa] Poland, 2004

In spring the ME was about zero. The RMSE error increased with forecast range and it was smaller for summer than for winter (Fig. 8).

10 m wind speed

The wind speed is overpredicted with minimum of error at 18 UTC (Fig. 9).

The ME for wind speed is from 0 to 1 m/s. In RMSE error for daily amplitude with forecast range was very little and also the difference of RMSE among several months was small (Fig. 10).

The previous pictures show the mean errors from all stations, and the next three figures (11-13) represented the distribution of errors for one month (March 2004) for a 36h forecast, for each of 53 SYNOP stations (without the three high mountainous stations). The error was different and depended on the location of the stations.

ME for temperature, wind speed and sea level pressure was different and sometimes they were below zero and sometimes above zero level (Fig. 11), but the dew point temperature

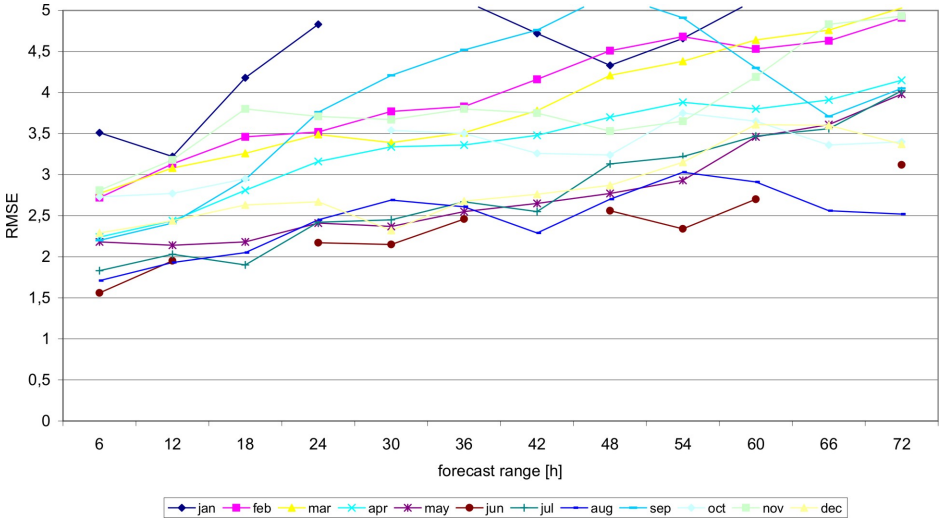

Figure 8: RMSE, Pressure [hPa] Poland, 2004

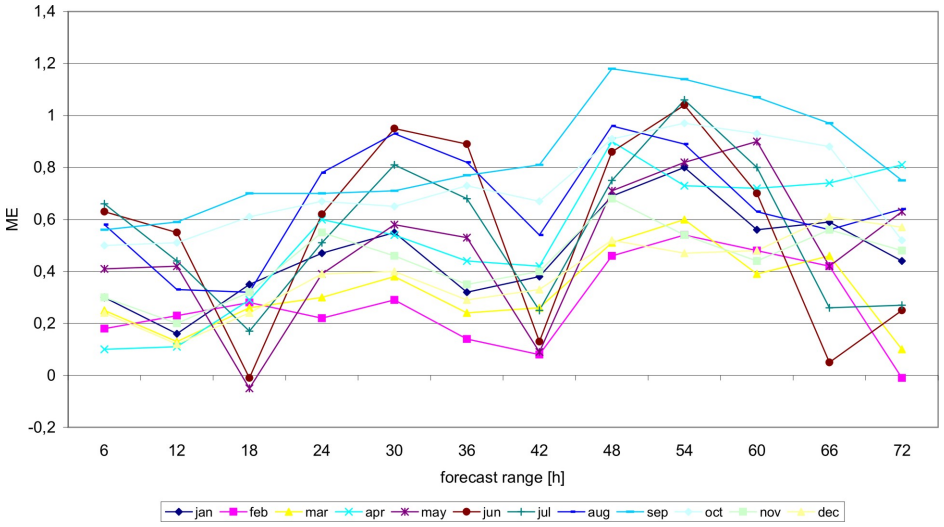

Figure 9: Mean error, Wind speed [m/s], Poland, 2004

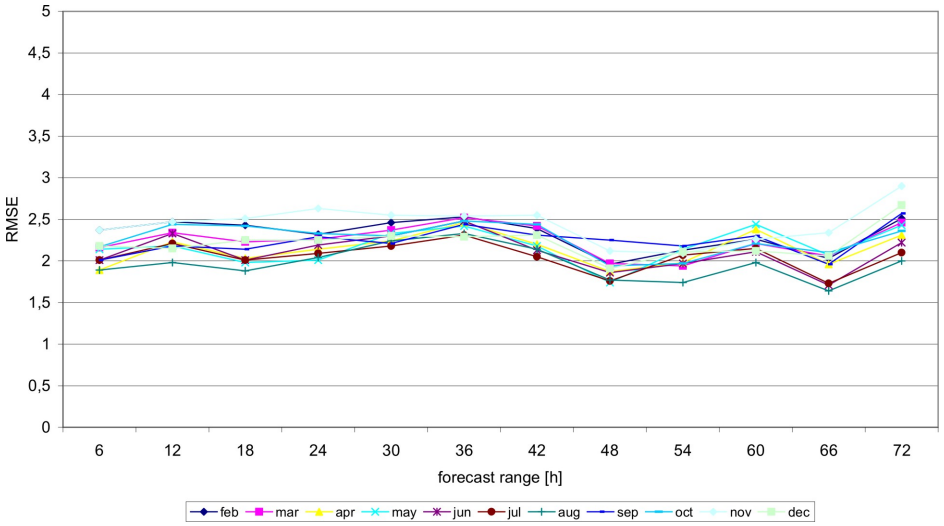

Figure 10: RMSE, Wind speed [m/s], Poland, 2004

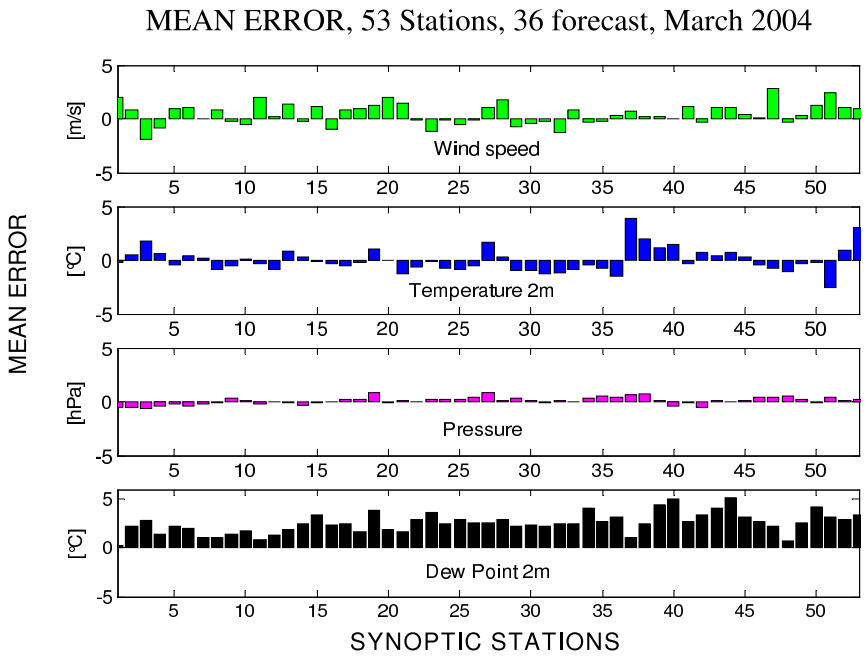

Figure 11: Mean error,53 stations, 36h forecast, March 2004

this month was overpredicted for all stations. In Fig. 12 we show RMSE for individual stations for the same month.

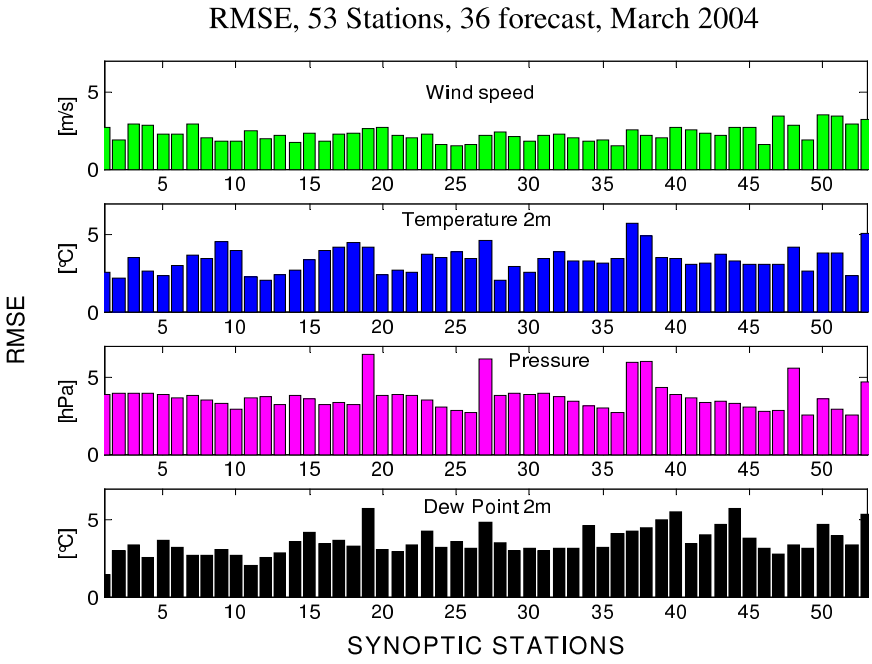

Figure 12: RMSE, 53 stations, 36h forecast, March 2004

2.2 Comparison with rain gauges

For precipitation we calculated indices from the contingency table for the 24 h accumulated forecast data and data from 308 stations (rain gauges). For verification of precipitation thresholds 0.5, 1,2.5,5,10,20,25,30 mm were used. For each threshold the following scores were calculated (the same are used at DWD): FBI (Frequency bias), POD (Probability of

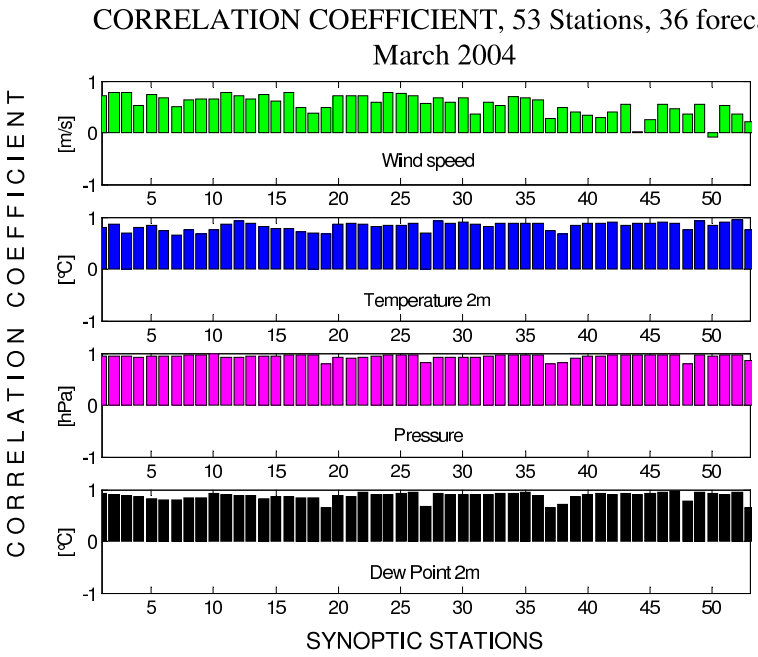

Figure 13: Correlation coefficient, 53 stations, 36h forecast, March 2004

detection of event), PON (Probability of detection of non-event) FAR (False alarm rate), TSS (True skill statistics), HSS (Heidke skill score), ETS (Equitable skill score).

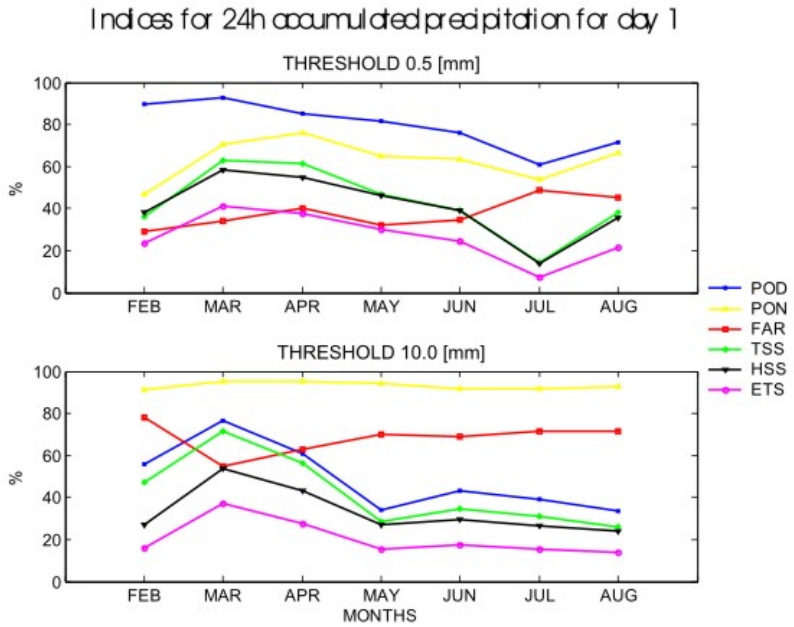

Figure 14: Indices for 24h accumulated precipitation for day 1

At Fig. 14 we show those indices for two thresholds 0.5 and 10 mm from February to August for the first day forecast. We have chosen March to present the indices for all thresholds for three days of forecast range (Fig. 15).

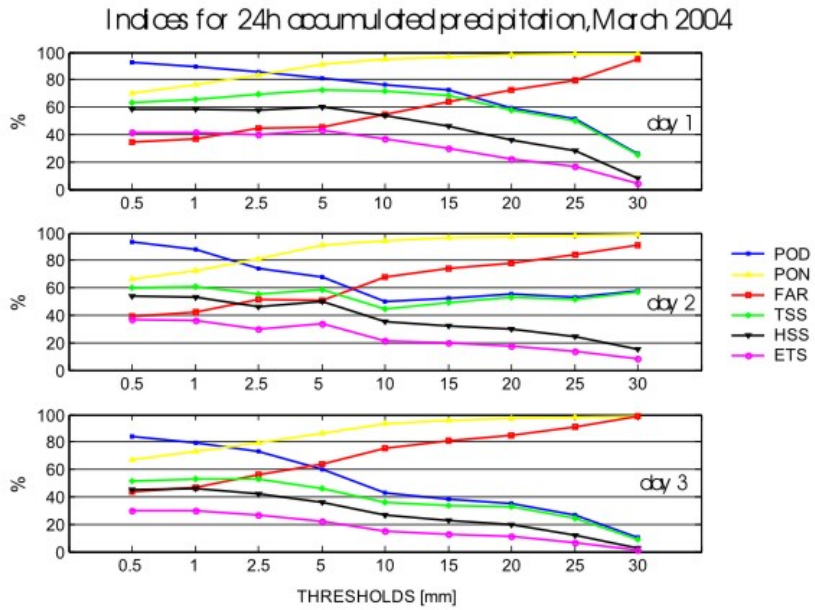

Figure 15: Indices for 24h accumulated precipitation, March 2004

3 Conclusions

1. We observed the diurnal and monthly cycle of RMSE of the 2m temperature and the 2m dew point temperature.
2. RMSE increased during the forecast, especially for the sea level pressure.
3. The distribution of RMSE for the wind speed was quite smooth with minimum values occurring at night (similar in every month).
4. ME is positive for the wind speed and the 2m dew point temperature, about zero or negative for the sea level pressure and changes a sign for temperature (negative in winter and positive in summer).
5. Precipitation amounts seem to be overestimated by the model.

Operational Verification of Vertical Profiles at Meteoswiss

Marco Aprpagaus

MeteoSwiss, Zürich, Switzerland

The operational upper-air verification at MeteoSwiss uses TEMP stations all over the integration domain to verify the vertical structure of the forecasts. For the operational setup of the Alpine Model (aLMo), refer to section 4 in this newsletter. However, note that the aLMo runs with the new two-category ice scheme since 11 May 2004 and with the prognostic precipitation scheme since 16 November 2004. Moreover, the model is integrated out to +72 hours since 16 September 2003 (recall that aLMo runs with ECMWF lateral boundary conditions rather than GME lateral boundary conditions since that date), which allows to compare verification results for +00 h, +24 h, +48 h, and +72 h, respectively.

In the following, we present the average vertical structure for 30 TEMP stations for the full climatic year 2004 (averaged over verification times 00 & 12 UTC; see Figs. 1 – 4; please note that the statistics for the uppermost level of 30 hPa is extremely limited, and hence the verification results at that level should be interpreted very carefully).

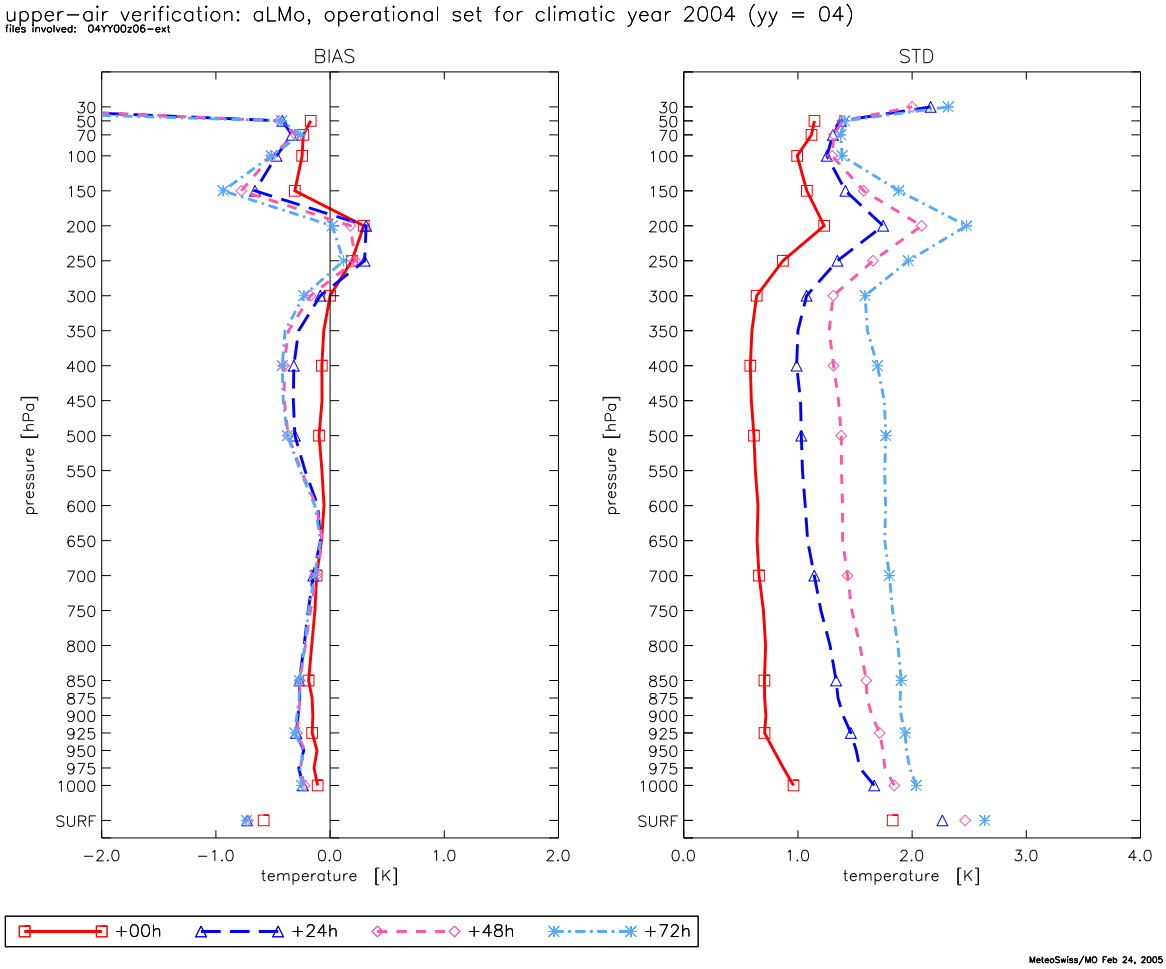

Figure 1: Mean error (BIAS) and standard deviation (STD) for temperature. Various forecast times (averaged over all stations and verification times 00 & 12 UTC) for the climatic year 2004 (1.12.2003 – 30.11.2004).

The verification plot for *temperature* (*cf.* Fig. 1) shows a cold bias throughout the troposphere, varying in magnitude between 0.1 K and 0.4 K. When looking at the different seasons (not shown), one finds that most seasons contribute similarly to this cold bias, except for the summer season, which shows a warm bias in between 800 hPa and 500 hPa, with a maximum at around 650 hPa, which is reflected in the minimum of the cold bias for the full climatic year at that level. At and above the tropopause level, a saw-like structure in the mean error of temperature can be observed, which is common to all seasons. The fact that most temperature biases increase with increasing forecast time hints at a systematic model deficiency. Concerning the standard deviation, largest spread is seen around the tropopause level.

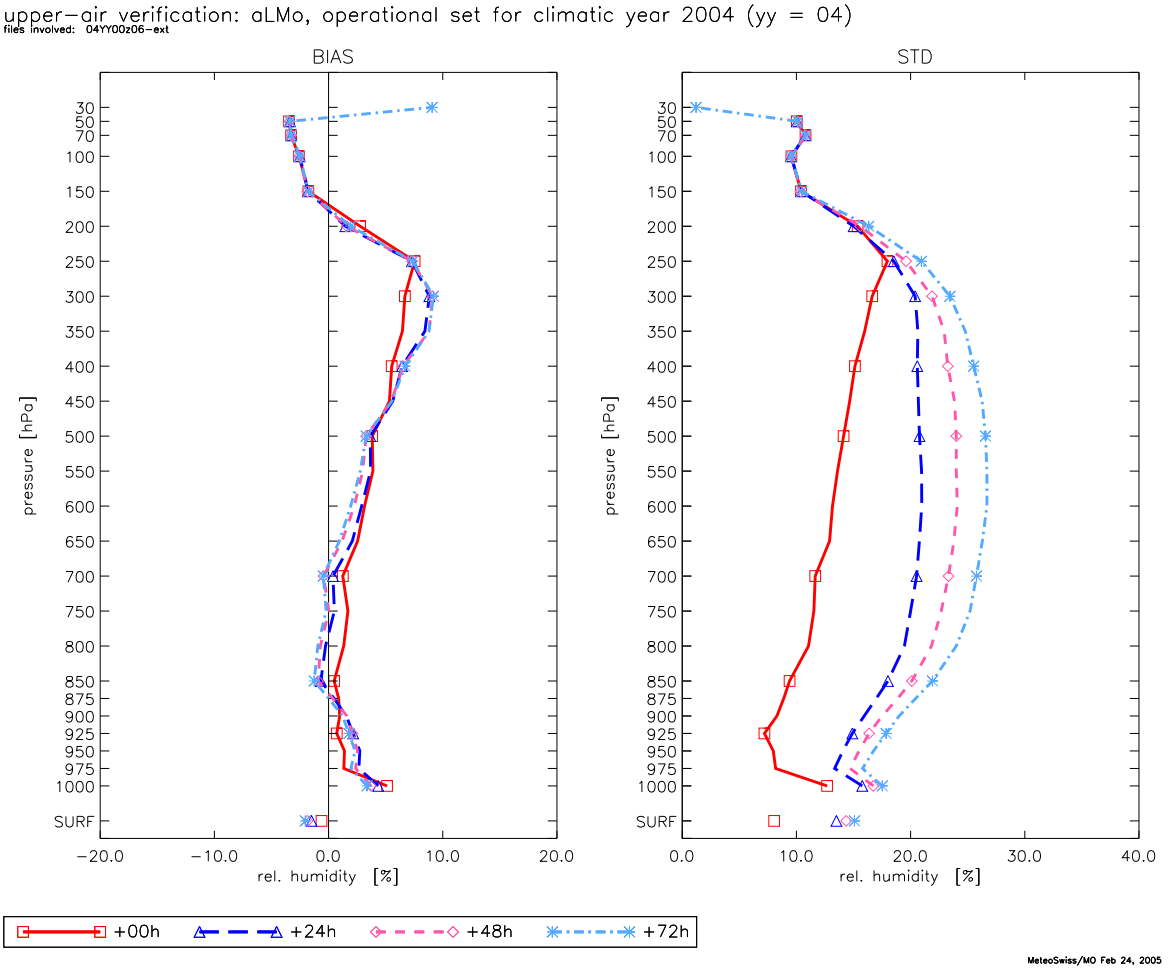

Figure 2: Mean error (BIAS) and standard deviation (STD) for relative humidity with respect to water. Various forecast times (averaged over all stations and verification times 00 & 12 UTC) for the climatic year 2004 (1.12.2003 – 30.11.2004).

Looking at the verification results for the *relative humidity* (*cf.* Fig. 2) the mean error is moderate up to 700 hPa, with a clear and increasing moist bias towards the surface. Above 700 hPa, relative humidity with respect to water is systematically biased towards positive values, since for the old grid-scale precipitation scheme (one-category ice scheme, *i.e.*, no cloud ice; in operation until mid 2004) specific humidity values need to be artificially increased at analysis time to compensate for the difference in saturation vapour pressure over water and ice at temperatures below freezing (for the two seasons after the switch to the new cloud ice scheme, the bias in relative humidity is at most 6% throughout the atmosphere; not shown). The standard deviation is reasonably uniform throughout the troposphere, with a slight increase towards the surface.

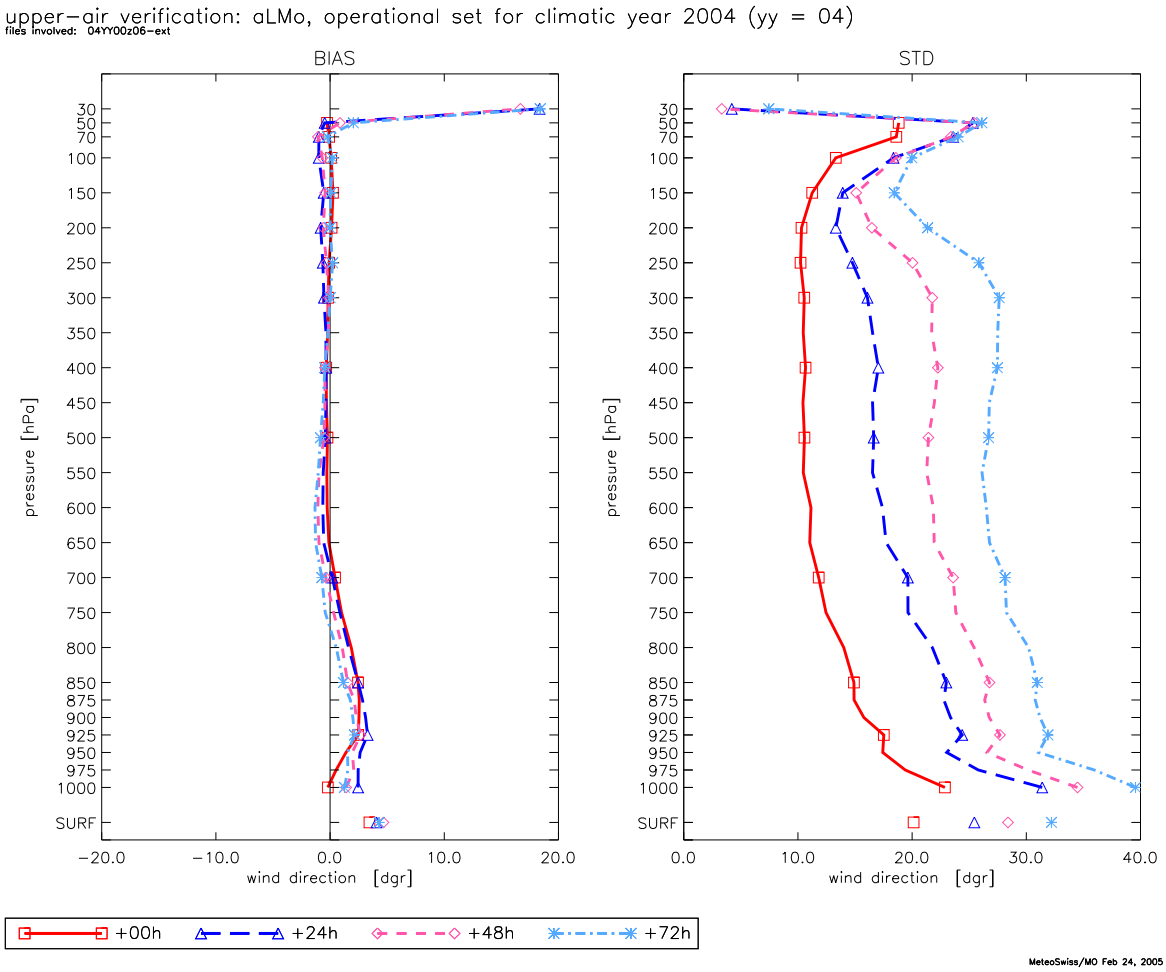

Figure 3: Mean error (BIAS) and standard deviation (STD) for wind direction. Various forecast times (averaged over all stations and verification times 00 & 12 UTC) for the climatic year 2004 (1.12.2003 – 30.11.2004).

Wind direction (*cf.* Fig. 3) exhibits a very small mean error, especially above the boundary layer. As expected, there is a marked increase for both mean error and standard deviation towards the surface. A deterioration of the standard deviation is also observed in the stratosphere.

The mean error of the *wind speed* (*cf.* Fig. 4) is small. The largest bias is observed for the boundary layer and around the tropopause height. Although seasonal differences in the (small) mean error are fairly small, the main contributions to the prevailing negative bias stem from the spring and summer seasons, whereas the positive bias in the boundary layer is largest in winter (not shown). The standard deviation is largest at the tropopause, consistent with the highest winds at this level.

Concerning the interplay between the assimilation scheme and the daily spread of the forecasts, we note that the standard deviation increases almost linearly from forecast time +06 h to +72 h with a substantially larger difference between analysis time (*i.e.*, +00 h) and +06 h for all parameters except the (un-nudged) geopotential (not shown).

Let us finally compare these verification results with other years (see older COSMO Newsletters for comparison), always bearing in mind that inter-annual differences in the weather situations may lead to larger differences in the verification results then possible model improvements. The systematic errors in temperature and especially wind speed observed in

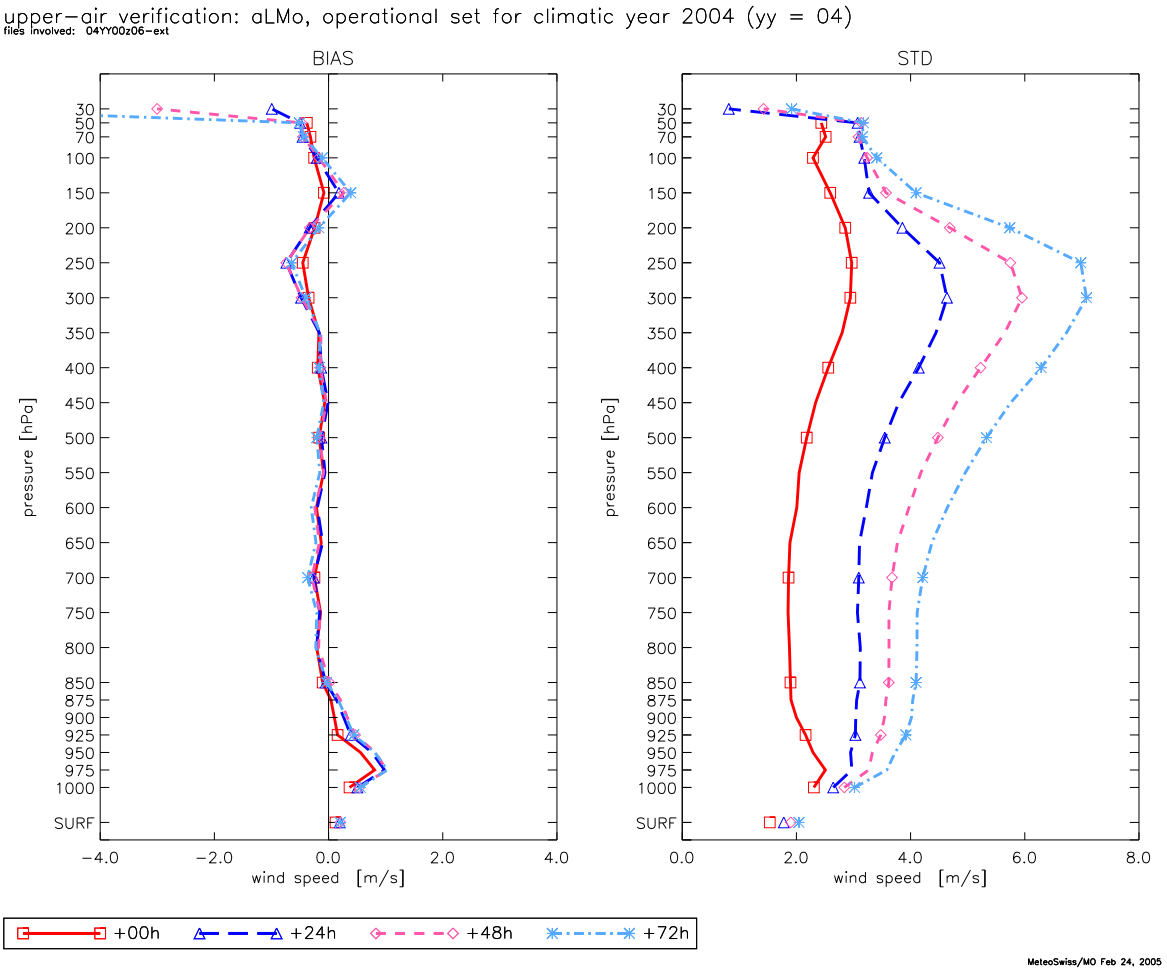

Figure 4: Mean error (BIAS) and standard deviation (STD) for wind speed. Various forecast times (averaged over all stations and verification times 00 & 12 UTC) for the climatic year 2004 (1.12.2003 – 30.11.2004).

earlier years, some of which may have been due to the driving global model, have disappeared. However, by using the ECMWF global forecasts (IFS) as lateral boundary conditions without any mechanism to damp reflections at the upper boundary (*i.e.*, no Rayleigh damping, since aLMo runs with IFS frames rather than full 3d fields), we may have introduced new problems, especially concerning the forecast of temperature in the stratosphere. Nevertheless, a clear improvement of the standard deviation as compared to the climatic year 2003 can be observed for all parameters verified (not shown).

Operational Verification of Vertical Profiles at DWD

Ulrich Pflüger

Deutscher Wetterdienst, P.O.Box 100465, 63004 Offenbach a.M., Germany

1 Introduction

The operational upper-air verification at the Deutscher Wetterdienst uses all available radiosonde stations over the integration domain of LM to verify the vertical structure of the forecasts. The parameters considered are geopotential, relative humidity, temperature, wind direction and wind velocity.

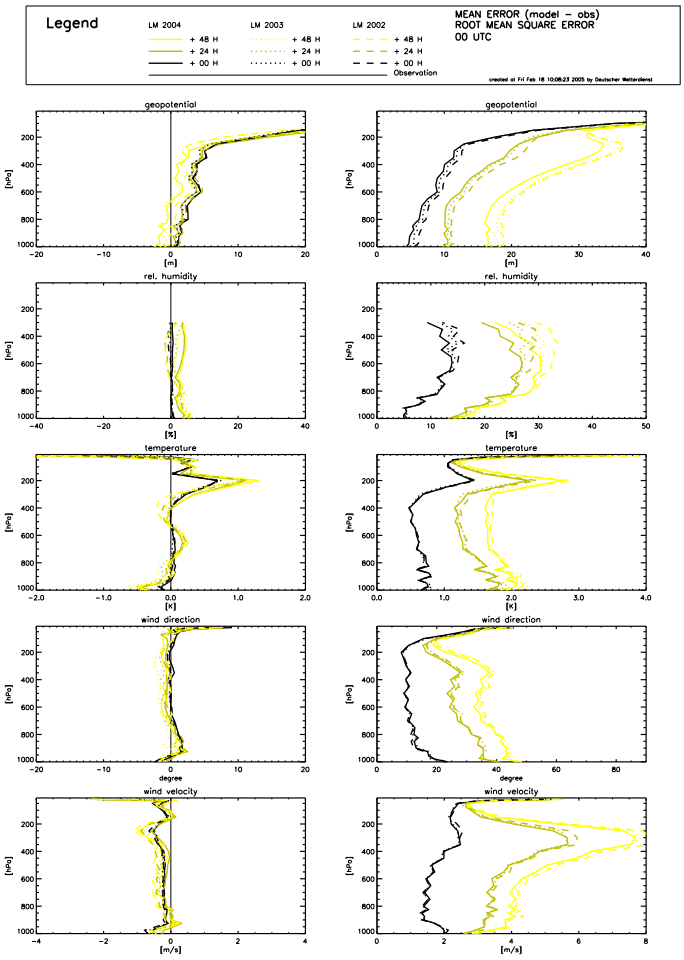

Figure 1: Vertical profiles of annual mean of bias (left columns) and rmse (right columns) at all radiosonde stations for different forecast times of LM runs and different years at DWD. Solid lines: 2004 00UTC, dotted lines: 2003 00 UTC, dashed lines: 2002 00 UTC. From top to bottom at each column: geopotential, relative humidity, temperature, wind direction and wind velocity.

Vertically the atmosphere is divided into bins of 25 hPa below the 800-hPa level and of 50 hPa between the 800-hPa and 100-hPa levels. Above 100 hPa, the bins are bounded by the pressure levels 100, 70, 50, 30, 20 and 10 hPa. Complying with the height, every observation, respectively every forecast increment is allocated to one bin.

2 Annual Mean Profiles of BIAS and RMSE

Figure 1 displays the profiles of the annual mean error (bias, left column) and the annual root mean square error (rmse, right column) against all radiosonde data at 00 UTC within the LM domain for different forecast times (analysis, 24h, 48h) and different parameters (geopotential, relative humidity, temperature, wind direction and wind speed from top to bottom) for 2004 (solid lines), 2003 (dotted lines) and 2002 (dashed lines).

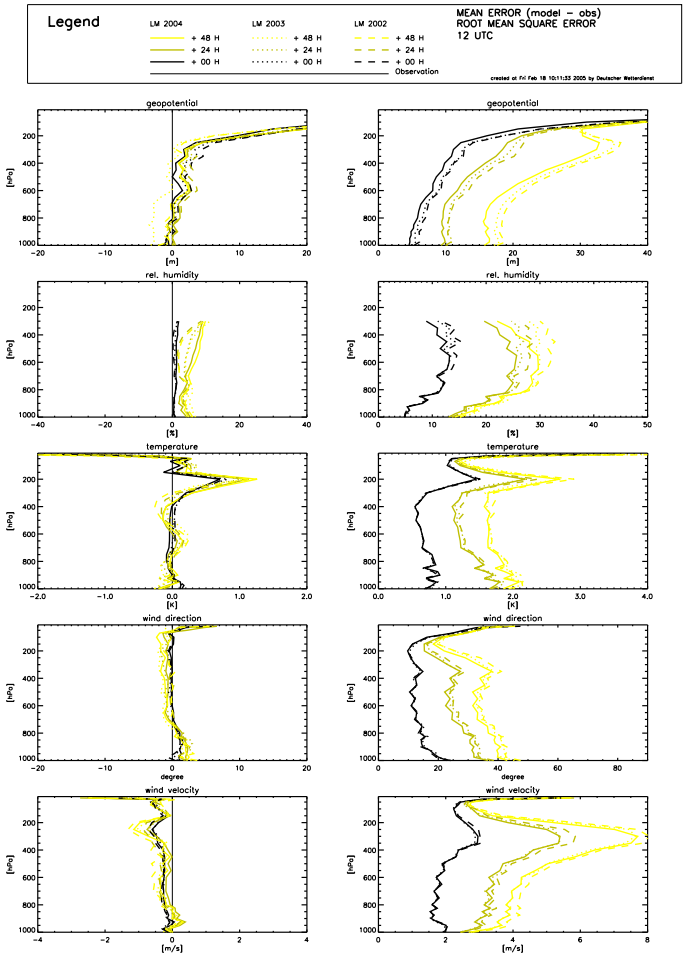

Figure 2: Vertical profiles of annual mean of bias (left columns) and rmse (right columns) at all radiosonde stations for different forecast times of LM runs and different years at DWD. Solid lines: 2004 12UTC, dotted lines: 2003 12 UTC, dashed lines: 2002 12 UTC. From top to bottom at each column: geopotential, relative humidity, temperature, wind direction and wind velocity.

Figure 2 shows the same illustration for verification time 12 UTC. The comparison of the corresponding profiles demonstrates that generally the annual mean profiles of bias and rmse do not change very much between the three years, but there are some exceptions. The bias of geopotential for 2004 remains in the range of the bias which is given with that of the years 2003 and 2002. The negative bias of the 48 h forecast below 600 hPa in 2003 at verification time 12 UTC seems to have been an exception. Changes in rmse are small but clearly visible, against 2003 a systematic rmse reduction of about 1 - 2 m has occurred, with increasing reduction the longer the forecast time is. Between 700 hPa and 300 hPa, there are some changes in the bias of relative humidity. At verification time 00 UTC the 24 h and 48 h forecasts show compared to 2002 and 2003 yet another increase of the bias, the slight positive bias in 2003 is partly more than reduplicated, but at 300 hPa the profiles of 2003

and 2004 meet together. At verification time 12 UTC, the stronger positive bias of 2003 increases for 2004 clearly and the profiles for all three years are meeting together at 300 hPa. The further reduction of rmse of relative humidity above 400 hPa in 2004 is ascribed to the implementation of a prognostic cloud ice scheme at 16 th of September 2003. Since that time there is a reduction of up to 10 monthly mean profiles. Unlike 2004 in the year 2003 only 3 and a half months are contributing to this effect, so in the year 2004 a stronger reduction of the rmse should occur. As remarked in the last Newsletter (Pflüger 2004), this is partly resulting form the smaller range of humidity values because, in contrast to the old scheme, the ice scheme rarely produces relative humidity values close to 100% at that height.

The differences in the bias of temperature remain in the range of the years before and also rmse of temperature remains predominantly unchanged, at the most a very slight improvement between 700 hPa and 400 hPa can be seen. The negative bias of wind direction, which has appeared above 700 hPa in 2003 up to 2 degrees, has mostly weaken. The rmse profiles of wind direction show a very slight improvement above 700 hPa. The bias of wind velocity has the same structure in 2004 as in the years before, the slight tendency for a decrease in 2003 hasn't continued in 2004. The rmse of wind velocity has very few changes between the years 2003 and 2004.

3 Time Series of Monthly Mean Profiles of BIAS and RMSE

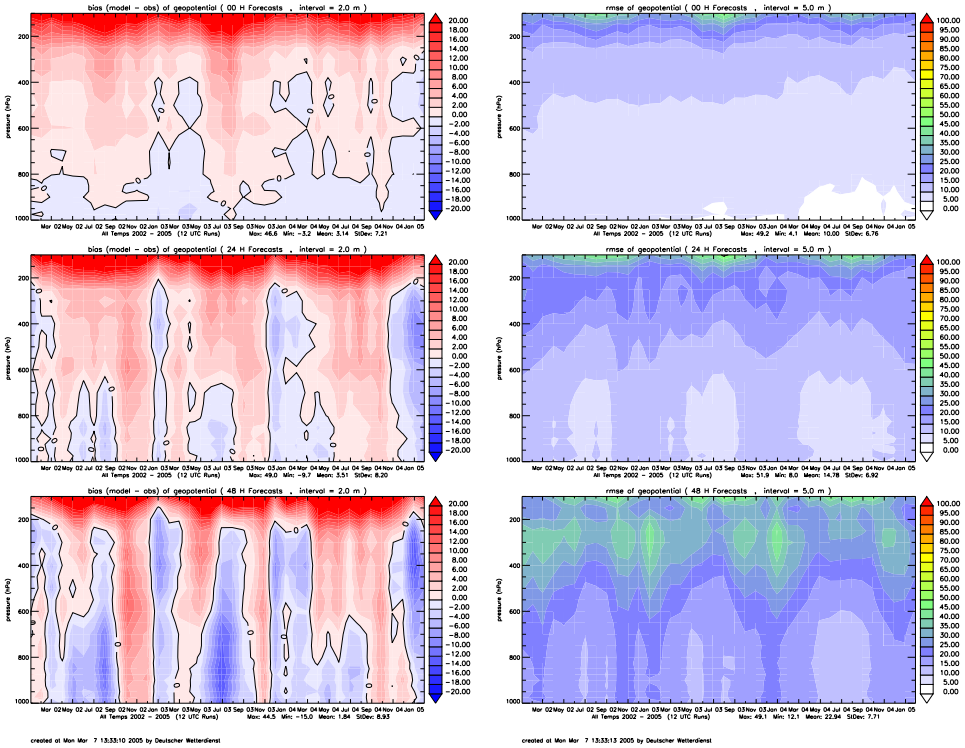

Figure 3: Time Series (January 2002 – Februray 2005) of gepotential bias (left columns) and rmse (right columns) against radiosondes based on monthly mean profiles for 12 UTC LM runs at DWD. From top to bottom: Analysis, 24 h, and 48 h forecast.

In order to show both, the seasonal and inter annual variation of the bias and rmse, time series (January 2002 until February 2005) of the vertical distribution of the monthly bias (left column) and rmse (right column) are presented in Figures 3, 4, 5, 7 and 8 for geopotential height, relative humidity, temperature, wind direction and wind velocity. Figure 6 displays for December 2004 additionally the daily mean values for temperature bias and rmse. All

Figures show the verification time 12 UTC for 3 forecast times (analysis, 24 h and 48 h, from top to bottom). Verification time 00 UTC has basically the same behaviour and is not shown.

Figure 3 displays the time series of the vertical profiles of the monthly geopotential bias and rmse against radiosonde data. It can be seen that the seasonal variation of the bias stated in the last Newsletter (Pflüger 2004), with values less than -10 m in summer and up to +8 m during the rest of the year, isn't that strong in 2004. The rmse is reduced in 2004 up to 5 m mainly in Summer in the lower troposphere and in Winter above 400 hPa.

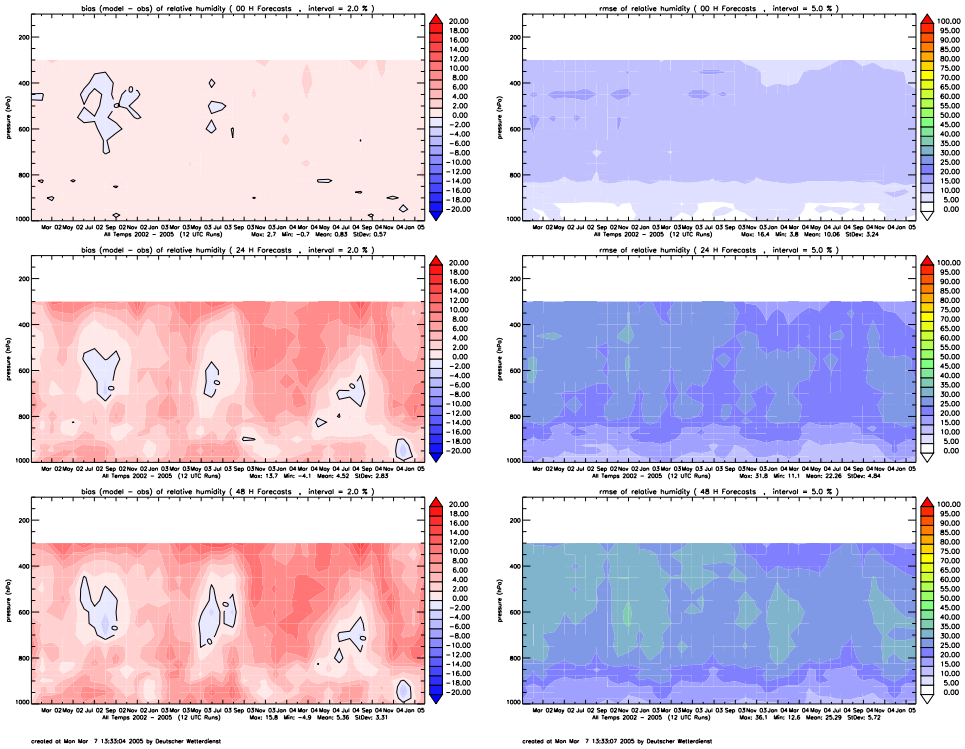

Figure 4: Time Series (January 2002 – February 2005) of relative humidity bias (left columns) and rmse (right columns) against radiosondes based on monthly mean profiles for 12 UTC LM runs at DWD. From top to bottom: Analysis, 24 h, and 48 h forecast.

Figure 4 shows that in 2004 compared to 2003 and 2002, there is a further increase of the positive bias of relative humidity in the middle atmosphere during the autumn and winter months and a slight decrease of the negative bias during summer at forecast times 24 h and 48 h. This can also be seen in the profiles of the annual means as aforementioned. Below 800 hPa, a positive bias during spring and summer months is found. It was larger in the year 2003 and has reduced again in 2004 to that of the 2002. The aforementioned decrease of rmse of relative humidity above 400 hPa due to the implementation of prognostic cloud ice in October 2003 is left in the year 2004.

Figure 5 displays the time series of the vertical profiles of the monthly temperature bias and rmse against radiosondes. The bias patterns of the years 2002 and 2003 are recurring more or less in the year 2004. The positive bias in summer in the middle troposphere is reduced and also the negative bias in the lower troposphere is less pronounced in 2004. The rmse of temperature in the middle troposphere is reduced to values below 2 degrees in 2004, however in December 2004 there is a maximum rmse of 3.2 K at 950 hPa.

This was caused by a 10 day period with an strong temperature inversion in the boundary layer which wasn't resolved by the LM. Figure 6 displays the daily mean of temperature bias

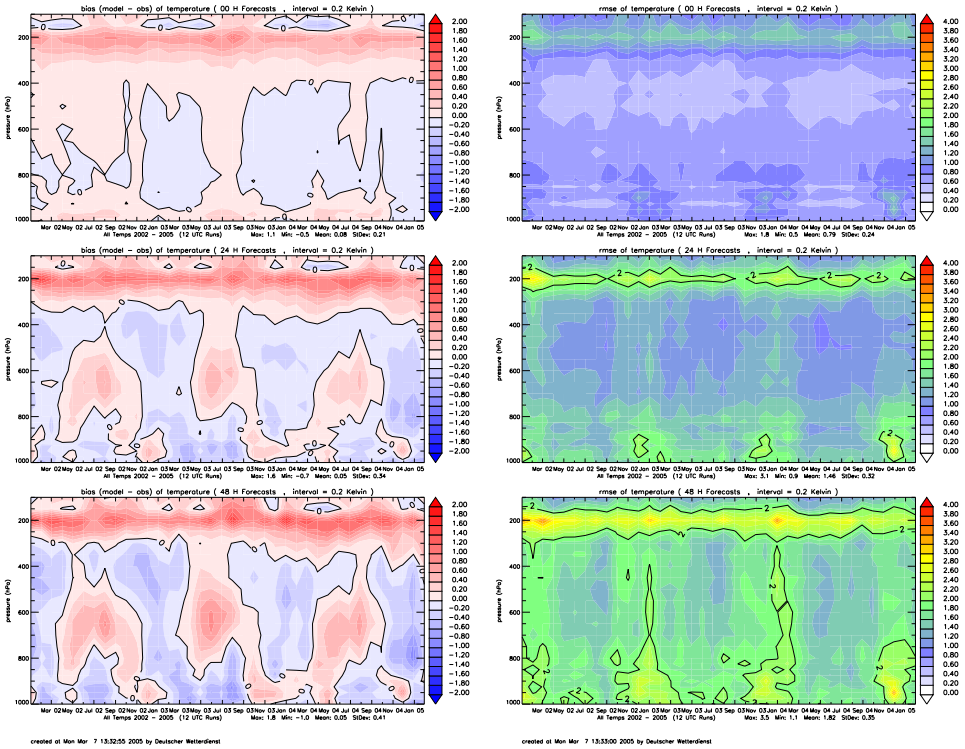

Figure 5: Time Series (January 2002 – February 2005) of temperature bias (left columns) and rmse (right columns) against radiosondes based on monthly mean profiles for 12 UTC LM runs at DWD. From top to bottom: Analysis, 24 h, and 48 h forecast.

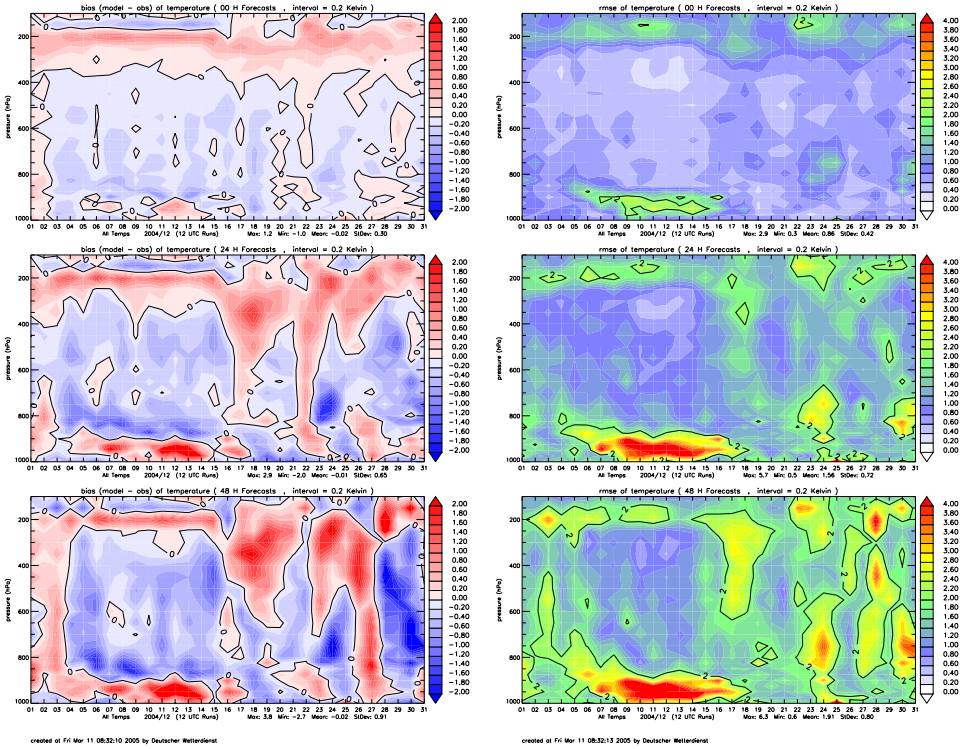

Figure 6: Time Series (December 2004) of temperature bias (left columns) and rmse (right columns) against aircraft data based on daily mean profiles for 12 UTC LM runs at DWD. From top to bottom: Analysis, 24h, and 48h forecast.

and rmse for December 2004. In the period with the temperature inversion, the daily mean of rmse reached values up to 6.3 K at the 950 hPa level and a daily mean bias of + 3.8 K.

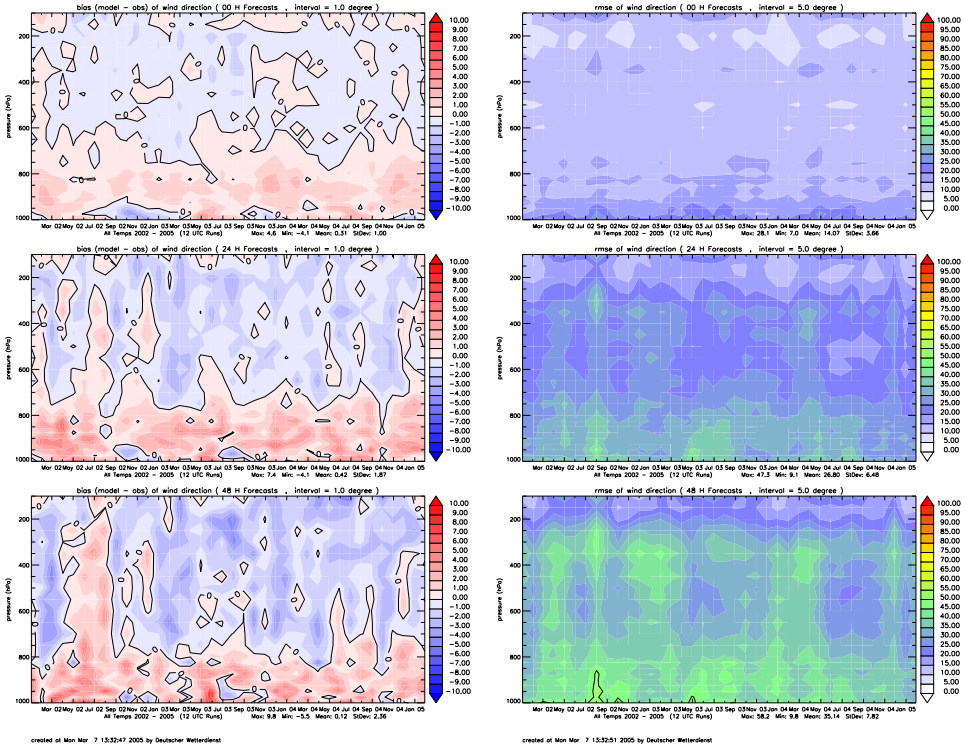

Figure 7: Time Series (January 2002 – February 2005) of wind speed bias (left columns) and rmse (right columns) against radiosondes based on monthly mean profiles for 00 UTC LM runs at DWD. From top to bottom: Analysis, 24 h, and 48 h forecast.

Figure 7 displays bias and rmse for the wind direction. The bias of wind direction is mainly positive in the lower troposphere and negative in the middle and upper troposphere. No significant change in the behaviour over the years 2002 until 2004 is recognisable. The rmse of wind direction below 700 hPa shows a seasonal variation with lower values in winter and higher values in summer. In the middle and upper troposphere the behaviour of rmse is viceversa and between 500 and 600 hPa the minimum value of rmse occur. Overall in 2004, compared to 2003 a slight reduction of rmse can be seen.

Figure 8 displays bias and rmse for the wind velocity. The bias of wind velocity is mainly positive in the lower troposphere in winter and negative in summer, whereas in the upper troposphere a negative bias through the whole year is prevailing. Since October 2004 this has changed, now a stronger positive bias from ground until up to 400 hPa can be seen. The reason for this change is quite not clear but in October 2004 the resolution of the global model which delivers the boundary values for LM was increased to a 40 km grid (from 60 km before) and to 40 vertical layers (from 31 before). Rmse of wind velocity remains nearly unchanged in summer half, whereas between winter half 2003/2004 and winter half 2004/2005 a rmse reduction of about 0.5 m/s can be stated below 600 hPa. In the 300 hPa level the maximum value of more than 9 m/s in winter 2003/2004 is reduced to 8 m/s in winter 2004/2005.

References

Pflüger U., 2004: Operational verification of vertical profiles at DWD. COSMO Newsletter no 4, pp. 95 - 103, available at www.cosmo-model.org

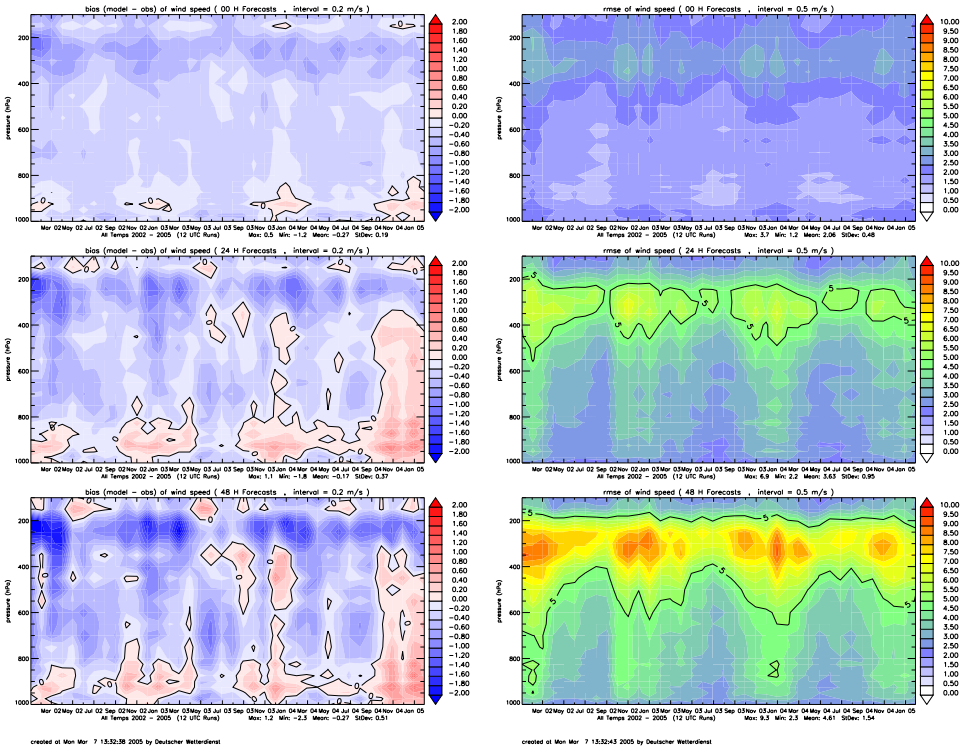

Figure 8: Time Series (January 2002 – February 2005) of wind direction bias (left columns) and rmse (right columns) against radiosondes based on monthly mean profiles for 00 UTC LM runs at DWD. From top to bottom: Analysis, 24 h, and 48 h forecast.

Verification of aLMo with SYNOP and GPS data over Europe

Pirmin Kaufman

MeteoSwiss, Zurich, Switzerland

1 Introduction

The development of the surface verification of aLMo over the whole model domain continued in 2004. The last two of the six statistical measures that are now routinely plotted (Table 1) have been added in 2004.

Table 1: Routinely plotted verification parameter.

ME	Mean Error	Bias, average difference between model and observation
MAE	Mean Absolute Error	Average difference between model and observation, independent of sign
STDE	Standard Deviation of Error	Variability of error
RMSE	Root Mean Square Error	Error independent of sign, more weight to larger deviations
COR	Correlation	Correspondence of model fluctuations with observation
NOBS	Number of observations	Data availability

13 more statistical values (Table 2) are now also calculated but not routinely plotted because of their limited usability. The verification now also includes the parameters 10 m wind speed and direction, cloud cover, and 12-hourly precipitation sums.

Table 2: Routinely calculated but not plotted verification parameters.

NMOD	Number of model values
N	Number of valid (mod,obs) pairs, i.e. number of valid error values
MINE	Minimum of error
MAXE	Maximum of error
COV	Covariance
MMOD	Mean model
MOBS	Mean observation
STDMOD	Standard deviation of model
STDOBS	Standard deviation of observation
MINMOD	Minimum of model
MINOBS	Minimum of observation
MAXMOD	Maximum of model
MAXOBS	Maximum of observation

For the latter two, categorical statistics (Table 3) have been implemented but are not yet operationally plotted. The thresholds are set to 30% and 80% for cloud cover and to 0.1, 1, 2,

Table 3: Routinely calculated categorical scores (plots to be implemented).

OF	Observed frequency
ACC	Accuracy (or percent correct, by few authors called hit rate)
FBI	Frequency bias
POD	Probability of detection
FAR	False alarm ratio
THS	Threat score (or critical success index)
ETS	Equitable threat score
TSS	True skill statistics (or Pierce skill score, or Hanssen-Kuipers Discriminant)
HSS	Heidke skill score

10, 20, 30, and 50 mm for 12h-precipitation sums. A more sophisticated search algorithm for the assignment of the observation sites to model grid points has been implemented. Under the constraint that land points are always preferred over water points, the sum of the vertical plus the horizontal distance between observation site and model grid point is minimized, with a weighting factor for the vertical distance currently set to 500. This means that a grid point with 20 m height difference has the same summed distance than one at equal height but 10 km horizontal distance. The search area for model grid points is now circular instead of quadratic, with a radius over water of 2 grid points and over land of sqrt(2) grid points. Stations with height difference greater than 100 m are excluded as before. This algorithm allows optimizing the observation site to grid point relationship also below 100 m height difference. The algorithm agreed on within COSMO WG 5 (COSMO, 2000) would not allow this, even when the nearest grid points have nearly the same horizontal distance and only differ in height.

2 Results

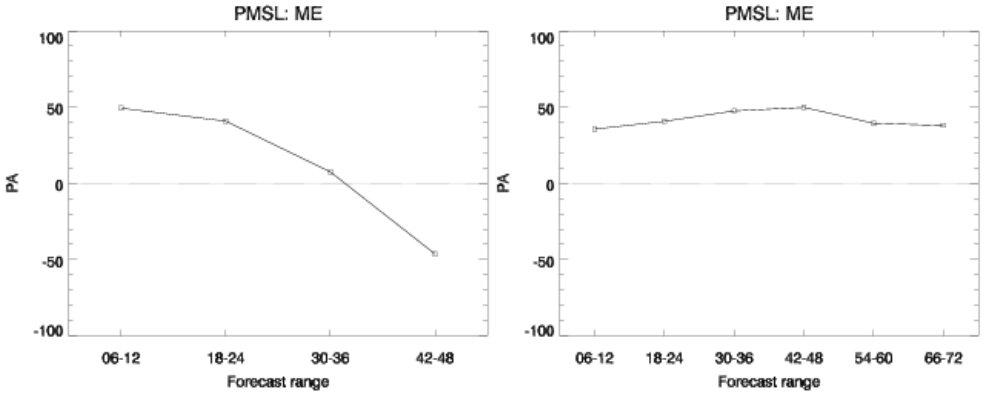

Figure 1: Evolution of pressure bias with forecast time for a) summer 2003 b) summer 2004.

The pressure bias increases with forecast time in winter, but decreases in summer. This general pattern of the pressure bias evolution however has changed for the summer season between 2003 and 2004. While still valid in summer 2003 (Fig 1a), in summer 2004 the pressure bias remained close to zero (0.2 hPa) over the whole forecast range of 72 hours (Fig. 1b). The comparison of the IFS-driven parallel test chain with the operational GME-driven aLMo in summer 2003 indicates that this is probably due to the IFS boundary conditions,

which became operationally used in autumn 2003. The standard deviation of the pressure error over the northern half of the model domain is usually considerably higher in winter (∼ 3 hPa, 48 h forecast range) than in summer (∼ 1.5 hPa). In winter 2004/05, the elevated standard deviation only appears over the northernmost part of the domain and is smaller than in previous winters.

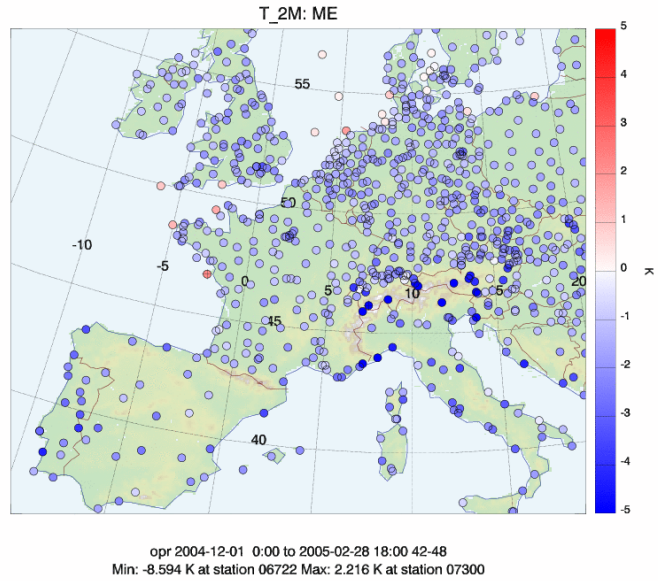

Figure 2: Temperature (2 m) bias for winter 2004/05 and forecast range 42-48 h. Blue indicates model is too cold, red model is too warm.

The well-known cold bias of the 2 m temperature in winter continues to exist and is more negative in 2004/05 (Fig. 2; whole model domain: -1.7 deg C at +48 h) than in previous winters (e.g. -1.4 deg C in 2003/04). Coastal stations (near seas or lakes) in winter produce large positive biases (up to 6 deg C) when used to verify with model grid points that have water as surface type. The verification results with land points instead of water points gives considerably better results. Some small islands and oil platforms however do verify well with water grid points in the model (light red and white dots in Fig. 2) and should not be eliminated from the verification, thus water points are still allowed if no land points are available within the search radius. The standard deviation of the 2 m-temperature error increases with the complexity of the terrain (not shown).

The wind speed has a slight negative bias when measured over the whole model domain. There is however an important difference between coastal and inland stations (Fig. 3). While the bias is strongly negative at coastal stations (down to -6 m/s), it is strongly positive at many inland stations (up to 3.7 m/s), especially during winter. Interestingly, island and oil-platform stations that are compared with model grid points over water also show a positive bias, indicating that the wind speed over water is also overestimated. The standard deviation of the error (2 m/s) is larger near the coast than at the inland stations. This is probably due to the varying sign of the error depending on the wind blowing off the sea or off the land.

The wind direction bias over Europe (Fig. 4) amounts to 10 - 20 degrees and is much more evenly distributed than the speed bias. The positive bias indicates that the model wind direction has a clockwise offset. As opposed to the wind speed, the standard deviation of the wind direction error increases with distance form the coast from 30 degree to 100 degree in the complex terrain of the Alps. This large standard deviation is due to the variable winds at low wind speeds which are not excluded in this verification and are more frequent in complex terrain due to topographic shielding, channeling, and local thermal wind systems.

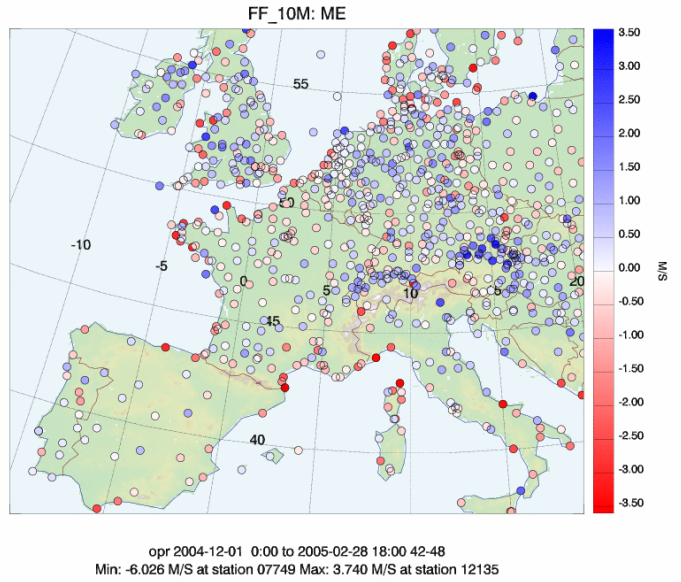

Figure 3: Wind speed (10 m) bias for winter 2004/05 and forecast range 42-48 h. Red indicates model wind is too slow, blue too strong.

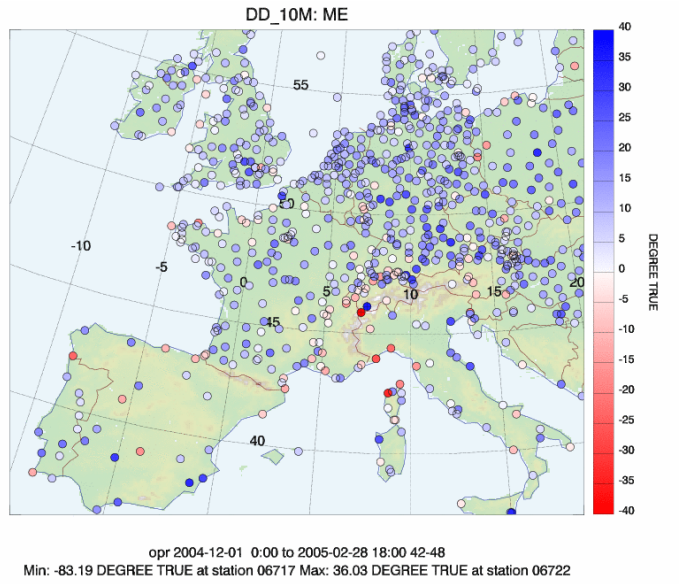

Figure 4: Wind direction (10 m) bias for winter 2004/05 and forecast range 42-48 h. Positive bias indicates clockwise offset.

The cloud cover bias is mostly slightly negative (-7%, independent of the season). A positive bias is often present over Belgium and sometimes also over the Netherlands, northern Germany, Denmark, and Poland. The standard deviation of the error is around 35% (+48 h) for the whole model domain.

The model bias against GPS-derived integrated water vapor (IWV) is more negative in summer (-1.4 mm at +48 h, all European sites processed by Swisstopo) and in complex terrain (up to 6 mm) than in winter (-0.5 mm) or flat terrain. The most probable explanation for the more negative bias in summer is the increased specific humidity content that leads to larger absolute errors even when the relative errors stay the same. In complex terrain, the increased height differences between GPS antennae, SYNOP station and model grid point in complex terrain probably lead to larger errors in the calculation of the IWV. The standard

deviation of the error (summer $\sim$ 5 mm, winter $\sim$ 2.5 mm at +48 h) is not affected by complex terrain, supporting the assumption that the bias is due to these height differences.

3 Conclusions

The change of the driving model from GME to IFS in autumn 2003 had a positive effect in the summertime pressure bias. The verification results for newly added parameters wind, cloud cover, and precipitation are not yet available for the seasons before the change. For temperature and dew point temperature, the variation from year to year is larger than an eventual change due to the driving model.

The fact that many U.K. stations that report reduced pressure dont report the pressure at station height, and that many stations in Spain, Italy and the Balkans do not report any measurements at nighttime, remains a nuisance for an all-European verification.

References

COSMO, 2000: Verification Workshop report, 14-15 February 2000, Bologna, Italy, available from www.comso-model.org (private pages).

Vertical Profiles - A Comparison between German, Italian and Swiss Verification

P. Kaufman[1], M. Arpagaus[1], P. Emiliani[2], E. Veccia[2], A. Galliani[2], U. Pfluger[3]

[1] *MeteoSwiss* [2] *UGM* [3] *DWD*

1 Introduction

The verification of vertical profiles is an important part of the operational verification of a limited area model. In addition to the separate verification of each operating centre, a lot can be learned about the influence of the differing model set-up by comparing the verification results of the different Local Model installations of each country. For the COSMO General Meeting of 2004, the German, Swiss and Italian responsibles for the upper-air verification contributed their results of summer 2004 to a common presentation.

The model set-ups involved are named as follows: The German operational Local Model set-up with 35 layers in the vertical, soil-moisture analysis and nudging for the initial conditions, GME boundary conditions, and the prognostic-tke surface-layer scheme is named LM. The Italian version running at Bologna, with 35 layers, nudging for the initial conditions, and GME boundary conditions and prognostic-tke surface-layer scheme is called LAMI. The Swiss set-up finally, with 45 layers, nudging for initial conditions, IFS for boundary conditions, and the old surface-layer scheme is referred to as the aLMo (Alpine Model).

While the differences in the model set-ups rend the comparison of the verification results interesting, there are also differences in the verification itself, which is to some extent detrimental to the direct comparison. The German upper-air verification use all available radiosonde stations over the model domain (Pflger 2004). The Swiss aLMo is verified at 30 selected sites evenly distributed over the model domain (Arpagaus 2004). The Italian verification, in contrast, uses a set of 7 stations in the Italian area (Emiliani et al. 2004). A similar verification with 6 stations south of the Alps is available for aLMo but not for the LM. Due to the different set of stations involved, the following figures will either contain overlay of LM and aLMo results for the whole model domain, or overlays of LAMI and aLMo results for the Italian part of the model domain. The humidity verification can only be compared between LM and aLMo both using use relative humidity, whereas LAMI on the other side verifies dewpoint temperature.

Another difference in the LAMI verification is the definitions of the seasons. The summer season is usually defined as the calendar months of June, July and August. The LAMI verification for summer 2004 originally included July, August and September. For the purpose of this paper however the LAMI verification only includes July and August.

2 Results

Fig. 1 shows the geopotential height verification for LM (black, green, and yellow) and aLMo (red, blue, magenta, and cyan). The aLMo bias shows a see-saw in the upper troposphere. This is probably an artifact stemming from a vertical interpolation error (Arpagaus 2002).

The standard pressure levels (markers in Fig. 1) however are not affected and give meaningful results. In the lower troposphere, the LM starts at the initial time with a positive bias of

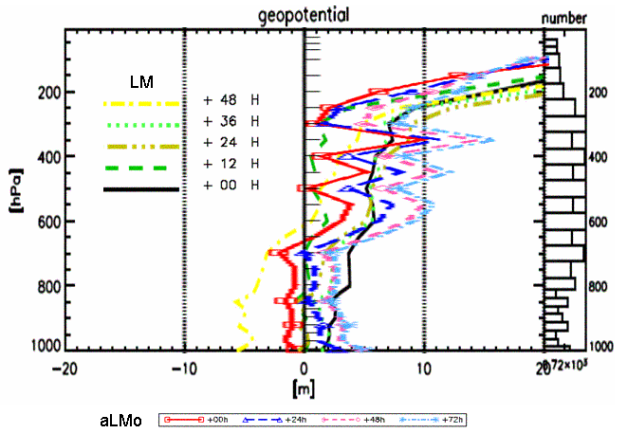

Figure 1: Bias of geopotential height for LM (black-green-yellow) and aLMo (red-blue-magenta-cyan) for summer 2004.

2 to 3 m, which is slowly reduced towards zero throughout the integration until 36 h, then jumps to -5 m at 48 h. The aLMo, in contrast, starts with a slightly negative bias of about -1 to -2 m, which increases gradually to +3 m.

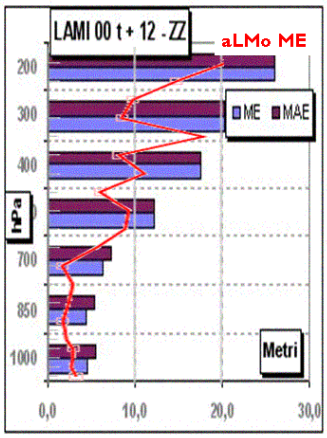

Figure 2: Bias of geopotential height for LAMI (blue bars) and aLMo (red line) for summer 2004 at forecast hour 12.

For the stations south of the Alps (Fig. 2 and 3), the aLMo shows a slight increase of the bias from the initial time (Fig. 2) to 48 h forecast (Fig. 3), like for the whole model domain.

LAMI, with a bias decreasing with increasing forecast range, behaves as LM did for the whole domain, although with a larger value (-10 m at 48 h) of the bias. The reason of this mass deficit in LM and LAMI in the 48 h forecast is unknown. The fact that aLMo showed the same behavior in summer 2002 and 2003 hints to the GME boundary conditions as possible reason.

The temperature profiles of LM and aLMo behave in a comparable manner, except that the aLMo bias is shifted to slightly lower values (Fig. 4). The negative bias peak in the boundary layer is at 975 hPa for the LM, but at 925 hPa for aLMo. This could be caused by the choice of verification sites. For the region south of the Alps (Fig. 5), aLMo shows a bias similar to the one for the whole domain. LAMI shows a bias profile with a positive

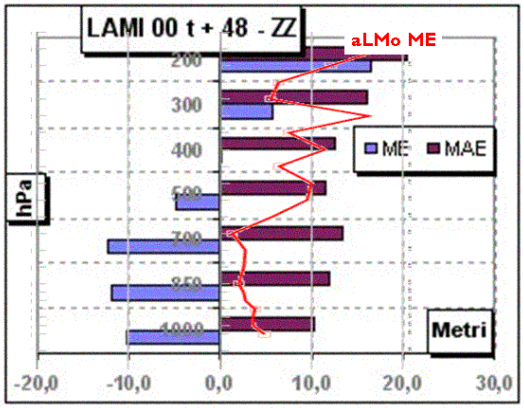

Figure 3: Bias of geopotential height for LAMI (blue bars) and aLMo (red line) for summer 2004 at forecast hour 48.

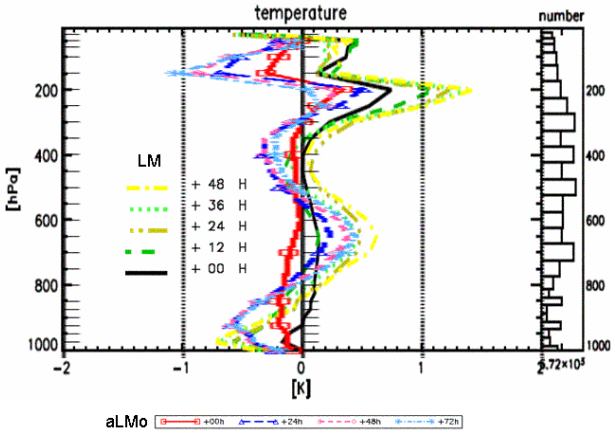

Figure 4: Temperature bias for LM (black-green-yellow) and aLMo (red-blue-magenta-cyan) for summer 2004.

peak at 400 hPa, a feature present neither in LM nor in aLMo.

The relative humidity bias is nearly equal for LM and aLMo (Fig. 6). As mentioned above, the LAMI verification does not use relative humidity but dewpoint temperature and cannot be compared to the LM and aLMo verifications. The positive peak of the aLMo bias at 1000 hPa at the initial time (red line in Fig. 6) could be the result of using the old turbulence scheme without prognostic tke.

The wind speed bias for LM and aLMo is largest (around -1 m/s) below and above the tropopause region (Fig. 7). It is also large between 800 hPa and 500 hPa in all models. The amount of the bias differs: In the whole domain at 48 h, it is -0.75 m/s for the LM and -0.5 m/s for aLMo. Remarkable is the different sign of the bias in the boundary layer: while the LM bias is negative, the aLMo has a positive bias below 900 hPa. No such difference is found in the wind direction (not shown). South of the Alps (Fig. 8), the wind speed bias is -1.5 m/s for LAMI and -1 m/s aLMo.

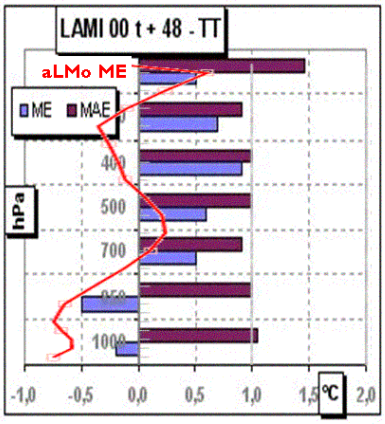

Figure 5: Temperature bias for LAMI (blue bars) and aLMo (red line) for summer 2004 at forecast hour 48.

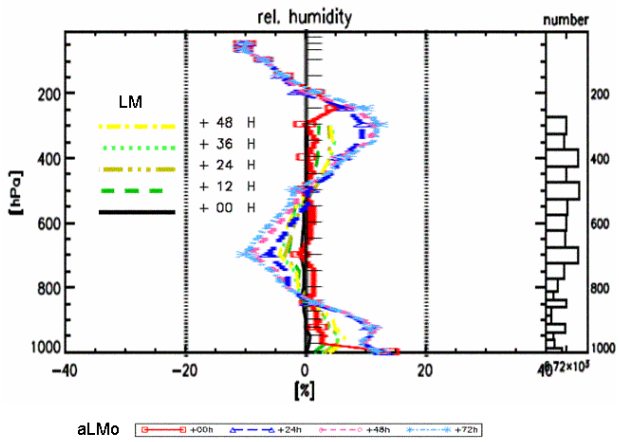

Figure 6: Relative humidity bias for LM (black-green-yellow) and aLMo (red-blue-magenta-cyan) for summer 2004.

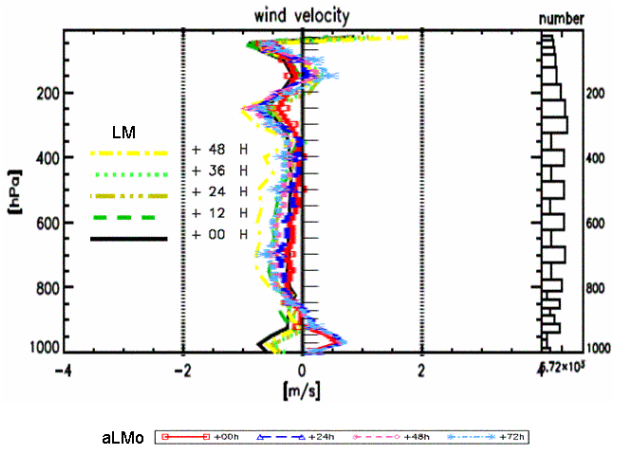

Figure 7: Wind velocity bias for LM (black-green-yellow) and aLMo (red-blue-magenta-cyan) for summer 2004.

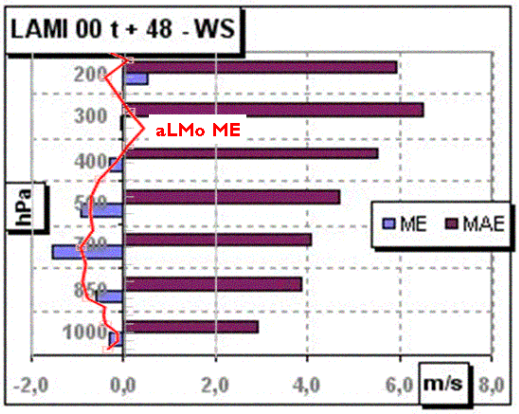

Figure 8: Wind velocity bias for LAMI (blue bars) and aLMo (red line) for summer 2004 at forecast hour 48.

3 Conclusion

The two model set-ups LM and LAMI both show a similar drop-off of the near-surface geopotential at the 48 h forecast range, and are driven by the same boundary conditions. The other common features of LM and LAMI that distinguishes them from aLMo are the tke surface-layer scheme and the number of vertical levels. These are however unlikely candidates to explain the difference in the pressure bias. They might however be causing differences in temperature and humidity near the ground. The verification results of these parameters are less consistent. With the existing differences in verification, it is difficult to decide whether and what differences in the model set-up cause different model behavior. For a more in-depth comparison, it would be helpful if the participating operating centers could agree on a common set of sounding stations, a common definition of seasons and some additional common statistical measures other than the bias. As an alternative, the model forecast could be exchanged and each country could not only verify its own, but also the other models. This would avoid the danger of still having unrecognized differences in the model verification that could mislead the interpretation.

References

Arpagaus, M., 2002: Operational verification at MeteoSwiss. COSMO Newsletter no 2, pp. 65 68, available at www.cosmo-model.org

Arpagaus, M., 2004: Operational verification of vertical profiles at MeteoSwiss. COSMO Newsletter no 4, pp. 104–106, available at www.cosmo-model.org

Emiliani, P., M. Ferri, A. Galliani, and E. Veccia, 2004: Verification of vertical profiles at UGM. COSMO Newsletter no 4, pp. 107–112, available at www.cosmo-model.org

Pfluger, U., 2004: Operational verification of vertical profiles at DWD. COSMO Newsletter no 4, pp. 95–103, available at www.cosmo-model.org.

9 Model Development and Application

This section includes several reports on various research topics and model applications as well as progress and status reports of the COSMO Working Groups. Within this section, we omit a subdivision by themes and the numbering of equations and figures refers to each paper. The contributions are ordered such that they follow the topics of WG1 – WG4 and WG6. Papers related to model verification have been included in the preceding section.

Most of the papers included in this section are write-ups from the COSMO annual meeting 2004 in Milano (Italy). Many thanks to all who provided contributions for the present issue of the Newsletter.

We have not included longer reports that have been or are going to be published in the COSMO Technical Report (TR) series. The TRs are intended for a documentation of research activities, to present and discuss results from model applications and from verification and interpretation, and to document technical changes and new components of the LM package. The purpose of these reports is to communicate results, changes and progress related to the LM model system relatively fast within the COSMO consortium. Technical Reports No. 1 - 8 are available at www.cosmo-model.org (see Appendix C).

Latent Heat Nudging and Prognostic Precipitation

Stefan Klink and Klaus Stephan

Deutscher Wetterdienst, P.O.Box 100465, 63004 Offenbach a.M., Germany

1 Introduction

Within the framework of the development of LMK (LM Kürzestfrist), which is a meso-γ-scale version of the operational nonhydrostatic limited area model LM, it is intended to use remote sensing data for the continuous data assimilation stream of LMK (Doms and Förstner, 2004). As the main focus of LMK is on the prediction of severe weather, which often forms in context with deep moist convection (such as super- and multi-cell thunderstorms, squall-lines, mesoscale convective complexes and mesocyclones), we expect a beneficial impact on the assimilation cycle of LMK from radar measurements of these meso-γ-scale structures. Thus, in addition to the assimilation of conventional data, like surface and radiosonde measurements, as a first step 2D radar reflectivities derived from the German radar network will be introduced in the nudging-type analysis of LMK. Using the Latent Heat Nudging (LHN) technique (Leuenberger and Rossa, 2003) the thermodynamic quantities of the atmospheric model are adjusted in that way, that the modelled precipitation rates resemble the observed precipitation rates. Due to complaints from forecast meteorologists as well as from hydrological authorities on a non-realistic distribution of precipitation in mountainous terrain, given by the operational forecasts of LM, a reconsideration of the numerical treatment of precipitation quantities within LM took place. These investigations on the topic of "Prognostic Precipitation" have been carried out by Gassmann (2003) and Baldauf and Schulz (2004). Resulting from this, since April 2004, the advection of hydrometeors is taken into account in the operational LM. Because the Latent Heat Nudging algorithm is highly sensitive on the 3D thermodynamical field of cloud and precipitation physics, the LHN has to be tested under these new circumstances of a changed treatment of grid scale precipitation, which will also be used in the LMK version. Results from preliminary experiments with a purely diagnostic precipitation scheme have shown that precipitation patterns can be assimilated, using the LHN algorithm, in good agreement with those observed by radar, both in position and amplitude (Klink and Stephan, 2004 and Leuenberger and Rossa, 2003) but later experiments using the "prognostic precipitation" revealed some problems with the LHN. However, some recent tests show, that several adaptations to the conventional LHN scheme are necessary in order to reestablish the good performance of LHN during the assimilation run and to get a positive impact on the free forecasts.

2 Interaction of Prognostic Precipitation and Latent Heat Nudging

In order to test the performance of the LHN algorithm under the conditions and constraints of a prognostic treatment of precipitation (Gassmann, 2003 and Baldauf and Schulz, 2004) a case study has been conducted for a convective event in summer 2004. During the morning hours of the 9th June 2004 a convergence line reached the northerly parts of Germany. Hamburg has been hit by a severe thunderstorm, which was part of this squall line approaching the land from the North Sea. This is outlined by fig. 1, which shows the current precipitation rate measured by the German radar network at 6 UTC (fig. 1a) and 8 UTC (fig. 1b).

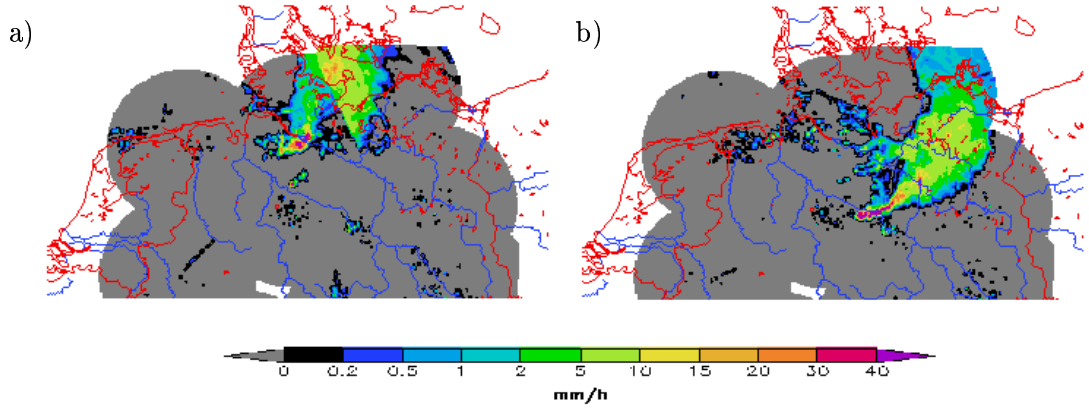

Figure 1: Current precipitation rate in mm/h (derived from radar) on 9th June 2004 at 6 UTC (a) and 8 UTC (b).

For this case different assimilation runs testing the LHN in connection with diagnostic and prognostic precipitation have been carried out. Figure 2 displays hourly accumulated precipitation heights for the hour from 8 to 9 UTC for the radar measurements (b), the control run (i.e. Nudging without LHN) (a), a LHN run with diagnostic precipitation (c) and a LHN run with prognostic precipitation (d). When comparing fig. 2b and 2c we can see, that the LHN run with the conventional diagnostic precipitation scheme almost perfectly meets the patterns given by the radar measurements. In contrast to this, the run with LHN and prognostic treatment of precipitation (fig. 2d) shows a distinct overestimation of the mean precipitation amount. Furthermore the local maxima and minima, visual in the radar data (fig. 2b), are not in the correct position for this LHN run (fig. 2d). The results from other experiments sustained the impression, that there is a typical overestimation of precipitation and a misplacement of local extremes when using LHN in combination with prognostic precipitation.

When searching for reasons for this bad performance of LHN under the conditions of a prognostic precipitation scheme we have reconsidered the general outline of the LHN algorithm and the basic assumption one acts on, when using this assimilation method for radar data. The basic assumption for LHN is the proportionality between vertically integrated latent heat release and surface precipitation rate in one single column (Leuenberger and Rossa, 2003). This is based on the observation that relatively little moisture is stored in clouds. The proportionality itself allows to scale the modelled latent heating rate with the ratio of observed to modelled precipitation rate. But this relation is just valid for large scales and long time periods, where we can assume, that cloud and precipitation producing (mainly condensation) and cloud dissipating (precipitation) processes are balanced, which means that no net storage of cloud liquid water and precipitation quantities takes place inside one column. A horizontal grid length of roughly 3 km in combination with an appropriate time step and an additional prognostic treatment of precipitation can be understood as a step towards cloud resolving models. This means, that the model itself is able to distinguish between updrafts and downdrafts inside convective systems. Because the main part of positive latent heat release (due to condensation) occurs in updrafts and strong precipitation rates are often connected with downdrafts, we can expect, that on cloud resolving scales areas with positive latent heating and patterns with strong precipitation rates will be located at different horizontal positions. Figure 3b exemplifies the changed thermal structures in convection cells, when advection of precipitation is taken into account, while fig. 3a shows the well known strong correlation of latent heat release and precipitation rate for a simulation

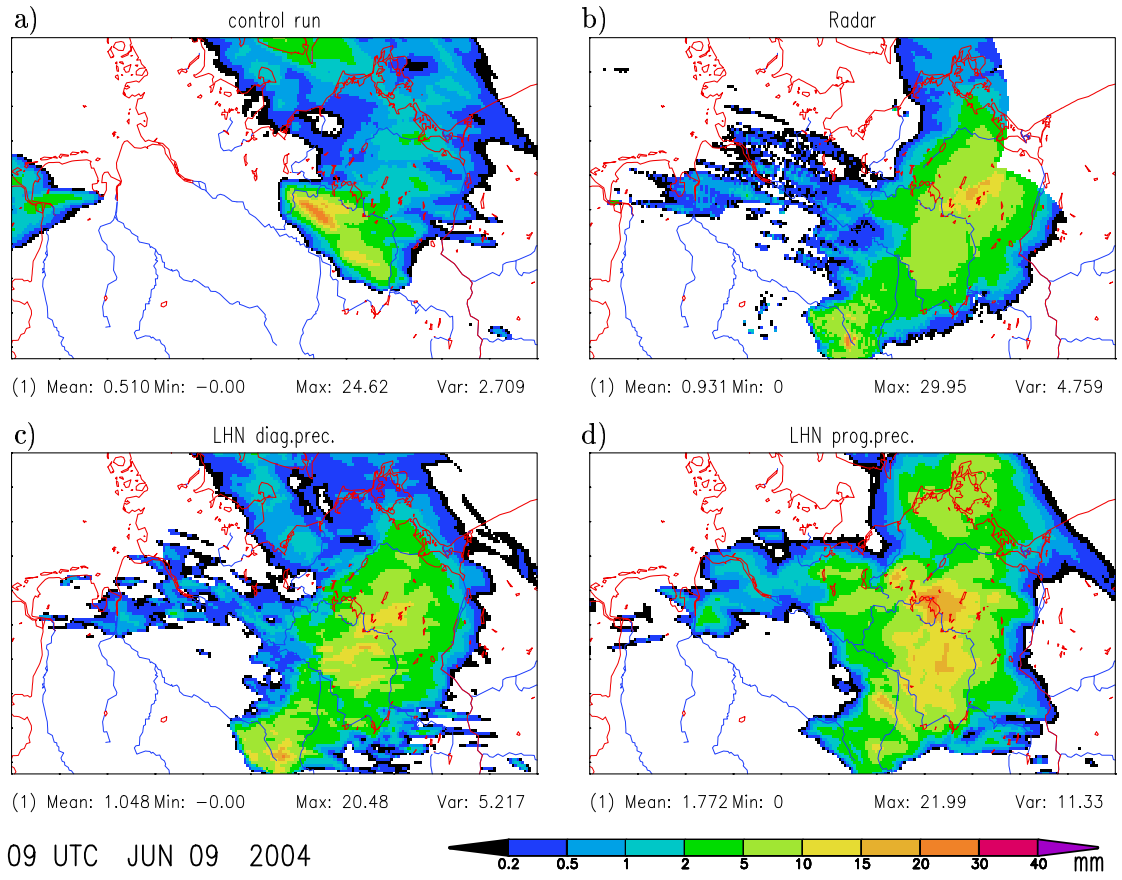

Figure 2: Hourly accumulated precipitation heights in mm on 9th June 2004 8-9 UTC: control run (a), radar observation (b), LHN run with diagnostic precipitation (c) and LHN with prognostic precipitation (d).

with diagnostic treatment of gridscale precipitation. Recognizing a northwesterly flow in this case, one finds that the area of positive latent heat release, which marks the region of cloud and precipitation formation, is a little bit ahead of the surface precipitation area (see fig. 3b). Due to this displacement the problem arises, that LHN temperature increments will probably be inserted in the wrong locations. The fact, that the correlation between the vertically integrated rate of latent heat release and the surface precipitation rate is significantly smaller for the simulation with prognostic precipitation compared to the diagnostic run is shown by Fig. 4. Thus, we have to state, that the use of prognostic precipitation at least weakens the validity of the basic assumption of the LHN algorithm. Furthermore it takes some time for the precipitation to reach the ground when advection is considered. For this reason no immediate response of the model to temperature increments of the LHN algorithm is possible. The scheme does not notice, if precipitation has already been activated by the LHN. On account of this new situation the LHN scheme, implemented in the LM, had to be revised. Which adaptations are possible and useful, will be described in the following section.

3 Possible Adaptations to the conventional LHN scheme

As mentioned above there are two major challenges when treating the precipitation prognostically. First of all, it is strongly related to the temporal and spatial characteristics of

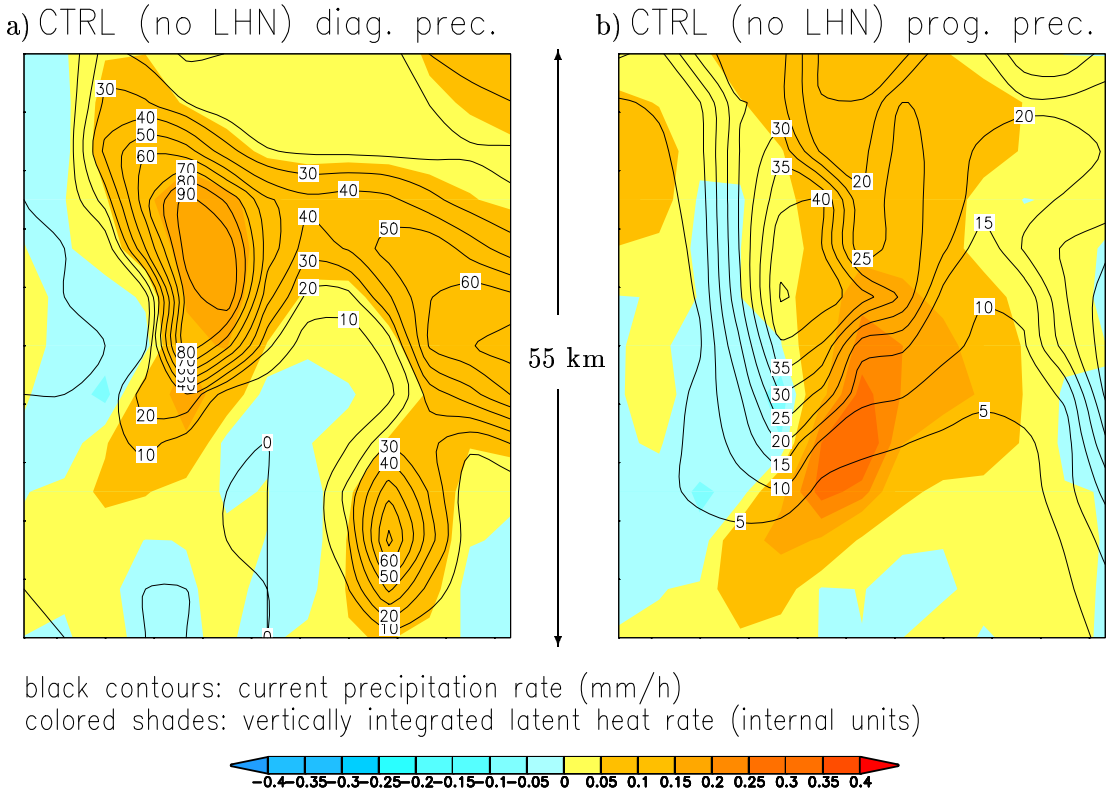

Figure 3: Horizontal fields of vertically integrated latent heat rate (shaded colours) and current precipitation rate at the ground (black contours) for a run with diagnostic precipitation (a) and prognostic precipitation (b).

the prognostic precipitation itself. One can show that the temporal effect of drifting of precipitation particles is much more important for the LHN-approach than the spatial displacement. However, one suggestion is, to spatially smooth the fields of observed as well as modelled surface precipitation rate and the 3D field of latent heat release, in order to get a better correlation of precipitation and latent heating. Of course, this would lead to a loss of information on the grid scale. The temporal delay leads to a lack of feedback between the temperature increment and the forced precipitation. To tackle this problem an immediate information, of how much precipitation the temperature increment has initialised already, is necessary within each time step. This information is used as a reference in the comparison of modelled with the observed precipitation rates to measure the essential scaling factor. Remember, the LHN increment is calculated with respect to the ratio of observed to modelled precipitation rate. This ratio minus 1 gives the essential scaling factor:

$$\begin{aligned} \Delta T_{LHN}(z) &= \alpha \cdot \Delta T_{LatentHeatRelease}(z) \qquad \text{with} \\ \alpha &= \left(\frac{RR_{Obs}}{RR_{Mod}} - 1 \right) \end{aligned}$$

Such a reference could be the diagnostically calculated precipitation rate. For this purpose an additional call of the former cloud microphysics scheme (`HYDCI`) is enforced. This additional calculation must not have any further effect on the simulation. No feedback on other model variables has to be performed. It just diagnoses the amount of precipitation what would fall out at once within each separate vertical column. This precipitation rate can not be compared with the precipitation rate of the former diagnostic treatment. It is quite different

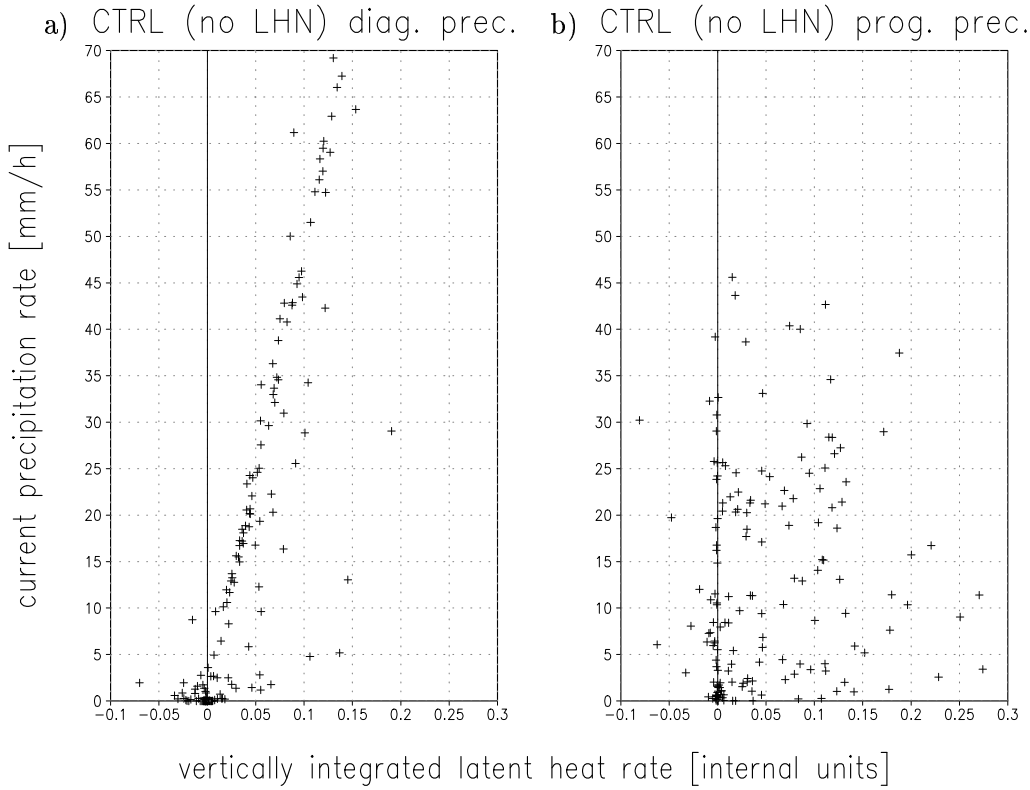

Figure 4: Scatter plots of vertically integrated latent heat rate and current precipitation rate at the ground for a run with diagnostic precipitation (a) and prognostic precipitation (b).

to both the former diagnostic and the newer prognostic precipitation rate. It still gives an important hint of the efficiency of the LHN so far. Unfortunately this precipitation rate is hardly to interpret. It does not match the actual rate and therefore has to be calibrated. A more sophisticated solution might be the application of the vertical integrated precipitation flux as a reference.

The second challenge is to be found as the change of the spatial structure of latent heat release within the model. In contrast to a diagnostic treatment of precipitation, latent heat release is now layered more horizontally than vertically. Very high values of latent heat release will be found in the updraft regions at the leading edge of a convective cell. No precipitation will reach the ground, there. Further upstream the release of latent heat becomes weaker and the precipitation rate arises. In terms of correlation of precipitation rate and latent heat release it means that within the same vertical column there is a weak correlation at an early state of a convective cell, a higher positive correlation in the middle of its lifetime and a weak negative correlation at the end of the lifetime. This feature strongly influences the effects of LHN. To consider these influences, the original LHN routine has to be checked, if it is still consistent. Especially all the control parameters have to be recalibrated in order to take into account the higher amounts of latent heat release. One essential effect will be discussed here in more detail. Performing prognostic precipitation will get vertical columns with a certain precipitation rate at the ground but no appreciable latent heat release above it. This will take place mainly in upstream regions of a convective cell, where the cell is almost dissipated. At these locations the model generally produces negative values of latent heat release due to evaporation of precipitation. In the case, that too much precipitation is modelled at these grid points (i.e. $\alpha < 0$), the resulting temperature increment will be positive. This of course will increase the precipitation rate instead. Therefore it is necessary to assure that increments will only be inserted at the right vertical layers. At grid points, where the

precipitation rate of the model has to be increased, only positive temperature increments are added and negative increments at grid points where the model produces higher amounts than the observations. There is now implemented a check of the sign of the increment and the scaling factor within each model layer, which decides, if the increment will be used or not.

Figure 5 shows the hourly sum of precipitation for different LHN configurations (panels c to h) in comparison with the radar observation (panel a) and a simulation without LHN at all (panel b) for the 8th July 2004 9 UTC after 6 hours of assimilation. For panel c we just used the LHN configuration maintained in all the runs with diagnostic precipitation. This means, using

- an additional moisture adjustment,
- vertical filtering of the increments,
- grid point search for grid points without appreciable precipitation and
- LHN parameters as follows:
  - upper limit of the ratio is set to 3.0 (i.e. $\alpha <= 2$),
  - lower limit of the ratio 0.3 (i.e. $\alpha >= -0.7$) and
  - nudging coefficient equal 1.0.

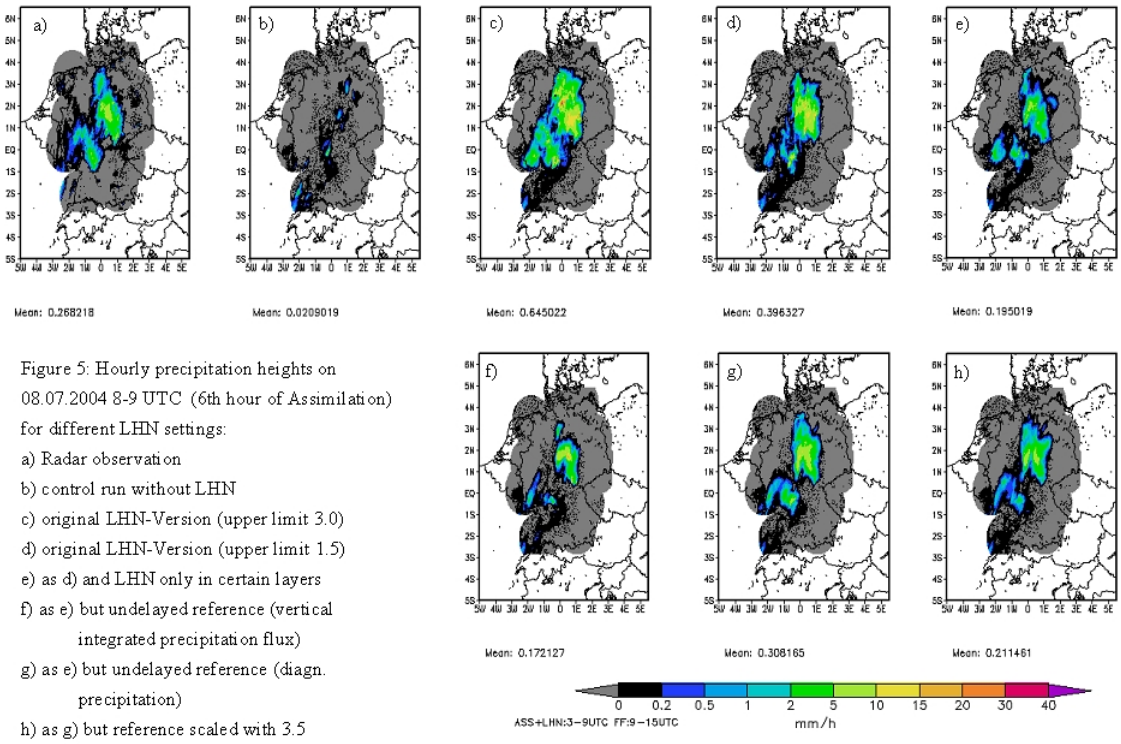

Figure 5: Hourly precipitation heights on
08.07.2004 8-9 UTC (6th hour of Assimilation)
for different LHN settings:
a) Radar observation
b) control run without LHN
c) original LHN-Version (upper limit 3.0)
d) original LHN-Version (upper limit 1.5)
e) as d) and LHN only in certain layers
f) as e) but undelayed reference (vertical
integrated precipitation flux)
g) as e) but undelayed reference (diagn.
precipitation)
h) as g) but reference scaled with 3.5

Figure 5: Hourly precipitation heights on 8th July 2004 8-9 UTC (6th hour of assimilation run) for different LHN configurations.

Again, we get a strong overestimation of precipitation due to the LHN. In the simulation for panel d we just changed the upper limit of the ratio to 1.5 (i.e. $\alpha <= 0.5$). Only this little change has a distinct effect on the forecast. The overestimation is not as strong as before and

the locations of the patterns fit better, as well. In the next step of development we only apply the LHN increments in certain vertical layers as mentioned above. The results look quite good, even though the precipitation is underestimated now. So far, all the LHN simulations used the delayed prognostic precipitation as reference. Using an undelayed reference yields some additional benefits, especially in position and structure of the precipitation patterns. As a matter of fact, the application of an undelayed precipitation reference within the LHN approach is still under development.

4 Case Study with LHN and an undelayed reference precipitation

In order to test the previously mentioned adaptations to the LHN algorithm and to assess the effectiveness of LHN under the new circumstances, we carried out an assimilation run covering 5 days and also started 00, 12 and 18 UTC forecasts at each of these days. The period starting on the 7th July 2004 mainly covers convective precipitation events. For the simulations we used LM version 3.13 and we chose LMK configurations for the general model setup. Some additional LHN features are:

- use of an undelayed precipitation (diagnostic precipitation),
- spatial averaging (20 gridpoints) of latent heating and precipitation fields,
- LHN-coefficient: 0.5,
- applying temperature increments only in certain layers (more or less only in clouds).

For the purpose of comparison a control experiment without LHN was made. Figure 6 shows mean Equitable Threat Scores (ETS) and mean Frequency Biases (FBI) for hourly accumulated precipitation heights for a threshold of 0.1 mm for the assimilation run and the free forecasts starting at 18 UTC. The use of the LHN algorithm leads to continuously improved analysis states during the assimilation. This is shown by the higher values of ETS in fig. 6a. This positive impact of radar data is visible in the free forecasts for up to 7 hours (fig. 6b) on average. However, there is also a weak but persistent increase in the FBI present, which most of the time during assimilation tends towards the desired value of 1.0 (see fig. 6c). Unwanted are the greater values of FBI after the 8th hour of the 18 UTC forecasts (fig. 6d). But these values as well as the values in the night time hours of the assimilation run can probably be explained by a too low number of precipitation events during the hours from 0 until 6 UTC.

5 Summary and Outlook

Applying the Latent Heat Nudging approach in combination with a prognostic treatment of precipitation, we had to realise a bad performance of the LHN scheme. A distinct overestimation of surface precipitation took place. The features of the so called "prognostic precipitation" weaken the validity of the basic assumption of the LHN-approach. Several investigations were caried out. In the end two features could be identified to be the main reasons for the bad interaction of LHN and prognostic precipitation. First, precipitation needs a certain time to reach the ground and second, the change of spatial distribution of latent heat release in the model. After adapting the scheme, the model is again able to simulate the precipitation patterns in good agreement with radar observations. Over all we can state, that after tackling the challenges due to prognostic precipitation, the skill scores of

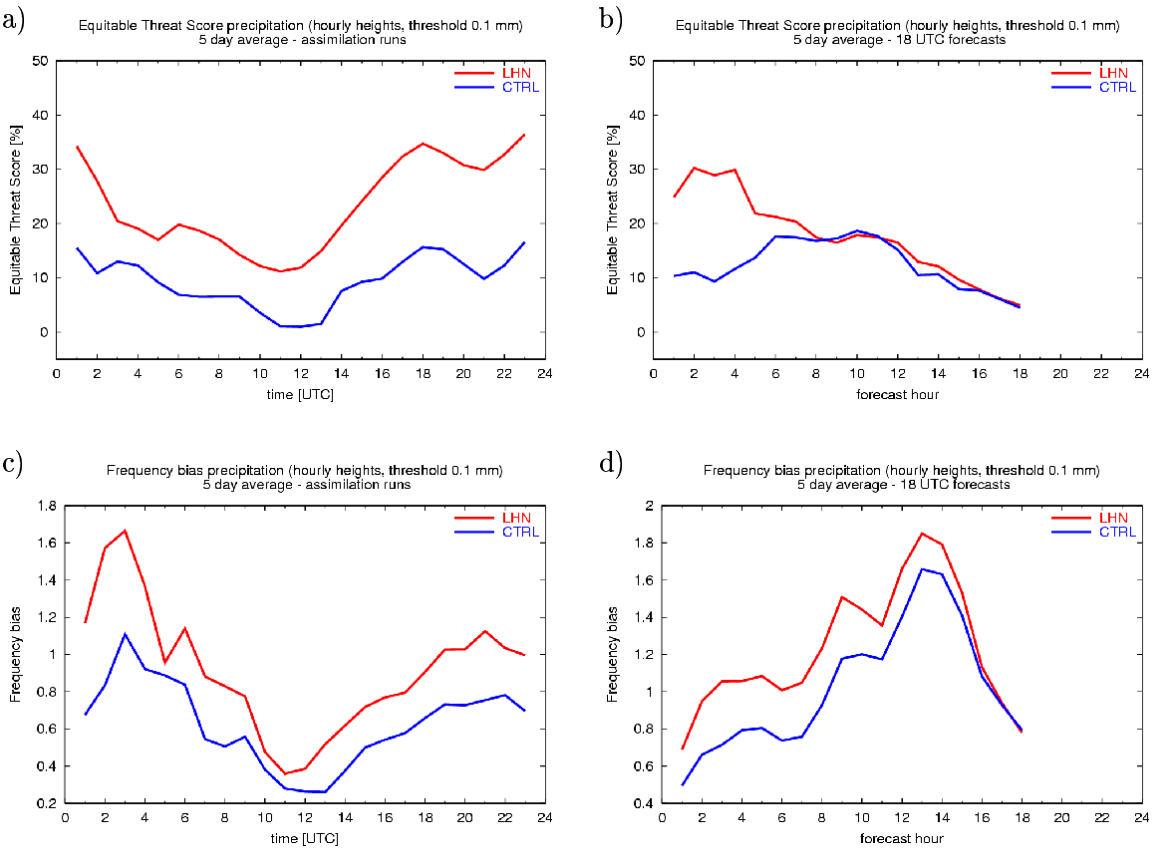

Figure 6: Mean Equitable Threat Scores and Mean Frequency Biases for hourly precipitation heights (threshold 0.1 mm) for assimilation runs (a) and (c) and for 18 UTC forecasts (b) and (d). The Mean scores were obtained by averaging over a 5 day period.

simulations with LHN are better than for simulations with the former diagnostic treatment of precipitation. With respect to a short simulation period in summer 2004, we can observe a benefit of LHN up to several hours within the free forecast. Further adaptations of the LHN scheme are possible and should allow to tune the results, as for instance spatial smoothing of precipitation fields and fields of latent heat release. In addition, simulations over longer periods in summer and winter are necessary, to decide on the operational use of the LHN approach.

References

Baldauf, M. and J.-P. Schulz, 2004: Prognostic Precipitation in the Lokal Modell (LM) of DWD. COSMO Newsletter, No. 4, 177-180.

Doms, G. and J. Förstner, 2004: Development of a Kilometer-Scale NWP-System: LMK. COSMO Newsletter, No. 4, 159-167.

Gassmann, A., 2003: Case Studies with the 2-Timelevel Scheme and Prognostic Precipitation. COSMO Newsletter, No. 3, 173-176.

Klink, S. and K. Stephan, 2004: Assimilation of Radar Data in the LM at DWD. COSMO Newsletter, No. 4, 143-150.

Leuenberger, D. and A. Rossa, 2003: Assimilation of Radar Information in aLMo. COSMO Newsletter, No. 3, 164-172.

The Coordinate Transformations of the 3-Dimensional Turbulent Diffusion in LMK

M. Baldauf

Deutscher Wetterdienst, Kaiserleistr. 42, D-63067 Offenbach a.M., Germany

1 Introduction

At the Deutscher Wetterdienst the numerical weather forecast model LMK (LM-Kürzestfrist) is currently under development. It is based on the LM (Lokal Modell) and shall be used for very short range forecasts (up to 18 hours) and with a resolution on the meso-γ-scale (about 2.8 km). Among other new parameterizations, e.g. a 6-class cloud microphysics scheme with graupel and a shallow convection parameterization, LMK shall contain a 3-dimensional (3D) turbulence model instead of the 1-dimensional column physics designed for the current LM resolution (Raschendorfer 2004). An appropriate 3D turbulence formulation is already contained in LLM, the large eddy simulation version of LM (Herzog, 2002a, and Herzog, 2002b) which was transferred into LMK (Förstner, 2005). Despite the fact, that it is not yet clear if a 3D turbulence is really required at the meso-γ-scale, for further applications of the model with increasing horizontal resolutions a 3D formulation of turbulence will surely be necessary.

The LLM was mainly designed for very small scale climatology studies with horizontal resolutions of about $\Delta x \sim 100$ m and therefore it uses cartesian coordinates instead of terrain following coordinates required for regional numerical weather prediction models. As a first step, this work derives the terms associated with terrain following coordinates both for the fluxes of momentum and arbitrary scalars and for the divergence of these fluxes. In principle, these terms were already derived in the LM documentation (Doms and Schättler, 2002; Doms et.al., 2005), but an error was found in their derivation: especially the divergence of a vector and a second-order tensor was handled identical there, which is not correct. Consequently a new derivation of these terms is presented here.

2 The flux divergences

To derive the coordinate transformation of the diffusion terms, in the equation of motion we only consider the time derivative of the velocity components and the divergence of the momentum fluxes

$$\frac{\partial v^i}{\partial t} = -\frac{1}{\rho}\nabla_j T^{ij} = -\frac{1}{\rho}\left(\frac{\partial}{\partial x^j}T^{ij} + \Gamma^i_{jk}T^{kj} + \Gamma^j_{jk}T^{ik}\right). \tag{1}$$

This equation is valid in *every arbitrary* coordinate system (e.g. Stephani, 1988). T^{ij} are the 2-fold contravariant components of the momentum flux tensor, v^i are the contravariant components of the velocity vector. Γ^k_{ij} are the Christoffel-symbols of 2. kind, defined by

$$\Gamma^k_{ij} = \frac{1}{2}g^{kh}\left(g_{ih,j} + g_{jh,i} - g_{ij,h}\right). \tag{2}$$

g^{ij} is the metric tensor; partial derivatives are denoted by a comma ',',.

A special quality of the LM coordinate system consists in the fact, that on the one hand it is spherical and terrain-following, but on the other hand it uses base vectors of a purely spherical coordinate system. Beyond this, not the contravariant components are used, but the so called physical components (i.e. they are related to normalized base vectors). Because of that, the elegant and compact formulation in (1) is lost, unfortunately.

To express equation (1) in the special LM coordinate system, it turns out to be convenient to apply it in purely spherical coordinates $x^i = (r, \lambda, \phi)$. This reflects on the one hand the usage of the spherical base vectors. On the other hand, the metric tensor and the Christoffel symbols are well known for spherical coordinates and can be found in many text books (see also Appendix A) instead of deriving them for the fully spherical and terrain-following coordinates.

Starting from Eq. (1) we first introduce physical components. Here we denote them with a star $*$, in contrast to the LM-documentation (Doms et.al., 2005), e.g.:

$$v^{*i} = \sqrt{g_{(ii)}} v^i. \tag{3}$$

A bracket (..) around indices means, that the summation convention must not be applied to them. A summation is only carried out if there is also a double occurence of the same indices without brackets, so that they only 'run in common' (one should not confuse this with symmetrising brackets, partially used in the literature).

From Eq. (1) follows

$$\begin{aligned} \rho \frac{\partial v^{*i}}{\partial t} = \rho \sqrt{g_{(ii)}} \frac{\partial v^i}{\partial t} &= -\sqrt{g_{(ii)}} \left[\frac{\partial}{\partial x^j} \left(T^{*ij} \frac{1}{\sqrt{g_{(ii)}}} \frac{1}{\sqrt{g_{(jj)}}} \right) + \right. \\ &\left. + \Gamma^i_{jk} T^{*kj} \frac{1}{\sqrt{g_{(jj)}}} \frac{1}{\sqrt{g_{(kk)}}} + \Gamma^j_{jk} T^{*ik} \frac{1}{\sqrt{g_{(ii)}}} \frac{1}{\sqrt{g_{(kk)}}} \right]. \end{aligned} \tag{4}$$

The transition to terrain following coordinates (denoted with x'^i) only means an application of the chain rule in the first term on the right side. Simultaneous application of the product rule delivers

$$\begin{aligned} \rho \frac{\partial v^{*i}}{\partial t} &= -\sqrt{g_{(ii)}} \left[\frac{1}{\sqrt{g_{(ii)}}} \frac{1}{\sqrt{g_{(jj)}}} \frac{\partial x'^l}{\partial x^j} \frac{\partial}{\partial x' l} T^{*ij} \right. \\ &\quad + T^{*ij} \left(\frac{1}{\sqrt{g_{(jj)}}} \frac{\partial}{\partial x^j} \frac{1}{\sqrt{g_{(ii)}}} + \frac{1}{\sqrt{g_{(ii)}}} \frac{\partial}{\partial x^j} \frac{1}{\sqrt{g_{(jj)}}} \right) \\ &\quad \left. + \Gamma^i_{jk} T^{*kj} \frac{1}{\sqrt{g_{(jj)}}} \frac{1}{\sqrt{g_{(kk)}}} + \Gamma^j_{jk} T^{*ik} \frac{1}{\sqrt{g_{(ii)}}} \frac{1}{\sqrt{g_{(kk)}}} \right]. \end{aligned} \tag{5}$$

Derivatives of the metric tensor can be expressed by Christoffel-symbols (by solving Eq. (2)) to derive the equation

$$\frac{\partial}{\partial x^j}\frac{1}{\sqrt{g_{(ii)}}} = -\frac{1}{2\sqrt{g_{(ii)}}^3}\, g_{(ii),j} = -\frac{1}{\sqrt{g_{(ii)}}^3}\, g_{k(i)}\, \Gamma^k_{(i)j}. \tag{6}$$

It follows

$$\begin{aligned}\rho\frac{\partial v^{*i}}{\partial t} = & \underbrace{-\frac{1}{\sqrt{g_{(jj)}}}\frac{\partial x'^l}{\partial x^j}\frac{\partial}{\partial x'^l}T^{*ij}}_{(a)} \underbrace{+T^{*ij}\frac{1}{\sqrt{g_{(jj)}}}\frac{1}{g_{(ii)}}g_{k(i)}\Gamma^k_{(i)j}}_{(b)} \underbrace{+T^{*ij}\frac{1}{\sqrt{g_{(jj)}}^3}g_{k(j)}\Gamma^k_{(j)j}}_{(c)} \\ & \underbrace{-\Gamma^i_{jk}T^{*kj}\frac{1}{\sqrt{g_{(jj)}}}\frac{1}{\sqrt{g_{(kk)}}}\sqrt{g_{(ii)}}}_{(d)} \underbrace{-\Gamma^j_{jk}T^{*ik}\frac{1}{\sqrt{g_{(kk)}}}}_{(e)}.\end{aligned} \tag{7}$$

This equation generally describes the temporal change and the diffusion term of the physical components refered to a (normalized) base (in a coordinate system x^j), where all the fields are defined in a coordinate system x'^j.

Now we will specify the LM coordinate system. In Appendix A the metric tensor and Christoffel-symbols for spherical coordinates x^i are given; in Appendix B the transformation to terrain-following coordinates x'^i. Equations (46), (47) and (49) have to be inserted in Eq. (7) and after cumbersome, but uncomplicated calculation one finally arrives at

$$\begin{aligned}\rho\frac{\partial u^*}{\partial t} = & -\frac{1}{r\cos\phi}\frac{\partial T^{*11}}{\partial\lambda} - \frac{J_\lambda}{\sqrt{G}}\frac{1}{r\cos\phi}\frac{\partial T^{*11}}{\partial\zeta} - \frac{1}{r}\frac{\partial T^{*12}}{\partial\phi} - \frac{J_\phi}{\sqrt{G}}\frac{1}{r}\frac{\partial T^{*12}}{\partial\zeta} + \frac{1}{\sqrt{G}}\frac{\partial T^{*13}}{\partial\zeta} \\ & -\frac{3}{r}\,T^{*13} + \frac{2\tan\phi}{r}\,T^{*12},\end{aligned} \tag{8}$$

$$\begin{aligned}\rho\frac{\partial v^*}{\partial t} = & -\frac{1}{r\cos\phi}\frac{\partial T^{*12}}{\partial\lambda} - \frac{J_\lambda}{\sqrt{G}}\frac{1}{r\cos\phi}\frac{\partial T^{*12}}{\partial\zeta} - \frac{1}{r}\frac{\partial T^{*22}}{\partial\phi} - \frac{J_\phi}{\sqrt{G}}\frac{1}{r}\frac{\partial T^{*22}}{\partial\zeta} + \frac{1}{\sqrt{G}}\frac{\partial T^{*23}}{\partial\zeta} \\ & -\frac{3}{r}\,T^{*23} - \frac{\tan\phi}{r}\,(T^{*11} - T^{*22}),\end{aligned} \tag{9}$$

$$\begin{aligned}\rho\frac{\partial w^*}{\partial t} = & -\frac{1}{r\cos\phi}\frac{\partial T^{*13}}{\partial\lambda} - \frac{J_\lambda}{\sqrt{G}}\frac{1}{r\cos\phi}\frac{\partial T^{*13}}{\partial\zeta} - \frac{1}{r}\frac{\partial T^{*23}}{\partial\phi} - \frac{J_\phi}{\sqrt{G}}\frac{1}{r}\frac{\partial T^{*23}}{\partial\zeta} + \frac{1}{\sqrt{G}}\frac{\partial T^{*33}}{\partial\zeta} \\ & -\frac{2}{r}\,T^{*33} + \frac{1}{r}\,(T^{*11} + T^{*22}) + \frac{\tan\phi}{r}T^{*23}.\end{aligned} \tag{10}$$

Now the diffusion terms for scalar quantities s with an appropriate diffusion flux H^i shall be derived:

$$\frac{\partial s}{\partial t} = -\nabla_j H^j = -\frac{\partial}{\partial x^j}H^j - \Gamma^j_{jk}H^k. \tag{11}$$

The derivation is analogous to the former, but now some terms can be neglected from the starting point and it remains

$$\frac{\partial s}{\partial t} = -\frac{1}{\sqrt{g_{(jj)}}}\frac{\partial x'^l}{\partial x^j}\frac{\partial}{\partial x'^l}H^{*j} + \frac{1}{\sqrt{g_{(jj)}}^3}g_{k(j)}\Gamma^k_{(j)j}H^{*j} - \Gamma^j_{jk}\frac{1}{\sqrt{g_{(kk)}}}H^{*k}. \tag{12}$$

This corresponds obviously to the terms (a), (c) and (e) in Eq. (7). By insertion of the terms from Appendices A and B, it follows

$$\begin{aligned}\frac{\partial s}{\partial t} = & -\frac{1}{r\cos\phi}\frac{\partial H^{*1}}{\partial\lambda} - \frac{J_\lambda}{\sqrt{G}}\frac{1}{r\cos\phi}\frac{\partial H^{*1}}{\partial\zeta} - \frac{1}{r}\frac{\partial H^{*2}}{\partial\phi} - \frac{J_\phi}{\sqrt{G}}\frac{1}{r}\frac{\partial H^{*2}}{\partial\zeta} + \frac{1}{\sqrt{G}}\frac{\partial H^{*3}}{\partial\zeta} \\ & -\frac{2}{r}\,H^{*3} + \frac{\tan\phi}{r}\,H^{*2}.\end{aligned} \tag{13}$$

The single terms of this equation can be interpreted descriptive. The 1st, 3rd, and 5th term in the first line are corresponding completely to the x-, y-, and z-derivative in the calculation of the divergence in cartesian coordinates:

$$\frac{1}{r\cos\phi}\frac{\partial H^{*1}}{\partial\lambda} = \left.\frac{\partial H^{*1}}{\partial x}\right|_{\phi,\zeta}, \tag{14}$$

$$\frac{1}{r}\frac{\partial H^{*2}}{\partial\phi} = \left.\frac{\partial H^{*2}}{\partial y}\right|_{\lambda,\zeta}, \tag{15}$$

$$-\frac{1}{\sqrt{G}}\frac{\partial H^{*3}}{\partial\zeta} = \left.\frac{\partial H^{*3}}{\partial z}\right|_{\lambda,\phi}. \tag{16}$$

The 2nd and 4th terms give a correction from the terrain-following coordinate system, which obviously is given alone from the ζ-derivative

$$\frac{J_\lambda}{\sqrt{G}}\frac{1}{r\cos\phi}\frac{\partial H^{*1}}{\partial\zeta} = \frac{\left.\frac{\partial z}{\partial\lambda}\right|_\zeta}{-\frac{\partial z}{\partial\zeta}}\frac{1}{r\cos\phi}\frac{\partial H^{*1}}{\partial\zeta} = -\left.\frac{\partial z}{\partial x}\right|_\zeta\cdot\left.\frac{\partial H^{*1}}{\partial z}\right|_{\lambda,\phi}, \tag{17}$$

$$\frac{J_\phi}{\sqrt{G}}\frac{1}{r}\frac{\partial H^{*2}}{\partial\zeta} = \frac{\left.\frac{\partial z}{\partial\phi}\right|_\zeta}{-\frac{\partial z}{\partial\zeta}}\frac{1}{r}\frac{\partial H^{*2}}{\partial\zeta} = -\left.\frac{\partial z}{\partial y}\right|_\zeta\cdot\left.\frac{\partial H^{*2}}{\partial z}\right|_{\lambda,\phi}. \tag{18}$$

One has to obey, that the relations (14) - (18) are valid only on a local tangential plane (with $dx = r\cos\phi\, d\lambda$, and $dy = r\, d\phi$) and are presented here only for illustration purposes. Analogous relations follow for the momentum flux divergences (8)-(10) above.

The two terms in the second line of (13) are given by the spherical basis and can be illustrated in the following manner. We prescribe a constant (in the spherical base) scalar flux field $H^{*i} = const. = (0, 0, h)$, that means a radially outside directed vector field with constant absolute value. Starting from the integral form of the balance equation (11)

$$\int_V \frac{\partial s}{\partial t} dV = -\int_{\partial V} \mathbf{H}\cdot\mathbf{d}\sigma \tag{19}$$

and choosing an infinitesimal spherical segment as integration volume

$$dV = d\sigma\cdot dr \tag{20}$$

with the surface element

$$d\sigma = (r\, d\phi)\cdot(r\cos\phi\, d\lambda) \tag{21}$$

it follows

$$\frac{\partial s}{\partial t}\cos\phi\, d\phi\, d\lambda\, r^2 dr = -H^{*3}\left[((r+dr)d\phi)\cdot((r+dr)\cos\phi\, d\lambda) - (r\, d\phi)\cdot(r\cos\phi\, d\lambda)\right] \tag{22}$$

and finally by expansion

$$\frac{\partial s}{\partial t} = -H^{*3}\frac{2}{r} + \dots . \tag{23}$$

Therefore this correction term follows from the divergence of the radial base vectors in the spherical coordinate system. Obviously, this term is not contained in the original derivation in Doms, et.al., 2005, [Eq. (3.3)].

Analogously the 2nd term in the second line of Eq. (13) can be explained by the convergence (on the northern hemisphere) of the meridional base vectors. To see this, one chooses $H^{*i} = const. = (0, h, 0)$ and the same infinitesimal volume element; the flux divergence now arises from the lateral boundary surfaces (this term also arises in Doms, et.al., 2005, [Eq. (3.3)], but without the factor 2). This also explains, why there are no such terms for the H^{*1}-component: the zonal base vectors do not possess such a convergence/divergence.

The same considerations can be made for the equations of motion (8)-(10). Again, the terms in the second line arise by the spherical basis due to the curvature of the earth. Nevertheless the vectorial character of these equations complicates a quantitative illustration compared to the scalar equation.

How strong is the practical relevance of these terms? Let us first look to the terms which are only addressed to the earth curvature. In the equations of motion, we have terms of the form $T^{*ij}/r/\rho$. For rough estimations we can set $T^{*ij}/\rho \sim TKE$, where we can limit $TKE < 10\ \mathrm{m}^2/\mathrm{s}^2$; this occurs in nearly neutral boundary layers with very strong winds. Now we can estimate (where we take the biggest occuring coefficient of 3)

$$\max \frac{3|T^{*ij}|}{r\rho} \sim \max 3\frac{TKE}{R_E} \sim 3\frac{10\,m^2/s^2}{6\cdot 10^6\,m} \sim 0.5\cdot 10^{-5}\frac{m}{s^2} \tag{24}$$

(R_E = earth radius). Even this extreme case is more than one order less than a Coriolis force for small wind velocities with $2\Omega \times v \sim 10^{-4} s^{-1} \cdot 1\,m/s \sim 10^{-4}\,m/s^2$ and therefore such terms can be neglected.

In the equation for the scalar flux divergence, we roughly estimate $H^{*i} \sim |s| \cdot \sqrt{TKE}$ and find

$$\max \frac{|H^{*i}|}{r} \sim \max |s| \cdot \frac{\max \sqrt{TKE}}{R_E} \sim \max |s| \cdot \frac{3\,m/s}{6\cdot 10^6\,m} \sim \frac{\max |s|}{2\cdot 10^6 s} \sim \frac{\max |s|}{20\,d} \tag{25}$$

These terms mean at most a very slow change of the scalar variable in the order of about 20 days and therefore can be neglected, too.

Next, we look at the terms connected with the terrain-following coordinate. At least near the bottom, we can estimate for the typical LMK resolution and area (Germany and the most part of the Alpines) a maximum terrain slope of

$$\max \left|\frac{\partial z}{\partial x}\right| \approx \max \frac{|\Delta h|}{\Delta x} \approx \frac{1000\,m}{2800\,m} \approx 0.3 \tag{26}$$

Normally, the vertical part of the flux divergences are stronger than the horizontal parts, therefore, as can be seen from Eq. (17), terms connected with the terrain-following coordinate cannot be neglected.

3 The transformation of the turbulence closure

For calculating the momentum fluxes we start from a formulation with a scalar eddy viscosity K, which connects the fluxes with the deformation tensor D^{ij} in a gradient ansatz:

$$T^{ij} = -\rho K D^{ij} = -\rho K(g^{il}\nabla_l v^j + g^{jl}\nabla_l v^i). \tag{27}$$

Often, a diagonal term $2/3 g^{ij} E$, where E is the turbulent kinetic energy, is added to the right hand side. Such a term guaranties consistency for an incompressible (and therefore divergence free) medium; this can be seen by taking the trace of (27). We neglect it here,

because it is not used in Herzog, 2002a. But because of its simple form (E is a scalar), it is not affected by the following transformations and can be implemented directly. Using the physical components delivers

$$\frac{T^{*ij}}{\sqrt{g_{(ii)}}\sqrt{g_{(jj)}}} = -\rho K \left[g^{il}\frac{\partial}{\partial x^l}\left(\frac{v^{*j}}{\sqrt{g_{(jj)}}}\right) + g^{il}\Gamma^j_{lk}\frac{v^{*k}}{\sqrt{g_{(kk)}}} + g^{jl}\frac{\partial}{\partial x^l}\left(\frac{v^{*i}}{\sqrt{g_{(ii)}}}\right) + g^{jl}\Gamma^i_{lk}\frac{v^{*k}}{\sqrt{g_{(kk)}}}\right] \tag{28}$$

and introduction of terrain-following coordinates, application of the product rule and Eq. (6) yields

$$\begin{aligned} T^{*ij} = \quad & -\rho K \left[\sqrt{g_{(ii)}} g^{il}\frac{\partial x'^m}{\partial x^l}\frac{\partial v^{*j}}{\partial x'^m} - \frac{g^{il}}{g_{(jj)}}\sqrt{g_{(ii)}}g_{k(j)}\Gamma^k_{(j)l}v^{*j} + \frac{g^{il}}{\sqrt{g_{(kk)}}}\sqrt{g_{(ii)}}\sqrt{g_{(jj)}}\Gamma^j_{lk}v^{*k} \right. \\ & \left. \sqrt{g_{(jj)}} g^{jl}\frac{\partial x'^m}{\partial x^l}\frac{\partial v^{*i}}{\partial x'^m} - \frac{g^{jl}}{g_{(ii)}}\sqrt{g_{(jj)}}g_{k(i)}\Gamma^k_{(i)l}v^{*i} + \frac{g^{jl}}{\sqrt{g_{(kk)}}}\sqrt{g_{(ii)}}\sqrt{g_{(jj)}}\Gamma^i_{lk}v^{*k} \right]. \end{aligned} \tag{29}$$

By inserting the metric tensors and Christoffel symbols from Appendices A and B, the components

$$\frac{T^{*11}}{\rho K} = -\frac{2}{r\cos\phi}\left(\frac{\partial v^{*1}}{\partial\lambda} + \frac{J_\lambda}{\sqrt{G}}\frac{\partial v^{*1}}{\partial\zeta}\right) + \frac{2\tan\phi}{r}v^{*2} - \frac{2}{r}v^{*3}, \tag{30}$$

$$\frac{T^{*12}}{\rho K} = -\frac{1}{r\cos\phi}\left(\frac{\partial v^{*2}}{\partial\lambda} + \frac{J_\lambda}{\sqrt{G}}\frac{\partial v^{*2}}{\partial\zeta}\right) - \frac{1}{r}\left(\frac{\partial v^{*1}}{\partial\phi} + \frac{J_\phi}{\sqrt{G}}\frac{\partial v^{*1}}{\partial\zeta}\right) - \frac{\tan\phi}{r}v^{*1}, \tag{31}$$

$$\frac{T^{*13}}{\rho K} = -\frac{1}{r\cos\phi}\left(\frac{\partial v^{*3}}{\partial\lambda} + \frac{J_\lambda}{\sqrt{G}}\frac{\partial v^{*3}}{\partial\zeta}\right) + \frac{1}{\sqrt{G}}\frac{\partial v^{*1}}{\partial\zeta} + \frac{1}{r}v^{*1}, \tag{32}$$

$$\frac{T^{*22}}{\rho K} = -\frac{2}{r}\left(\frac{\partial v^{*2}}{\partial\phi} + \frac{J_\phi}{\sqrt{G}}\frac{\partial v^{*2}}{\partial\zeta}\right) - \frac{2}{r}v^{*3}, \tag{33}$$

$$\frac{T^{*23}}{\rho K} = -\frac{1}{r}\left(\frac{\partial v^{*3}}{\partial\phi} + \frac{J_\phi}{\sqrt{G}}\frac{\partial v^{*3}}{\partial\zeta}\right) + \frac{1}{\sqrt{G}}\frac{\partial v^{*2}}{\partial\zeta} + \frac{1}{r}v^{*2}, \tag{34}$$

$$\frac{T^{*33}}{\rho K} = \frac{2}{\sqrt{G}}\frac{\partial v^{*3}}{\partial\zeta} \tag{35}$$

follow. Here, the last terms in the right hand sides of each of the equations (30), (32), (33) and (35) are not contained in Doms, et.al., 2005. Analogous to this, the (much more simple) derivation for the scalar fluxes follows

$$H^i = -\rho K_s g^{ij}\nabla_j s, \tag{36}$$

from which the physical components can be derived

$$H^{*i} = -\rho K_s\sqrt{g_{(ii)}}g^{ij}\frac{\partial x'^m}{\partial x^j}\frac{\partial s}{\partial x'^m}, \tag{37}$$

or for the single components

$$H^{*1} = -\rho K_s\frac{1}{r\cos\phi}\left(\frac{\partial s}{\partial\lambda} + \frac{J_\lambda}{\sqrt{G}}\frac{\partial s}{\partial\zeta}\right), \tag{38}$$

$$H^{*2} = -\rho K_s\frac{1}{r}\left(\frac{\partial s}{\partial\phi} + \frac{J_\phi}{\sqrt{G}}\frac{\partial s}{\partial\zeta}\right), \tag{39}$$

$$H^{*3} = +\rho K_s\frac{1}{\sqrt{G}}\frac{\partial s}{\partial\zeta}, \tag{40}$$

which agrees to Doms, et.al., 2005.

Again, we want to estimate the relevance of the terms. In principle LMK shall resolve the bigger parts of deep convection. Therefore all the velocity components can have the same order and we can roughly estimate

$$\max \frac{|v^{*i}|}{r} \sim \frac{100\,m/s}{6 \cdot 10^6\,m} \sim 10^{-5}\frac{1}{s} \tag{41}$$

Compared to this any vertical deformations are much bigger, for example

$$\frac{1}{\sqrt{G}}\frac{\partial v^i}{\partial \zeta} \sim \frac{\Delta v}{\Delta z} \sim \frac{1\,m/s}{100\,m} \sim 10^{-2}\frac{1}{s}, \tag{42}$$

(we used an arbitrary value of $\Delta v \sim 1$ m/s, which is certainly not very much, because we assumed a strong wind case). Even horizontally we would expect

$$\frac{\Delta v}{\Delta x} \sim \frac{0.3\,m/s}{2800\,m} \sim 10^{-4}\frac{1}{s}. \tag{43}$$

Again, all the terms connected with the earth curvature are at least one order less than the gradient terms and therefore can be neglected. But, as before, all the terms connected with the terrain slope cannot be neglected.

4 Conclusions

Turbulent fluxes and flux divergences of momentum and arbitrary scalars were derived for the special LM/LMK coordinate system und base vectors. It occurred, that there are discrepancies between this derivation and the original LM documentation. A test of correctness of this derivation is the fact, that some of the 'new' terms can be motivated illustratively.

Nevertheless, the discrepancies are not of practical importance, because they occur only in terms corresponding to the earth curvature. The neglection of terms connected with the earth curvature can be motivated also by the following qualitative consideration. The maximum vertical length scale of turbulence is on the one hand determined by the depth of the planetary boundary layer ($L_v \sim 1$ km) and on the other hand is sureley not greater than the depth of the troposphere ($L_v \sim 10$ km), if one regards deep convection as a kind of turbulence, too. The horizontal length scale of turbulence cannot exceed very much this vertical length scale. Therefore, we have a maximum turbulence length scale of the order $L_{turb} < 10$ km. This is almost 3 orders less than the earth radius $R \sim 6400$ km. Therefore all the terms connected with the pure earth curvature can be neglected.

In summary, in the flux divergences of momentum (8)-(10) and arbitrary scalars (13) all the terms which contain the fluxes themself and not their spatial derivatives can be neglected (that means, all the second lines can be neglected). Similarly, in the turbulent fluxes of momentum (30)-(35) all the terms which contain the velocities itself and not their spatial derivatives can be neglected. In contrast, terms connected with the terrain slope have to be maintained.

Appendix A: Spherical coordinates

We use a spherical coordinate system with coordinates

$$x^1 = \lambda, \quad x^2 = \phi, \quad x^3 = r. \tag{44}$$

If one compares this with the literature, one should obey a possibly different relation with the cartesian coordinates. Here we use

$$x = r\cos\phi\cos\lambda, \quad y = r\cos\phi\sin\lambda, \quad z = r\sin\phi. \tag{45}$$

Note, that we define $\phi \in [-\pi/2, \pi/2]$ and therefore $\cos\phi \geq 0$.

For completeness we list the metric tensor

$$g_{ij} = \begin{pmatrix} r^2\cos^2\phi & 0 & 0 \\ 0 & r^2 & 0 \\ 0 & 0 & 1 \end{pmatrix} \quad \Leftrightarrow \quad g^{ij} = \begin{pmatrix} \frac{1}{r^2\cos^2\phi} & 0 & 0 \\ 0 & \frac{1}{r^2} & 0 \\ 0 & 0 & 1 \end{pmatrix}, \tag{46}$$

and the Christoffel symbols

$$\Gamma^1_{ij} = \begin{pmatrix} 0 & -\tan\phi & 1/r \\ -\tan\phi & 0 & 0 \\ 1/r & 0 & 0 \end{pmatrix},$$

$$\Gamma^2_{ij} = \begin{pmatrix} \cos\phi\cdot\sin\phi & 0 & 0 \\ 0 & 0 & 1/r \\ 0 & 1/r & 0 \end{pmatrix}, \quad \Gamma^3_{ij} = \begin{pmatrix} -r\cos^2\phi & 0 & 0 \\ 0 & -r & 0 \\ 0 & 0 & 0 \end{pmatrix}. \tag{47}$$

Appendix B: Terrain-following coordinates

The transition to terrain-following coordinates is described by

$$x^1 = x'^1 = \lambda, \qquad x^2 = x'^2 = \phi, \qquad x^3 = r(\lambda, \phi, \zeta). \tag{48}$$

Therefore we get for the required derivatives

$$\begin{aligned} &\frac{\partial x'^1}{\partial x^1} = 1, \quad \frac{\partial x'^1}{\partial x^2} = 0, \quad \frac{\partial x'^1}{\partial x^3} = 0, \\ &\frac{\partial x'^2}{\partial x^1} = 0, \quad \frac{\partial x'^2}{\partial x^2} = 1, \quad \frac{\partial x'^2}{\partial x^3} = 0, \\ &\frac{\partial x'^3}{\partial x^1} = \frac{\partial \zeta}{\partial \lambda} \equiv \frac{J_\lambda}{\sqrt{G}}, \quad \frac{\partial x'^3}{\partial x^2} = \frac{\partial \zeta}{\partial \phi} \equiv \frac{J_\phi}{\sqrt{G}}, \quad \frac{\partial x'^3}{\partial x^3} = \frac{\partial \zeta}{\partial z} \equiv -\frac{1}{\sqrt{G}}, \end{aligned} \tag{49}$$

where we introduced the abbreviations J_λ, J_ϕ and $\sqrt{G}$ analogous to the LM-documentation (Doms and Schättler, 2002).

References

Doms, G. and U. Schättler, 2002: A Description of the Nonhydrostatic Regional Model LM, Part I: Dynamics and Numerics. Deutscher Wetterdienst, Offenbach, Germany, November 2002.

Doms, G., J. Förstner, E. Heise, H.-J. Herzog, M. Raschendorfer, T. Reinhardt, and G. Vogel, 2005: A Description of the Nonhydrostatic Regional Model LM, Part II: Physical Parameterizations. Deutscher Wetterdienst, Offenbach, Germany, April 2005.

Förstner J., H.-J. Herzog, and G. Vogel, 2005: Implementation of a 3D-turbulence parameterization for the very short range forecast model LMK. *WGNE Blue Book*, 2005.
(see: `http://www.cmc.ec.gc.ca/rpn/wgne/`).

Herzog H.-J., U. Schubert, G. Vogel, A. Fiedler, and R. Kirchner, 2002a: LLM - the High-Resolving Nonhydrostatic Simulation Model in the DWD-Project LITFASS (Part I: Modelling Technique and Simulation Method) COSMO Technical Report No. 4. Deutscher Wetterdienst, Offenbach, Germany, March 2002.

Herzog H.-J., G. Vogel, and U. Schubert, 2002b: LLM - a nonhydrostatic model applied to high-resolving simulations of turbulent fluxes over heterogeneous terrain. *Theor. Appl. Climatol.*, 73, 67–86, 2002.

Raschendorfer M., 2004: A new TKE-based Scheme for Vertical Diffusion and Surface-Layer Transfer. Deutscher Wetterdienst, Offenbach, Germany, 2004.

Stephani H., 1988: *Allgemeine Relativitätstheorie.* Dt. Verlag d. Wiss., Berlin, 1988.

A new Option for Rayleigh Damping: Preliminary Tests

Lucio Torrisi

CNMCA, Via Pratica di Mare 45, 00040 Pomezia (RM), Italy

1 Introduction

An absorbing layer is used in a non-hydrostatic model to reduce spurious downward reflections of vertically propagating waves from the rigid top boundary (rigid lid condition), which can completely distort the numerical solution. This viscous damping layer is usually applied at the top of the computational domain to absorb upward propagating wave disturbances, before they reach the rigid top boundary. The prevention of wave energy reflection at the upper boundary is of crucial importance for a proper simulation of orographically induced flow. In the numerical model formulation a damping term is added to all the prognostic equations. In the traditional Rayleigh friction formulation, the damping term is defined by:

$$R_\phi = -r(z) \cdot (\phi - \phi_{base\ state}) \,, \tag{1}$$

where $r(z) \neq 0$ (increasing with z) in the damping layer between the top z_T (top boundary) and the base z_D. In LM it is

- $z_D = 11000$ meters (base of the damping layer),
- $\phi = T, u, v, w, p', q_v, q_c, q_i$, and
- $\phi_{base\ state}$ = large scale fields provided by the driving model (boundary condition fields).

The current LM Rayleigh damping formulation does not work with frames, because it requires boundary condition fields defined on a full grid. Although LM forecast fields, which come from runs without any absorbing layer, may be contaminated by spurious reflected waves, IFS *frames* are routinely used in EuroLM (UGM) and aLMo (MeteoSwiss) model configuration. A possible solution to the spurious waves' problem for these configurations is, to have boundary fields defined on the full grid above a certain model level, where the Rayleigh damping is active (three dimensional frames). Unfortunately, inaccurate calculations of the pressure perturbation p' from the boundary condition fields can generate further contamination in the numerical solution. A more satisfactory solution to the spurious waves' problem than the damping layer would be to specify a radiative upper boundary condition at the domain top. The implementation of the radiative upper boundary condition in LM is work in progress and its impact both from the numerical and from the computational point of view has still to be evaluated (Herzog, 2004).

2 A new Rayleigh damping option

A simple and effective way to overcome the spurious waves' problem is to change the formulation of the base state fields currently used in the Rayleigh damping layer. The *new* base state fields $\phi_{base\ state}$ are obtained by spatially filtering the LM forecast fields ϕ instead of using large scale fields provided by the driving model (boundary conditions fields). The basic idea is to have base state fields consistent with the LM prognostic variables. This is not always true in the current Rayleigh damping formulation, because of the difference in resolution, parameterization, numerics, etc. between LM and the driving model used. Inconsistencies between the LM and the driving model forecast could turn the damping layer in a source of further contamination.

The representation of the base state in the new Rayleigh damping option is strongly dependent on the choice of the filter applied to the LM fields. The current parallelization strategy (decomposition in subdomains surrounded by a 2 grid-line halo) allows the use of a filter with length=1 (using 9 points) without an excessive increase of the communication time. The digital filter has to be applied each time step to the prognostic fields $(T, u, v, w, p', q_v, q_c, q_i)$ The new Rayleigh damping option can also be switched on with boundary condition fields defined on a frame. The namelist variable `itype_spubc` (1 old, 2 new) is used to switch on the old or the new option. It was implemented in the LM version 3.14.

3 Preliminary tests

Preliminary tests of the new Rayleigh damping option were performed using real data. The EuroLM configuration showed in Table 1 was used in this experiment.

Table 1: **LM Configuration (Version 3.11)**

Domain Size	465 x 385 gridpoints
Horizontal Grid Spacing	0.0625° (∼ 7 km)
Number of Layers	35, base-state pressure based hybrid
Time Step and Integration Scheme	40 sec, 3 time-level split-explicit
Forecast Range	60 h
Initial Time of Model Runs	12 UTC
Lateral Boundary Conditions	Op. IFS (preproc. with CNMCA-IFS2LM)
L.B.C. update frequency	3 hrs.
Initial State	Op. IFS (preproc. with CNMCA-IFS2LM)
Orography	Filtered (`eps=0.1`)
Initialization	None

Three different runs were performed (12 UTC - 12 September 2004): the first one using the old option, the second one using the new option and the other one without any damping layer. 60 h accumulated total precipitation fields from these runs (Fig. 1) and their differences (Fig. 2) were compared to each other, in order to evaluate the impact of each option.

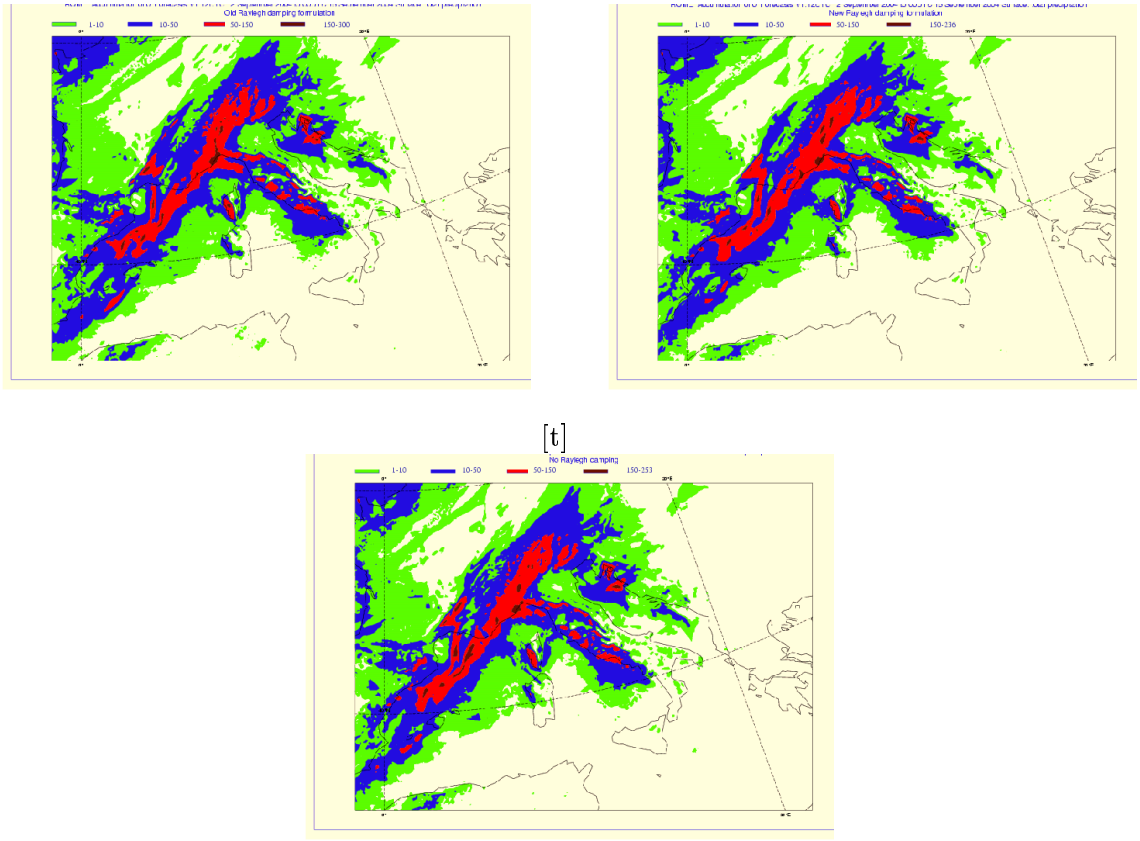

Figure 1: 60 h accumulated total precipitation fields from runs with the old (upper left) and the new (upper right) damping option and with no damping at all (lower).

The comparison of the old and new option runs to the run without any damping layer showed:

- a slight eastern shift in the precipitation pattern of the old option run;
- no significant distortion in the precipitation pattern of the new option run.

The following results were also verified for a three month period:

- runs with the new option have less accumulated total precipitation over the domain ($1.027 \cdot 10^6$ mm for the 12 September run) than runs with the old option ($1.044 \cdot 10^6$ mm for the 12 September run) and runs without any Rayleigh damping layer ($1.030 \cdot 10^6$ mm for the 12 September run);
- runs with the old option have often more accumulated total precipitation over the domain than runs without any Rayleigh damping layer.

This last result and the shift of the precipitation pattern previously found could be the indications that the old Rayleigh damping option is not working correctly, due to the inconsistencies between the LM and the driving model forecast mentioned before. On the other hand, the new Rayleigh damping option seems to work in the right direction decreasing the amount of spurious precipitation.

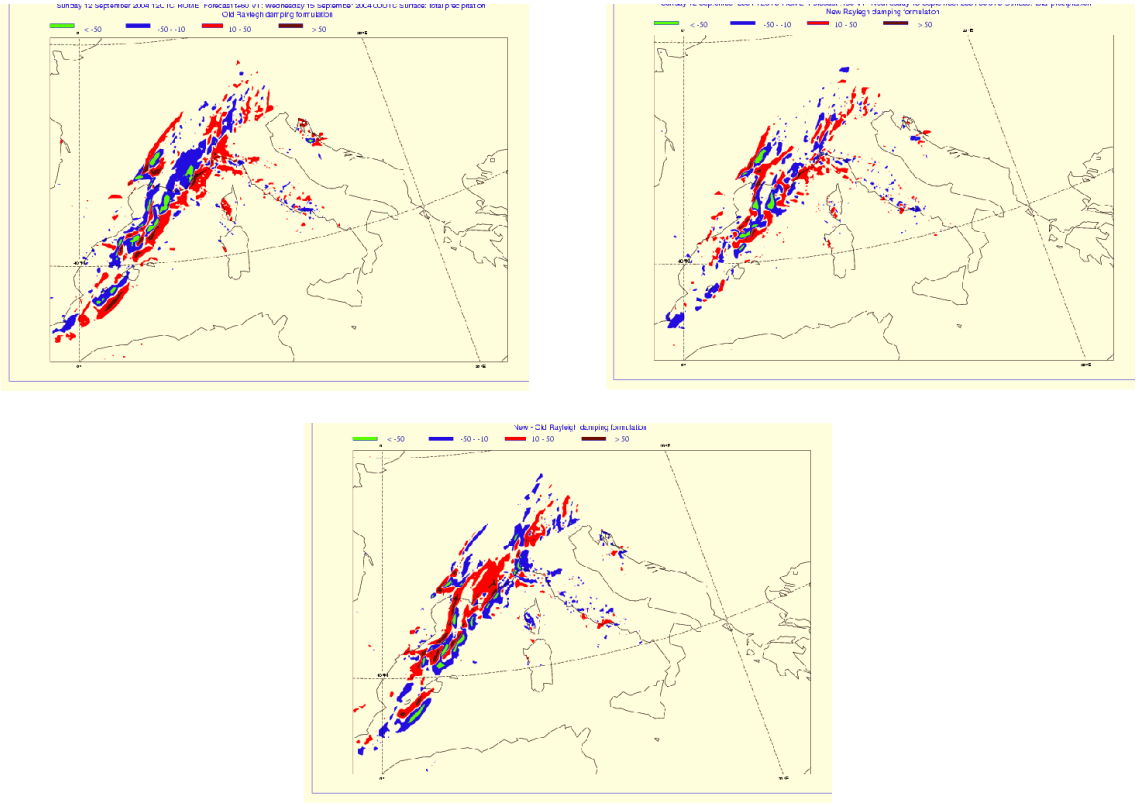

Figure 2: Differences of the accumulated total precipitation fields: old option - no damping (upper left); new option - no damping (upper right) and old - new damping option (lower).

4 Conclusions

A new option for the Rayleigh damping layer near the top boundary was implemented in LM code. It is recommended for LM runs with frames, but it can be used even if the boundary conditions are defined on a full grid. Preliminary tests using the new Rayleigh damping option have showed less accumulated total precipitation over the domain than runs with the old option and runs without any damping layer. These results are a clear indication that the new option is working correctly decreasing the amount of spurious precipitation, but further studies (idealized tests, such as the linear hydrostatic mountain wave test) are necessary to evaluate the impact of the new Rayleigh damping option on LM forecasts and to tune the new base (filtered) state formulation.

References

Herzog, H.-J., 2004: Tests of the radiative upper boundary condition. Presentation at the COSMO General Meeting, 2005 - Milano.

Impact of Domain Size on LM Forecast

Lucio Torrisi

CNMCA, Via Pratica di Mare 45, 00040 Pomezia (RM), Italy

1 Introduction

The impact of the domain size on LM forecast was investigated in the period 1 March – 30 June 2004. LM was integrated on LAMI and EuroLM domain (Fig. 1) domain. EuroLM is the UGM version of LM covering Italy and the western part of Europe and the Mediterranean Sea. The LM configuration used in this experiment is shown in Table 1. IFS fields were used as initial and boundary conditions. The LM forecast fields were objectively evaluated through comparisons with radiosonde and conventional surface observations. Mean error and root mean square error (RMSE) vertical profiles are computed for the Italian radiosounding stations (Milano, Udine, Pratica, Brindisi, Cagliari, Trapani, Bologna, Cuneo). Surface parameters are verified for about one hundred synop lowland stations satisfying the COSMO WG5 specification ($H_s < 700$ meters, $|H_s - H_n| < 100$ meters, where H_s is the station height and H_n is the height of the nearest land grid point).

Table 1: **LM Configuration (Version 3.11)**

Domain Size	234 × 272 grid points (LAMI) 465 × 385 grid points (EuroLM)
Horizontal Grid Spacing	0.0625° (∼ 7 km)
Number of Layers	35, base-state pressure based hybrid
Time Step and Integration Scheme	40 sec, 3 time-level split-explicit
Forecast Range	60 h
Initial Time of Model Runs	12 UTC
Lateral Boundary Conditions	3 hourly from op. IFS
Initial State	Op. IFS

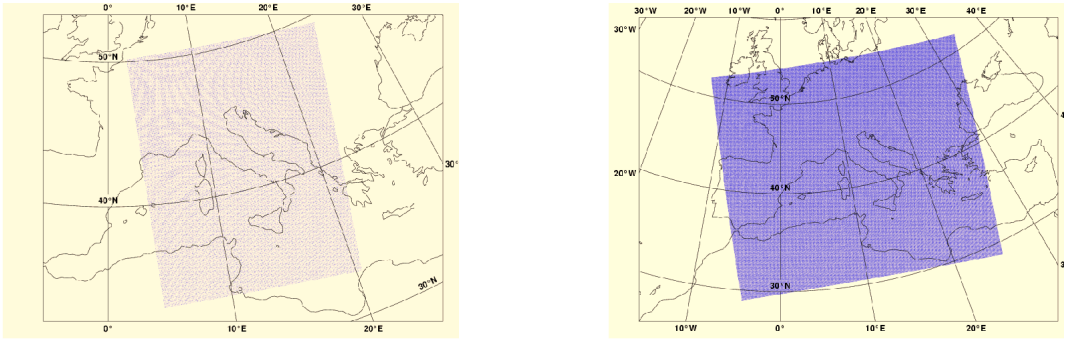

Figure 1: LAMI (left) and EuroLM (right) integration domain.

2 Vertical profiles

Temperature ME and RMSE vertical profiles of LM forecasts T+12 h, T+24 h, T+36 and T+48h are shown in Fig. 2 for the LAMI (red dashed line) and EuroLM configurations (blue solid line). RMSE for EuroLM (larger domain) is greater than for the LAMI between around 250 hPa at T+24h and below 250 hPa after T+36h. A warmer bias for the larger domain configuration is found at the jet level.

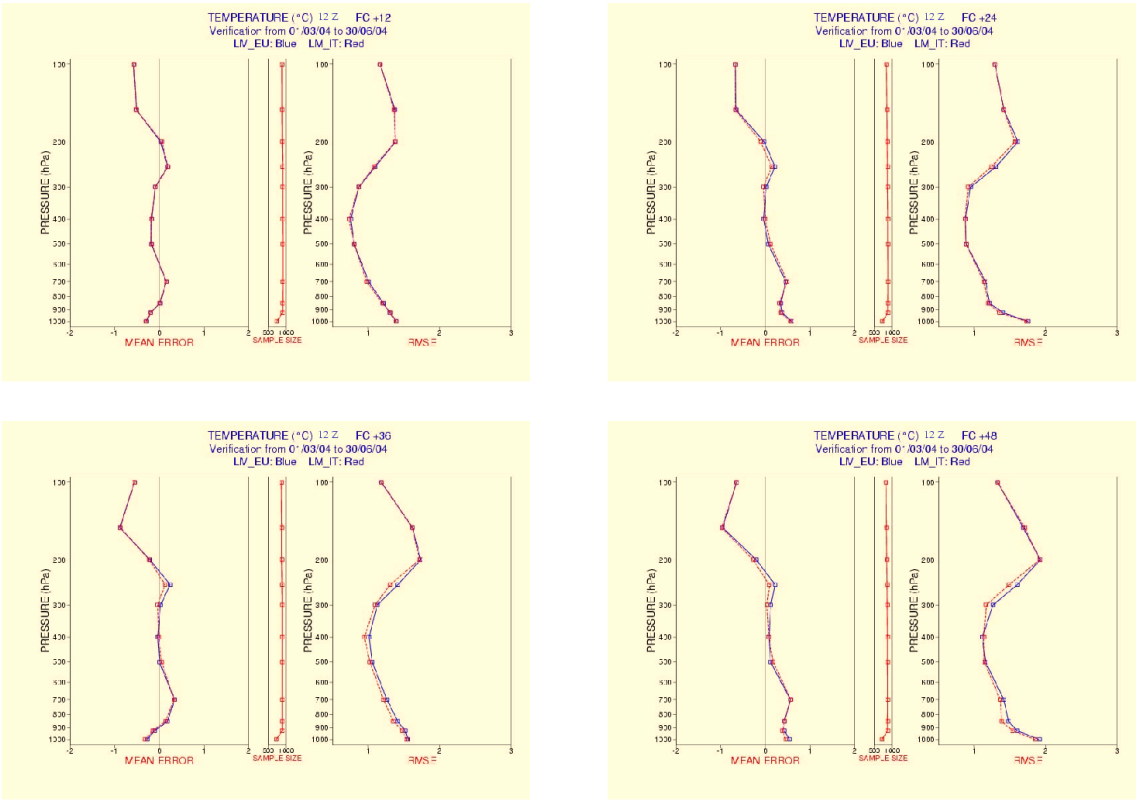

Figure 2: Temperature mean error and root mean square error vertical profiles of 12/24/36/48 h forecasts for LAMI and EuroLM.

Wind speed ME and wind vector RMSE vertical profiles of LM forecasts T+12 h, T+24 h, T+36 and T+48h are shown in Fig. 3 for the LAMI (red dashed line) and EuroLM configurations (blue solid line). Wind vector RMSE for the EuroLM runs is greater than for LAMI in the layer 250 hPa – 500 hPa at T+12h and below 250 hPa after T+24h. A slower bias for the smaller domain configuration in the wind speed bias is also found.

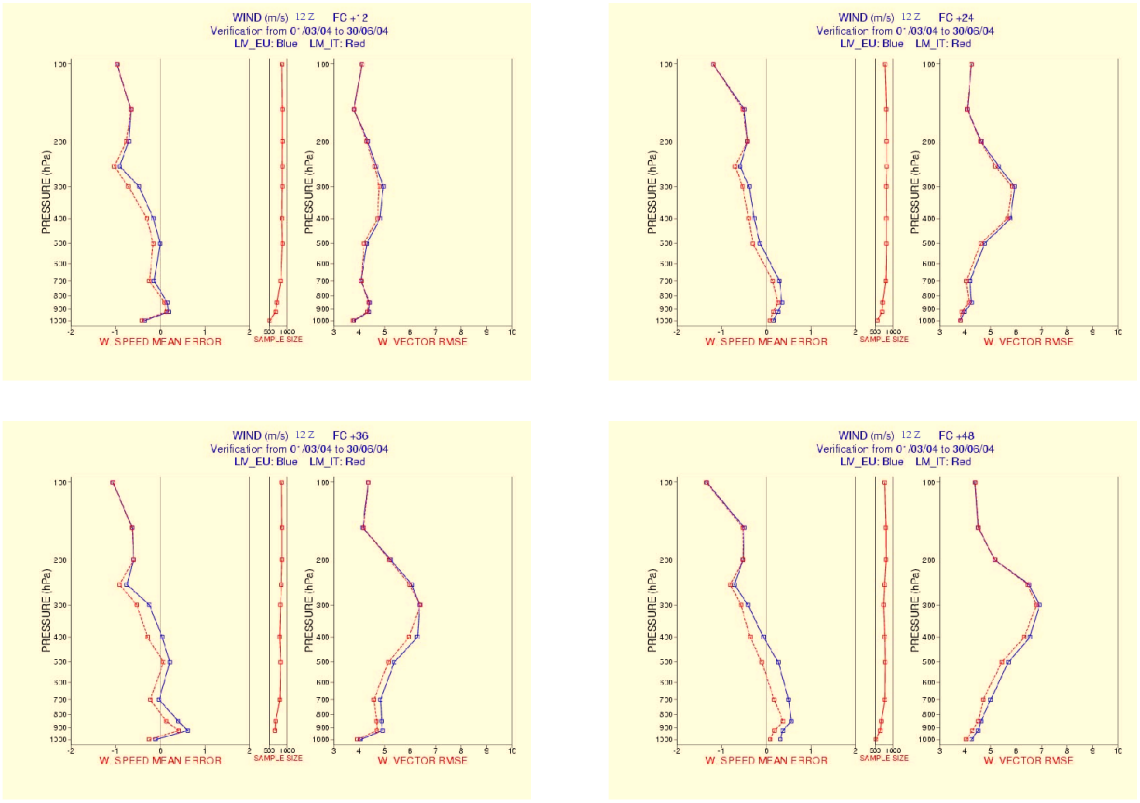

Figure 3: Wind speed mean error and wind vector root mean square error vertical profiles of 12/24/36/48 h forecasts for LAMI and EuroLM.

3 Surface variables

Mean error and RMSE of two meter temperature, two meter dew point, ten meter wind speed and mean sea level pressure (MSLP) as a function of the forecast time are represented in the Fig. 4 for the LAMI (red dashed line) and EuroLM configurations (blue solid line). MSLP ME and RMSE for LAMI are less than for the EuroLM after T+12h. Similar results to those of MSLP are found for the ten meter wind speed, but with smaller differences. Two meter temperature and dew point scores for both configurations have no significant differences.

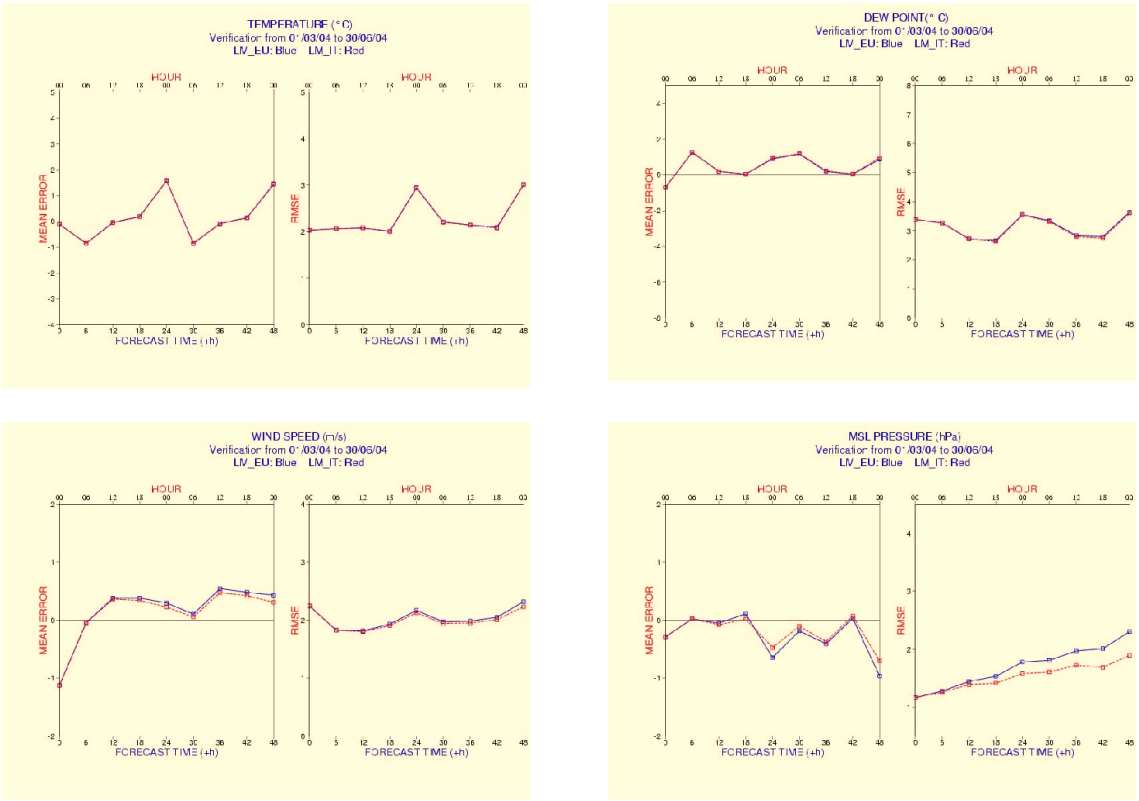

Figure 4: Mean error and RMSE of 2m temperature, 2m dew point, 10m wind speed and mean sea level pressure of LAMI and EuroLM.

4 Conclusions

The results of the domain size impact study on LM forecast are surprising. Statistical verification results have showed that the enlargement of the domain has a measurable negative impact on LM forecast skill. In particular the wind vector and the MSLP have the worst scores after T+24h. It seems that LM dynamics does not give a good representation of the meteorological evolution in the larger domain. It may be related to the accuracy of the discretization scheme currently used in LM (Leapfrog with second order spatial differencing). On the other hand, BC fields definitely affect the weather system evolution in the smaller domain, since the domain borders are closer to the location of the verification stations used in this experiment. The use of more accurate discretization schemes than the operational one seems to be necessary not only for very high-resolution application, but also for integration on large domains.

A Z-Coordinate Version of the Nonhydrostatic Model LM

Jürgen Steppeler[1], H.-W. Bitzer[2], Z. Janjic[3], U. Schättler[1]
P. Prohl[1], J. Parfiniewicz[4], U. Damrath[1], E. Avgoustoglou[5]

[1] *Deutscher Wetterdienst, P.O.Box 100465, 63004 Offenbach a.M., Germany*
[2] *Amt für GeoInformationswesen der Bundeswehr, Gruppe MetBW, Germany*
[3] *National Center for Environmental Prediction, Washington DC., USA*
[4] *Institute for Meteorology and Water Management, Warsaw, Poland*
[5] *Hellenic National Meteorological Service, Athens, Greece*

The Eulerian version of the LM-Z uses the numeric scheme described in Steppeler et.al. 2002. Mountains are represented by linear splines, as opposed to the step mountain approach of Mesinger et al. (1988) using a representation of the topography by piecewise constant functions. This technique is also known as brick (or Legoland) approach and it was shown by Gallus and Klemp (2000) that there are serious problems with this approach in the presence of wind. In test problems it could be shown that the solution does not converge. The technique used in the LM-Z is free from this error.

A number of idealized and real forecast tests have been performed. The large scale features of clouds are captured by LM-Z and LM. Concerning meso scale cloud structures there are substantial differences between the two forecasts. In particular the distinction between cellular and stratiform clouds is more realistic for LM-Z. A case of low stratus over southern Sweden was forecasted as layered cloud with LM-Z and rather broken with LM.

The case shown here is the 30 h forecast starting from the 28th of March 1997 00 UTC, representing a strong wind situation. The rather interesting differences in the forecast of meso scale cloud structures result in different precipitation forecasts. Fig 1 shows the observed precipitation sum 28 to 29 March 1997 06 to 06 UTC and Fig. 2 the corresponding forecasts of LM and LM-Z. There is a substantial improvement by the LM-Z.

References

Gallus, W. and J. Klemp, 2000: Behaviour of flow over steep orography. *Mon. Wea. Rev.*, 128, 1153-1164.

Mesinger, F., Z. Janjic, S. Nicovic, D. Gavrilov and D. Deaven, 1988: The step-mountain coordinate: Model description and performance for cases of Alpine lee cyclogenesis and for a case of Appalachian redevelopment. *Mon. Wea. Rev.*, 116, 1493-1518.

Steppeler, J., H.-W. Bitzer, M. Minotte and L. Bonaventura, 2002: Nonhydrostatic atmospheric modelling using a z-coordinate representation, *Mon. Wea. Rev.*, 130, 2143-2149.

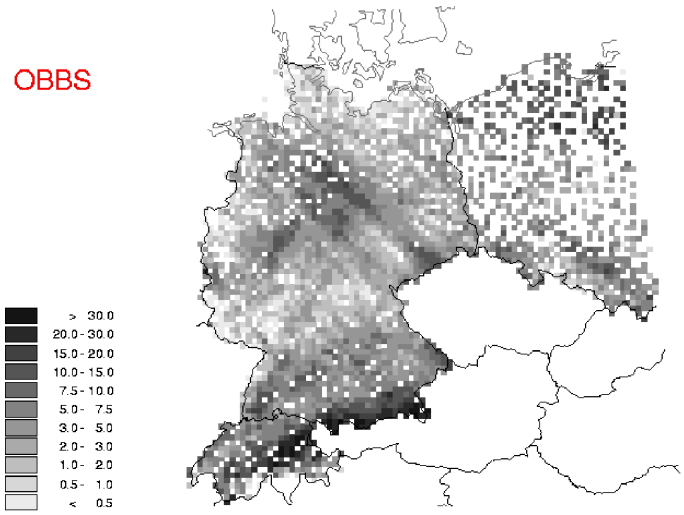

Figure 1: The precipitation sum as observed by the climatological network from 28 March 1997 6 UTC to 29 March 1997 6 UTC. Data from Germany, Switzerland and Poland were used.

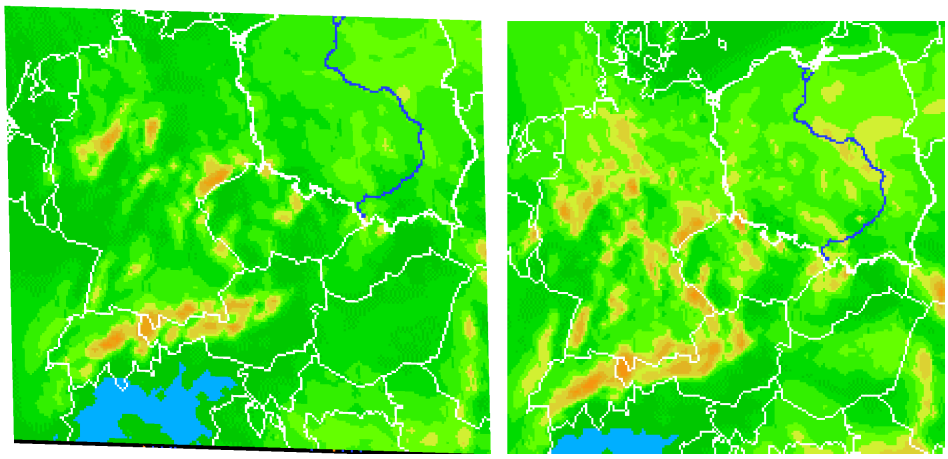

Figure 2: The same as in Fig. 1, but for forecasts of LM (left) and LM-Z (right).

A new Method for T2M Forecast in Complex Orography Areas

Daniele Cane[1,2], Massimo Milelli[1]

[1] *ARPA Piemonte, Italy*
[2] *Organizing Committee for the XX Winter Olympic Games Torino 2006*

1 Introduction

Meteorological parameter forecast is a quite challenging task in the Alpine region, due to complex geography and orography and to inexact parametrization of several physical processes. Limited area models also can show strong systematic and random errors in the parameter forecast, compared to the values observed by ground stations. As an example, consider the Figures 1 and 3, showing the mean temperature values in Piedmont observed in January and June 2004 respectively, compared with limited area models forecasts: errors up to 8°C can be observed.

Many post-processing methods are available for parameter forecast correction, see Kalman (1960) for instance, but usually they impose some hypothesis on parameter behaviour, such as Gaussian error distribution or no-correlation between errors. Krishnamurti (1999) introduced the so-called Multimodel technique, a post-processing method using several model outputs to obtain parameter forecasts. The Multimodel SuperEnsemble technique (see also Krishnamurti, 2000) takes into account the different model outputs, weighted by parameters calculated in a training period.

In this study we apply for the first time the SuperEnsemble technique on the operational model runs (00 UTC runs) of the 7 km resolution version of LM. We consider the outputs of Local Area Model Italy by UGM, ARPA-SIM, ARPA Piemonte (nud00), Lokal Modell by Deutscher Wetterdienst (lkd00) and Alpine Model (aLMo) by MeteoSwiss (alm00). We evaluate the model performances with respect to our regional high resolution network. Here presented are the results of 2 m temperature forecasts, compared with the measurements of 201 stations, divided in altitude classes ($< 700\ m$, $700 - 1500\ m$, $> 1500\ m$).

2 Multimodel Theory

As suggested by the name, the Multimodel SuperEnsemble method requires several model outputs, which are weighted with an adequate set of weights calculated during the so-called training period. The simple ensemble method with biased (Eq. 1) or bias-corrected (Eq. 2) data respectively, is given by

$$S = \overline{O} + \frac{1}{N}\sum_{i=1}^{N}(F_i - \overline{F_i}) \tag{1}$$

and

$$S = \overline{O} + \frac{1}{N}\sum_{i=1}^{N}(F_i - \overline{O}) \tag{2}$$

The conventional superensemble forecast (Krishnamurti, 2000) constructed with bias-corrected data is given by

$$S = \overline{O} + \sum_{i=1}^{N} a_i (F_i - \overline{O}) \tag{3}$$

where N is the number of models, F_i is the i^{th} forecast by the model, $\overline{F_i}$ and $\overline{O}$ are the mean forecasts and the mean observation during the training period T.

The calculation of the parameters a_i is given by the minimization of the mean square deviation

$$G = \sum_{k=1}^{T} (S_k - O_k)^2 \tag{4}$$

by derivation $\left(\frac{\partial G}{\partial a_i} = 0\right)$ we obtain a set of N equations, where N is the number of models involved $(i, j = 1, N)$:

$$\left(\sum_{k=1}^{T} \left(F_{i_k} - \overline{F_i}\right) \left(F_{j_k} - \overline{F_j}\right) \right) \cdot (a_i) = \left(\sum_{k=1}^{T} \left(F_{j_k} - \overline{F_j}\right) \left(O_k - \overline{O}\right) \right) \tag{5}$$

We then solve these equations using the Gauss-Jordan method (see Press et.al., 1992).

3 Results

3.1 Multimodel post-processing results: JANUARY 2004

We calculated Multimodel Ensemble and SuperEnsemble forecast using the three LM versions for the month of January 2004. Instead of using a fixed long training period, as in Krishnamurti (2000), we preferred to use a dynamic training period to take into account the seasonal variation of model performances. Then for each forecast day, forecast time and station we considered the 90 days before as training period, we calculated the forecast and observation means and the Multimodel weights and then we obtained Ensemble and SuperEnsemble forecast.

We evaluated the forecast improvement by comparison with observed values in the given period. Figure 1 shows the mean value confrontation. It has to be pointed out the strong systematic error of the direct model outputs, mainly in the medium mountain area (700 $m < height <$ 1500 m). More details can be found in Fig. 2, where Root Mean Square Error (RMSE) and Mean Error (or Bias) are shown. The model systematic error is about 6-8°C on the mountains, with significant increase around noon (+12 hr and +36 hr forecast time). Multimodel Ensemble and SuperEnsemble strongly reduce this bias, and RMSE shows the better performance of SuperEnsemble.

3.2 Multimodel post-processing results: JUNE 2004

We repeated the same procedure for the month of June 2004. The mean values of Fig. 3 do not show a strong systematic error, as they did in January, but the diurnal cycle is not well described by direct model outputs. Multimodel SuperEnsemble and Ensemble again perform better, as shown in Fig. 4. The RMSE shows again a better performance of SuperEnsemble with respect to Ensemble.

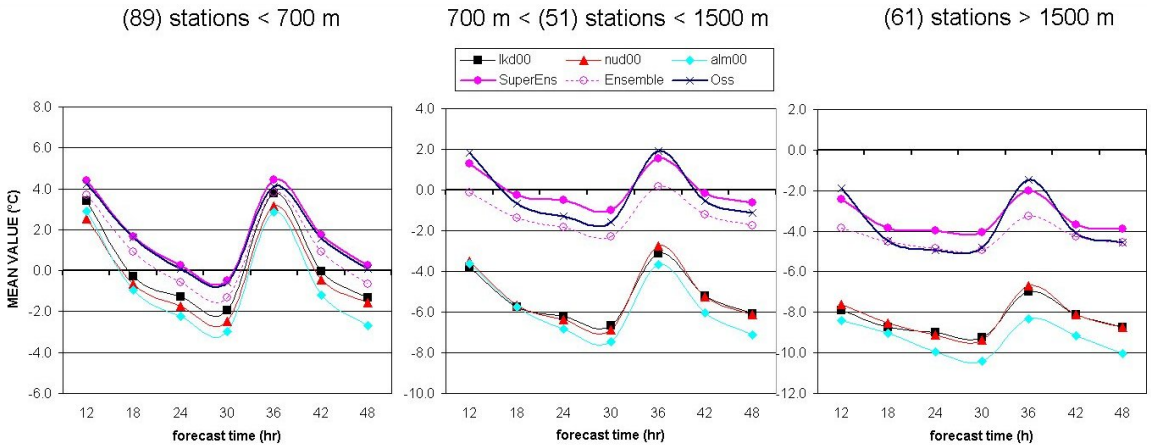

Figure 1: Mean temperatures for 201 Piedmontese weather stations: observed values (obs), SuperEnsemble (SuperEns) and Ensemble (Ensemble) forecast, LM forecast (alm00, nud00, lkd00), JANUARY 2004

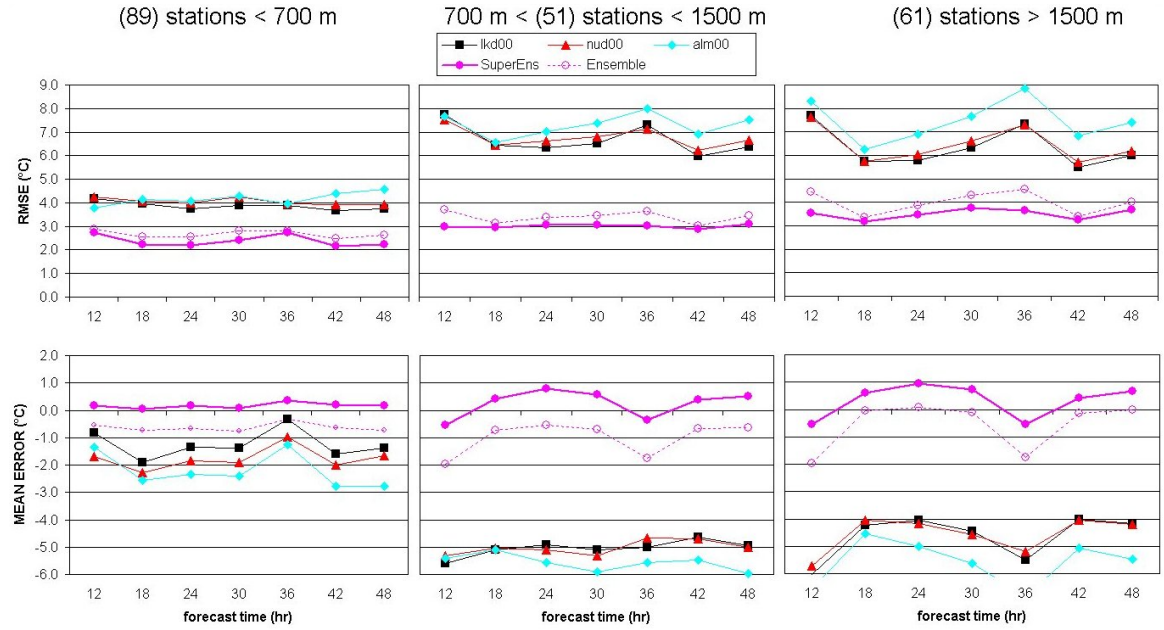

Figure 2: Root Mean Square Error (top) and Mean Error (bottom) for 201 Piedmontese weather stations: SuperEnsemble (SuperEns) and Ensemble (Ensemble) forecast, LM forecast (alm00, nud00, lkd00), JANUARY 2004

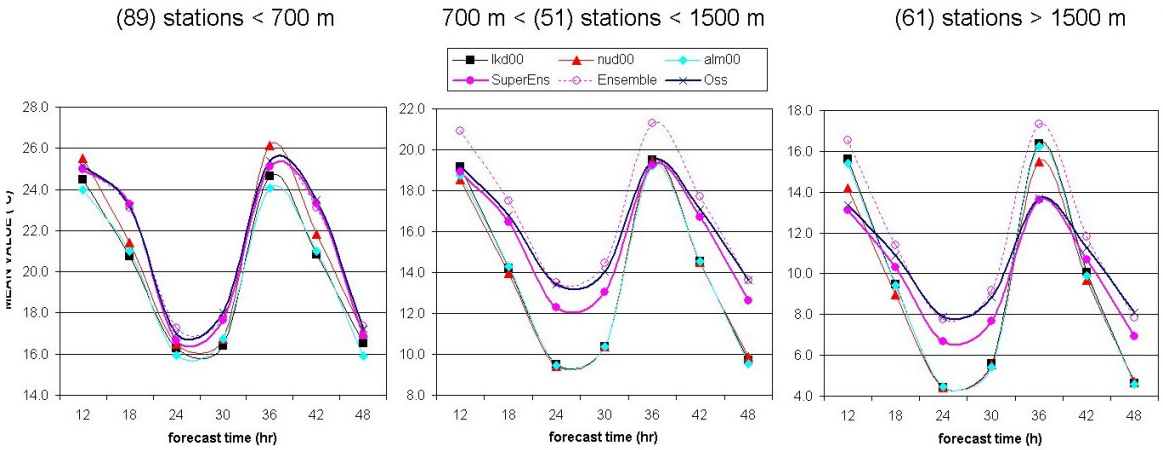

Figure 3: Mean temperatures for 201 Piedmontese weather stations: observed values (obs), SuperEnsemble (SuperEns) and Ensemble (Ensemble) forecast, LM forecast (alm00, nud00, lkd00), JUNE 2004

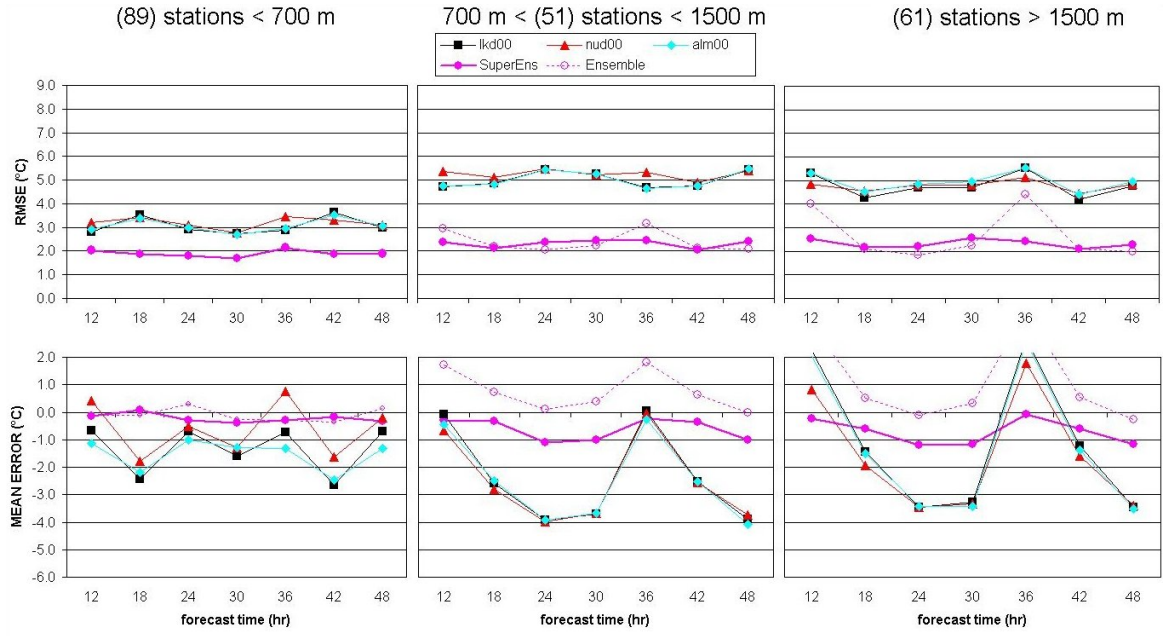

Figure 4: Root Mean Square Error (top) and Mean Error (bottom) for 201 Piedmontese weather stations: SuperEnsemble (SuperEns) and Ensemble (Ensemble) forecast, LM forecast (alm00, nud00, lkd00), JUNE 2004

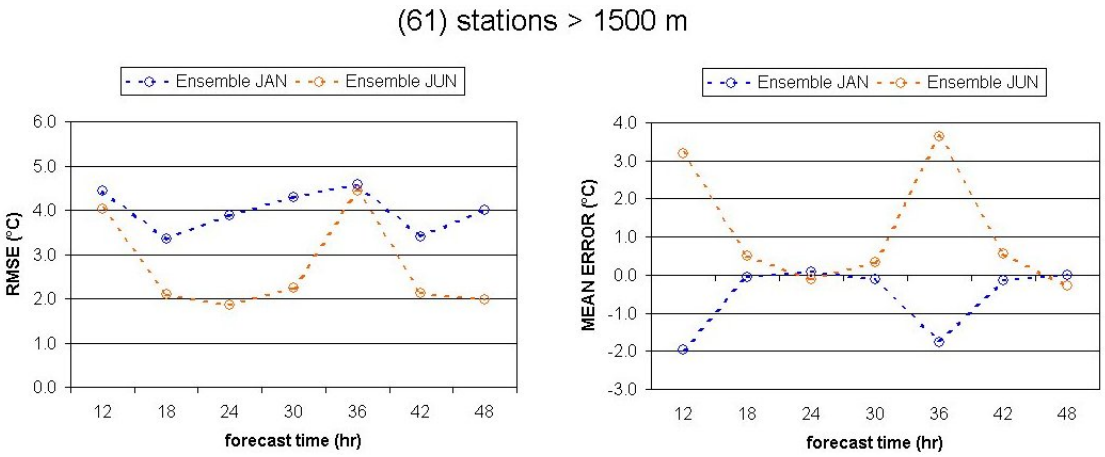

Figure 5: Root Mean Square Error (left) and Mean Error (right) for higher ($> 1500m$) weather stations: confrontation between Multimodel Ensemble January - June forecast

Actually Multimodel Ensemble is nothing but an unbiased mean of the direct model outputs, so it is quite interesting the comparison of 2m temperature RMSE for higher stations (> 1500 m). As shown before, it is worse during daytime hours (+12 hr and +36 hr forecasts), and the bias is opposite during winter (models underestimate the observed values) with respect to summer (models overestimate). A possible explanation is the uncorrect parametrization of the presence of snow on the ground, with its influence on heat flux calculation (see Fig. 5).

4 A comparison with Kalman filter results

A version of the Kalman filter (Kalman, 1960) post-processing on the direct output of ECMWF run at 12UTC is currently used every day for the 2m temperature forecasts over the entire Piedmont, but we register a degradation of the predicted values with increasing height of the weather stations. The same problem is evident also in the filtering of the limited area model outputs. The reason for this degradation can be found in the strong variability of the performances of the models day by day in the alpine region. In fact Kalman filter is very good in reducing the strong systematic errors, but fails when the difference between predicted and observed values varies strongly from one day to the next one.

Here we present the comparison between a test run of Kalman filter post-processing method on LM-DWD and the Multimodel method results. Figure 6 and 7 show the results for January 2004 and June 2004 respectively. Kalman filter and Multimodel SuperEnsemble give similar results, both in bias and RMSE.

5 Conclusions and perspectives

Direct Model Output 2m temperature forecasts show a noticeable degradation in the Alpine region, with strong systematic and random errors in any version of LM. Consequently, a new approach named Multimodel technique has been tested for the first time on limited area

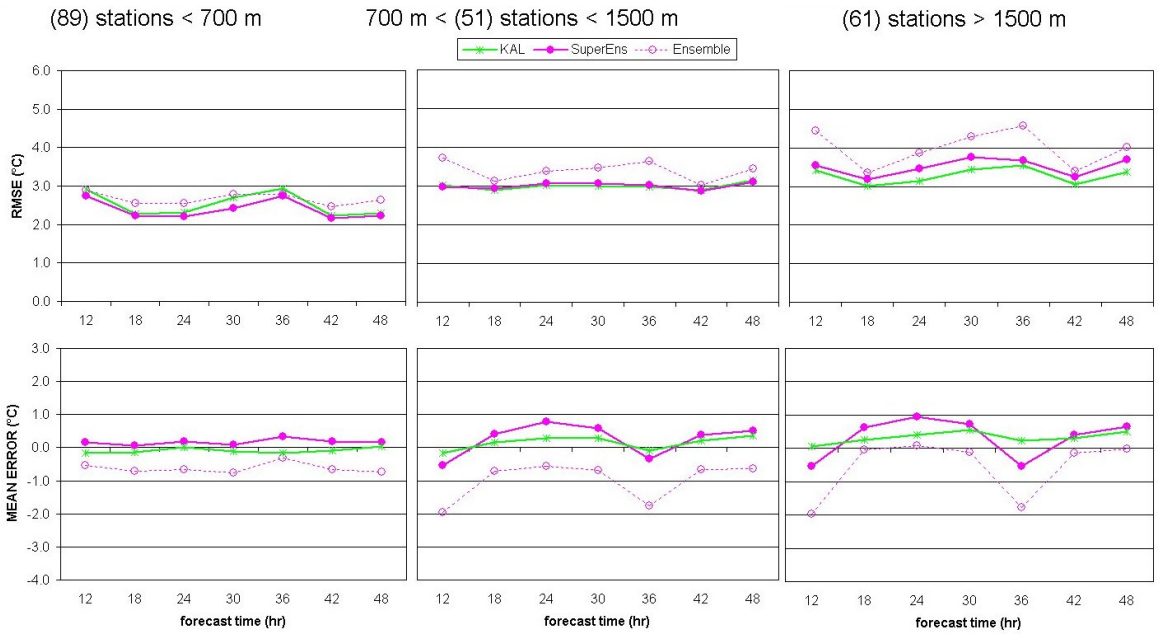

Figure 6: Root Mean Square Error (top) and Mean Error (bottom) for 201 Piedmontese weather stations: SuperEnsemble (SuperEns) and Ensemble (Ensemble) forecast, Kalman filter based on LM-DWD (KAL), JANUARY 2004

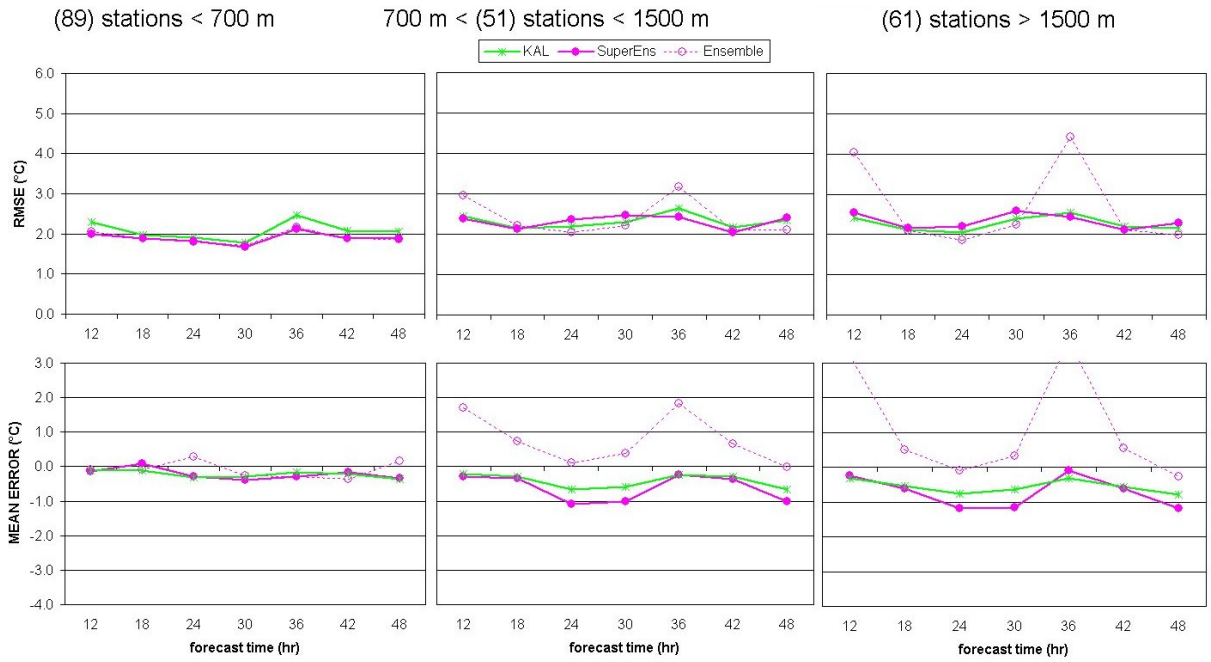

Figure 7: Root Mean Square Error (top) and Mean Error (bottom) for 201 Piedmontese weather stations: SuperEnsemble (SuperEns) and Ensemble (Ensemble) forecast, Kalman filter based on LM-DWD (KAL), JUNE 2004

models. The Multimodel SuperEnsemble improves the forecasts in high mountains locations, both in bias and RMSE and its performances are similar to those from Kalman filter, the latter being a much more complex technique, not suitable for all kind of variables. The hope is to obtain also good results in extending the Multimodel method to other parameters such as humidity and precipitation.

Acknowledgements

We wish to thank the Deutscher Wetterdienst and MeteoSwiss for providing the model outputs for this research work.

References

Kalman R. E., 1960. *Journal of Basic Engineering*, 82 (Series D), 35-45.

Krishnamurti, T. N. et al., 1999. *Science*, 285, 1548-1550.

Krishnamurti, T. N. et al., 2000. *J. Climate*, 13, 4196-4216.

Press et al., 1992. Numerical Recipes in Fortran, Cambridge University Press.

Introducing the Lokal-Modell LME at the German Weather Service

Jan-Peter Schulz

Deutscher Wetterdienst, Kaiserleistr. 42, D-63067 Offenbach a.M., Germany

1 Introduction

In order to fulfill new requirements of both external and internal customers, for instance in aviation, sea traffic or air pollution modelling, the German Weather Service (DWD) decided to expand the model domain of the operational limited area model, the Lokal-Modell (LM, Doms and Schättler, 2002).

2 The model LME

The current version covers basically Central Europe, including Germany and its neighbouring countries. The new version shall cover almost entire Europe and will therefore get the name LM Europe (LME). The integration domain of LME is shown in Fig. 1. The number of grid points per layer will be enhanced from 325×325 to 665×657, while the mesh size is kept unchanged at 7×7 km^2. The number of vertical layers is increased from 35 to 40. The additional layers are mainly located in the lower troposphere, the height of the lowest layer is reduced from 33 m to 10 m. This is in accordance with the new 40-km version of the driving global model GME which started operation at DWD in September 2004. The poles of the rotated LME coordinate system are different from the LM system. The LME system is rotated in a way that the equator is located within the center of the model domain. This has the advantage that the grid cells have a similar size and shape throughout the entire domain or, in other words, the divergence of the longitude rows is minimal. The main non-technical model change will be the introduction of a new multi-layer soil model, the same that was incorporated into GME in 2004.

3 Preliminary results

The introduction of LME at DWD is done in several steps. First of all, two experiments were set up at ECMWF in 2004, namely LME and LM, running daily forecasts driven by GME. Here, the influence of the domain size or the distance between the boundaries and the region of interest, respectively, can be tested. It turns out that in most weather situations there is very little influence. But, there are sporadic cases where for example the development of a cyclone evolves significantly differently. First results of an objective verification shows some advantage for LME forecasts for precipitation and gusts and some disadvantage for mean sea level pressure.

During spring 2005 LME data assimilation and forecasts are tested in an operational parallel suite at DWD. All postprocessing procedures have to be adjusted. Further subjective and objective verification is carried out. The operational start of LME at DWD is planned in autumn 2005.

Reference

Doms, G. and U. Schättler, 2002: A description of the nonhydrostatic regional model LM.

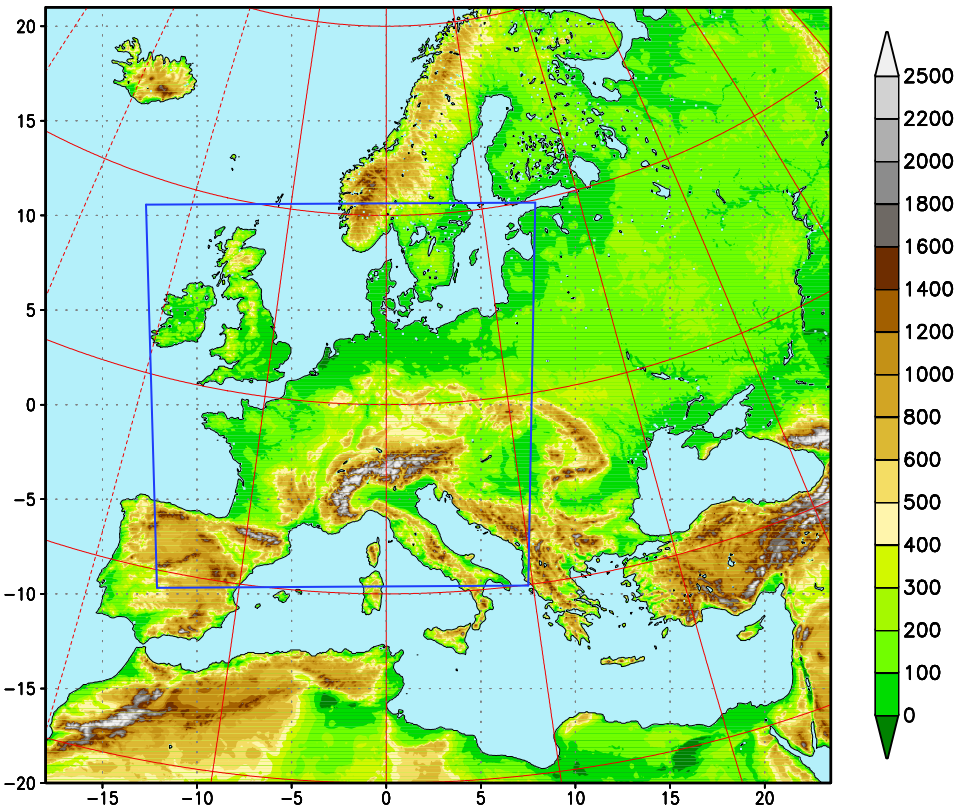

Figure 1: Model domain of LME. Topographical height (m) for land fractions > 50% (for the operationally used filtered orography). The frame in the figure depicts the integration domain of LM.

10 Collaboration and External Users of LM

All national weather services of COSMO are members of EUMETNET, the network of meteorological services within Europe. EUMETNET provides a framework to organize co-operative programmes between the members in the various fields of basic meteorological activities such as observing systems, data processing, basic forecasting products, research and development, and training (*www.eumetnet.eu.org*). COSMO's activities are embedded in this network and are especially related to EUMETNET programmes such as MAP-NWS (Mesoscale Alpine Programme - National Weather Services) and EUCOS (EUMETNET Composite Observing System).

Since the 1st of January 2000, EUMETNET provides a Coordinator for the SRNWP (Short Range Numerical Weather Prediction) Group. Representatives of the NWP branches of European National Meteorological Services meet in this group on a yearly basis to organize co-operative activities in development of numerical atmospheric models. The present SRNWP-coordinator is J. Quiby from MeteoSwiss. Within the SRNWP Group, Lead Centres have been selected for different topics. The Lead Centres have the responsibility to organize intercomparisons, workshops and to ensure the flow of information between participants. DWD has taken the role as the Lead Centre for Nonhydrostatic Modelling (responsible for this LC is Jürgen Steppeler from DWD) and UGM acts as Lead Centre for Short Range Ensemble Prediction Systems (responsible is Massimo Ferri from UGM). For more information on SRNWP and its Lead Centres see `http://srnwp.cscs.ch`.

All COSMO partners are also members of EWGLAM (European Working Group on Limited Area Modelling). This group meets once a year to exchange information on the current status and on recent developments in high-resolution numerical weather prediction.

Another type of collaboration with other European meteorological services is via COST, an intergovernmental framework for European *Co-operation in the field of Scientific and Technical Research*, allowing the co-ordination of nationally funded research on a European level (for more information about COST see *www.netmaniacs.com/cost*).

10.1 International Projects

This section lists the current participation of COSMO partners in international research projects which are related to LM. This list will be updated in the forthcoming issues.

- **SPP 1167** *Priority Program of the DFG: Quantitative Precipitation Forecast*
  Type: Funded by the german national science foundation *Deutsche Forschungsgemeinschaft* (DFG).
  Aim: Research of atmospheric processes and models to enhance the predictability of quantitative precipitation.
  DWD-contribution: *Central coordination for using DWD models (LM, NUmerical EXPerimentation System NUMEX) and data.*
  MeteoSwiss-contribution: *Improving short-term quantitative precipitation forecasts using radar rainfall assimilation with latent heat nudging.*
  Information: `http://www.meteo.uni-bonn.de/projekte/SPPMeteo`.

- **COST 722** *Short range forecasting methods of fog, visibility and low clouds.*
  Type: COST concerted research action
  MeteoSwiss contribution: *Coupling of the 1d COBEL model with the aLMo.*
  Information: `http://137.248.191.94/cost/`.

- **COST 731** *Propagation of Uncertainty in advanced meteo-hydrological Forecast Systems.*
  Type: COST concerted research action (will begin at the end of June)
  Aim: The Action will address the problem of forecasting (heavy) precipitation events and the corresponding hydrological processes in connection with the uncertainty inherent in this task. Building on experiences in COST 717 the established cross community communication between hydrologists, radar scientists and NWP modellers will be further strengthened.
  DLR contribution: *Application and further development of the regional ensemble system building on COSMO-LEPS, remote sensing observations (Satellite, Radar) and corresponding synthetic imagery and a pattern recognition algorithm.*
  Information: web-site not yet available

- **CLOUDNET** *Development of a European pilot network of stations for observing cloud profiles.*
  Type: EU funded project.
  Aim: Optimization of the use of existing data sets to develop and validate cloud remote sensing synergy algorithms; provision of data for the improvement of the representation of clouds in climate and weather forecast models.
  DWD contribution: *Provision of LM data for selected grid points for statistical and process-related verification.*
  Information: `http://www.met.rdg.ac.uk/radar/cloudnet`.

- **FUMAPEX** *Integrated Systems for Forecasting Urban Meteorology Air Pollution and Population Exposure* Type: EU funded project.
  DWD contribution: *Application of NWP for air-quality forecasting; improvement and urbanization of LM (at a very high resolution up to 1.1 km) and dispersion models; mesoscale model intercomparison.*
  ARPA-SIM contribution: *Preparing an urban air quality information system.*
  MeteoSwiss/EPF Lausanne-contribution: *Investigation of near-surface exchange processes, especially urban turbulence parameterization.*
  Information: `http://fumapex.dmi.dk`

Furthermore, a number of activities of COSMO members are related to the *Mesoscale Alpine Project* (MAP). For more information, see the MAP homepage at *www.map.ethz.ch.*

10.2 National Projects and Collaboration

This section lists LM-related projects and collaboration of COSMO members on a national level. At present, the list is by no means complete. Please inform the editors on such activities, especially those with national funding, in order to get a more complete list in the next COSMO newsletter.

- **DWD / Ruhr-Universität Bochum / Gesellschaft für wasserwirtschaftliche Planung und Systemforschung / Büro für angewandte Hydrologie (Berlin): Mulde-Projekt**
  Type: Funded by BMBF ("Verbundprojekt").
  Aim: Installation and pre-operation of an improved system for flood-warnings by a tighter coupling of the different components involved in flood forecasting.
  DWD-contribution: *Provide precipitation scenarios with probabilities for hydrological modelling derived from forecasts of LMK, COSMO-LEPS and SRNWP-PEPS. Of importance are mainly the quantifications of the uncertainties in the precipitation forecast and a consistent description of these by all scenarios.*

- **MeteoSwiss/NCCR Climate**
  National Centre of Competence in Research - Climate.
  Type: Nationally funded research project
  Information: `http://www.meteoswiss.ch/nccr`.

- **MeteoSwiss/University of Berne**
  Extraction of snow-cover, lake-temperature, NDVI, LAI, land surface temperature and albedo from NOAA satellites, primarily for the data assimilation suite.
  Type: bilateral project, partially funded by MeteoSwiss

- **MeteoSwiss/ETH Zürich**
  Extraction of snow-cover from Meteosat satellites, primarily for the data assimilation suite.
  Type: bilateral project, funded by EUMETSAT (Fellowship)

- **MeteoSwiss/EMPA**
  Determination of typical source regions of air pollutants for stations of the national air quality observing network.
  Type: BUWAL project with partial funding (EMPA only)
  Information: `http://www.empa.ch` > Organisation > Mobilität und Umwelt > Luftfremdstoffe / Umwelttechnik > Ausbreitungsmodellierung

- **MeteoSwiss/PMOD-WRC**
  Longwave radiation measurements compared to radiative transfer model and aLMo (terminated autumn 2004).
  Type: Swiss National Science Foundation Project "Greenhouse-effect in the Alps: by models and observations".
  Information: `http://www.pmodwrc.ch/pmod.php?topic=asrb`.
  Publication: Duerr, B., Philipona, R., Schubiger, F. and Ohmura, A. (2005): " Comparison of modeled and observed cloud-free longwave downward radiation over the Alps", to appear in Met. Z.

- **MeteoSwiss/PartnerRe**
  High-resolution re-analysis of extreme weather events. Computation with LM [at the Swiss Center for Scientific Computing (CSCS)] of winter storms (1957-2002) over

Europe based on initial and boundary fields from the ECMWF ERA-40 Project. Calculation of wind gusts with an alternative approach by Brasseur (2001) using the height of the balance between turbulent kinetic energy and the buoyancy force.

- **MeteoSwiss/HSK**
  Development of a new system for the security surveillance of atomic power plants in Switzerland, based on a high resolution implementation of the aLMo and new remote sensing capabilities.
  Type: Bilateral project.

- **CLM**
  In autumn 2001, the German community on regional climate modelling decided to use the Lokal-Modell as a basis for a new regional climate model. The first version of CLM (Climate Version of the LM) has been derived from the release 2.14 of LM. Meanwhile, CLM 3 (based on LM Version 3.1) is used. In 2004 a *Community Agreement* was signed by several partners on the use of CLM, which is supported by DWD. The major extensions to LM necessary for the climate version will be taken over to LM. You find information on this modelling group and the related model developments at the CLM web-site `http://w3.gkss.de/CLM/index.html`.

- **ICON**
  The Max Planck Institute for Meteorology in Hamburg (MPI) and DWD have started a joint research project to develop ICON (ICOsahedral Nonhydrostatic), a unified global model to be used both for climate studies and operational short range weather forecasting. The model will employ finite volume numerical techniques to discretize the fully compressible nonhydrostatic equations on a geodesic, icosahedral grid. More information is available at the ICON web site `http://icon.enes.org`.

- **AFO2000**
  The German Atmospheric Research Programme 2000-2006 (AFO200) is funded by the Federal Ministry for Education and Research. It aims to improve the understanding of the atmospheric system including earth-surface interactions, chemistry, dynamics, radiation and their interactions, multiphase processes, and atmosphere-system analysis. DWD contributes with LM-based studies in various subprojects. More information is available at the web site `http://www.afo-2000.de`.

10.3 External Users of LM

The source code of the LM-package is available free of charge for scientific and educational purposes to third parties outside COSMO. Such external users, however, must register and sign a special agreement with a COSMO meteorological service. For questions about the request and the agreement, please contact Dieter Frühwald (dieter.fruehwald@dwd.de) from the COSMO Steering Committee.

Meanwhile, a number of universities and research institutes have received the model software. Once a year, there is a *User Workshop on Scientific Applications of the LM* organized by Jürgen Steppeler at DWD (contact: juergen.steppeler@dwd.de, see also Section 7.4). There is, however, not always a feedback on the activities or on results and problems. The following table lists the current registered users of the LM (outside the COSMO group).

Institution	Country	Research Activities
Academy of Science, Hydrometeorological Institute	Bulgaria	unknown
Academy of Science, Institute for Physics of the Atmosphere, Prague	Czech Republic	Clouds and precipitation at high resolution
Alfred Wegener Institut, Bremerhaven	Germany	Cloud physics
Center for Marine Research Rudjer Boskovic Institute	Croatia	Ocean model simulations
Frontier Research, Institute for Global Change Research	Japan	Tests on time-splitting methods
German Aerospace Centre, Institute of Atmospheric Physics, Oberpfaffenhofen	Germany	Turbulence studies, model intercomparison
GKSS Research Centre Geesthacht	Germany	Regional climate simulations,
Institute for Tropospheric Research (IFT), Leipzig	Germany	Z-coordinate model version, turbulence studies
Konrad-Zuse Institut, Berlin	Germany	Scientific visualization
Massachusetts Institute of Technology, Cambridge MA	USA	unknown
Meteorological Research Institute	Japan	Model intercomparison
Meteorological Research Institute	Korea	unknown
National Center for Atmospheric Research, Boulder CO	USA	unknown
Norwegian Meteorological Institute (DNMI), Oslo	Norway	Model intercomparison
Potsdam Institute for Climate Impact Research (PIK), Potsdam	Germany	Regional climate studies, low Mach-number dynamics
Swiss Institute of Technology (ETH), Zürich	Switzerland	Regional climate studies High resolution experiments
Swiss Institute of Technology (EPF), Lausanne	Switzerland	Urban turbulence
Turkish State Meteorological Service	Turkey	Coastal wind simulations
University of Berlin	Germany	unknown
University of Bern	Switzerland	Land use and regional climate
University of Bonn	Germany	Physical initialization, statistical postprocessing, regional evaporation and water resource management
University of Bremen	Germany	Influence of water vapor in the upper troposphere on the climate

Institution	Country	Research Activities
University of Cologne	Germany	unknown
University of Dresden	Germany	Case studies
University of Frankfurt	Germany	Numerics and cloud physics
University of Genua	Italy	Dynamics of convective cells
University of Göttingen	Germany	Regional climate studies
University of Hamburg	Germany	unknown
University of Hannover	Germany	Aircraft icing
University of Hohenheim	Germany	Assimilation of LIDAR data
University of Karlsruhe	Germany	Soil modelling, case studies climate modelling, chemistry
University of Kiel	Germany	3D cloud models, radiation transport
University of Leipzig	Germany	Cloud physics, hydrology
University of Ljubljana	Slovenia	Latent heat nudging
University of Munich	Germany	Model comparison, case studies
University of Milano	Italy	Numerics, shaved elements

References

Note: The LM documentation, the COSMO Newsletters and COSMO Technical Reports are available at `http://www.cosmo-model.org` or `http://cosmo-model.cscs.ch`.

Baldauf. M. and J.-P. Schulz, 2004: Prognostic precipitation in the Lokal-Modell (LM) of DWD. *COSMO Newsletter*, No. 4, 177–180.

Davies, H. C. and R. E. Turner, 1977: Updating prediction models by dynamical relaxation: An examination of the technique. *Quart. J. Roy. Meteor. Soc.*, 103, 225–245.

Doms, G., and U. Schättler, 1999: The Nonhydrostatic Limited-Area Model LM (Lokal-Modell) of DWD. Part I: Scientific Documentation. Deutscher Wetterdienst (DWD), Offenbach. January 1999.

Doms, G., 2001: A scheme for monotonic numerical diffusion in the LM. *Cosmo Technical Report*, No. 3.

Doms, G., 2002: The LM cloud ice scheme. *COSMO Newsletter*, No. 2, 128–136.

Doms, G., Gassmann, A., Heise, E., Raschendorfer, M., Schraff, C. and R. Schrodin, 2002: Parameterization issues in the non-hydrostatic NWP-model LM. *ECMWF Seminar on Key Issues in the Parameterization of Subgrid Physical Processes*, 205-252.

Doms, G. and U. Schättler, 2002: A Description of the Nonhydrostatic Regional Model LM. Part I: Dynamics and Numerics. Deutscher Wetterdienst (DWD), Offenbach. November 2002

Doms, G., J. Förstner, E. Heise, H.-J. Herzog, M. Raschendorfer, T. Reinhardt, and G. Vogel, 2005: A Description of the Nonhydrostatic Regional Model LM. Part II: Physical Parameterizations. Deutscher Wetterdienst (DWD), Offenbach. April 2005.

Doms, G. and J. Förstner, 2004: Development of a Kilometer-Scale NWP-System: LMK. *COSMO Newsletter*, No. 4, 159–167.

Dudhia, J., 1993: A nonhydrostatic version of the Penn State / NCAR mesoscale model: Validation tests and simulation of an Atlantic cyclone and cold front. *Mon. Wea. Rev.*, 121, 1493–1513.

Förstner, J. and G. Doms, 2004: Runge-Kutta time integration and high-order spatial discretization of advection: a new dynamical core for LM. *COSMO Newsletter*, No. 4, 168–176.

Förstner J., H.-J. Herzog, and G. Vogel, 2005: Implementation of a 3D-turbulence parameterization for the very short range forecast model LMK. *WGNE Blue Book*, 2005.

Gallus, W. and J. Klemp, 2000: Behaviour of flow over steep orography. *Mon. Wea. Rev.*, 128, 1153–1164.

Gassmann, A., 2001: Filtering of LM-orography. *COSMO Newsletter*, No. 1, 71–78.

Gassmann, A., 2002: 3D-transport of precipitation. *COSMO Newsletter*, No. 2, 113–117.

Gassmann, A., 2002: A two timelevel integration scheme for the LM. *COSMO Newsletter*, No. 2, 97–100.

Gassmann, A., 2003: Case Studies with the 2-Timelevel Scheme and Prognostic Precipitation. *COSMO Newsletter*, No. 3, 173–176.

Herzog H.-J., U. Schubert, G. Vogel, A. Fiedler, and R. Kirchner, 2002: LLM - the High-Resolving Nonhydrostatic Simulation Model in the DWD-Project LITFASS (Part I: Modelling Technique and Simulation Method) COSMO Technical Report No. 4. Deutscher Wetterdienst, Offenbach, Germany, March 2002.

Herzog H.-J., G. Vogel, and U. Schubert, 2002: LLM - a nonhydrostatic model applied to high-resolving simulations of turbulent fluxes over heterogeneous terrain. *Theor. Appl. Climatol.*, 73, 67–86, 2002.

Hess, R., 2001: Assimilation of screen-level observations by variational soil moisture analysis. *Meteor. Atmos. Phys.*, 77, 155–166.

Jacobsen, I. and E. Heise, 1982: A new economic method for the computation of the surface temperature in numerical models. *Contr. Atmos. Phys.*, **55**, 128–141.

Kalman, R. E., 1960: *Journal of Basic Engineering*, 82 (Series D), 35–45.

Kessler, E., 1969: On the distribution and continuity of water substance in the atmospheric circulations. *Meteor. Monogr.*, 10, No. 32, Amer. Met. Soc., 84pp.

Klemp, J. B. and R. Wilhelmson, 1978: The simulation of three-dimensional convective storm dynamics. *J. Atmos. Sci.*, 35, 1070–1096.

Klink, S. and K. Stephan, 2004: Assimilation of Radar Data in the LM at DWD. *COSMO Newsletter*, No. 4, 143–150.

Krishnamurti, T. N., et.al., 1999: *Science*, 285, 1548–1550.

Krishnamurti, T. N., et.al., 2000: *J. Climate*, 13, 4196–4216.

Leuenberger, D. and A. Rossa 2003: Assimilation of Radar Information in aLMo. *COSMO Newsletter*, No. 3, 164–172.

Lorenc, A. C., R. S. Bell and B. Macpherson, 1991: The Meteorological Office analysis correction data assimilation scheme. *Quart. J. Roy. Meteor. Soc.*, 117, 59–89.

Louis, J.-F., 1979: A parametric model of vertical eddy fluxes in the atmosphere. *Bound. Layer Meteor.*, **17**, 187–202.

Lynch, P., D. Girard and V. Ivanovici, 1997: Improving the efficiency of a digital filtering scheme. *Mon. Wea. Rev.*, **125**, 1976–1982.

Majewski, D., 1998: The new global icosahedral-hexagonal grid point model GME of the Deutscher Wetterdienst. *ECMWF Seminar on Numerical Methods in Atmospheric Models.*

Majewski, D., D. Liermann, P. Prohl, B. Ritter, M. Buchhold, T. Hanisch, G. Paul, and W. Wergen, 2002: The operational global icosahedral-hexagonal gridpoint model GME: Description and high-resolution tests. *Mon. Wea. Rev.*, 130, 319–338.

Mellor, G. L. and T. Yamada, 1974: A hierarchy of turbulence closure models for planetary boundary layers. *J. Atmos. Sci.*, 31, 1791–1806.

Mellor, G. L. and T. Yamada, 1982: Development of a turbulence closure model for geophysical flow problems. *Rev. Geophys. and Space Phys.*, 20, 831–857.

Mesinger, F., Z. Janjic, S. Nicovic, D. Gavrilov and D. Deaven, 1988: The step-mountain coordinate: Model description and performance for cases of alpine lee cyclogenesis and for a case of Appalachian redevelopment. *Mon. Wea. Rev.*, 116, 1493–1518.

Montani, A., M. Capaldo, D. Cesari, C. Marsigli, U. Modigliani, F. Nerozzi, T. Paccagnella, P. Patruno and S. Tibaldi, 2003: *ECMWF Newsletter Summer 2003*, 98, 2–7.

Press, et.al., 1992: Numerical Recipes in Fortran. Cambridge University Press.

Raschendorfer, M., 2004: A new TKE-based Scheme fro Vertical Diffusion and Surface-Layer Transfer. Deutscher Wetterdienst, Offenbach, Germany, 2004.

Raymond, W. H., 1988: High-order low-pass implicit tangent filters for use in finite area calculations. *Mon. Wea. Rev.*, **116**, 2132–2141.

Ritter, B. and J. F. Geleyn, 1992: A comprehensive radiation scheme for numerical weather prediction models with potential applications in climate simulations. *Mon. Wea. Rev.*, **120**, 303–325.

Schär, C., D. Leuenberger, O. Fuhrer, D. Lüthi and C. Girard, 2002: A new terrain-following vertical coordinate formulation for atmospheric prediction models. *Mon. Wea. Rev.*, 130, 2459–2480.

Schraff, C., 1996: Data assimilation and mesoscale weather prediction: A study with a forecast model for the Alpine region. Publication No. 56, Swiss Meteorological Institute.

Schraff, C., 1997: Mesoscale data assimilation and prediction of low stratus in the Alpine region. *Meteorol. Atmos. Phys.*, **64**, 21–50.

Schraff, C. and R. Hess, 2003: A description of the nonhydrostatic regional model LM. Part III: Data assimilation. Deutscher Wetterdienst (DWD), Offenbach. June 2003 (available at www.cosmo-model.org).

Schrodin, R. and E. Heise, 2001 : The multi-layer version of the DWD soil model TERRA_LM. *Cosmo Technical Report*, No.2 (available at www.cosmo-model.org).

Skamarock, W. C. and J. B. Klemp, 1992: The stability of time-split numerical methods for the hydrostatic and the nonhydrostatic elastic equations. *Mon. Wea. Rev.*, **120**, 2109–2127.

Sommeria, G. and J. W. Deardorff, 1977: Subgrid-scale condensation in models of non-precipitating clouds. *J. Atmos. Sci.*, 34, 344–355.

Stauffer, D. R. and N. L. Seaman, 1990: Use of four-dimensional data assimilation in a limited-area mesoscale model. Part I: Experiments with synoptic-scale data. *Mon. Wea. Rev.*, 118, 1250–1277.

Stauffer, D. R. and N. L. Seaman, 1994: Multiscale four-dimensional data assimilation. *J. Appl. Meteor.*, 33, 416–434.

Stephani, H., 1988: *Allgemeine Relativitätstheorie*. Dt. Verlag d. Wiss., Berlin, 1988.

Steppeler, J., H.-W. Bitzer, M. Minotte and L. Bonaventura, 2002: Nonhydrostatic atmospheric modelling using a z-coordinate representation. *Mon. Wea. Rev.*, 130, 2143–2149.

Steppeler, J., G. Doms, U. Schättler, H.-W. Bitzer, A. Gassmann, U. Damrath and G. Gregoric, 2003: Meso-gamma scale forecasts using the non-hydrostatic model LM. *Meteorol. Atmos. Phys.*, 82, 75-96.

Thomas, S., C. Girard, G. Doms and U. Schättler, 2000: Semi-implicit scheme for the DWD Lokal-Modell. *Meteorol. Atmos. Phys.*, **75**, 105–125.

Tiedtke, M., 1989: A comprehensive mass flux scheme for cumulus parameterization in large-scale models. *Mon. Wea. Rev.*,**117**, 1779–1799.

Wicker, L. and W. Skamarock, 1998: A time-splitting scheme for the elastic equations incorporating second-order Runge-Kutta time differencing. *Mon. Wea. Rev.*, **126**, 1992–1999.

Wicker, L. and W. Skamarock, 2002: Time-splitting methods for elasic models using forward time schemes. *Mon. Wea. Rev.*, **130**, 2088–2097.

Appendix A: The GRIB Binary Data Format used for LM I/O

All input and output arrays of the LM and of the preprocessor programs providing interpolated initial conditions and the boundary values are stored in a compressed binary data format called GRIB-code. GRIB means "gridded binary" and is designed for the international exchange of processed data in the form of grid-point values expressed in binary form.

The GRIB-code is part of the FM-system of binary codes of the World Meteorological Organization (WMO). Currently, we use Edition 1 of the GRIB-code with number FM 92-VIII. For coding details, see the *Manual on Codes, International Codes, Volume 1.2* of WMO (WMO Publication No. 306, 1995). In this section, we describe only the basic features of the GRIB code which are relevant for the I/O of the LM-system.

A.1 Code Form

Each GRIB-coded record (analysis or forecast field) consists of a continuous bit-stream which is made up of a sequence of octets (1 octet = 8 bits). The representation of data by means of series of bits is independent of any particular machine representation. The octets of a GRIB messsage are grouped in sections (see Table 1, where the length of the record and the length of the sections are expressed in octets. Section 0 has a fixed length of 4 octets and section 5 has a fixed length of 4 octets. Sections 1, 2, 3 and 4 have a variable length which is included in the first three octets of each section.

Table 1: *Form of GRIB-code*

Section number	**Name**	**Contents**
0	Indicator Section	"GRIB"; length of record; GRIB edition number
1	Product Definition Section	Length of section; identification of the coded analysis/forecast field
2	Grid Description Section (optional)	Length of section; grid geometry, as necessary
3	Bit-map Section (optional)	Length of section; the bit per grid-point, placed in suitable sequence
4	Binary Data Section	Length of section; data values
5	End Section	7777

Octets are numbered 1, 2, 3, etc., starting at the beginning of each section. Bit positions within octets are referred to as bit 1 to 8, where bit 1 is the most significant bit and bit 8 is the least significant bit. Thus, an octet with only bit 8 set to 1 would have the integer value 1.

A.2 Indicator and End Section

The Indicator Section has a fixed length of 8 octets. The first four octets shall always be character coded as "GRIB" (according to the CCITT International Alphabet No.5). The remainder of the section shall contain the length of the entire GRIB-record (including the Indicator Section) expressed in binary form over the left-most 3 octets (i.e. 24 bits in octet 5-7), followed by the GRIB edition number (currently 1), in binary, in the remaining octet 8.

The End Section has a fixed length of 4 octets. These octets are character coded as '7777'

according to the International Alphabet No.5.

Thus, the beginning and the end of a GRIB-record can be identified by the character coded words "GRIB" and "7777". All other octets included in the code represent data in binary form. Each input or output array defined on the rotated lat/lon grid of the LM (e.g the surface pressure or the temperature at a specified model level) is coded as a GRIB-record. Various such records can be combined in a single GRIB-file.

A.3 Product Definition Section

The Product Definition Section (PDS) contains the necessary information to identify the binary coded field contained in the GRIB-record. The most important octet in this section is the indicator of the meteorological parameter. The indicator relates a specific meteorological element to an integer number. This indicator number is also referred to as GRIB-number or element-number and is defined in a separate code table. More than one indicator code tables may be used in GRIB-code. Thus, one can have the same element-number but different code table numbers for various fields. The element-numbers and code tables used by LM are described below.

The program `grbin1` of the supplementary GRIB-library `griblib` of the LM-system can be used to decode GRIB binary code. Besides the decoded data set, this program does also retrieve the contents of the octets of the PDS in an integer array `ipds`. To illustrate the structure of the PDS, Table 2 shows the contents of the product definition section of a binary coded LM output array, the total cloud cover (CLCT). The GRIB-record for this field is valid for 28.10.1998 00 UTC + 11 h and was created at 28.10.1998 7.04 UTC by an LM forecast.

Octet 4 (ipds(2)) assigns a table number to the parameter indicator number given in octet 9. Currently, we use 4 additional code tables besides the WMO-table (see Table 3), where table 205 is used to code synthetic satellite products (from LM version 3.7 and higher). A full list of variables defined by these tables is available from DWD.

Octet 6 (ipds(4)) indicates the process identification number which is allocated by the originating centre. Currently, we use only two different process numbers for forecasts or analyses (see Table 4).

The level or layer for which the data are included in the GRIB-record is coded in octets 10 - 12 (ipds(8) - ipds(10)), where octet 10 indicates the type of level and octets 11 and 12 indicate the value of this level. Table 5 shows the code figures used for LM. For reserved values, or if not defined, octets 11 and 12 shall contain zero.

All 3-D variables of LM except the vertical velocity are defined on terrain-following main levels. In GRIB, these main levels are coded as level-type 110: hybrid layers between two adjacent hybrid levels - which are the LM half levels, i.e the layer interfaces. In this case, octet 11 contains the level index of the upper half level and octet 12 contains the level index of the lower half level. The vertical velocity and the height of the half levels are coded as level type 109: hybrid levels, i.e. the LM half levels. In this case, octet 11 contains zero and octet 12 contains the level index of the model half level. Pressure levels (ipds(8) = 100) and height levels (ipds(8) = 105) are used when the interpolation from model to specified p- or z-surfaces is switched on for model output. For synthetic satellite images (table number 205 and level-type 222), the octets 11 - 12 are used to code the channel of a satellite: ipds(9) = 0 and ipds(10) contains the channel number.

Table 2: ***Contents of the Product Definition Section***

array ipds(i)	Octet number	Contents of PDS Value	Remarks
1	1-3	54	Length of the PDS (in octets)
2	4	2	Version number of the GRIB indicator table (see Table 3)
3	5	78	Identification of originating/generating centre (DWD has WMO number 78)
4	6	132	Generating process identification number (allocated by originating centre, see Table 4)
5	7	255	Number of grid used - from catalogue defined by the originating centre. Octet 7 set to 255 indicates a non-cataloged grid, in which case the grid is defined in the grid description section.
6	8	128	Block-flag; the value 128 indicates that the grid description section is included.
7	9	71	Indicator of parameter (element number) from GRIB-table in ipds(2); see Section 3.7
8	10	1	Indicator of type of level, see Table 5
9-10	11-12	0	Value of level (height, pressure, etc.) for which the data are included (see Table 5)
11	13	98	Year (start time of forecast; analysis time)
12	14	10	Month (start time of forecast; analysis time)
13	15	28	Day (start time of forecast; analysis time)
14	16	0	Hour (start time of forecast; analysis time)
15	17	0	Minute (start time of forecast; analysis time)
16	18	1	Indicator of unit of time range (see Table 6)
17	19	11	P1 - period of time (number of time units);
			time units given by octet 18 (ipds(16))
18	20	0	P2 - period of time (number of time units);
			time units given by octet 18 (ipds(16))
19	21	0	time range indicator (see Table 7)
20	22-23	0	Number of forecasts included in average, when octet 21 (ipds(19)) indicates an average or accumulation of forecasts (or analyses); otherwise set to zero.
21	24	0	Number of forecasts missing from averages or accumulations.
22	25	20	Century of reference time of data given by octets 13- 17
23	26	255	Sub-centre identification, national use
24	27-28	0	Units decimal scale factor (D)
25-36	29-40	0	Reserved: need not to be present
37	41	254	Octets 41-54 are reserved for the originating centre. The integer value 254 indicates that additional data follow. We use this part as follows:
38	42	0	not used
39	43-45	0	not used
40	46	0	not used
41	47	0	Additional indicator for a GRIB element number
42	48	98	Year of production of GRIB-record
43	49	98	Month of production of GRIB-record
44	50	11	Day of production of GRIB-record
45	51	2	Hour of production of GRIB-record
46	52	0	Minute of production of GRIB-record
47	53-54	1	Version number, currently 1 for LM

Table 3: *GRIB-tables for parameter (element) indicator number*

Version number of GRIB-table; ipds(2)	**Comment**
2	WMO-table of indicator parameters
201	national table of DWD for internal use
202	national table of DWD for internal use
203	national table of DWD for internal use
205	national table of DWD for internal use

Table 4: *Process identification numbers*

process id-number; ipds(4)	**Comment**
131	LM-analyses from data assimilation cycle
132	LM-forecasts and initialized analyses

Table 5: *Types of fixed levels or layers used by LM*

level type ipds(8)	**Meaning**	**ipds(9)**	**ipds(10)**
1	Ground or water surface	0	0
2	Cloud base level	0	0
3	Level of cloud tops	0	0
4	Level of $0°C$ isotherm	0	0
8	Top of atmosphere	0	0
100	Pressure (isobaric) level	0	Pressure in hPa
102	Mean sea level	0	0
103	Specified height above mean sea level	0	Height in m
105	Specified height level above ground	0	Height in m
109	Hybrid level (half levels)	0	Level number (k)
110	Hybrid layer (main level) between two hybrid levels	Level number of top (k)	Level number of bottom (k+1)
111	Depth below land surface	0	Depth in cm
112	Layer between two depths below land surface	Depth of upper surface in cm	Depth of lower surface in cm
222	Satellite images	0	Satellite Channel

Octets 13-17 contain the reference time of the data: the start of a forecast, the time for which an analysis is valid or the start of an averaging or accumulation period. The year of the century is coded in octet 13 and the century (100 years) in octet 25. For a reference time within the year 2000, octet 13 will contain the integer value 100 and octet 25 will contain the integer value 20.

The time or time interval for which the data are valid with respect to the reference time is coded in octets 18-21 (ipds(16)-ipds(19)). Octets 19 and 20 contain two periods of time, P1 and P2. The units of the values of P1 and P2 are defined in octet 18. Currently, we use hours as the time unit, but other values may be more appropriate for special applications of the model as the maximum integer number in an octet is 256. Thus, for long-term climate runs or short-term cloud simulations, other time units must be chosen. In LM version 3.15 time units of 15 minutes (`ipds(16)=13`) and 30 minutes (`ipds(16)=14`) have been implemented.

Note, that these values are DWD extensions and not GRIB standard. The WMO code-table for the unit of time in P1 and P2 is given in Table 6.

Table 6: *Code table for unit of time*

ipds(16)	Meaning	ipds(16)	Meaning	ipds(16)	Meaning
0	Minute	5	Decade	11	6 hours
1	Hour	6	Normal	12	12 hours
2	Day	7	Century	13(!)	15 minutes
3	Month	8-9	Reserved	14(!)	30 minutes
4	Year	10	3 hours	15-253	reserved
				254	second

The meaning of the time period P1 in octet 19 (ipds(17)) and of the time period P2 in octet 20 (ipds(18)) - given in the units coded in octet 18 - depends on the time-range indicator, which is contained in octet 21 (ipds(19)). The WMO code-table allows for a large number of indicators including averages and accumulation over a number of forecasts and analyses. For the LM-system, we use only a few standard indicators as shown in Table 7. In order to distinguish output from the nudging assimilation cycle from other external analysis products, as e.g. the sea surface temperature or snow depth, all nudging products will have a time-range indicator 13.

Table 7: *Time range indicators used by LM*

ipds(19)	Meaning
0	Forecast product valid for reference time + P1 (if P1 > 0) or uninitialized analysis product valid for reference time (P1 = 0)
1	initialized analysis product valid for reference time (P1 = 0)
2	Product with a valid time ranging between reference time + P1 and reference time + P2
3	Average from reference time + P1 to reference time + P2
4	Accumulation from reference time + P1 to reference time + P2; product valid for reference time + P2
13	Nudging analysis product, valid for reference time (P1 = 0) Note: All output from a nudging assimilation cycle will have time-range indicator 13, also fields which usually have ipds(19) = 2, 3 or 4.

A.4. Grid Description Section

Section 2 of a GRIB-record, the grid description section GDS, contains all information about the geometry of the grid on which the data are defined. For all input and output files of the LM, this section is coded completely for every field contained in the file. The program `grbin1` of the supplementary GRIB-library `griblib` retrieves the contents of the GDS in an integer array `igds`.

The contents of the grid description section of an LM GRIB-record is illustrated in Table 8 for the model domain used operationally at DWD. The octets corresponding to the integer array `igds` are numbered relative to this section.

Table 8: ***Contents of the Grid Description Section***

array igds(i)	Octet number	Contents of GDS Value	Meaning
1	1-3	202	Length of GDS (in octets) including the vertical coordinate parameters. (here for $ke = 35$ layers, i.e. $ke + 1 = 36$ half levels)
2	4	40	NV: Number of vertical coordinate parameters (four base state parameters + $(ke + 1)$ values of the vertical coordinates of the half levels)
3	5	43	PV: Location (octet number) of the list of vertical coordinate parameters
4	6	10	Data representation type according to WMO code-table 6; '10' assigns a rotated latitude/longitude grid
5	7-8	325	Number of gridpoints in 'zonal' direction
6	9-10	325	Number of gridpoints in 'meridional' direction
7	11-13	-17000	Rotated latitude of the first gridpoint in millidegrees
8	14-16	-12500	Rotated longitude of the first gridpoint in millidegrees
9	17	0	Resolution flag according to WMO code-table 7; '0' means that the grid spacing is not given
10	18-20	3250	Rotated latitude of the last gridpoint in millidegrees
11	21-23	7750	Rotated longitude of the last gridpoint in millidegrees
12	24-25	0	Longitudinal direction increment (grid spacing in λ-direction, not given)
13	26-27	0	Meridional direction increment (grid spacing in ϕ-direction, not given)
14	28	64	Scanning mode flag according to WMO code-table 8 '64' means that points scan in +i and +j direction and adjacent points in i-direction are consecutive
15-19	29-32	0	Reserved (set to zero)
20	33-35	-32500	Geographical latitude of rotated southern pole in millidegrees
21	36-38	10000	Geographical longitude of rotated southern pole in millidegrees
22	39-42	0	Angle of rotation
26-65	43-202	.....	List of vertical coordinate parameters, each packed on 4 octets (length = 4 x NV octets). first the three parameters defining the base state: `igds(26)=p0sl`, `igds(27)=t0sl`, `igds(28)=dt0lp`; then the parameter `igds(29)=vcflat` of the hybrid coordinate system; and finally the $ke + 1$ values of the vertical coordinate $\eta(k)$ of the model half levels for $k = 1, \ldots, ke + 1$ in `igds(30)`,..., `igds(65)`.

Appendix B: Available LM Output Fields

This appendix summarizes the GRIB parameter indicators (element numbers), the table numbers and the dimensions of the direct model output variables. Any changes will be updated in the next COSMO Newsletter.

B.1 General Remarks

For direct model output, we distinguish between so-called *multi-level fields* which are defined on model layers or levels or on fixed pressure or height levels, and *single level fields* which are defined at the surface or on another fixed level.

The fields contained in the model output GRIB-files can be freely chosen by the user: The names of the model variables to be written out have to be specified on the following NAMELIST input character arrays:

- `yvarml` for output on the model grid and for single level data,
- `yvarpl` for output on constant pressure levels
- `yvarzl` for output on constant height levels.

If latter two variables are empty, the model-internal interpolation to pressure and height levels is omitted. If they are set, the values of the corresponding pressure and height levels can be specified by the NAMELIST input arrays `plev` and `zlev`. By default, some multi-level variable are interpolated to 10 pressure levels and 4 height levels:

- p-levles: 1000, 950, 850, 700, 600, 500, 400, 300, 250, 200 hPa.
- z-levles: 1000, 2000, 3000, 5000 m (above sea level).

B.2 Element and Table Numbers used by LM

The name of an input/output field is specified as a CHARACTER variable (in capital letters, names must be 8 characters long, filled with blanks) in NAMELIST input. The model then relates this name internally to a corresponding GRIB element number and table number as well as the corresponding global model variable (which has usually the same name but with small letters). However, some names of output variables are not related to a globally defined model variable. In these cases, the output array is calculated locally only at the output time step.

Table 1 shows the GRIB-element numbers (ee) and table numbers (tab) for the multi-level fields available for LM output files. The level-types (lty) and the corresponding values in octet 11 (lvt) and octet 12 (lv) as well as the physical units (unit) are also included. For variables with level-types 109 and 110, the integer level numbers denoted by k (and k+1) are stored in octets 11 and 12. For pressure levels the constant pressure value in hPa is stored in octet 12 (denoted by pres), and for height levels the constant height level in m above sea level (denoted by z) is stored in octet 12.

Some of the multi-level fields in Table 1 can only be put on the output list if certain parameterization schemes are switched on. These variables are denoted as optional fields. All variables on the list for constant pressure and constant height levels are in the default output list.

Table 1: ***Multi-level fields of LM GRIB-output***

Name	Meteorological Element	ee	tab	lty	lvt	lv	unit
Multi-level fields on model layers/levels k							
U	Zonal wind component (rotated grid)	33	2	110	k	k+1	m/s
V	Meridional wind component (rotated grid)	34	2	110	k	k+1	m/s
W	Vertical wind component	40	2	109	-	k	m/s
P	Pressure	1	2	110	k	k+1	Pa
PP	Pressure perturbation	139	201	110	k	k+1	Pa
T	Temperature	11	2	110	k	k+1	K
QV	Specific humidity	51	2	110	k	k+1	kg/kg
QC	Specific cloud water content	31	201	110	k	k+1	kg/kg
CLC	Fractional cloud cover	29	201	110	k	k+1	%
HHL	Height of half levels (i.e. layer interfaces) constant with time, written only at t=0	8	2	109	-	k	m
Optional multi-level fields on model layers/levels k							
QI	Specific cloud ice content	33	201	110	k	k+1	kg/kg
QR	Specific water content of rain	35	201	110	k	k+1	kg/kg
QS	Specific water content of snow	36	201	110	k	k+1	kg/kg
QG	Specific water content of graupel	39	201	110	k	k+1	kg/kg
QRS	Specific content of rain and snow	99	201	110	k	k+1	kg/kg
TKE	Specific turbulent kinetic energy	152	201	109	-	k	m^2/s^2
TKVM	Turbulent diffusion coefficient for vertical momentum transport	153	201	109	-	k	m^2/s
TKVH	Turbulent diffusion coefficient for vertical heat transport	154	201	109	-	k	m^2/s
Optional multi-level fields of soil layers m between depth z_m and z_{m+1}							
T_SO	Temperature of soil layer m	197	201	112	z_m	z_{m+1}	K
W_SO	Water content of soil layer m	198	201	112	z_m	z_{m+1}	kg/m^2
W_ICE	Ice content of soil layer m	199	201	112	z_m	z_{m+1}	kg/m^2
Multi-level fields interpolated on pressure levels pres (in hPa)							
U	Zonal wind component (rotated grid)	33	2	100	-	pres	m/s
V	Meridional wind component (rotated grid)	34	2	100	-	pres	m/s
OMEGA	Vertical motion	39	2	100	-	pres	Pa/s
T	Temperature	11	2	100	-	pres	K
RELHUM	Relative humidity	52	2	100	-	pres	%
FI	Geopotential	6	2	100	-	pres	m^2/s^2
Multi-level fields interpolated on height levels z (in m)							
U	Zonal wind component (rotated grid)	33	2	103	-	z	m/s
V	Meridional wind component (rotated grid)	34	2	103	-	z	m/s
W	Vertical wind component	40	2	103	-	z	m/s
T	Temperature	11	2	103	-	z	K
P	Pressure	1	2	103	-	z	Pa
RELHUM	Relative humidity	52	2	103	-	z	%

Table 2 shows the GRIB-element numbers (ee) and table numbers (tab) for the single-level forecast fields available for LM output files. As in the previous table, the level-types (lty) and the corresponding values in octet 11 (lvt) and octet 12 (lv) as well as the physical units (unit) of the fields are also included. See Table 5 in Appendix A for the units of the numbers stored in lvt and lv for the corresponding level-type.

Table 2: ***Single-level fields of LM GRIB-output***

Name	Meteorological Element	ee	tab	lty	lvt	lv	unit
Single-level fields: valid at output time							
PS	Surface pressure	1	2	1	-	-	Pa
PMSL	Mean sea level pressure	2	2	102	-	-	Pa
U_10M	Zonal 10m-wind	33	2	105	-	10	m/s
V_10M	Meridional 10m-wind	34	2	105	-	10	m/s
T_2M	2m-temperature	11	2	105	-	2	K
TD_2M	2m-dewpoint temperature	17	2	105	-	2	K
T_G	Temperature at the interface surface-atmosphere	11	2	1	-	-	K
T_SNOW	Temperature of snow surface (surface temperature if no snow)	203	201	1	-	-	K
T_S	Temperature below snow (surface temperature if no snow	85	2	111	-	0	K
T_M	Temperature at the bottom of first soil layer	85	2	111	-	9	K
QV_S	Specific humidity at the surface	51	2	1	-	-	kg/kg
W_SNOW	Water content of snow	65	2	1	-	-	kg/m^2
W_I	Water content of interception store	200	201	1	-	-	kg/m^2
W_G1	Water content of upper soil layer	86	2	112	0	10	kg/m^2
W_G2	Water content of middle soil layer	86	2	112	10	100	kg/m^2
TCM	Turbulent transfer coefficient for momentum at the surface	170	201	1	-	-	-
TCH	Turbulent transfer coefficient for heat and moisture at the surface	171	201	1	-	-	-
Z0	Roughness length (land and water)	83	2	1	-	-	m
ALB_RAD	Surface albedo (shortwave radiation)	84	2	1	-	-	%
CLCT	Total cloud cover	71	2	1	-	-	%
CLCH	High cloud cover (0 - 400 hPa)	75	2	1	-	-	%
CLCM	Middle cloud cover (400-800 hPa)	74	2	1	-	-	%
CLCL	Low cloud cover (800hPa-surface)	73	2	1	-	-	%
CLCT_MOD	Total cloud cover (modified for graphics)	204	203	1	-	-	-
CLDEPTH	Normalized cloud depth (modified for graphics)	203	203	1	-	-	-
HTOP_DC	Top height of dry convection (height above mean sea level)	82	201	1	-	-	m
HZEROCL	Height of $0°C$ isotherm (above mean sea level)	84	201	1	-	-	m
MFLX_CON	Massflux at convective cloud base	240	201	1	-	-	$kg/(m^2s)$
CAPE_CON	Convective available potential energy	241	201	1	-	-	J/kg
QCVG_CON	Moisture convergence below convective cloud base	242	201	1	-	-	1/s
TKE_CON	Convective turbulent kinetic energy	243	201	1	-	-	J/kg
TWATER	Total column water	41	201	1	-	-	kg/m^2
TQV	Total column water vapour	54	2	1	-	-	kg/m^2
TQC	Total column cloud water	76	2	1	-	-	kg/m^2
TQI	Total column cloud ice	58	2	1	-	-	kg/m^2
SNOWLMT	Height of Snow-fall limit	85	201	1	-	-	m

Name	Meteorological Element	ee	tab	lty	lvt	lv	unit
PRR_GSP	Grid-Scale surface rain flux	100	201	1	-	-	kg/(m^{2}s)
PRS_GSP	Grid-Scale surface snow flux	101	201	1	-	-	kg/(m^{2}s)
PRS_CON	Convective surface rain flux	111	201	1	-	-	kg/(m^{2}s)
PRS_CON	Convective surface snow flux	112	201	1	-	-	kg/(m^{2}s)
FRESHSNW	Indicator for age of snow	129	201	1	-	-	-
ZTD	Total zenith delay	121	202	1	-	-	-
ZWD	Wet zenit delay	122	202	1	-	-	-
ZHD	Hydrostatic zenith delay	123	202	1	-	-	-
	Single-level fields: Accumulated since start of the forecast						
RAIN_GSP	Amount of grid-scale rain	102	201	1	-	-	kg/m^2
SNOW_GSP	Amount of grid-scale snow	79	2	1	-	-	kg/m^2
RAIN_CON	Amount of convective rain	113	201	1	-	-	kg/m^2
SNOW_CON	Amount of convective snow	78	2	1	-	-	kg/m^2
TOT_PREC	Total precipitation amount	61	2	1	-	-	kg/m^2
RUNOFF_S	Surface water run-off	90	2	112	0	10	kg/m^2
RUNOFF_G	Ground water run-off	90	2	112	10	100	kg/m^2
TDIV_HUM	Total column divergence of specific humidity	42	201	1	-	-	kg/m^2
AEVAP_S	Accumulated flux of surface moisture	57	2	1	-	-	kg/m^2
	Single-level fields: Averaged over the forecast period						
AUMFL_S	Surface u-momentum flux	124	2	1	-	-	N/m^2
AVMFL_S	Surface v-momentum flux	125	2	1	-	-	N/m^2
ASHFL_S	Surface sensible heat flux	122	2	1	-	-	W/m^2
ALHFL_S	Surface latent heat flux	121	2	1	-	-	W/m^2
ASOB_S	Solar radiation budget at the earth surface	111	2	1	-	-	W/m^2
ASOB_T	Solar radiation budget at the top of the atmosphere	113	2	8	-	-	W/m^2
ATHB_S	Thermal radiation budget at the earth surface	112	2	1	-	-	W/m^2
ATHB_T	Thermal radiation budget at the top of the atmosphere	114	2	8	-	-	W/m^2
APAB_S	Budget of photosynthetic active radiation at the earth surface	5	201	1	-	-	W/m^2
	Single-level fields: Extreme values over certain time intervals						
TMIN_2M	Minimum of 2m-temperature	16	2	105	-	2	K
TMAX_2M	Maximum of 2m-temperature	15	2	105	-	2	K
VMAX_10M	Maximum of 10m-wind speed	187	201	105	-	10	m/s
HTOP_CON	Top height of convective clouds (above mean sea level)	69	201	3	-	-	m
HBAS_CON	Base height of convective clouds (above mean sea level)	68	201	2	-	-	m
TOP_CON	Main-level index of convective cloud top	73	201	1	-	-	-
BAS_CON	Half-level index of convective cloud base	72	201	1	-	-	-
	Single-level fields: Constant and climatological fields						
FIS	Geopotential of earth surface	6	2	1	-	-	m^2/s^2

Name	Meteorological Element	ee	tab	lty	lvt	lv	unit
HSURF	Geometrical height of surface	8	2	1	-	-	m
FR_LAND	Land fraction of a grid area	81	2	1	-	-	-
SOILTYP	Soil texture for land fraction (key number 1-8, over water =9)	57	202	1	-	-	-
RLAT	Geographical latitude	114	202	1	-	-	° N
RLON	Geographical longitude	115	202	1	-	-	° E
PLCOV	Fractional plant cover	87	2	1	-	-	-
LAI	Leaf area index of vegetation	61	2	1	-	-	-
ROOTDP	Root depth of vegetation	62	202	1	-	-	m
FC	Coriolis parameter	113	202	1	-	-	s^{-1}
T_CL	Temperature of the lowest soil layer (climatological value)	85	2	111	-	36	K
W_CL	Water content of the lowest soil layer (climatological value)	86	2	112	100	190	kg/m^2
VIO3	Vertically integrated ozone	65	202	1	-	-	Pa O3
HMO3	Height of ozone maximum	64	202	1	-	-	Pa
Single-level fields: Synthetic satellite products							
SYNME5	METEOSAT-5, MVIRI instrument	1	205	222	0	nc	-
SYNME6	METEOSAT-6, MVIRI instrument	2	205	222	0	nc	-
SYNME7	METEOSAT-7, MVIRI instrument	3	205	222	0	nc	-
SYNMSG	MSG, SEVIRI instrument	4	205	222	0	nc	-

With respect to synthetic satellite images, only the element numbers 3 and 4, i.e. the MVIRI instrument on METEOSAT-7 and the SEVIRI on MSG, respectively, are supported by LM at present. To each channel number 'nc' coded in octet 12 (ipds(10) or 'lv' in the table above) corresponds a physical channel with a specific wavelength, as shown in Table 3.

Table 3: ***Coding of channels for synthetic satellite products***

ee	Satellite/Instrument	lv	channel	wavelength (μm)
3	METEOSAT-7 / MVIRI	1	1	WV 6.4
3	METEOSAT-7 / MVIRI	2	2	IR 11.5
4	MSG / SEVIRI	1	4	IR 3.9
4	MSG / SEVIRI	2	5	WV 6.2
4	MSG / SEVIRI	3	6	WV 7.3
4	MSG / SEVIRI	4	7	IR 8.7
4	MSG / SEVIRI	5	8	IR 9.7
4	MSG / SEVIRI	6	9	IR 10.8
4	MSG / SEVIRI	7	10	IR 12.1
4	MSG / SEVIRI	8	11	IR 13.4

Table 4: ***Specific synthetic satellite products***

ipds(41)	Product	unit
1	Cloudy brightness temperature	K
2	Clear-sky brightness temperature	K
3	Cloudy radiance	$mW/(m^2$ sr cm)
4	Clear-sky radiance	mW/m^2 sr cm)

For each channel on a specified satellite instrument, four different fields are calculated. These products are distinguished by a value for the additional element number (ipds(41), octet 47) in the product definition section, as indicated in Table 4.

All variables required on the input and boundary data files use also the corresponding GRIB table and element numbers from the above tables. The preprocessor programs to interpolate initial and/or boundary conditions to the LM-grid require the GRIB-files containing the external parameter data sets. The table and element numbers of the external parameter fields are shown in Table 5.

Table 5: ***Single-level fields in the LM external parameter files***

Name	**Meteorological Element**	**ee**	**tab**	**lty**	**lvt**	**lv**	**unit**
FIS	Geopotential of earth surface	6	2	1	-	-	m^2/s^2
HSURF	Geometrical height of surface	8	2	1	-	-	m
FR_LAND	Land fraction of a grid area	81	2	1	-	-	-
Z0	Roughness length (land and water)	83	2	1	-	-	m
SOILTYP	Soil texture for land fraction (key number 1-8, over water =9)	57	202	1	-	-	-
PHI	Geographical latitude	114	202	1	-	-	° N
RLA	Geographical longitude	115	202	1	-	-	° E
PLCOV_MX	Plant cover, vegetation period	67	202	1	-	-	%
PLCOV_MN	Plant cover, rest period	68	202	1	-	-	%
LAI_MX	Leaf area index, vegetation period	69	202	1	-	-	-
LAI_MN	Leaf area index, rest period	70	202	1	-	-	-
ROOTDP	Root depth of vegetation	62	202	1	-	-	m

Appendix C: List of COSMO Newsletters and Technical Reports

All Newsletters and Technical Reports are available for download from the COSMO Website: www.cosmo-model.org (or the mirror site cosmo-model.cscs.ch).

COSMO Newsletters

Newsletter No. 1, February 2001.

Newsletter No. 2, February 2002.

Newsletter No. 3, February 2003.

Newsletter No. 4, February 2004.

Newsletter No. 5, April 2005.

COSMO Technical Reports

No. 1, Dmitrii Mironov and Matthias Raschendorfer (2001):
Evaluation of Empirical Parameters of the New LM Surface-Layer Parameterization Scheme. Results from Numerical Experiments Including the Soil Moisture Analysis.

No. 2, Reinhold Schrodin and Erdmann Heise (2001):
The Multi-Layer Version of the DWD Soil Model TERRA_LM.

No. 3, Günther Doms (2001):
A Scheme for Monotonic Numerical Diffusion in the LM.

No. 4, Hans-Joachim Herzog, Ursula Schubert, Gerd Vogel, Adelheid Fiedler and Roswitha Kirchner (2002):
LLM - the High-Resolving Nonhydrostatic Simulation Model in the DWD - Project LITFASS. Part I: Modelling Technique and Simulation Method.

No. 5, Jean-Marie Bettems (2002):
EUCOS Impact Study Using the Limited-Area Non-Hydrostatic NWP Model in Operational Use at MeteoSwiss.

No. 6, Heinz-Werner Bitzer and Jürgen Steppeler (2004):
Documentation of the Z-Coordinate Dynamical Core of LM.

No. 7, Hans-Joachim Herzog and Almut Gassmann (2005):
Lorenz- and Charney-Phillips vertical grid experimentation using a compressible nonhydrostatic toy-model relevant to the fast-mode part of the 'Lokal-Modell'

No. 8, Chiara Marsigli, Andrea Montani and Tiziana Paccagnella (2005):
Evaluation of the Performance of the COSMO-LEPS System